CASCADE PROCESSES AND FULLY DEVELOPED TURBULENCE

by

Antoine Saucier, M. Sc. A.

Department of Physics, McGill University

A thesis submitted to the Faculty of Graduate Studies and Research
in partial fulfillment of the requirements for the degree of
Doctor of Philosophy

Department of physics
McGill University
Montréal, Canada
January 1991

à mes parents,
Elaine et Jean Saucier

Au fou et au vent il faut livrer passage

Spanish saying

ABSTRACT

The energy cascade process in turbulent flows is studied. Kolmogorov inertial range theories are critically reviewed and the multifractal characterization is discussed. Multiplicative cascade models are compared to the energy dissipation field (EDF) measured in the atmosphere. Landau's objection to the 1941 Kolmogorov theory is extended to the predictions of statistical fluid mechanics. The hypothesis $\Delta v(\lambda L) \stackrel{d}{=} \lambda^{1/3} \Delta v(L)$ is rejected with a statistical test. The moments $<(\log\varepsilon(L))^p>$, where $\varepsilon(L)$ denotes the EDF averaged over a volume of size L, are shown to be gaussian. For the EDF: Convergence tests showed that the exponents $\tau(q)$ were not reliable for $q < 0$; the correlations obey $<(\mu_x(\delta))^p(\mu_{x+\delta}(\delta))^q> \propto \delta^{\gamma(p,q)}$ but γ does not always equal the value obtained with a multinomial measure; a privileged scale ratio $r \approx 1/2$ is suggested by the prefactor oscillations of the correlation function. The implications of these results for the modelling of the EDF are discussed.

RÉSUMÉ

On étudie le processus de cascade d'énergie dans les écoulements turbulents. On propose une revue critique des théories de l'intervalle d'inertie de Kolmogorov et la caractérisation multifractale est discutée. Les processus multiplicatifs sont comparés au champ de dissipation d'énergie (CDE) mesuré dans l'atmosphère. L'objection de Landau à la théorie the Kolmororov (1941) est étendue aux predictions de la mécanique statistique des fluides. L'hypothèse $\Delta v(\lambda L) \stackrel{d}{=} \lambda^{1/3} \Delta v(L)$ est rejetée avec un test statistique. On montre que les moments $<(\log\varepsilon(L))^p>$, où $\varepsilon(L)$ est le CDE moyenné sur un volume de taille L, sont gaussiens. Pour le CDE: Des tests de convergence ont montré que les exposants $\tau(q)$ ne sont pas fiables pour $q < 0$; les corrélations satisfont $<(\mu_x(\delta))^p(\mu_{x+\delta}(\delta))^q> \propto \delta^{\gamma(p,q)}$ mais γ n'est pas toujours égal à la valeur obtenue avec une mesure multinomiale; un rapport d'échelle privilégié $r = 1/2$ est suggéré par l'étude des oscillations du préfacteur de la fonction de corrélation. Les implications de ces résultats pour la modélisation du CDE sont discutées.

ACKNOWLEDGMENTS

I thank Geoffrey Austin from the McGill physics department for his overall scientific and financial support, for the confidence he always had in me and especially for the freedom I had to explore my own ideas in a very rich but rather difficult field. Without his worries about the lack of communication between theoreticians and experimentalists, that convinced me to do turbulence measurements as well that theory, my project would not have been as complete. However, the essential scientific supervision of my thesis was made by Thomas Warn, from the McGill meteorology department, without whom this project would not have been possible We spent together uncountable hours of discussion, trying to elucidate the mysteries of the Kolmogorov hypotheses and of the multifractal theories, and he provided the critical expertise and thesis editing that was needed to achieve my goals. His willingness to jump with me in a field that was a bit outside of his specialization, his passion for physics and mathematics as well that his virtuoso's ability to ally logical rigor to intuition were always a source of inspiration The experimental part of this project would not have been possible without Ishtar Zawadski, from the physics department of *Université du Québec à Montréal*, who provided the technical assistance (personal computer with digitizer) and moral support (invitations to his cottage with the gastronomy of his wife Dominique) necessary to do the experiments.

I thank Shaun Lovejoy from the McGill physics department for providing inspirational guidelines to my project. I thank the people of the St-Anne de Bellevue Radar for lending me with enthusiasm a P.C. for the data analysis at the end of my project. I thank Mike Duncan for his patient cooperation in the surface layer fluxes project, the editing he did on parts of my thesis and his moral support. I thank Peter Schuepp, from Macdonald College, who lent me his hot wire anemometer for long periods of time. I thank Yiri Muller, from the *National Norwegian Institute of Energy and Technology* , for his sustained interest in my project and for the

up-to-date literature he sent me. I thank Michel Beauchamp and Biono Saverio, technicians at the Rutherford physics building, for lending me various pieces of equipment

Special thanks go to my friends in physics for making the graduate student life possible in the white U-boat corridors of the Rutherford building dungeon. Robert Plamondon, Andre Longtin, Gadjendra Sarma - Musashi, Jean Wilson, André Giguère, Christopher Lander, Anthony Davis, François Dumais, Jacques Mainville, Ian Graham, Daniel Lavallee, Yves Tessier Charles Hoodge. I thank my friends of the *McGill Daily français*, Luc Gremer, Benoit Leblanc, Nicolas Desaulniers-Soucy, Allan Bowman, Anick Goulet, who helped me keeping in touch with my mother tongue, french, and organized great parties. I thank Myriam Garçon for blowing a fresh breeze in my life during the endless I-should-deposit-tomorrow stage of my thesis. I also thank the people of the Thompson House, and especially Brenda Barclay, for providing smiles and beer in times of despair.

TABLE OF CONTENTS

LIST OF FIGURES

CONTRIBUTIONS TO ORIGINAL KNOWLEDGE

This thesis is an attempt to bridge the physical theories of turbulence with the fractal characterizations. This connection was made to reach a better understanding of an essential energy transfer mechanism common to all turbulent flows: The energy cascade process. Another related goal was to develop new characterization methods for irregular fields. We chose to group our main contributions to these problems in two sections: Turbulence and fractals.

TURBULENCE

1) Landau's objection to the 1941 Kolmogorov theory: The possibility of extending Landau's objection to most of the predictions of statistical fluid mechanics does not appear to have been emphasized previously (chapter 2). The principle of invariance with respect to the composition of statistical subensembles may provide constraining guidelines in the construction of adequate statements in statistical fluid mechanics.

2) Third Kolmogorov hypothesis: On the basis of the properties of multiplicative processes we proposed an alternate weaker form of the third Kolmogorov hypothesis. Our hypothesis states that the moments $\log(\varepsilon(L))$ can be obtained using the gaussian approximation (chapter 3), while the original third Kolmogorov hypothesis states that $\varepsilon(L)$ is distributed according to a lognormal law. The use of the lognormal law for the calculation of $\langle(\varepsilon(L))^q\rangle$ does not yield accurate predictions (Anselmet, 1984). By contrast, our hypothesis was found to be reasonably well supported by the data (section 7.3). Our study clarifies the implications of the central limit theorem on the calculation of moments and also supports the use of multiplicative processes in the modelling of the energy cascade.

3) Simple scaling of the velocity field: Our method for testing the simple scaling of $\Delta v(L)$ based on a χ^2 comparative test on normalized histograms obtained for different

separations L appears to be original. It allowed us to reject the null hypothesis of simple scaling without necessarily having an accurate estimation of high order moments (chapter 7). This test also resolved a controversy in turbulence theory about the breakdown of $<|\Delta v(L)|^h> \propto L^{h/3}$ for high values of h.

4) Correlations in multifractals: Our experimental verification on the energy dissipation field of the relation between the scaling exponents of $<(\mu_l(\delta))^p(\mu_{l+n}(\delta))^q> \propto \delta^{\gamma(p,q)}$ and $<(\mu_l(\delta))^{p+q}>$ appears to be original. In particular, we found that γ did not equal for all (p, q) the value corresponding to the random multinomial measure. These scaling exponents therefore allow to distinguish the energy dissipation field from single scale multiplicative processes.

5) Spurious scaling: The lack of reliability of the mass exponents $\tau(q)$ (spurious scaling) in the negative range does not seem to have been noticed previously.

6) Spatially localized energy cascade: Our simultaneous observations of several spectral bands of the velocity field does not appear to have been used previously to support the existence of a spatially localized energy cascade (chapter 7).

7) Physically distinguished scale ratios in the dissipation field: We presented a first attempt to discover privileged scale ratios by measuring the prefactor oscillations of the correlation functions $\Omega_q(L)$ in the energy dissipation field (8.2.4). The analysis of $\Omega_q(L)$ revealed oscillating prefactors with fairly regular up and downs, but our estimation of the prefactors was not accurate enough to establish periodicity. In the isotropic range (i.e. $L \leq 3$ m) the oscillations suggest a periodicity with a scale ratio $r \approx 1/2$; in the non-isotropic range (i.e. $L > 3$ m), they suggest a rough periodicity with $r \approx 1/1.4$. In any case the prefactors are not periodic over the whole scaling range, which means that the hypothesis of a single scale ratio does not hold.

FRACTALS

1) Renormalization: The possibility of understanding the scaling properties of self-similar sets and self-similar measures, either deterministic or random, with a unique renormalization equation does not appear to have been emphasized previously (chapter 4 and 5 and the appendix 4.1) and allows a simple and unified presentation.

2) Non-concave multifractal spectrum: The possibility of a non-concave $f(\alpha)$ giving rise to a concave $\tau(q)$ does not appear to have been noticed previously. It implies that the true $f(\alpha)$ cannot be deduced from τ with a Legendre transform, unless $f(\alpha)$ is smooth and concave

3) Canonical multiplicative processes: Our presentation of the canonical random multinomial measure is simpler than the original presentation (Mandelbrot, 1974) In the divergent case our results suggest that the measure is composed of a multifractal measure plus a finite number of isolated and intense "spikes" that determine entirely high order moments (chapter 5).

4) Correlations in multifractals: Our derivation of the scaling exponents of the correlation generating function for separated self-similar measures using a renormalization equation appears to be original (section 5.5.2). The exact connection of $<\mu_i(\delta)\mu_{i+n}(\delta)>$ and $<\mu_i(\delta)(\mu_{i+n}(\delta))^2>$ with single box moments does not appear to have been noticed previously (section 5.5), and the existence of more general constraints satisfied by higher order order correlations $<(\mu_i(\delta))^p(\mu_{i+n}(\delta))^q>$ was never pointed out. We gave the first derivation of the correlation generating function for the family of single-scale random multinomial measures (section 5.5.4) Previous calculations involved only specific quasi-deterministic examples of measures.

5) Oscillations in self-similar sets and measures involving a privileged scale ratio: The sensitivity of the prefactor of $N_B(\delta)$ to the box-counting grid does not appear to have been emphasized previously (chapter 4). The discussion of prefactor oscillations in the

generating function of multinomial measures appears to be original (chapter 5). Our definitions of $C_q(L)$ and $\Omega_q(L)$ (chapter 8) are original and provide new "grid insensitive" methods for measuring prefactors or scaling exponents. The effect of the separation condition and of randomness on the periodic prefactor of $C_q(L)$ and $\Omega_q(L)$ in single scale sets and measures does not appear to have been studied previously (sections 8.2.1, 8.2.2). We presented a first numerical experiment with the Novikov "pulse-in-pulse" model (section 8.2.3) that suggests that the prefactor oscillations have a small amplitude (a few percent of the average prefactor).

Chapter I
INTRODUCTION

Vent, vent, tout n'est que vent
Breton saying

The existence of two sharply different types of flows, today called laminar and turbulent, had already been noticed in the first half of nineteen century. However, the first theory of turbulence came only with the pioneering works of Osborne Reynolds (1883-1894). Reynolds first studied the conditions under which a laminar flow of fluid in a pipe becomes turbulent The characteristic property of any turbulent flow is the irregular random variations of the velocity field (as well that other fields) over wide ranges of spatial and temporal scales Reynolds discovered that pipe flows became turbulent, in contrast to laminar which implies steady and smooth, for large enough fluid velocities in the pipe and he proposed a general criterion for the transition to turbulence based on the famous Reynolds number Since these heroic times it has been recognized that the majority of flows encountered in nature and technology are actually turbulent flows, while laminar flows occur only as rare exceptions. The various motions of air in the atmosphere, from slight breezes to general atmospheric circulation at planetary scales, the motions of water in rivers, lakes and oceans as well that the motions of gases in interstellar nebulae are turbulent.

Turbulence plays a fundamental role in various mechanisms such as the transfer of heat and moisture by air masses, the spreading of admixtures in the air, the exchange of carbon dioxide and oxygen between plants and animal life, the scattering of pollen and the lighter seeds, the production of wind currents in the oceans etc... All these processes are crucially involved in the development of life on earth as well that in pollution problems. Turbulence is therefore all around us and its study is consequently extremely important from the practical point of view. Turbulence is also very interesting from a theoretical perspective of nonlinear mechanical

systems with a very great number of degrees of freedom. Indeed, turbulent fields are described by functions of a complex nature involving a huge number of Fourier components. Such systems demand a statistical description that is the object of statistical fluid mechanics (Monin and Yaglom, 1975). The atmosphere is sometimes regarded as a unique laboratory for investigating the properties of these systems.

In numerical simulations of the atmosphere, the huge number of degrees of freedom characteristic of turbulence is one of the first difficulty encountered because computers are still very far from being able to process the necessary amount of data. As a simplifying modelling hypothesis, it is often argued that velocity variations on small spatial or temporal scales cannot be considered as meteorologically significant, and that smoothed versions of the same fields should provide the relevant dynamical information. Such arguments usually involve the hypothesis of a scale separation, made in the hope that small scale details do not play a dynamically significant role. In these approximations, known as parametrization methods, small scale motions are expressed in terms of larger scale motions. Small scales are in that sense "slaved" by larger scales, and ad hoc pseudo viscosities must be introduced to avoid the accumulation of energy that would normally be absorbed by small scale dissipation. An interesting alternative to such slaving principles is the hypothesis of self-similarity, proposed by Mandelbrot (1983) in a general geometrical context, and developed in atmospheric physics by Schertzer and Lovejoy (1985, 85, 87, 89). From this point of view, there is no need to introduce a scale separation because the statistics at a given scale are assumed to be related in some relatively simple way to smaller or larger scales statistics. Small and large scale variability are regarded as part of a unique process, and the goal is to find effective ways to describe and characterize fields that are very irregular over a wide range of temporal and spatial scales, i.e. *fractal* fields.

In this thesis we shall focus on what may be the simplest state of a turbulent fluid: Inertial range fully developed turbulence. The main reasons for studying this type of flow are twofold

Firstly the concept of "locally isotropic turbulence" introduced by Kolmogorov, supplemented with hypotheses about the energy cascade process inspired from the ideas of Lewis Richardson and Geoffrey Taylor, lead to accurate predictions about the energy spectrum and had a profound impact on our understanding of turbulence. The success of these theories suggests that there may exist some *universal* state for high-Reynolds-number small scale turbulence, which is an attractive possibility. The work of Kolmogorov has served as a basis for most subsequent developments of the theory of the local structure of turbulence. From the broader perspective of the statistical mechanics of systems with a large number of degrees of freedom, Kolmogorov dimensional arguments have also been applied to nonlinear systems other than fluids with encouraging results (e.g Bartello and Warn, 1988) Secondly, these theories opened the way to an ensemble of phenomenological approaches to the modelling of turbulence, and more precisely of the energy cascade process. This process, by which the energy is carried from large to small scales, is of general interest and is an essential ingredient of the dynamics of all turbulent flows. These phenomenological cascade models are perhaps the beginning of a new stochastic approach to the modelling of turbulence, providing an alternative to other avenues, such as the direct numerical simulation of the Navier-Stokes equations - still very limited by the capacities of today's computers - or the closure theory developed in particular by Robert Kraichnan, which do not account for the characteristic intermittency of a turbulent flows.

The connection of cascade models with real fluids is phenomenological, and their exact link with the dynamics remains rather vague at this stage. In this thesis we shall study these models and compare them with real turbulent flows. The emphasis will therefore be on the accuracy of this descriptive approach to turbulence modelling. It has been argued by Mandelbrot that the development of an efficient description was a necessary and preliminary step to the process of making predictions. Indeed, how the elliptical trajectories of the planets could have been predicted without the invention of calculus? In this perspective, our goal is to bring together inertial range turbulence theory and the fractal description, which happens to be a natural

framework for turbulent fluids. We will try to determine which phenomenological energy cascade models, among the growing list of possibilities proposed in the literature, are the most relevant candidates to the modelling of turbulent flows. More precisely, we would like to find to what extent the multifractal characterization allows different models to be distinguished, and eventually go beyond this characterization.

On the theoretical side two preliminary steps were found to be essential to reach our goal. Firstly, a good understanding of the Kolmogorov inertial range theories was needed. A critical review of these theories with an emphasis on what appears to be the most significant problems and controversies is therefore presented in chapters two and three. Secondly, a clear statement of the fractal ideas was also needed. Indeed, the large number of possible models consistent with a given scale symmetry demands a work of classification, as well that the development of techniques allowing different classes to be distinguished, and therefore the fractal characterization methods are directly relevant. In this perspective, we propose in chapter 4 and 5 an original turbulence-oriented synthesis of the concepts and methods appropriate for fractal sets and fractal measures respectively. This synthesis was mainly motivated by the lack of systematic reviews on fractal measures, and it covers a literature scattered over several fields, such as topology, non-linear dynamical systems, chaos theory, geophysics and fluid mechanics.

Ultimately, the experimental verification of any hypothesis is necessary, especially when dealing with loosely specified phenomenological models that relate only qualitatively to the Navier-Stokes equations, by sharing some (scale) symmetries with them. On the experimental side, high frequency measurements of the velocity field in the atmospheric surface layer were collected using a hot wire anemometer and an analog-to-digital converter installed on a personal computer. Chapter six first concentrates on preliminary analyses of this data by reproducing well known results about inertial range turbulence. Previous scaling studies on the subject are next criticized and some new original analyses related to correlations in multifractal are

presented. In chapter seven two aspects of inertial range turbulence theories, namely simple scaling and intermittency, are examined with original methods and a new test of the validity of multiplicative processes is proposed, based on the central limit theorem. In chapter eight one the simplest family of cascade model, involving a single scale ratio, is compared with the energy dissipation field.

The faculty of Graduate Studies and Research of McGill University requires that the following text from the **GUIDELINES CONCERNING THESIS PREPARATION** be cited in full in the introductory sections of any thesis to which it applies.

MANUSCRIPTS AND AUTHORSHIP

The candidate has the option, subject to the approval of the Department, of including as part of the thesis the text, or duplicated published text (see below), of an original paper, or papers In this case the thesis must still conform to all other requirements explained in Guidelines Concerning Thesis Preparation. Additional material (procedural and design data as well as description of equipment) must be provided in sufficient detail (e.g. in appendices) to allow a clear and precise judgement to be made of the importance and originality of the research reported. The thesis should be more than a mere collection of manuscripts published or to be published. It must include a general abstract, a full introduction and literature review and a final overall conclusion. Connecting texts which provide logical bridges between different manuscripts are usually desirable in the interests of cohesion.

It is acceptable for theses to include as chapters authentic copies of papers already published, provided these are duplicated clearly on regulation thesis stationery and bound as an integral part of the thesis. Photographs or other materials which do not duplicate well must be included in their original form. In such instances, connecting texts are mandatory and supplementary explanatory material is almost always necessary.

The inclusion of manuscripts co-authored by the candidate and others is acceptable but the candidate is required to make an explicit statement on who contributed to such work and to what extent, and supervisors must attest to the accuracy of the claims, e.g. before the Oral Committee. Since the task of the Examiners is made more difficult in these cases, it is in the candidate's interest to make the responsibilities of authors perfectly clear. Candidates following this option must inform the Department before it submits the thesis for review.

Chapter II

REVIEW OF THE KOLMOGOROV INERTIAL RANGE THEORIES AND THE ORIGIN OF CASCADE MODELS

A major defect of the current theoretical study of turbulence is that it separates into at least two disconnected parts. One part includes the successful phenomenology put forth in Kolmogorov 1941 (.). And the other part includes the differential equations of hydrodynamics, due to Euler for nonviscous fluids, and to Navier (and Stokes) for viscous fluids. These two parts remain unrelated. If "explained" and understood mean "reduced to basic equations," the Kolmogorov theory is not yet explained or understood. And Kolmogorov has not helped solve the equations of fluid motion.

Benoit B. Mandelbrot (from *The fractal geometry of nature*)

This thesis is mostly concerned with phenomenological approaches involving statistics, fractals and scaling, applied to the modelling of turbulent flows. In the field of statistical fluid mechanics, scaling hypotheses and "fractal" ideas probably started with the Kolmogorov inertial range theories. We shall therefore begin this dissertation with a critical review of these theories. We emphasize some unresolved controversies and try to interpret them in the framework of the classical theories. This presentation relies in particular on Kolmogorov (1941a, 1962), Kraichnan (1974), Monin & Yaglom (1975), Orszag (1977), Frisch and Sulem (1978), Schertzer and Lovejoy (1984) and Frisch and Orszag (1990).

2.1 REVIEW OF THE 1941 KOLMOGOROV HYPOTHESES

The simplicity of the 1941 Kolmogorov theory (in short the K41 theory) and the accuracy of its most famous prediction, namely the $k^{-5/3}$ energy spectrum, make this theory one of the most remarkable in the field of turbulence. As is often the case with dimensional analysis, an important tool in this theory, the derivation of the result is easier than its interpretation in dynamical terms. Even today, no formal analysis by means of perturbation theory, the moment equation hierarchy, or renormalization techniques can settle whether a power spectrum of the form k^{-p} is compatible with the Navier-Stokes equations (Kraichnan, 1974). Nevertheless, the

success of Kolmogorov energy spectrum certainly supported the idea that scale invariance was an important property of turbulent flows.

The K41 theory is concerned with the small scale behavior of incompressible fluids at high Reynolds number. By "small scale" we mean small with respect to the smallest macroscale L_0, defined by the geometry of the flow. In the simplest case of a fluid contained in a cubic box, L_0 would be the size of the box. In more realistic situations, for example the velocity field in the atmosphere above a flat terrain, L_0 would be the distance from the boundary if the thermal effects (i.e. motion generated by the fluctuations of the air density) were negligible. The fluid considered is subject to some large scale forcing mechanism injecting in the flow a mean energy production rate f_0 per unit mass. In a dynamical equilibrium, this energy production is balanced by the mean energy dissipation rate per unit mass ε_0, so that $\varepsilon_0 = f_0$.

The energy contained in the largest scales of the turbulent velocity field is transfered, via non-linear interactions, into the smaller scales. For large scales the energy is transfered without losses. This statement can be justified by considering the spectral form of the Navier-Stokes equation. If the velocity field is expanded in Fourier series in cyclic boxes, i.e.

$$\mathbf{v}(\mathbf{x},t) = \sum_j \mathbf{v}(\mathbf{k}_j)\, e^{i\mathbf{k}_j\cdot\mathbf{x}},$$

the dissipation term $-\nu\, \partial^2\mathbf{v}(\mathbf{x},t)/\partial x_i \partial x_i$ of the Navier-Stokes equation takes the spectral form $T_D = -\nu\, \|\mathbf{k}\|^2 \mathbf{v}(\mathbf{k}_j)$. T_D is large only for large $\|\mathbf{k}\|$, i.e. for small scales, for which the viscous forces become important and convert the kinetic energy into heat. The non-dissipative energy transfer from large to smaller scales, driven by non-linear interactions, is usually called the *energy cascade process*. It was first described by Richardson who envisioned a sequence of eddies of all sizes in which smaller eddies "feed" on the energy of larger eddies. Similar breakage processes were studied by Kolmogorov (1941b).

Kolmogorov argued that for high Reynolds number the small scales of the flow should have a universal structure, independent of the larger scale geometry of the flow, the details of the forcing and of the boundary conditions being "forgotten". More specifically the K41 theory is based on two hypotheses. The first supposes that the n-variate probability distributions of the velocity differences $\Delta v_i(\mathbf{L}) = v_i(\mathbf{x}+\mathbf{L}) - v_i(\mathbf{x})$ are universal isotropic functions solely of the difference vector $\mathbf{L}$, the kinematic viscosity ν and ε_0, provided that $\|\mathbf{L}\| = L$ is small with respect to L_0. Using these parameters a dissipation scale (or inner scale) $\eta_0 = \nu^{3/4} \varepsilon_0^{-1/4}$ can be formed, usually interpreted as an estimate of the smallest scale in the velocity field. This leads immediately, by dimensional analysis, to

$$< |\Delta v_i(\mathbf{L})|^h > \; = \; F_h(\eta_0/L) \; (\varepsilon_0 L)^{h/3}, \;\; L << L_0, \qquad (2.1.1)$$

where F_h is an unknown function. The second hypothesis states that the above n-variate distributions are independent of ν if L lies in the inertial-range, i.e. if $\eta_0 << L << L_0$. Indeed for large enough scales the dissipation term defined above is small, and it becomes plausible to assume that large scales statistics become independent of ν in the limit $\nu \rightarrow 0$. The second hypothesis implies that the high-Reynolds-number expression of the velocity structure function is

$$< |\Delta v_i(L)|^h > \; = \; F_h(0) \; (\varepsilon_0 L)^{h/3} \; , \; \eta_0 << L << L_0, \qquad (2.1.2)$$

which is one form of the celebrated Kolmogorov law.

These results can be stated in the spectral form. The characteristic wavenumber associated with the dissipation scale is $k_d = (\varepsilon_0/\nu^3)^{1/4}$ and marks the transition from the inertial range $k_0 < k < k_d$ ($k_0 = 1/L_0$, where L_0 is the smallest macroscale) to the dissipation range $k > k_d$. The energy spectrum E(k) is defined so that

$$\frac{<v_i'^2>}{2} = \int_0^\infty E(k) \, dk \;\; ,$$

where $v_i' = v_i - \langle v_i \rangle$. Assuming that E(k) falls off in the dissipation range rapidly enough with increasing k, (2.1.1) with h = 2 leads by Fourier transformation to the inertial range spectrum law

$$E(k) = \varepsilon_0^{2/3}\, k^{-5/3}\, f(k/k_d), \qquad (2.1.3)$$

where f(x) an unknown universal function (for more details on the energy spectrum see Monin and Yaglom (1975), section 12.1 and 21.4, volume 2). Alternatively, (2.1.3) can be obtained directly with dimensional analysis. The second hypothesis implies that the k_d dependence disappears for $k << k_d$, i.e. $f(x) \to C$ as $x \to 0$, where C is a constant. In the inertial range, the energy spectrum then becomes

$$E(k) = C\ \varepsilon_0^{2/3}\, k^{-5/3}\ . \qquad (2.1.4)$$

Kolmogorov theory does not predict the value of C, which can be determined experimentally ($C \approx 1.6$).

In Kraichnan's words the 1941 Kolmogorov theory, and especially the prediction (2.1.4), "has achieved an embarrassment of success". Since the first experiments of Grant, Stewart and Moilliet (1962), numerous other experiments in wind tunnels as well as in the atmosphere have shown that (2.1.2) is well obeyed for h = 2, that the energy spectrum in the dissipation range $k > k_d$ scales according to (2.1.3) and that (2.1.4) often holds over a range of scales wider than expected *a priori*. Actually, an approximate $k^{-5/3}$ energy spectrum is often observed in flows for which the Reynolds number is too small for a distinct inertial range to exist and in conditions where substantial departures from isotropy occur.

One might be tempted to use the the same dimensional arguments with other fields, for example the energy dissipation field

$$\varepsilon(\mathbf{x},t) = 1/2\ \nu \sum_{i,j} (\partial u_i/\partial x_j + \partial u_j/\partial x_i)^2.$$

The first and second hypothesis applied to $\varepsilon(\mathbf{x},t)$ imply that the power spectrum of $\varepsilon(\mathbf{x},t)$ has the form $F_\varepsilon(k) = C\,\varepsilon_0^2\,k^{-1}$ in the low-k range. However this spectrum was experimentally found to be proportional to k^{-s} where $s \approx 0.6$ (see for example Pond and Stewart (1965)). This means that the dimensional argument of the K41 cannot be applied to $\varepsilon(\mathbf{x},t)$, probably because $\varepsilon(\mathbf{x},t)$ always depends on the kinematic viscosity.

The K41 theory makes useful predictions for flows having a wide range of scales. The necessity for a wide range of scales in fully-developed turbulence follows from the balance between dissipation and the driving force. The mean energy dissipation rate can be expressed in the form

$$\varepsilon_0 = 2\nu \int_0^\infty k^2\, E(k)\, dk = \nu\ \Omega, \qquad (2.1.5)$$

where $E(k)$ is the energy spectrum (Monin and Yaglom (1975), section 12.3) and Ω the *enstrophy*. In the limit $R_e \to \infty$ (or $\nu \to 0$) with ε_0 finite, (2.1.5) implies that $\Omega \to \infty$ and therefore the energy distribution must become broader in k-space if $E(k)$ remains finite.

Despite its success, the K41 theory was immediately criticized by Landau in 1944 (see Landau and Lifchitz, 1989) on theoretical grounds, and was consequently modified by Obukhov (1961) and Kolmogorov (1962). More recently, some experimental evidence of the failure of the prediction (2.1.2) at large h was obtained by Anselmet (1984). We shall now discuss the physical arguments, rather delicate and often introduced in a cavalier manner, explaining the limitations of the K41 theory.

2.2 REEXAMINATION OF THE K41 THEORY AND THE MODIFIED SIMILARITY HYPOTHESES

In the spirit of the K41 theory the small scales of the fluid velocity field are assumed to reach a statistical equilibrium determined by the energy injected at larger scales. A given spatial region of the fluid is therefore expected to adjust to an energy flux that is somehow local in real space. This concept of localness, linked to the energy cascade, was first pointed out by Landau as a basic objection to the K41 theory. *Global* universality seems untenable since the intensity of the small scales in any particular region is clearly related to the intensity of the local external driving. Consequently it seems inescapable that the statistics of the small-scales depend on spatial and temporal variations of the driving, which are in essence non-universal.

On the experimental side, it was noticed by Obukhov (1961) that the $k^{-5/3}$ energy spectrum is observed locally in the atmosphere. He noticed that power spectra measured on long enough samples in the atmosphere do exhibit a $k^{-5/3}$ energy spectrum, but that the prefactor was changing significantly from a sample to the other. From the standpoint of the K41 theory, the variations of the prefactor are due to changes in the local energy dissipation rate ε_{local} (at this stage ε_{local} can be thought to be an average obtained with a finite sample). The validity of the $k^{-5/3}$ energy spectrum for samples questions the universality of the constant C in (2.1.4), because in general $<(\varepsilon_{local})^{2/3}> \neq (<\varepsilon_{local}>)^{2/3}$. This difficulty arises from the fact that the law $E(k) = C\ \varepsilon_0^{2/3}\ k^{-5/3}$ is not invariant with respect to the composition of statistical sub-ensembles. To illustrate this property, suppose that a set of samples is split in two sub-sets according to the mean energy dissipation rate ε obtained for each sample: A sample belongs to the first sub-ensemble if $\varepsilon > \varepsilon_*$ (ε_* is an arbitrary threshold) and belongs to the second sub-ensemble otherwise. It seems reasonable to expect the $k^{-5/3}$ law to hold separately for each sub-ensemble, i.e.

$$E_1(k) = C\ <\varepsilon>_1^{2/3}\ k^{-5/3} \quad \text{and} \quad E_2(k) = C\ <\varepsilon>_2^{2/3}\ k^{-5/3},$$

where $\langle\varepsilon\rangle_1$ and $\langle\varepsilon\rangle_2$ denote the mean energy dissipation rate for each sub-ensemble. If p_1 and p_2 denote the probabilities of belonging to each statistical sub-ensemble, then the energy spectrum of the complete ensemble is obtained by

$$\begin{aligned} E(k) &= p_1\ E_1(k) + p_2\ E_2(k) \\ &= C\ [\ p_1\ \langle\varepsilon\rangle_1^{2/3} + p_2\ \langle\varepsilon\rangle_2^{2/3}\ ]\ k^{-5/3} \\ &\neq C\ \langle\varepsilon\rangle^{2/3}\ k^{-5/3}, \end{aligned}$$

unless ε has a special probability distribution. The $k^{-5/3}$ law relates the average quantity E(k) to the $2/3^{th}$ power of an average, which breaks the invariance with respect to the composition of statistical sub-ensemble. A statistical statement that respect this invariance must relate average quantities in a *linear* way, e.g. $\langle A\rangle = k\langle B\rangle$. It would therefore seem that the $k^{-5/3}$ law cannot hold in principle.

Obukhov's observations and Landau's objection suggested the possibility of a local application of the Kolmogorov similarity hypotheses. Obukhov proposed to redefine the statistical ensemble of the K41 theory. The basic idea is to define a sub-ensemble of flows, contained in some imaginary sphere of diameter L, for which the volume-averaged energy dissipation $\varepsilon(L)$ is fixed. $\varepsilon(L)$ is regarded as an estimate of the "local" energy flux. The K41 theory is then assumed to hold for this sub-ensemble, with ε_0 replaced by $\varepsilon(L)$.

This idea has been criticized mostly because of the arbitrariness of the choice of $\varepsilon(L)$ as a candidate for a "local energy flux". Indeed, the dynamical quantity responsible for the dynamics of the scales L is the spectral energy flux from scales L to smaller scales. In general, this spectral flux does not equal $\varepsilon(L)$ (Kraichnan, 1974). Despite its arbitrariness, this hypothesis is still used nowadays to relate the energy dissipation field to the velocity field (Anselmet (1984), Schertzer and Lovejoy (1985), Meneveau and Sreenivasan (1990, 1987b, 1987c), Novikov (1990)). The idea of studying the properties of a field as a function of the properties of another

field, allowing the introduction of a conditional ensemble, is commonly used in the analysis of turbulent fields and is usually called conditional sampling (Antonia (1981), Raupach (1981), Shaw and Businger (1985)).

The idea of Obukhov lead Kolmogorov to propose a modified version of the K41 theory, based on the concept of local energy dissipation rate. The refined hypotheses are similar to the original hypotheses, except that they apply to a conditional ensemble. **x** and **x+L** are assumed to be contained in a sphere of diameter L having a fixed value ε for $\varepsilon(L)$. The first refined hypothesis naturally leads to the definition of a local dissipation scale $\eta = \nu^{3/4} \varepsilon^{-1/4}$. From dimensional analysis follows the expression of the conditional velocity structure function:

$$\text{For } L << L_o, \quad < (\Delta v(L))^h >_{\varepsilon(L)=\varepsilon} = F_h(\eta/L) (\varepsilon L)^{h/3} . \qquad (2.2.1)$$

Similarly, the second refined hypothesis states that the n-variate distributions of the velocity differences are independent of ν when $\eta << L << L_0$, i.e. when the local dissipation scale is small enough. This implies that the moments given by equation (2.2.1) become independent of η as $\eta \to 0$. Therefore

$$\text{as } \eta \to 0, \quad < (\Delta v(L))^h >_{\varepsilon(L)=\varepsilon} \sim F_h(0) (\varepsilon L)^{h/3} . \qquad (2\ 2.2)$$

These two hypothesis are assumed to be valid for a "pure regime", i.e. for the conditional ensemble described above. A real flow is a "mixed regime" where a range of values for $\varepsilon(L)$ exists. It follows that there is also a spectrum of local dissipation scales η. If the global Reynolds number of the flow is large enough, it becomes plausible to assume that the condition $\eta << L$ is always satisfied except for a few events weighted by a small probability. Following this argument, the unconditional ensemble average can be obtained by an ensemble average on the equation (2.2.2):

$$< (\Delta v(L))^h > = F_h(0) L^{h/3} < (\varepsilon(L))^{h/3} >. \qquad (2.2.3)$$

Notice that this equation is invariant with respect to the composition of statistical sub-ensembles because it relates linearly two averages. (2.2.3) is the modified form of (2.1.2), taking into account the Reynolds number dependence of the velocity field through $<(\varepsilon(L))^h>$ It connects the statistics of two random variables without specifying either of them, which is a qualitative difference between the modified and original theories. The modified theory is therefore much less predictive than the K41 theory because $<(\varepsilon(L))^h>$ remains unknown. The refined theory, and especially the prediction (2.2.3), are still regarded as controversial (Landau and Lifchitz, 1989 (revised edition), section 34).

It is interesting to note that for $h = 3$ the prediction (2.2.3) of the modified theory yields is $<(\Delta v(L))^3> \propto \varepsilon_0 L$ (because $<\varepsilon(L)> = \varepsilon_0$) and is therefore identical to the prediction of the K41 theory. The order-3 velocity structure function is therefore insensitive to intermittency. It is also worth stressing that the exact expression of $<(\Delta v(L))^3>$ can be derived from the Navier-Stokes equation. Assuming isotropy (landau and Lifchitz, 1989, section 34), it can be shown that

$$B_3(L) = -\frac{4}{5}\,\varepsilon_0 L + 6\nu\frac{dB_2}{dL}, \qquad (2.2.4)$$

where $B_n(L) = <(\Delta v_i(L))^n>$. Assuming that ε_0 remains finite as $\nu \to 0$, (2.2.4) becomes

$$B_3(L) = -\frac{4}{5}\,\varepsilon_0 L. \qquad (2.2.5)$$

This is an important result since it is essentially *exact* for fully-developed isotropic turbulence. *A priori* (2.2.5) might suggest that $B_n(L)$ can be expressed for any n only in terms of L and ε_0, in which case one falls back on the original K41 theory. However, in the light of Landau's objection the universality of (2.2.5) is regarded as an interesting but special property of the order-3 moment of $\Delta v_i(L)$, and moments of order $h \neq 3$ are expected in general to be

non-universal. Note that $B_3(L)$ depends linearly on ε_0 and therefore the exact result (2.2.5) is invariant with respect to the composition of statistical sub-ensembles.

It is interesting to look back at the K41 theory from the point of view of the refined theory The prediction (2.2.3) would be consistent with (2.1.2) if the condition

$$<(\varepsilon(L))^h> = \varepsilon_0{}^h \qquad (2.2.6)$$

was satisfied for $L >> \eta$. In general (2.2.6) is not satisfied, although $<\varepsilon(L)> = \varepsilon_0$ always holds for a spatially homogeneous field. Nevertheless (2.2.6) could still be satisfied if the variations of $\varepsilon(L)$ were restricted to the dissipation range only, i.e. if $\varepsilon(L) \approx \varepsilon_0$ when $L > \eta$. However the variability of the energy dissipation field and in particular its *intermittency*, which produce sequences of "dead" or "live" regions of size $L > \eta$, is not compatible with this behavior. In the perspective of the refined theory, the K41 theory fails because $\varepsilon(L)$ varies significantly when L lies in the inertial range.

The intermittency of the energy dissipation field (Batchelor and Townsend (1949), Sandborn (1959), Kuo and Corrsin (1971)) was discovered by looking at the high-passed filtered velocity field (figure 2.1). The resulting signal exhibits a sequence of active regions separated by inactive gaps where the velocity is almost vanishing. The bulk of the dissipation takes place in the intense regions, where the velocity derivatives are large. It was observed that the mean size of the active regions decreased as the Reynolds number increased. As a phenomenological observation, intermittency implies that the bulk of the dissipation in a fully-developed turbulent fluid occurs in a small volume-fraction of the whole space, and that this fraction decreases with increasing Reynolds number. We will return to these high-passed filtered velocity fields in an experimental study (chapter 7).

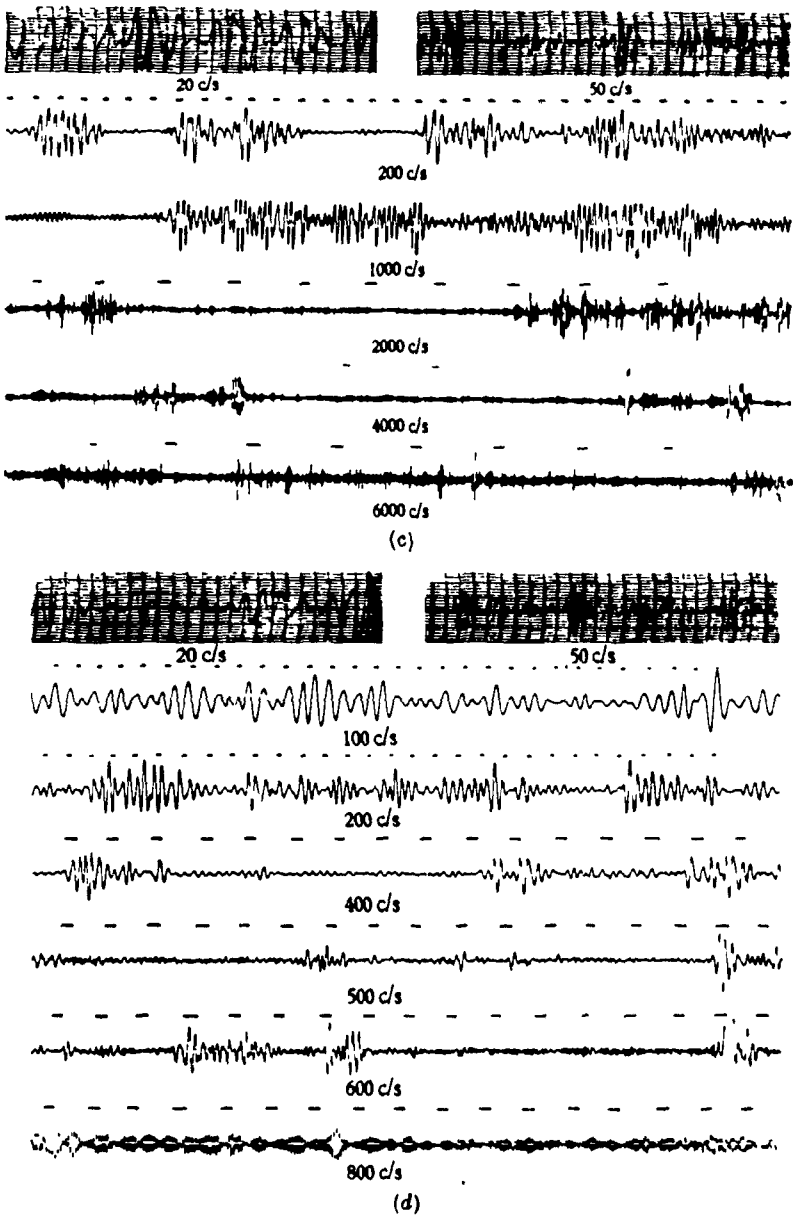

Figure 2.1: A velocity signal measured with a hot wire anemometer in a 15x150 cm boundary layer channel was filtered, so that the traces shown are within a narrow frequency band around the frequency noted. The small scale turbulence appears to be contained in quite sharply defined lumps or bursts. (c) and (d) refer to samples at different locations (from Sandborn, 1959).

From a more fundamental point of view the existence of small scale intermittency reveals that the "gustiness" of a turbulent flow, observed in various conditions, is not always the effect of some large scale irregular forcing. It seems to be a natural property of the flow at large Reynolds number. Numerical experiments with one-dimensional truncated versions of the Navier-Stokes equation, involving a large number of degrees of freedom and sharing invariants with the three-dimensional Navier-Stokes equations, have been shown to exhibit intermittency (Bartello and Warn, 1988).

Landau's objection can also be raised for most of the predictions of statistical fluid mechanics. Consider for example the law of the *logarithmic boundary layer* describing how the mean velocity u along an infinite flat surface changes as a function of the vertical distance z:

$$\frac{d\langle u(z)\rangle}{dz} = \frac{u_*}{\kappa z}, \quad z >> \delta \qquad (2.2.7)$$

where $u_* = \sqrt{\tau_0/\rho}$, $\tau_0 = -\rho \langle u'w' \rangle$, $\delta = \nu/u_*$ and κ is the von Karman constant. This follows from the Reynolds equations assuming a zero vertical pressure gradient (ρ is the fluid density, u' and w' are the velocity fluctuations parallel and normal to the surface respectively, see Monin and Yaglom (1975), section 5.1 for more details). (2.2.7) is a *universality statement* typical of statistical fluid mechanics: One assumes that an average quantity - here $d\langle u(z)\rangle/dz$ - can be expressed only in terms of a few *mean characteristics* of the flow, here the friction velocity u_*. As for the $k^{-5/3}$ spectral law, (2.2.7) is not invariant under the composition of statistical sub-ensembles because u_* is the square root of an average. We therefore conclude that this law cannot hold in principle, even if it provides a valuable approximation for flows that are not too intermittent. This could explain the scatter of the measurements of the von Karman constant, which is not universal from this standpoint.

More generally, the above considerations suggest that global universality might never hold and that a more complete specification of the statistical ensemble may be essential. It is

emphasized that this lack of global universality does not prevent some specific statistics, e.g. $B_3(L) = -4/5\ \varepsilon_0 L$, to be expressed only in terms of a few mean characteristics of the flow (here ε_0). By contrast with the statistical mechanics of systems in equilibrium, where various statistical ensembles are defined (e.g. microcanonical, canonical etc...), one must recognize that in the context of statistical fluid mechanics the nature of the ensembles is poorly understood. The possibility of extending Landau's objection to most of the predictions of statistical fluid mechanics does not appear to have been emphasized previously.

2.3 CONTROVERSY ABOUT THE BREAKDOWN OF THE K41 THEORY FOR HIGH ORDER MOMENTS OF $\Delta V(L)$

Despite the experimental validation of (2.1.3) and (2.1.4), measurements of the higher order moments (e.g. Anselmet, 1984) have shown that the law (2.1.2) breaks down for $h > 4$. As h increases the structure function keeps its power law behavior but the exponent is less than the predicted h/3. Hence, these analyses suggest that the correct law is of the form $\langle|\Delta v_l(\mathbf{L})|^h\rangle \propto L^{\zeta(h)}$, where $\zeta(h)$ is a non-linear function such that $\zeta(h) \approx h/3$ for $h \leq 4$ and $\zeta(h) < h/3$ for $h > 4$ (figure 2.2). This result is consistent with a failure of the first Kolmogorov hypothesis, as argued by Landau. In order to explain the non-linear scaling of the velocity structure functions, two main interpretations have been proposed.

We shall first examine the point of view of Frisch (1983) who obtained the result $\langle|\Delta v_l(\mathbf{L})|^h\rangle \propto L^{h/3}$ in the following alternate way. Since the forcing is confined to large scales and the dissipation is confined to small scales when the Reynolds number is large, it can be argued that intermediate scales (i.e. $\eta << L << L_0$) evolve according to Euler's equation which is invariant under the stretching transformation

$$\mathbf{x} \to \lambda \mathbf{x}, \quad \mathbf{v} \to \lambda^{\alpha} \mathbf{v}, \quad t \to \lambda^{1-\alpha} t, \tag{2.3.1}$$

i.e., if $\mathbf{v}(\mathbf{x},t)$ is a solution so is $\lambda^{-\alpha}\mathbf{v}(\lambda\mathbf{x},\lambda^{1-\alpha}t)$. Consider the velocity structure functions $B_n(\mathbf{L}) = \langle(\Delta v_i(\mathbf{L}))^n\rangle$, where $\Delta v_l(\mathbf{L}) = v_l(\mathbf{x}+\mathbf{L}) - v_l(\mathbf{x})$ and v_i is the component of $\mathbf{v}$ along $\mathbf{L}$. If the turbulence is homogeneous and isotropic then B_n depends only on L.

If it is also invariant under stretching, then for all λ

$$\Delta v_l(\mathbf{L}) \overset{d}{=} \lambda^{-\alpha}\, \Delta v_l(\lambda \mathbf{L}) \tag{2.3.2}$$

where " $\overset{d}{=}$ " denotes an equality in probability distribution and α is an unknown parameter. It

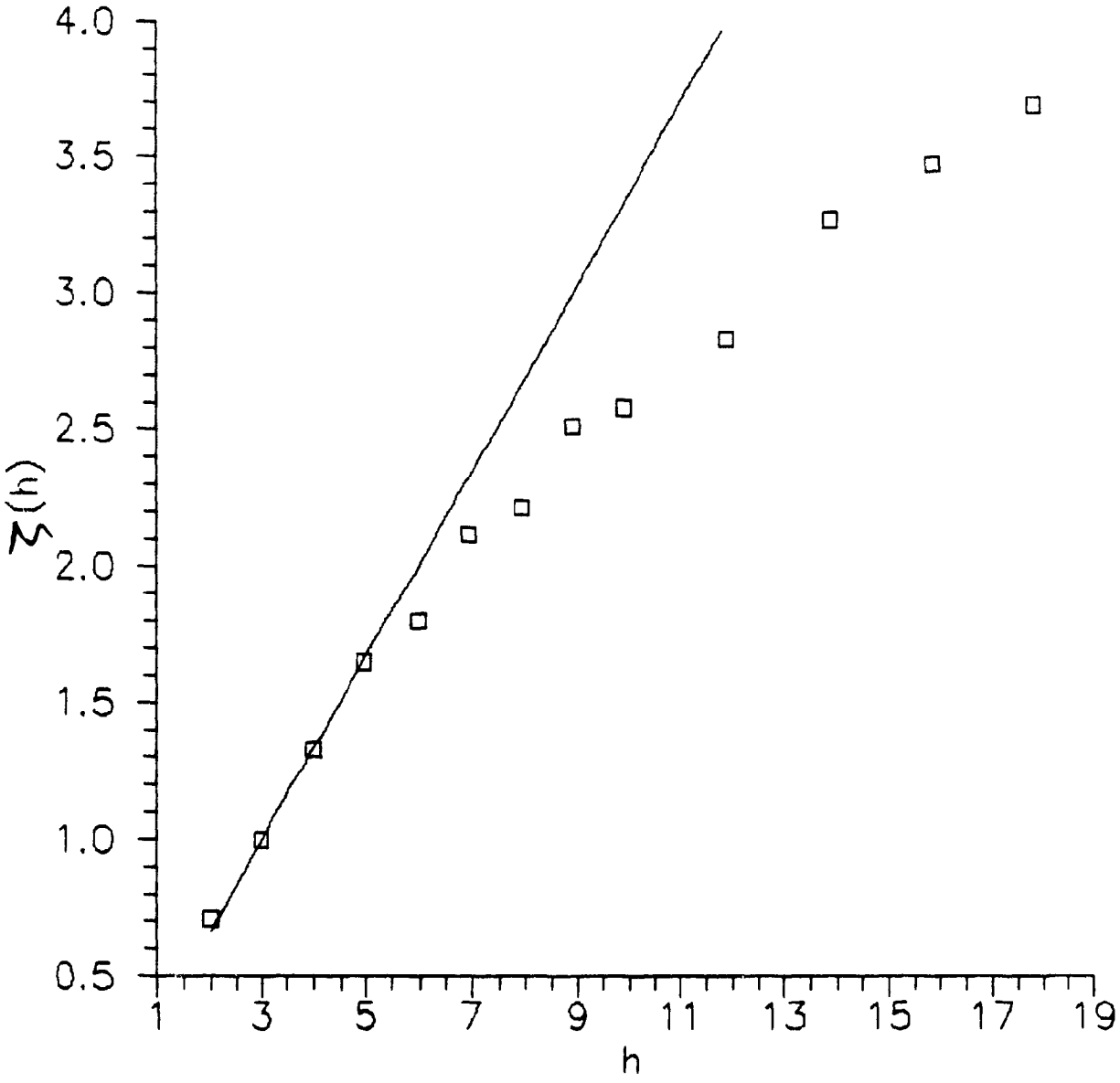

Figure 2.2 : The function $\zeta(h)$ as measured by Anselmet (1984). The non-linearity becomes clear for $h > 4$. The straight line is the prediction of the K41 theory, i.e. $\zeta(h) = h/3$.

follows from (2.3.2) that

$$B_n(L) = \lambda^{-\alpha n} B_n(\lambda L), \tag{2.3.3}$$

which on setting $\lambda = 1/L$ becomes

$$B_n(L) = c_n L^{\zeta_n} \tag{2.3.4}$$

where $\zeta_n = n\alpha$ and the c_n are constants. Since the exponents at all orders are determined by a single parameter α, the scaling is said to be *simple*. The scaling exponent α is a kind of irregularity index for the velocity field. For $L << \eta$, the field is smooth and Taylor's series arguments imply $\Delta u_l(L) \sim L$ (neglecting points where the derivative vanishes) and $\alpha = 1$. If $\alpha < 1$ for $L >> \eta$, then the velocity field is irregular on these scales. An ordinary function is said to satisfy *Holder condition* with *Holder exponent* β at x_0 if $|f(x) - f(x_0)| \leq K |x - x_0|^\beta$ for all x in some neighborhood of x_0 for some K. α is a kind of statistical Holder exponent for the velocity field.

Self-similarity implies simple scaling but does not fix the exponent α. Bounds on α can be obtained by noting that the Fourier transform of B_2 implies $E(k) = ck^{-2\alpha-1}$ for $k_0 << k << k_d$ if it is assumed that E is negligible outside the range. Since $k_d \to \infty$ as $R_e \to \infty$, then $2\alpha+1 > 1$ for finite energy and $2\alpha+1 \leq 3$ for infinite enstrophy (see (2.1.5)), i.e $0 < \alpha \leq 1$. The slope of the energy spectrum (in log-log coordinates) therefore lies between -1 and -3. On the other hand, using the exact result (2.2.5) together with (2.3.4) leads directly to $\alpha = 1/3$. By contrast with the K41 theory, it is emphasized that we do not need in this argument to give a privileged role to ε_0 in the velocity statistics to obtain the simple scaling (2.3.4) with $\alpha = 1/3$. The only assumption required is that ε_0 remains finite in the limit $\nu \to 0$. *Hence this symmetry argument yields the simple scaling (2.3.4) without specifying the c_n's, which may then remain non-universal.* From this standpoint Frisch interprets the measured

non-linearity of $\zeta(h)$ at large h as a *breaking of the formal scaling symmetry of the Euler's equation* in real flows.

Once the K41 theory is abandoned, a "Pandora's box" of possibilities is opened (Kraichnan, 1974). For example, one might try adding a dependence on some outer scale L_0 in the first Kolmogorov hypothesis, i.e. $<|\Delta v_l(\mathbf{L})|^h> = f(\varepsilon_0, L, h, \nu, L_0)$. This outer scale makes room for a possible influence of the large scales on the small scales. Unfortunately, in this case dimensional analysis no longer reveals the analytical form of the velocity structure functions or of the energy spectrum, and there is no basis in the hypothesis for concluding that these should be power laws, as observed. In other words, we are left with a non-predictive theory. Frisch and Parisi (Appendix of Frisch, 1983) assumed that $|\Delta v(L)|$ obeyed a *multiscaling law*, i.e. a scaling law with a non-linear $\zeta(h)$. They also introduced the notion of a multifractal spectrum to explain multiscaling. We shall come back in chapter five on this multifractal hypothesis.

On the other hand, Schertzer and Lovejoy (1984) suggested that the simple scaling $\Delta v(\lambda L) \stackrel{d}{=} \lambda^{1/3} \Delta v(L)$ holds ("$\stackrel{d}{=}$" denotes the equality in probability distribution), i.e. $<|\Delta v_l(L)|^n> = c_n L^{n/3}$, but that high order moments are spoiled by the statistical problem of divergence of moments. This interpretation is consistent with the possibility of an *unbroken scale symmetry* in a *non-universal* context. More precisely, they argued that for h large enough $<|\Delta v_l(\mathbf{L})|^h>$ diverges in the limit of infinite Reynolds number, which introduces a "spurious" scaling of $<|\Delta v_l(\mathbf{L})|^h>$ for h large enough, i.e. a scaling with $\zeta(h) \neq h/3$. If we try using their hypothesis together with the K41 theory (for simplicity), where the velocity structure function is given by $<|\Delta v_l(\mathbf{L})|^h> = (\varepsilon_0 L)^{h/3} F_h(\eta_0/L)$, their statement becomes

$$\text{As } x \to 0,\ F_h(x) \to \begin{cases} \text{constant} & \text{, if } 1 < h < \alpha_v \\ \infty & \text{, if } h > \alpha_v . \end{cases}$$

where $\alpha_v \approx 5$. From this point of view, the failure of simple scaling does not come from the direct influence of an outer scale L_0, but rather from the inner scale η_0. From the more general

standpoint of the refined theory, the prediction (2.2.3) could make room simultaneously for outer and inner scales dependence, which could jointly contribute to break simple scaling Resolving experimentally all these questions unambiguously is a difficult task. In chapter 7, we will return in an experimental study to some aspects of this controversy.

2.4 MODELLING OF THE ENERGY DISSIPATION FIELD

The refined theory remains incomplete because the velocity structure function cannot be predicted with (2.3.3) unless $<(\varepsilon(L))^h>$ is given. The need to predict the value of $<(\varepsilon(L))^h>$ as well that the search of a better understanding of the energy cascade process motivated researchers to invent several phenomenological models of the energy dissipation field. In this section three of these models are presented, starting with multiplicative processes. In these models the concept of self-similarity, implicit to the Richardson's phenomenology and the Kolmogorov theories, is used in different and non-equivalent ways. This diversity reflects the still controversial nature of the energy cascade process.

2.4.1 Multiplicative processes

According to (2.2.3), another obvious way of predicting multiscaling for $<|\Delta v_l(\delta)|^h>$ is to assume that $<(\varepsilon(\delta))^h>$ scales non-linearly with δ. This is one of the basic properties of multiplicative processes. In the early Yaglom's model (1966), we consider a set of cubic eddies of sizes $L_n = L_0/\lambda^n$ imbedded in each other and located on a regular grid. The energy dissipation $\varepsilon(L_{n+1})$ averaged over the volume of an eddy (i.e. a cube) of size L_{n+1} is assumed to be a random fraction of the energy dissipation averaged over the volume of the larger embedding eddy of size $L_n = \lambda L_{n+1}$ ($\lambda > 1$). In other terms $\varepsilon(L_{n+1}) = W\, \varepsilon(L_n)$, where W is a random multiplicative factor (see figure 2.3 and 2.4). The factors W are assumed to be statistically independent of each other at different scales and identically distributed. The choice of a scale invariant multiplicative factor W is the expression, in this model, of the concept of self-similarity. $\varepsilon(L_n)$ takes the form

$$\varepsilon(L_n) = W_1\, W_2 \ldots W_n\, \varepsilon_0, \qquad (2.4.1)$$

where ε_0 is the mean energy dissipation rate. In this model, the condition of conservation $<\varepsilon(L_n)> = \varepsilon_0$ implies that the random factors satisfy $<W> = 1$. More generally a discrete

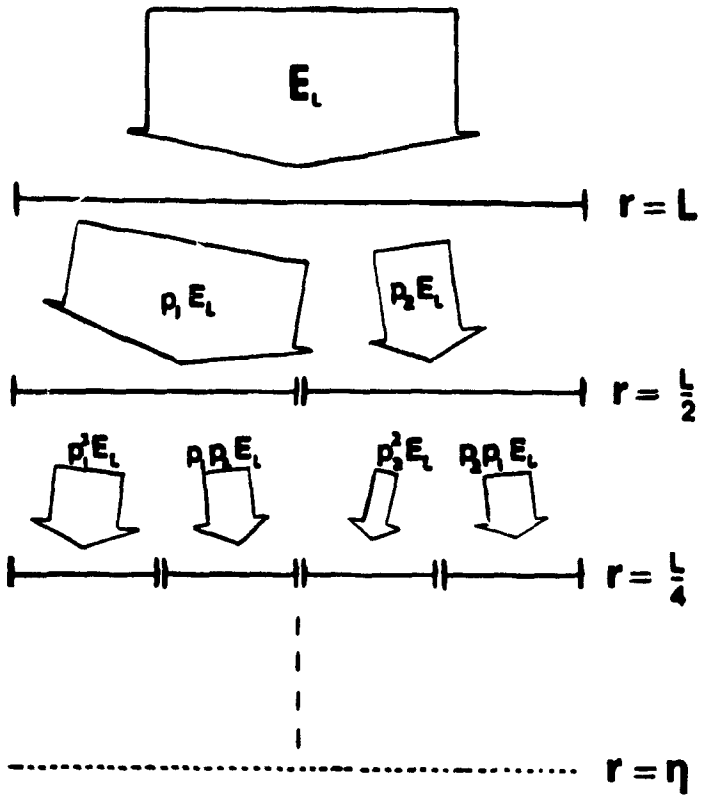

Figure. 2.3: One dimensional version of a cascade model of eddies, each mother eddy breaking down into 2 daughter eddies. The flux of kinetic energy to smaller scales is divided into different fractions p_1 and p_2. This cascade terminates when the eddies are of the size of the Kolmogorov scale, η (from Meneveau and Sreenivasan, 1987a).

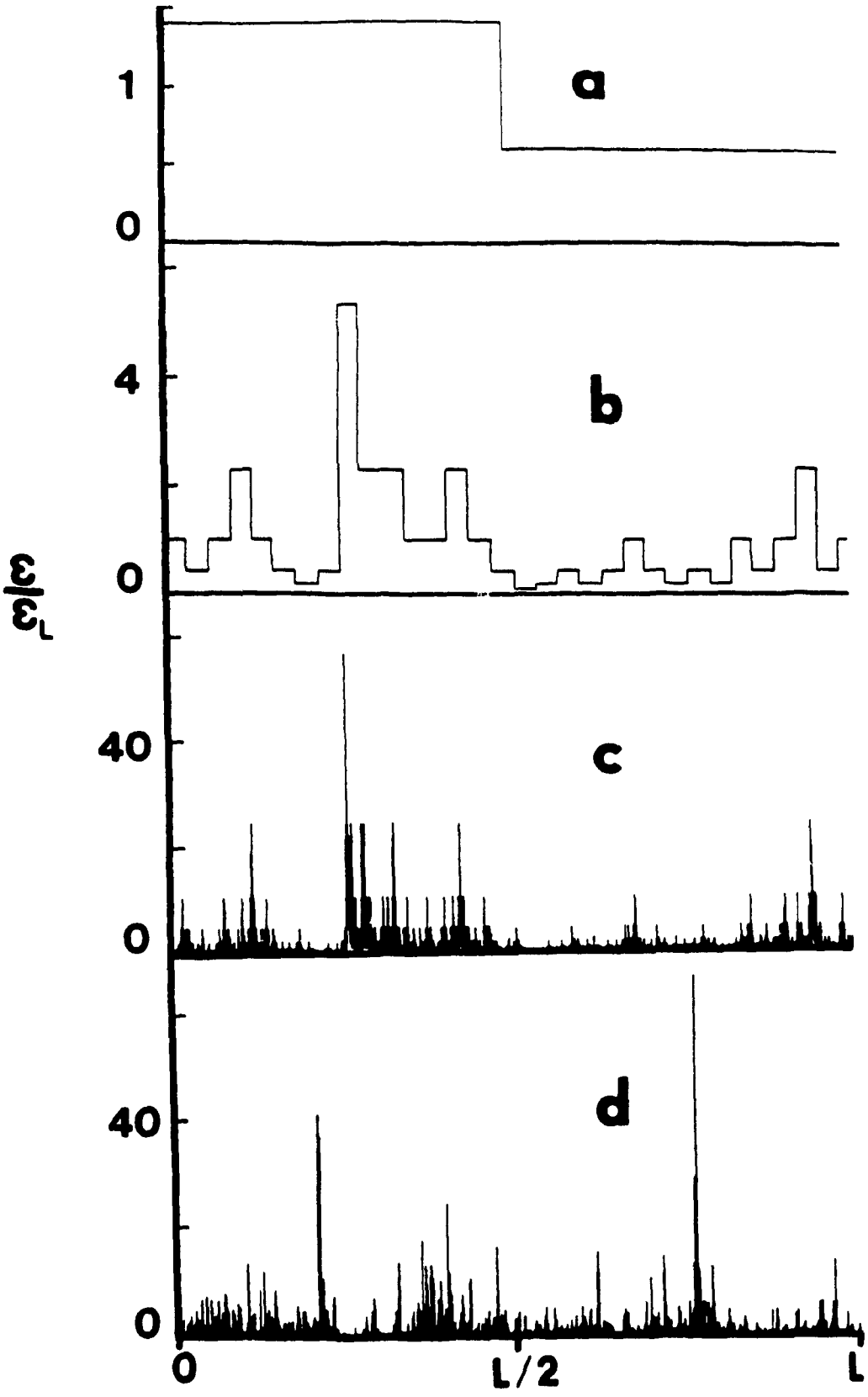

Figure 2.4: Different stages during the construction of the cascade model proposed in figure 2.3 (1st stage in a, 5th stage in b and 12th stage in c), and an experimental signal of ε in d (from Meneveau and Sreenivasan, 1987a)

sequence of random variables $\{X_n\}$ such that $X_{n+1} = W_n X_n$, where the multiplicative factors W_n are independent random variables identically distributed, will be called a *multiplicative process*. The independence of the W's in (2.4.1) leads to

$$< \varepsilon(L_n)^p > = <W^p>^n \varepsilon_0^p = (L_n/L_0)^{-K(p)} \varepsilon_0^p, \quad K(p) = \log_\lambda <W^p>. \qquad (2.4\ 2)$$

$< \varepsilon(L_n)^p >$ therefore depends on an outer scale L_0. This simple model has the virtue of producing a variance that increases with decreasing L_n, consistent with the measurements. It also predicts through (2.3.3) a power law dependence of the velocity structure function, i.e.

$$< (\Delta v(L))^h > \propto L^{h/3} (L/L_0)^{-K(h/3)}, \quad \zeta(h) = h/3 - K(h/3). \qquad (2.4.3)$$

The combination of the refined theory and of multiplicative processes therefore leads to multiscaling for $<(\Delta v(L))^h>$, as observed by Anselmet *et al.* (1984). This model also produces an irregular field $\varepsilon(\mathbf{x})$ in qualitative agreement with the observations of intermittency. Different kinds of multiplicative processes have been introduced by other authors, in particular Mandelbrot (1974) and Schertzer and Lovejoy (1987). Some of these models will be reexamined in chapter 5.

As pointed out by Kraichnan (1974), Yaglom's model is only one among a large class of scale invariant splitting models that can invented in the spirit of the Richardson's phenomenology. Kraichnan also claims that the eddy mitosis picture is made implausible by the physics of vortex stretching, which involves the stretching of thin vortex tubes rather than cubic eddies. Nevertheless, turbulent flows do have scaling properties and cascade models provide simple ways or generating fields with such properties. Various aspects of scaling fields can therefore be investigated through cascade models, and comparisons can be made with real geophysical fields. There is no need for the intermediate fields obtained during the construction of a multiplicative process to have a physical interpretation. It should also be noted that these

models can produce fields having different geometries because the scaling exponents K(h) do not characterize completely $\varepsilon(x)$.

2.4.2 The Frisch-Sulem-Nelkin β-model.

The β-model (Frisch, Sulem and Nelkin (1978)) is a simple conceptual model of intermittency. In the following it will be called the F.S.N. β-model in order to avoid confusion with the β-model discussed by Schertzer and Lovejoy (1985). The F.S.N. β-model is directly based on the "gusty" appearance of the high-passed velocity field, as observed by various experimenters. Frequency bands $[k_n, k_{n+1}]$ are defined, where $k_n = 1/L_n$ and $L_n = L_0/2^n$ If E(k) denotes the three dimensional energy spectrum, the energy E_n in the n^{th} band is defined by

$$E_n = \int_{k_n}^{k_{n+1}} E(k)\, dk \quad . \tag{2.4.4}$$

The velocity field in the n^{th} band is assumed to exhibit patches of activity of size L_n filling a fraction β_n of the space. A velocity scale v_n is defined by

$$E_n = \beta_n v_n^2 \ . \tag{2.4.5}$$

v_n is interpreted to be a velocity difference over a distance L_n in an active region. The time needed for an eddy of size L_n to transfer its energy to smaller scales eddies is the *turn-over time*, defined by

$$t_n = L_n / v_n \tag{2.4.6}$$

The energy flux from band to band is assumed to be constant and is therefore equal to the mean energy dissipation rate ε_0, from which follows that

$$\varepsilon_0 = E_n / t_n \quad . \tag{2.4.7}$$

Replacing (2.4.5) and (2.4.6) in (2.4.7) leads to

$$v_n = \beta_n^{-1/3} (\varepsilon_0 L_n)^{1/3} \quad . \tag{2.4.8}$$

The bursts of band n+1 are assumed to be nested in the larger scale bursts of band n in a self-similar way, so that $\beta_n = \beta^n$, where β is a real parameter. β can be expressed in terms of the fractal dimension d of the support of the active regions : $\beta = 2^{-C}$, where C = 3 - d (we will return in more details to the concept of dimension in chapter 4). Using $L_n = L_0/2^n$ yields $\beta_n = (L_n/L_0)^C$ and (2.4.8) then becomes

$$v_n = (\varepsilon_0 L_n)^{1/3} (L_n/L_0)^{-C/3} \tag{2.4.9}$$

Velocity structure functions are then given by

$$\langle v_n^h \rangle = \beta_n \; v_n^h = (\varepsilon_0 L_n)^{h/3} (L_n/L_0)^{C(1-h/3)} \tag{2.4.10}$$

and therefore

$$\zeta(h) = \tfrac{1}{3} (1-C)\, h + C,$$

i.e. $\zeta(h)$ is linear in h. (2.4.10) is a modified form of the Kolmogorov law $\langle (\Delta v(L))^h \rangle \propto L^{h/3}$ that takes into account the clustering of the dissipation field on a set of dimension d The power spectrum is obtained by replacing (2.4.9) in (2.4.5), which yields

$$E_n = (\varepsilon_0 L_n)^{2/3} (L_n/L_0)^{C/3}$$

and consequently

$$E(k_n) = \frac{E_n}{\Delta k_n} = L_n^2 E_n = \varepsilon_0^{2/3} k_n^{-5/3} (k_n/k_0)^{-C/3} \tag{2.4.11}$$

This model therefore predicts a correction to the $k^{-5/3}$ spectrum due to intermittency, i.e. the scaling exponent slightly exceeds 5/3 by C/3. There also exists a random version of this model

(Benzi *et al.*, 1984), where the fraction of space occupied by active eddies in the n^{th} band is not fixed to β^n, but rather takes the form $\beta_1 ... \beta_n$ where the β_i's are independent random variables with the same probability density. This random model leads in general to a nonlinear exponent $\zeta(h)$.

2.4.3 The Novikov "pulse-in-pulse" model

The Novikov (1966, 1990) model is based on the assumption that the energy dissipation field has a geometrically self-similar structure of nested "pulse-in-pulse" pattern. The energy dissipation field is constructed by centering pulse functions on each point of a set constructed as follows. Consider a system of random points x_{k_1} distributed by a Poisson law with mean density σ. We connect with each of the points x_{k_1} a system of points $x_{k_2} = x_{k_1} + \lambda_1 \theta_{k_1 l}$ ($l = 1, ..., m$), where $\theta_{k_1 l}$ are mutually independent random variables with the same probability distribution. This process is then repeated for each point according to the iteration rule

$$x_{k_{s+1}} = x_{k_s} + \lambda_s \theta_{k_s l} \quad (l = 1, ..., m), \tag{2.4.12}$$

where $\lambda_s = \lambda_1 \beta^{s-1}$ and $0 < \beta < m\beta < 1$. The geometrical similitude of this set is expressed in having the same number m and distribution law of the variables $\theta_{k_s l}$ for the same scale reduction coefficient β. We next define the stationary random function $\varepsilon_s(x)$, consisting of a sequence of pulse functions $I_s(x)$ centered on the points x_{k_s}:

$$\varepsilon_s(x) = \langle \varepsilon \rangle \alpha^{-1} (m\beta)^{1-s} \int I_s\left(\frac{x-x'}{\lambda_s}\right) \xi_s(x')\, dx' \tag{2.4.13}$$

where

$$\xi_s(x) = \sum_{k_s} \delta(x - x_{k_s}), \quad \langle \xi_s(x) \rangle = \sigma m^{s-1}$$

$$\alpha = \sigma\lambda_1, \quad \int I_s(\theta)\, d\theta = 1, \quad \langle \varepsilon_s(x) \rangle = \langle \varepsilon \rangle.$$

The function $\varepsilon_s(x)$ is interpreted as the energy dissipation field in a fully turbulent flow, and the limit $s \to \infty$ corresponds to the limit of infinite Reynolds number.

Novikov showed that the power spectrum of $\varepsilon_s(x)$ is of the form $k^{-1+\mu}\,\phi(\log(k))$, where $0 < \mu < 1$ and ϕ is a periodic function with period equal to $\ln\beta$ ($\mu = \log(m\beta)/\log\beta$) The period of the prefactor ϕ reveals the scale reduction coefficient of the set supporting $\varepsilon_s(x)$. Results reported by several experimenters (Monin and Yaglom, 1974, section 25.3) are consistent with a power spectrum of the form k^{-s}, $0 < s < 1$. Note that the power spectrum of the field generated by a discrete scale cascade model with a finite number of cascade steps is also proportional to k^{-s}, with $0 < s < 1$ (Monin and Yaglom, 1974, section 25.3). We shall return in chapter 8 to the Novikov model in a numerical study.

Chapter III

THE THIRD KOLMOGOROV HYPOTHESIS REVISITED

At present there is not enough solid knowledge about the Navier-Stokes equation to say with assurance that Kolmogorov's idea of multiple random cascade steps is qualitatively correct ( ) Even if the underlying idea of a multistage breakdown is correct, Kolmogorov's first and third hypothesis of 1962 do not necessarily follow

Robert H. Kraichnan (1974)

The modified Kolmogorov similarity hypotheses, by relating $<(\Delta v_l(L))^h>$ to $<(\varepsilon(L))^h>$, shifted the emphasis from velocity structure functions to the energy dissipation field. The third hypothesis is a statistical statement about the probability distribution of $\varepsilon(L)$ that gives a central role to lognormal distributions. This hypothesis differs qualitatively from the others, which are essentially scaling hypothesis. In geophysics the importance of these distributions has often been overestimated, and some misconceptions still persist in the field of turbulence. We propose in this chapter a critical review of the third Kolmogorov hypothesis.

3.1 THE THIRD KOLMOGOROV HYPOTHESIS OF LOGNORMALITY

Kolmogorov formulated a third hypothesis, according to which the volume-averaged energy dissipation rate $\varepsilon(L)$ is distributed according to a lognormal distribution (a random variable V is said to be lognormal with parameters μ and σ if $\log V = N(\mu,\sigma^2)$, where $N(\mu,\sigma^2)$ denotes a Gaussian random variable of mean μ and variance σ^2). This is assumed to hold for high-Reynolds-number flows when L lies in the inertial range. From a fundamental point of view, the third hypothesis is *a priori* interesting because it suggests the existence of universal probability distributions governing the dissipation field at small scale. In view of its theoretical importance, we shall examine the question of universality in the context of discrete multiplicative processes.

A plausible origin for the third hypothesis is found in the properties of the multiplicative processes associated with the eddy mitosis picture proposed by Richardson, as well that in the breakage processes studied earlier by Kolmogorov (1941b). For a multiplicative process $X_n = W_1 \ldots W_n$, the *central limit theorem* can be applied to $Z_n = \log X_n = \log W_1 + \ldots + \log W_n$. Provided that the mean $\mu = \langle \log W \rangle$ and the variance $\sigma^2 = \langle (\log W)^2 \rangle - \mu^2$ exist, then for every fixed β

$$\text{Prob}\{ \frac{\log X_n - n\,\mu}{\sqrt{n}\,\sigma} < \beta \} \rightarrow F_N(\beta) \qquad (3.1.1)$$

as $n \rightarrow \infty$, where $F_N(\beta)$ denotes the cumulative probability distribution of $N(0,1)$. Equivalently, $\log X_n$ tends as $n \rightarrow \infty$ to a Gaussian random variable $N(n\mu, n\sigma^2)$; in addition, X_n tends as $n \rightarrow \infty$ to the log-normal law $V_n = \log N(n\mu, n\sigma^2)$ (convergence of the integral probability distributions in both cases). Approximate log-normality therefore always holds for multiplicative processes.

It is not clear whether Kolmogorov meant the log-normal law to be exactly true, or simply approximate in the sense given above. A companion paper of Obukhov (1962) suggests the latter view. In any case the log-normality assumption has been taken literally by the experimenters (e.g. Anselmet, 1984), who used it in particular to compute $\langle (\varepsilon(L))^h \rangle$ and deduce with (2.4.3) the scaling exponents of $\langle (\Delta v(L))^h \rangle$, which in turn can be measured. We emphasize that the distinction between exact and approximate log-normality is crucial if one tries to estimate the moments. It is shown below that these are, in general, very far from the actual moments. Let us consider the order-q moments of the multiplicative process X_n. Using the independence of the multiplicative factors, we get

$$\langle (X_n)^q \rangle = \langle W^q \rangle^n = \exp\{ n \log \langle W^q \rangle \}. \qquad (3.1.2)$$

It follows that X_n does not approach a universal random variable as $n \rightarrow \infty$, because $\langle X_n^q \rangle$ and consequently the probability distribution of X_n is entirely determined by the non-universal

function $<W^q>$. On the other hand, X_n approaches as $n\to\infty$ a log-normal random variable $V_n = \log N(n\mu, n\sigma^2)$, and the q-order moments of V_n have the exact form

$$<V_n^q> = \exp\{ n q (\mu + \frac{1}{2} \sigma^2 q) \} \qquad (3.1.3)$$

(3.1.2) and (3.1.3) are in general different even as $n\to\infty$, unless the multiplicative factor W is exactly log-normal with $W = \log N(\mu,\sigma^2)$. It is emphasized that (3.1.2) and (3.1.3) do not converge to each other as $n\to\infty$. Indeed, their ratio

$$\frac{<X_n^q>}{<V_n^q>} = \exp\{ n [\log<W^q> - q (\mu + \frac{1}{2} \sigma^2 q)] \}$$

either diverges or goes to zero as $n\to\infty$. This difficulty with the log-normal approximation was noticed by Novikov (1970, 1990 and earlier references therein), Mandelbrot (1972, 1974), Kraichnan (1974).

3.2 WHY IS THE LOG-NORMAL APPROXIMATION UNTENABLE FOR MOMENTS CALCULATIONS ?

Consider the random variable

$$S_n = Y_1 + Y_2 + \ldots + Y_n, \qquad (3.2.1)$$

where the Y_i are identically distributed and independent random variables with $<Y> = 0$ and $\sigma^2 = \mathrm{Var}\{Y\} < \infty$. If Y satisfies a few additional constraints (see Appendix 3.1), Khinchin (1949) shows that for n large the probability density $G_n(s)$ of S_n is of the form

$$G_n(s) = g_n(s) + O(\frac{1}{n}) \qquad (3.2.2)$$

where

$$g_n(s) = \frac{1}{\sqrt{2\pi n}\,\sigma} \exp\{ - \frac{s^2}{2n\sigma^2} \},$$

i.e. $g_n(s)$ is the probability density of a Gaussian random variable $N(0,n\sigma^2)$. (3.2.2) holds under more restrictive conditions than the central limit theorem quoted in section 3.1, that requires only $<Y^2>$ to be finite. This form of the central limit theorem focuses on the probability density and shows explicitly that the Gaussian approximation holds only around the maximum of $G_n(s)$ in general. The error term is at most equal to C/n, where C is a constant, but can also vanish in the special case of exactly Gaussian increments Y_i. The error term is small for $(C/n)/g_n(s) << 1$ which implies

$$\frac{|s|}{\sigma} << \sqrt{n \log n} \ . \qquad (3.2.3)$$

The width of the range of validity of the Gaussian approximation therefore increases with increasing n.

According to the Gaussian approximation, for q even

$$<(N(0,n\sigma^2))^q> = \frac{2}{\sqrt{2\pi n}\,\sigma} \int_0^\infty \exp\{q\log s - \frac{s^2}{2n\sigma^2}\}\, ds$$

$$= (q-1)!!\ (\sqrt{n}\,\sigma)^q \qquad (3.2.4)$$

while $<(N(0,n\sigma^2))^q>$ vanishes for q odd. The main contribution of this integral comes from the range of values of x around the maximum of $\exp\{q\log s - s^2/(2n\sigma^2)\}$, which occurs in $s = \sigma\sqrt{nq}$. The order-q moment is therefore expected to be accurate provided that (3.2.3) holds, i.e. if $\sqrt{nq} << \sqrt{n\log n}$ which implies

$$q << \log n. \qquad (3.2.5)$$

Consequently the order-q moments of S_n obtained from the central limit theorem are not accurate if $q \geq \log n$. Conversely, $<S_n^q>$ is accurate as long that $n >> e^q$.

Next consider the central limit theorem applied to multiplicative processes. A multiplicative process X_n can always be associated to S_n with the change of variable

$$X_n = \exp(S_n) = e^{Y_1} \cdots e^{Y_n}. \qquad (3.2.6)$$

The multiplicative factors are $W_i = e^{Y_i}$. We can try to estimate $<X_n^q>$ using the Gaussian approximation for S_n, or equivalently using a log-normal distribution for X_n. This estimate is

$$<X_n^q> = <(e^{S_n})^q> = \frac{1}{\sqrt{2\pi n}\,\sigma} \int_{-\infty}^{+\infty} \exp\{sq - \frac{s^2}{2n\sigma^2}\}\, ds = \exp\{1/2\, n\sigma^2 q^2\} \qquad (3.2.7)$$

As previously this moment will be accurate if the maximum of the function $\exp\{sq - s^2/(2n\sigma^2)\}$ lies in the interval (3.2.3). This maximum occurs at $s = n\sigma^2 q$, and (3.2.3) yields $n\sigma q << \sqrt{n \log n}$ which implies

$$q << \frac{1}{\sigma}\sqrt{\frac{\log n}{n}}\,. \qquad (3.2.8)$$

Since that $\log(n)/n \to 0$ as $n \to \infty$, only the moments of order $q \approx 0$ are accurately estimated. Higher order moments depend on the distribution outside of the range of applicability of the central limit theorem (figure 3.1).

In summary, the width of the range of validity of the Gaussian approximation for S_n increases like $\sqrt{n \log n}$ while the main contributions to the moments of S_n and $\exp(S_n)$ come from $s = \sigma\sqrt{nq}$ and $s = n\sigma^2 q$ respectively. For n large enough, $<S_n^q>$ can always be calculated from the Gaussian approximation whereas none of the moments of $<|\exp(S_n)|^q>$ are accurate (except for the trivial case $q = 0$). Our explanation of this fact appears to be original and clarifies certain issues.

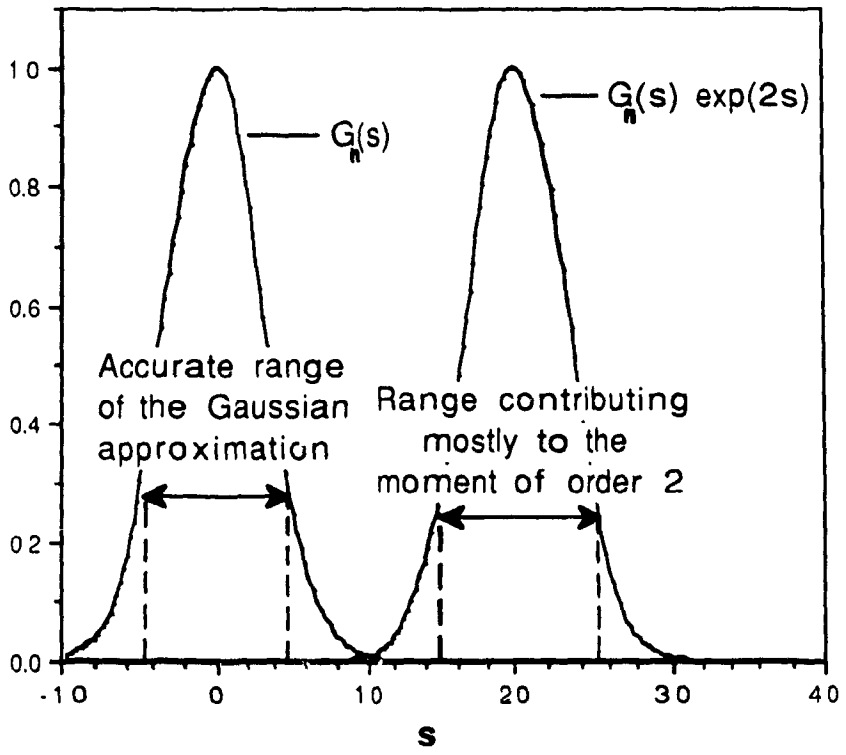

Figure 3.1: The density $g_n(s)$, with n=10 and σ=1, is plotted on the left side. The arrow indicates the range where $g_n(s)$ is expected to give a good approximation of the true distribution of S_n. On the right side is plotted $g_n(s)\, e^{2s}$ (normalized units were used in both cases). The arrow shows the range making the main contribution to $\langle (e^{S_n})^2 \rangle$. Both ranges do not even overlap and therefore $g_n(s)$ cannot be used to estimate $\langle (e^{S_n})^2 \rangle$ (see text).

What looked at first like a paradox is explained by the peculiar kind of convergence of the probability distribution of S_n to a Gaussian law. Although the integral (or cumulative) probability distributions of S_n and X_n approach the integral distributions of a gaussian and a log-normal law respectively (Novikov, 1990), the probability density of S_n is approximately Gaussian only around its maximum but remains in general non-Gaussian elsewhere (a property consistent with the name "central limit theorem"). In that sense, the convergence of the probability density is not uniform. This lack of normality away from the maximum of $G_n(s)$ has been known for a while (Novikov, 1990) and our explanation makes explicit its effect on the moments of S_n and X_n.

The implications of this discussion are important for several applications (economics, biology, particles decay, turbulence) where the use of log-normal distributions is justified by the existence of underlying multiplicative processes (Aitchison and Brown, 1976). In this context lognormal distributions are usually regarded as generic and various calculations, including moments, are made using an exactly lognormal probability density. We have shown that in general this choice is not justified.

The failure of the log-normal approximation for the estimation of $<X_n^q>$ raises the problem of finding a better approximation for the probability density of X_n. This approximate density should converge to the actual density and provide accurate estimates of $<X_n^q>$ in the limit $n \to \infty$. In the next section, we shall present a general method to compute probability distributions from the moments of a non-negative random variable Applied to multiplicative processes, this method will lead us to the general form of their probability distributions. While these distributions will be shown to be approximately log-normal around their maximum, they will produce valid estimates of the moments.

3.3 PROBABILITY DISTRIBUTIONS OF MULTIPLICATIVE PROCESSES IN THE LARGE N LIMIT

3.3.1 A general method to obtain the probability density from the moments of a non-negative random variable

It was shown that the moments of X_n are easily obtained by making use of the independence of the variables W (see (2.4.2)). It would therefore be convenient to have a systematic way to derive from $\langle X_n^q \rangle$ an expression for the probability density of X_n. Integral transforms can be used for that purpose, an interesting possibility that was noticed in particular by Fourcade and Tremblay (1987). For a random variable $0 \leq X \leq 1$, they show (using the change of variable $Y = -\log(X)$) that the moments $\langle X^q \rangle$ are related to the probability density $\rho(x)$ of X by $\langle X^q \rangle = L\{\rho(e^{-x})e^{-x}\}$, where L denotes the Laplace transform. $\rho(x)$ can therefore be obtained through the inverse transform of $\langle X^q \rangle$.

We generalize the method of Fourcade and Tremblay to any non-negative random variable by making use of the Mellin transform. The Mellin transform $F^*(z)$ of a function $F(x)$ are related by (see appendix 3.2 for a statement of the theorem)

$$F^*(z) = \int_0^\infty x^{z-1} F(x)\, dx \quad \text{and} \quad F(x) = \frac{1}{2\pi i} \int_{c-i\infty}^{c+i\infty} x^{-z} F^*(z)\, dz. \qquad (3.2.1)$$

It is obviously in a form related to the complex moments of order z - 1 of some non-negative random variable having F(x) as a probability density. It was shown in chapter 2 that multiplicative processes yield moments of the form

$$\langle X_n^q \rangle = e^{nK(q)}, \qquad (3.2.2)$$

where $K(q) = \log\langle W^q \rangle$. Using (3.2.1) a general expression for the probability density $\rho_n(x)$ of X_n is obtained:

$$\rho_n(x) = \frac{1}{2\pi i} \int_{c-i\infty}^{c+i\infty} x^{-z}\, e^{nK(z)}\, dz. \qquad (3.2.3)$$

We shall also consider the probability density $\gamma_n(\alpha)$ of the variable $\alpha_n = \log(X_n)/n$, which can be obtained from (3.2.3) with the corresponding change of variable:

$$\gamma_n(\alpha) = \frac{n}{2\pi i} \int_{c-i\infty}^{c+i\infty} e^{n(K(z) - \alpha z)}\, dz \qquad (3.2.4)$$

Asymptotic expansions of these integrals in the limit $n\to\infty$ can be obtained with the steepest descent method, but the integral (3.2.4) is more suitable because the prefactor of the exponential is not singular. In the next section the steepest descent method will be applied to (3.2.4) and asymptotic expressions of $\gamma_n(x)$ and $\rho_n(x)$ in the limit $n\to\infty$ will be obtained

Remark: In general, the integer moments do not determine the distribution (see Carleman's criterion in Feller, 1966). For example, Orszag (1970) showed that the lognormal distribution is not uniquely determined by its integer moments. We conclude that in general one must use integral transforms to solve the moment inversion problem.

3.3.2 Asymptotic expansions of the probability densities of X_n and $\log X_n/n$ for n large.

Equation (3.2.4) is in a form immediately suitable for the steepest descent method to be applied. This method applies to integrals in the complex plane of the form

$$I(n) = \int f(z)\, e^{n\phi(z)}\, dz. \qquad (3.2.5)$$

and yields an asymptotic expression of I(n) in the large n limit (see Bender and Orszag (1978), or Wong (1989)). Assuming that f(z) varies slowly with respect to $e^{n\phi(z)}$, that ϕ possesses a single stationary point z_0 such that $\phi'(z_0) = 0$, and provided that $\phi''(z_0) \neq 0$, I(n) takes as $n \to \infty$ the asymptotic form

$$I(n) = e^{n\phi(z_0)} \sqrt{\frac{2\pi}{nf''(z_0)}}\, e^{\pm i\pi/2} \{ f(z_0) + \frac{A(z_0)}{n} + O(\frac{1}{n}) \} \qquad (3.2.6)$$

where we use the factor $e^{i\pi/2}$ if $\phi''(z_0) > 0$ and the factor $e^{-i\pi/2}$ if $\phi''(z_0) < 0$. The term $A(z_0)/n$ is a higher order correction.

Using (3.2.6) with the integral (3.2.4), the stationary point is defined by $K'(z_0(\alpha)) = \alpha$. $z_0(\alpha)$ is unique because the function K(q), defined by (3.2.2), is convex (a theorem in probability theory (Feller, 1966) states that $\log\langle X_n^q \rangle$ is a convex function of q, i.e. $K''(q) \geq 0$). Note that for cascade processes the condition $\langle W \rangle = 1$ implies that $K(1) = 0$, and trivially $K(0) = 0$, therefore K posseses a unique minimum in the interval $]0,1[$. For n large, the expansion (3.2.6) yields

$$\gamma_n(\alpha) = \sqrt{\frac{n}{2\pi K''(z_0(\alpha))}}\, e^{-nf(\alpha)} \{1 + \frac{A(z_0(\alpha))}{n} + O(\frac{1}{n}) \} \qquad (3.2.7)$$

where

$$f(\alpha) = \alpha\, z_0(\alpha) - K(z_0(\alpha)) = \max_h \{\alpha h - K(h)\} \qquad (3.2.8)$$

$f(\alpha)$ is the Legendre transform of K(h) (Arnold, 1974), denoted by $f(\alpha) = L\{K(h)\}$. The Legendre transform satisfies $L^2 = 1$ and consequently

$$K(h) = \max_\alpha \{ h\, \alpha - f(\alpha) \}. \qquad (3.2.9)$$

$f(\alpha)$ characterizes the probability density of the multiplicative process. It follows from the definition (3.2.8) that

$$f''(\alpha) = 1/K''[z_0(\alpha)] \geq 0, \qquad (3.2.10)$$

and the unique minimum of f occurs in $\alpha_* = K'(0)$ where $f(\alpha_*) = -K(0) = 0$. Using (3.2.10), (3.2.7) becomes

$$\gamma_n(\alpha) = \sqrt{\frac{nf''(\alpha)}{2\pi}}\, e^{-nf(\alpha)} \{ 1 + \frac{A(z_0(\alpha))}{n} + O(\frac{1}{n}) \}, \qquad (3.2.11)$$

a form that depends only on $f(\alpha)$. Since that $\rho_n(x) = \frac{\gamma_n(\alpha)}{nx}$, for n large we also get

$$\rho_n(x) = \frac{1}{x}\sqrt{\frac{f''(\log(x)/n)}{2\pi n}}\, e^{-n\, f(\log(x)/n)}\ \left(1 + \frac{A(z_0(\log(x)/n))}{n} + O(\frac{1}{n})\right) \qquad (3.2.12)$$

The only "universal" features in the expression of $\gamma_n(\alpha)$ are the exponential dependence on n and the $\sqrt{n}$ prefactor. For a multiplicative process X_n, (3.2.11) and (3.2.12) will be shown to be effective asymptotic expansions of the probability densities of $\log(X_n)/n$ and X_n respectively.

By contrast with the log-normal approximation, the correct moments of X_n are recovered if the approximation (3.2.12) is used. The following expression of $\langle X_n^q \rangle$ is obtained from (3.2.11):

$$\langle X_n^q \rangle = \langle e^{n\alpha q} \rangle = \sqrt{\frac{n}{2\pi}} \int \sqrt{f''(\alpha)}\, e^{n(\alpha q - f(\alpha))}\, d\alpha\ .$$

For n large Laplace's method can be used to obtain an asymptotic expansion of this integral (see Bender and Orszag, 1978). The main contribution comes from the value of α that maximizes $\alpha q - f(\alpha)$, i.e. from $\alpha_0(q)$ defined by $f'(\alpha_0(q)) = q$. Therefore

$$\langle X_n^q \rangle \sim \sqrt{\frac{n}{2\pi}}\, \sqrt{f''(\alpha_0(q))}\, e^{n \max_\alpha \{\alpha q - f(\alpha)\}} \sqrt{\frac{2\pi}{n\, f''(\alpha_0(q))}}$$

$$= e^{n\, \mathrm{Max}_\alpha \{\alpha q - f(\alpha)\}} = e^{n\, K(h)},$$

which is indeed the exact form of $\langle X_n^q \rangle$.

Clearly the functional form (3.2.11) is not Gaussian while (3.2.12) is not a log-normal probability density. However, it can be checked that $\gamma_n(\alpha)$ is approximately Gaussian about the value $\alpha = \alpha_*$, which is the point where $\gamma_n(\alpha)$ is maximum for n large. This is done by expanding $f(\alpha)$ in Taylor series (2 terms) about $\alpha = \alpha_*$, which yields a mean $\mu = \langle \log W \rangle$

and a variance $\sigma^2 = n\ \mathrm{Var}(\log W)$. In the neighborhood of $\alpha = \alpha_*$ the probability density of $\rho_n(x)$ is therefore approximately lognormal, as expected.

3.3.3 Implications for the third Kolmogorov hypothesis

From the standpoint of breakage processes, the third Kolmogorov hypothesis holds in the sense that $\rho_n(x)$ is approximately lognormal around its maximum as $n \to \infty$, but in general $\rho_n(x)$ converges uniformly to a probability density that is not log-normal (see (3.2.12)). The above discussion also implies that the use of an exactly log-normal distribution for the calculation of $\langle(\varepsilon(\delta))^h\rangle$ finds no support in breakage processes.

A weaker version of the third hypothesis, avoiding this problem of approximate lognormality, could be based on the moments of the volume-averaged energy dissipation rate $\varepsilon(\delta)$. For example one could assume that

$$\frac{\log\langle(\varepsilon(\delta))^q\rangle}{\log\delta} \sim -K(h)$$

as $\delta \to 0$, where K is an unknown function. Equivalently, the third hypothesis could be based on the probability density $\rho(\gamma,\delta)$ of $\gamma(\delta) = -\frac{\log(\varepsilon(\delta))}{\log\delta}$, i.e.

$$\frac{\log\rho(\gamma,\delta)}{\log\delta} \sim C(\gamma)$$

as $\delta \to 0$, where $C(\gamma)$ is an unknown function. K and C are then related by

$$K(h) = \max_\gamma\{\gamma h - C(\gamma)\} \iff C(\gamma) = \max_h\{h\gamma - K(h)\} \qquad (3.3.1)$$

High Reynolds number turbulence could make room for universal functions $K(h)$ and $C(\gamma)$, but their analytical form cannot be derived in the context of Yaglom's type discrete multiplicative processes only. This weaker version of the third hypothesis basically states that moments and distributions scale and that the exponents are related by a Legendre transform. This form of the

third hypothesis is also the essential part of the *multifractal formalism*, in which $C(\gamma)$ is often interpreted as a *codimension*. We shall return to this interpretation in chapter 5.

Another weaker version of the third hypothesis is to assume that the moments of $\log(\varepsilon(\delta))$ can be determined from the gaussian approximation, as suggested by the above considerations. We will return to this second form of the 3rd hypothesis in an experimental study in chapter 7

Chapter IV

FRACTAL SETS: CONCEPTS, METHODS AND GENERAL RESULTS

Turbulence in fluids raises a variety of interesting and practically important problems of geometry, which have not, so far, received the full attention they deserve. The geometry of stochastic processes (much influenced, through N. Wiener, by Perrin's (1913) work on Brownian motion and G. I. Taylor's early papers on turbulence) has grasped fully the peculiar and "pathological" shapes of randomly generated lines, and either borrowed or developed analytic and geometric tools to describe this kind of irregularity. But geometry (in contrast to analysis) has hardly at all been applied to the specific random surfaces of turbulence. This failure is particularly surprising because turbulent shapes are readily visualized and therefore almost cry out for proper geometrical description.

Benoit B. Mandelbrot (1975)

In this chapter, we provide a comprehensive and turbulence-oriented synthesis of the characterization methods appropriate for fractal sets. In section 4.1 an introduction to the concepts of fractal field and fractal set is given and their use in the context of geophysics is motivated. Section 4.2 deals with the concept of fractal dimension and a fairly complete treatment of self-similar sets is presented. Efforts have been made to insert both self-similar sets and self-similar measures (introduced later in chapter 5) in a common mathematical framework based on scale renormalization.

4.1 VARIABILITY IN GEOPHYSICS - THE CONCEPT OF FRACTAL

4.1.1 Fractal fields

In geophysics one often encounters fields that involve structure over a wide range of spatial and temporal scales. Rain fields, for example, exhibit spatial structure over roughly nine orders of magnitude (about 1 mm for the raindrop diameter to 1000 km in the horizontal). The same complexity is observed in the velocity field in the planetary boundary layer: At low altitudes a temporal sampling rate as high as 20 kHz may be necessary if a smooth picture of the turbulent velocity signal is to be obtained. Figure 4.1 provides a sequential zoom in one such velocity signal and illustrates the intrinsic irregularity of a turbulent field.

Figure 4.1 : Zoom in one velocity signal measured in the atmospheric surface layer with a hot-film anemometer. In the next 3 pages are found six figures that exhibit graphs of the longitudinal velocity plotted as a function of time. The same string of data is shown successively in the ranges 0 - 20 sec, 0 - 10 sec, 0 - 5 sec, 0 - 2.5 sec, 0 -1sec and 0 - 0.5 sec. The approach of the Kolmogorov inner scale beyond which the signal is smooth can be felt clearly in the last screens.

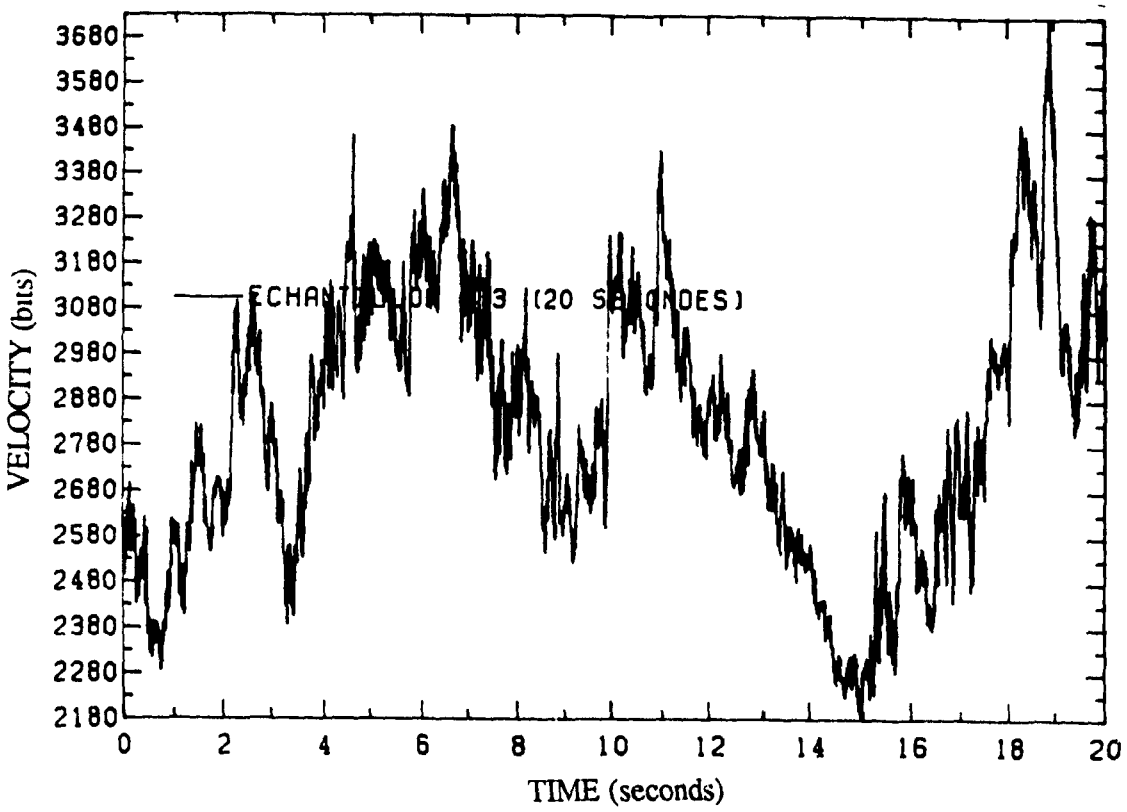
VELOCITY (bits)
3680
3580
3480
3380
3280
3180
3080
2980
2880
2780
2680
2580
2480
2380
2280
2180
0
2
4
6
8
10
12
14
16
18
20
TIME (seconds)

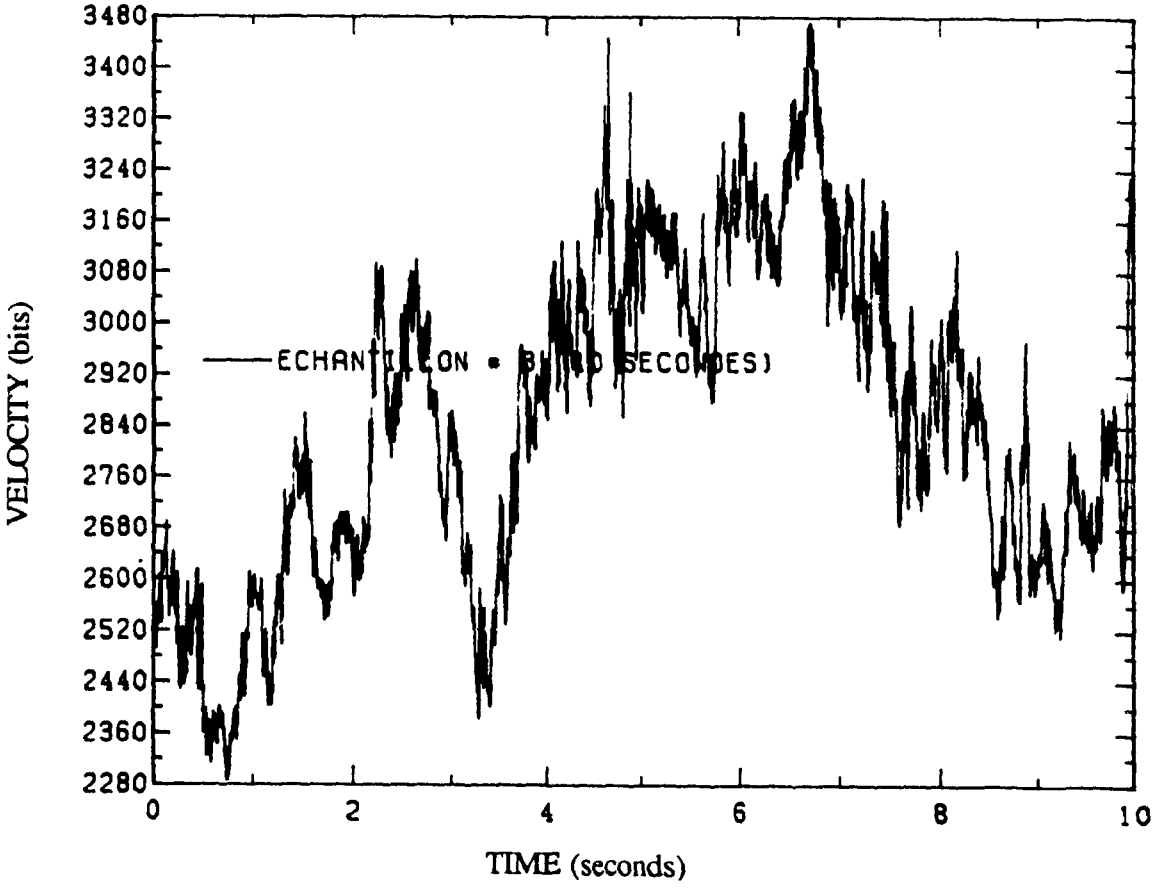
VELOCITY (bits)
3480
3400
3320
3240
3160
3080
3000
2920
2840
2760
2680
2600
2520
2440
2360
2280
0
2
4
6
8
10
TIME (seconds)

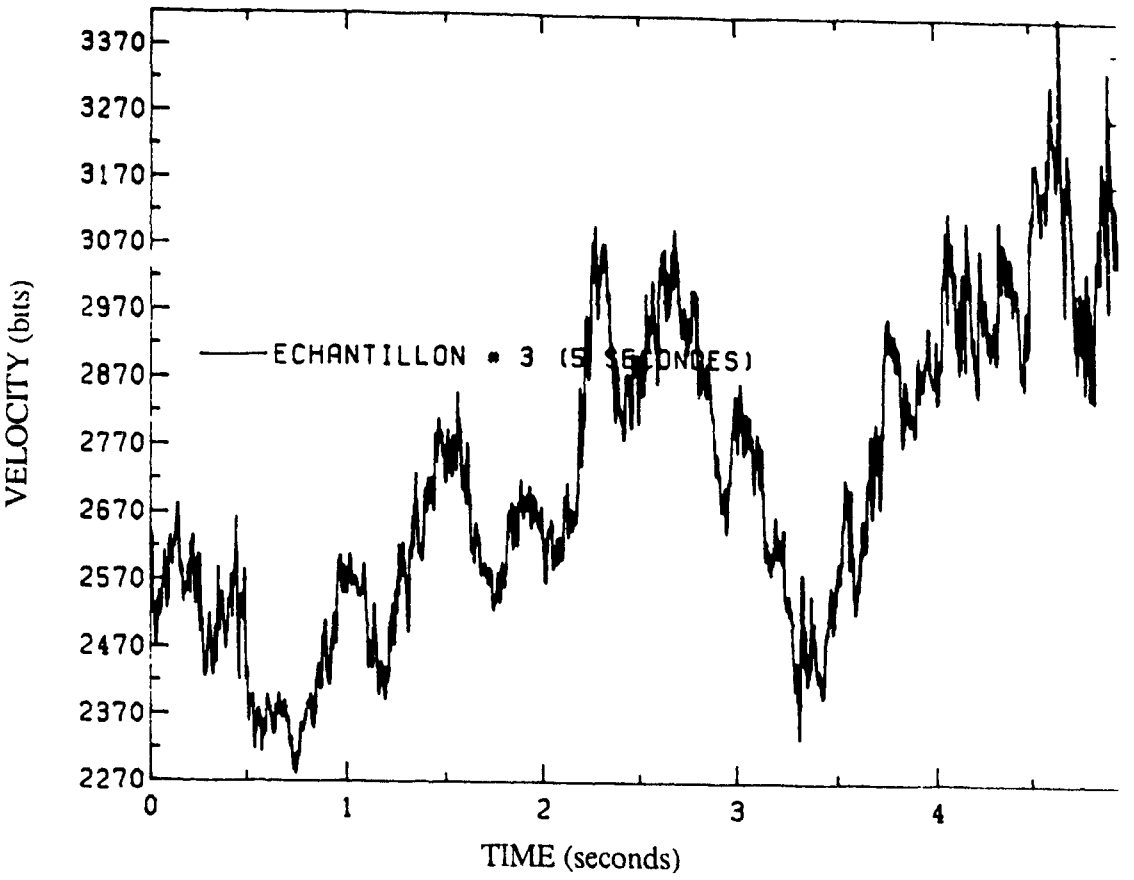
3370
3270
3170
3070
2970
2870
2770
2670
2570
2470
2370
2270
VELOCITY (bits)
ECHANTILLON # 3 (5 SECONDES)
0
1
2
3
4
TIME (seconds)

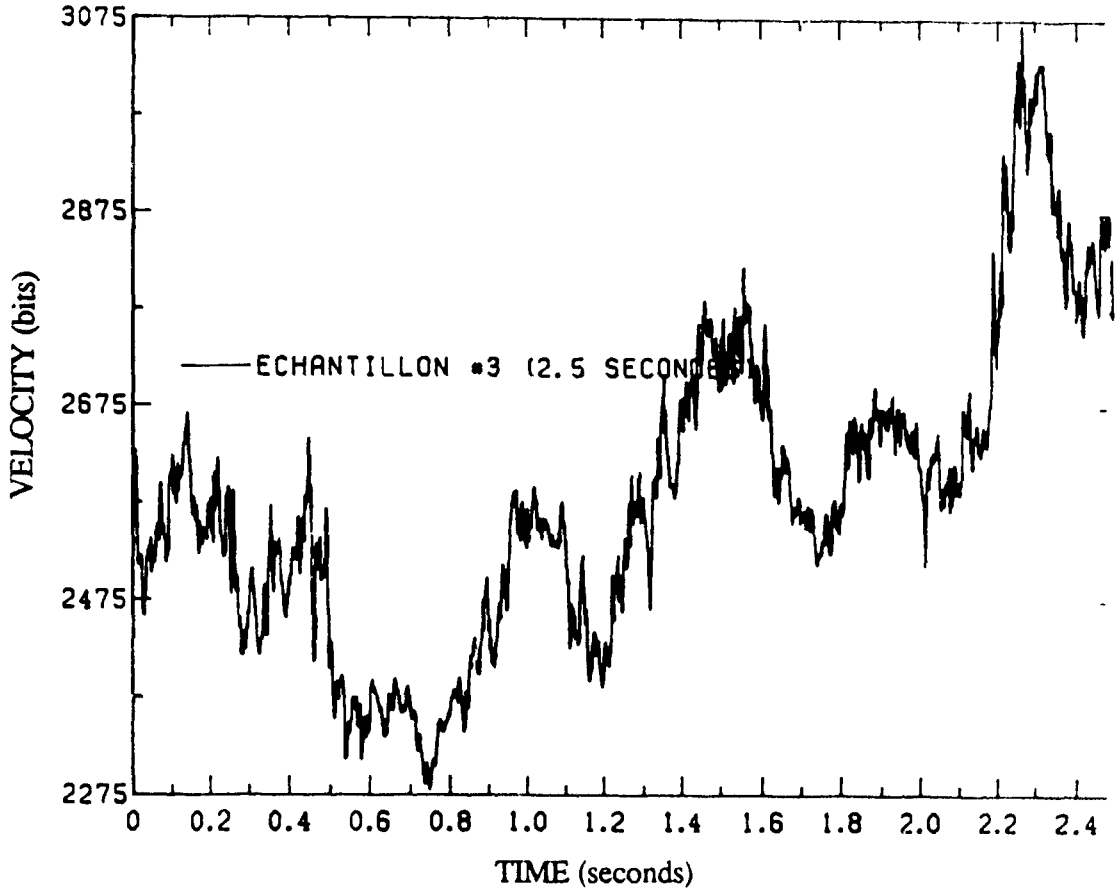
3075
2875
2675
2475
2275
VELOCITY (bits)
ECHANTILLON #3 (2.5 SECONDES)
0
0.2
0.4
0.6
0.8
1.0
1.2
1.4
1.6
1.8
2.0
2.2
2.4
TIME (seconds)

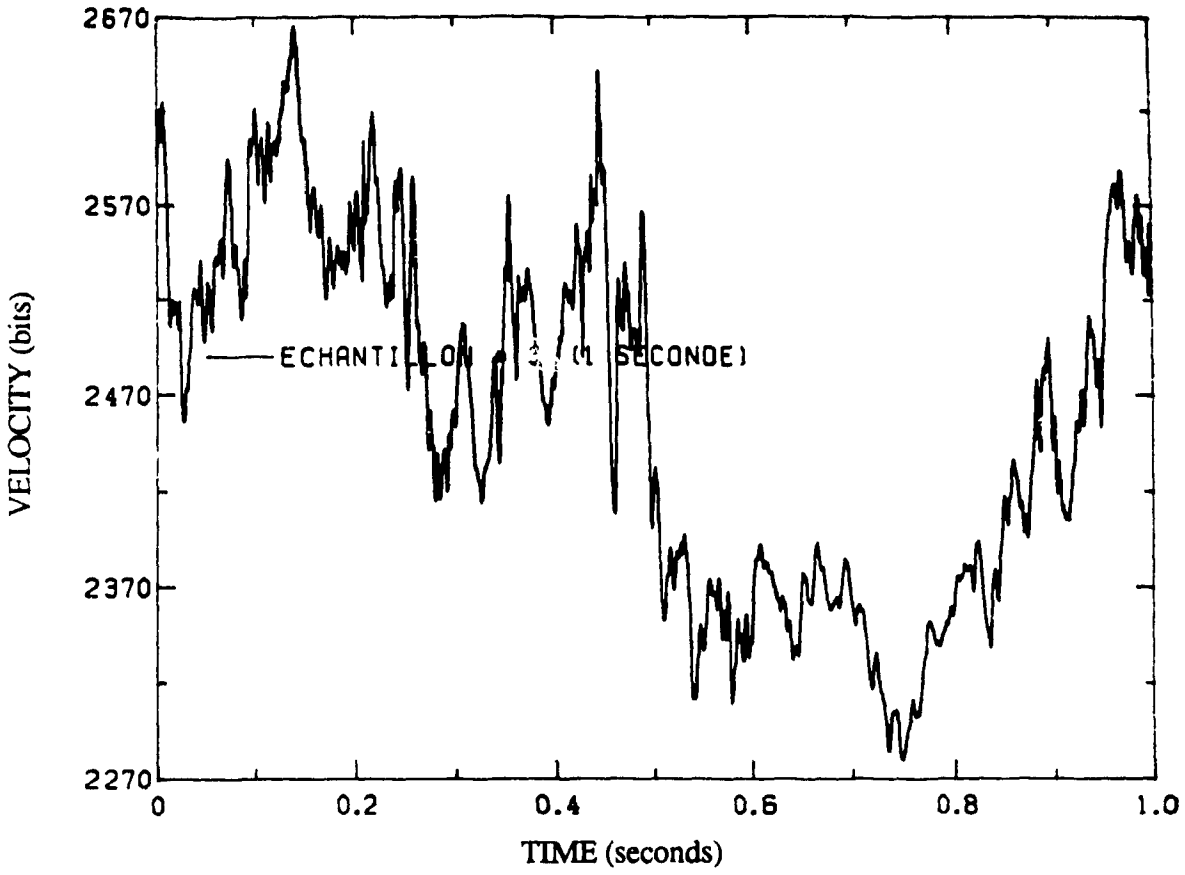
2670
2570
2470
2370
2270
VELOCITY (bits)
0
0.2
0.4
0.6
0.8
1.0
TIME (seconds)

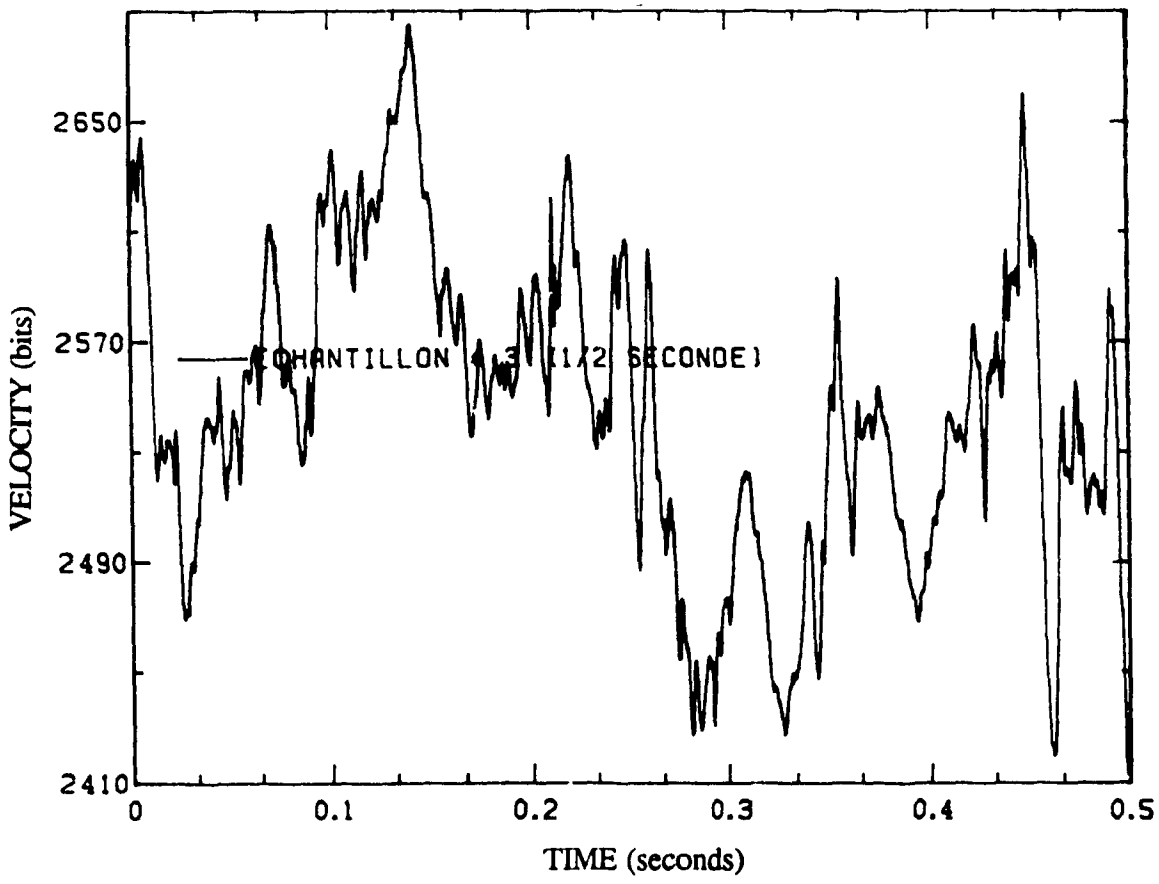
2650
2570
2490
2410
VELOCITY (bits)
0
0.1
0.2
0.3
0.4
0.5
TIME (seconds)

In practice however, geophysical measurements rarely resolve the natural *homogeneity scales* (or *inner scales*) beyond which the field is smooth. Remotely sensed data, e g. radar reflectivity or satellite pictures are the result of an averaging over volumes, areas or intervals much larger than the natural homogeneity scales. This resolution limit introduces unavoidable

biases in the measurements. Indeed, the statistical properties of measured fields are in general resolution-dependent. There is therefore a need for some scheme that would allow representations of the field at different resolutions to be related in some way

A field that is irregular and textured over several orders of magnitude of spatial or temporal scales appears to be *fractal* , i.e. a continued zoom always keeps revealing new structure and irregularities. If the range of irregularity scales is wide enough, some properties of the field at resolutions $L >> \eta$ (η is the inner scale) may be independent or only weakly sensitive to η In such cases it becomes convenient to ignore the inner scale. This is the content of the second hypothesis of the Kolmogorov 1941 theory, for which $\langle[\Delta v(L)]^2\rangle = C\ (\varepsilon L)^{2/3}$ is argued to become independent of η if $L >> \eta$ (see chapter 2). Another example is given by Brownian motion: The position x(t) of a particle in Brownian motion satisfies $\langle\{x(t+\tau)-x(t)\}^2\rangle = C'\ \tau$ if $\tau >> t_0$, where t_0 is the mean free time.

From this perspective certain fields may be regarded and modeled as *fractal fields*, i e fields that never become smooth under magnification. The term smooth is used here in the sense of differentiable: A "smooth" curve can be locally approximated by a straight line, while a smooth surface can be locally represented by a plane. By contrast, a fractal field is described by *non differentiable* functions. A fractal model of a geophysical field therefore shares some properties with the actual field in the appropriate range of scales but is more irregular at small scales It is also simpler because of the lack of an inner scale. An analogy with singular functions can be made: The Dirac distribution is singular and yet simpler to manipulate than the regular functions which it is used to approximate.

Our definition of fractal field is more general than other more common definitions (e g self-similarity, a special case examined in the next section), so general in fact that a wide family of geophysical fields appears to be fractal. The titles of the two books *The fractal geometry of Nature* (Mandelbrot, 1983) and *Fractals everywhere* (Barnsley, 1988) testify to the apparent ubiquity of fractals. Fractal fields are especially suitable for the description of rain fields, cloud fields, wind fields and various other geophysical fields. The scaling models currently used in the study of turbulence usually involve fractal fields.

Once the fractal character of a geophysical field has been recognized, the next step is to try to classify these fields and to develop tests allowing different classes to be distinguished. We hope this process will lead us to determine more precisely to which class actual flows actually belong. Fractal fields and fractal sets are closely related and an understanding of both is required for our study of turbulent flows. We shall now expose briefly the concept of fractal set.

4.1.2 Fractal sets and self-similar fractals

Even though various tentative definitions of fractal sets have been proposed, they still have not received a rigorous mathematical definition (Mandelbrot (1983), pp. 361). Avoiding at this point more technical definitions, we shall only say that fractal sets are *non-euclidian* sets. They are not straight lines, circles or triangles, nor are they cones or smooth surfaces, and they cannot be approximated by pieces of such sets. Fractal sets are irregular and their characteristic property is to have *structure on all scales*. Such sets arise naturally in geophysics; shapes like coastlines, mountains and vegetation are often viewed as fractal sets. Since the graph of a fractal field is a fractal set, there is an intimate link between fractal fields and fractal sets.

The simplest fractal sets are those which posses symmetry. In that spirit, Mandelbrot (1983) introduces the notion of self-similar sets as the simplest examples of fractal sets. Self-similar

sets are to fractal geometry what straight lines and points are to euclidian geometry A simple and often quoted example is the von Koch curve, obtained recursively by replacing each linear segment by four new segments that are shorter than the mother segment by a factor 1/3, beginning with the unit interval (figure 4 2). Being irregular on all scales, the limiting set is clearly fractal (the limiting set obtained after an infinite number of iterations can be shown to exist and to be closed and bounded (see Barnsley 1988)) This is an example of an *exactly self-similar* set. Indeed, each segment of this curve is an identical copy of the whole curve scaled down by a factor 1/3 (along with a rotation and a translation). The von Koch construction can be generalized to M-piece fractal curves by replacing each linear segment by M new segments that are shorter than the mother segment by a factor r at each stage

More generally if a set can be broken down in a sequence of disjoint or "just-touching" copies of itself scaled down by various different ratios, the set will be said to be *multiscale self-similar*. Exact self-similarity is then a special case of multiscale self-similarity with a single scaling ratio. If different length scales are used for each segment in the construction of the M-piece von Koch curve, a multiscale self-similar von Koch curve is obtained

It is worth stressing that self-similarity and fractality are treated here as distinct and independent concepts. For example, the interval [0,1] is obviously exactly self-similar (i e composed of a union of scaled-down copies of itself) but is not fractal. In general, fractal sets need not be self-similar. By contrast, some authors have proposed a definition based on self-similarity (e.g. see Feder (1988), p.11 or Devaney (1986), p.37).

A fractal is a set which is self-similar under magnification.

This statement, as well that our definition of fractal set avoid the problem of the mathematical characterization of fractal sets. Nevertheless, most authors retain the intuitive idea of structure on all scales.

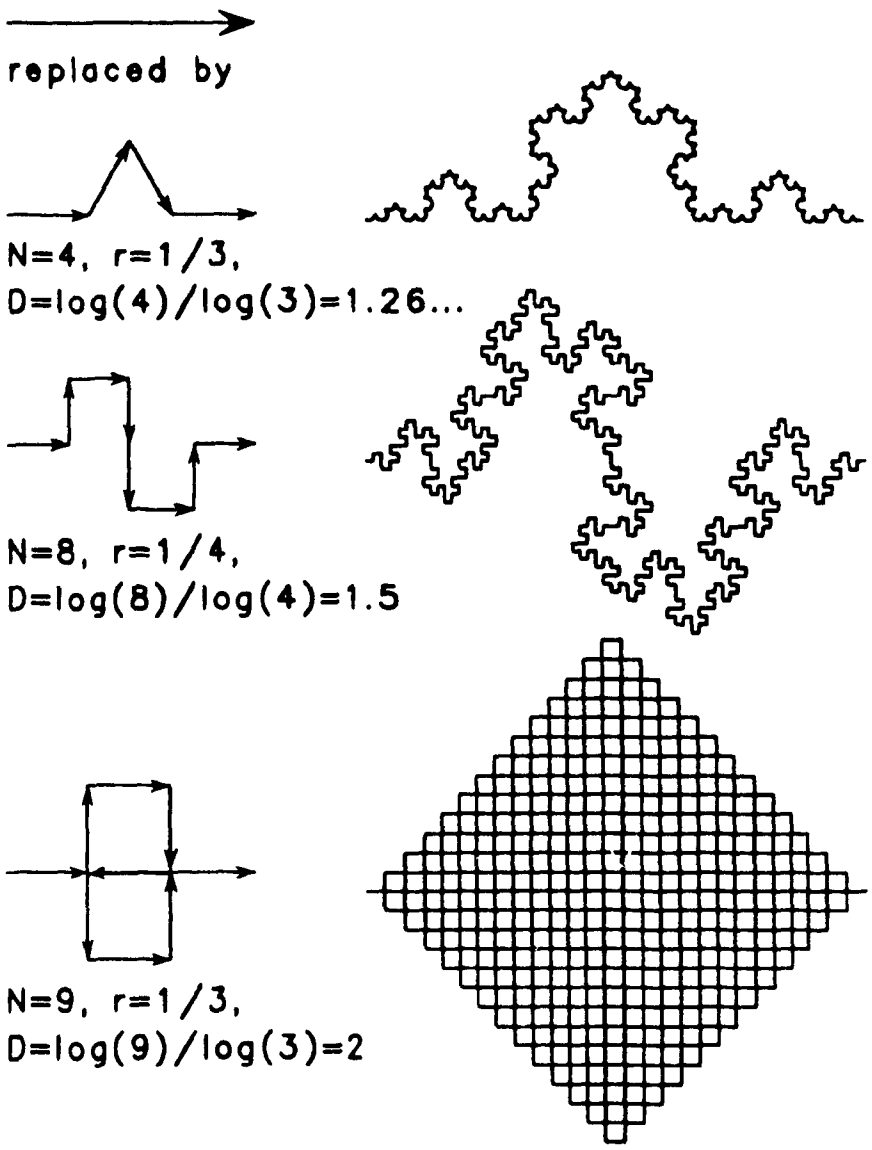

Figure 4.2 : Three examples of von Koch curve (from Peitgen 1988). In each case the number of sub-segments N and the ratio r is given, as well as the corresponding similarity dimension. The first example (on top) is the von Koch curve (or snowflake). The other curves are examples of generalized von Koch curves.

The reasons for emphasizing self-similarity and scaling in this thesis are threefold. Firstly, symptoms of scaling have been observed in turbulent flows (e g. Anselmet (1984), Meneveau and Sreenivasan (1987bc)) and in the atmosphere with remotely sensed data, such as radar reflectivities and satellite pictures (Schertzer and Lovejoy (1987, 1989)). Secondly, the scaling assumption can be argued to be a "first-order" simplification of the problem of fractal fields modelling. As discussed by Mandelbrot (1983, p. 19), " One must rather marvel that these first approximations are so strikingly reasonable ". Such an *a priori* simplifying modelling hypothesis should therefore be considered first. A similar point of view is defended by Schertzer and Lovejoy (1989), who claim that the " (scale) symmetry assumption is not only the simplest but also the only assumption acceptable in the absence of more information or knowledge ". Thirdly, it can be argued that a physical process involving no characteristic scale is likely to exhibit scaling. This is what happens for example in the Kolmogorov 1941 theory, where the velocity statistics becomes independent of viscosity and outer scales in the limit of infinite Reynolds number. In a wider context, scaling may also be obtained over other scale ranges in the atmosphere where other mechanisms rule the dynamics.

Very few general results are available on the topic of non self-similar fractals. One of the goal of the research in this area is to discover some kind of "multiscale fractal transform" that would go beyond the Fourier transform, currently the basis of almost all the techniques in signal analysis.

4.2 FRACTAL DIMENSIONS AS IRREGULARITY INDICES FOR SETS

4.2.1 Is there a general definition of fractal dimension ?

Fractal dimensions are *irregularity indices* for sets. Various different definitions of dimension exist, each being sensitive to various aspects of the "wiggliness" or "fatness" of the set. One of the goals of fractal geometry is to give a precise and objective mathematical meaning to the often ambiguous, although sometimes poetic, qualifiers used to describe complex textures. Dimensions are numbers that allow the comparison of different fractal sets and indicate their capacity to fill space. They do not provide by any means a complete characterization of a set. In contrast with topological dimension, the definition of fractal dimension always involves the notion of a metric, i.e. of distance (Mandelbrot, 1983).

The term dimension is sometimes used fairly loosely in the literature, usually in the vague sense of a scaling exponent d in some power law expression. In this thesis, we shall require that in order for a quantity d to qualify as a fractal dimension, it should

i) apply to sets.

ii) be a real number that satisfies $0 \leq d \leq D$, where D is the topological dimension of the Euclidian space $\mathbb{R}^D$ in which the set is imbedded.

iii) reduce to the topological dimension for simple Euclidian sets (points, lines, planes, volumes, circles, triangles etc...).

iv) satisfy $d(S) \leq d(S')$ if $S' \supset S$

Tricot (1973) also proposed the condition

v) For any countable and possibly infinite union of sets S_i

$$d(\bigcup_i S_i) = \sup_i \{ d(S_i) \},$$

where the sup denotes the supremum, i.e. least upper bound, of all the dimensions of the individual sets.

4.2.2 Similarity dimension for exactly self-similar sets

Similarity dimension arises naturally in the context of exactly self-similar fractal sets, such as the M-piece von Koch curve introduced above and is probably the simplest example of a fractal dimension. The similarity dimension can be introduced using an analogy with the topological dimension: In one dimension, a unit interval can be split into $M = 1/r$ subintervals of length r, in two dimensions, a unit square splits into $M = (1/r)^2$ subsquares of size r; in 3 dimensions, a unit cube splits into $M = (1/r)^3$ subcubes of size r. Similarly, the M-piece von Koch curve splits up into M identical smaller von Koch curves of size r. One may define by extension the similarity dimension to be the exponent d_S such that $M = (1/r)^{d_S}$, i.e.

$$d_S = \frac{\log M}{\log(1/r)} . \qquad (4.2.1)$$

Similarity dimension is in general non-integer and can be regarded as a natural generalization of the topological dimension for exactly self-similar sets. For simple euclidian sets d_S reduces to the topological dimension.

Another important example of an exactly self-similar set is the triadic *Cantor set* obtained by repeatedly removing middle third open intervals beginning with [0,1], as illustrated in figure 4.3. The similarity dimension of this set is

$$d_S = \frac{\log 2}{\log 3} \approx 0.6309 .$$

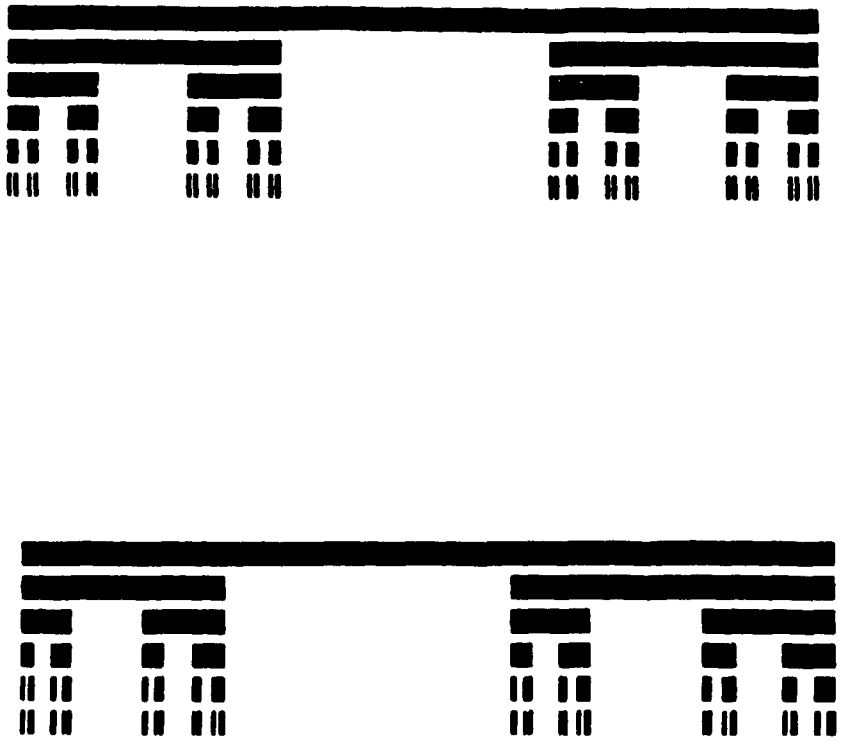

Figure 4.3 : Two examples of Cantor sets. The first one (on top) is the classical triadic Cantor set, formed by removing open middle thirds of intervals recursively. The second case is an example of multiscale Cantor set. At each step of construction, only closed segments scaled down by ratios 1/4 and 1/2 survive.

The *M-piece Cantor set* can be defined by analogy with the M-piece von Koch curves: At each iteration the surviving intervals of size L are replaced by M disjoint intervals of size rL. The similarity dimension is then given by (4.2.1). If the surviving disjoint intervals are chosen to have different length r_iL, a multiscale self-similar set called the *multiscale Cantor set* is obtained.

These sets can be directly generalized to higher dimensions by replacing the initial unit interval by a square or a cube, which does not affect the definition of d_S. Notice that d_S is not sensitive to the orientations of sub-segments in the M-piece von Koch curve, nor to the position or the surviving sub-segments at each stage of construction of the M-piece Cantor set. Many different fractal sets therefore share the same similarity dimension, a clear indication that they are only partially characterized by d_S.

It should be noted that the *splitting factor M* and the *scale ratio r* of an exactly self-similar set are not uniquely determined by d_S since sets with parameters (M,r) and (M^n,r^n) have the same dimension. This issue will be reexamined in section 4 2.3.2.

d_S is not defined for general sets since these cannot be split up into M copies. More flexible definitions are therefore needed to characterize sets.

4.2.3 Box dimension and self-similar sets

4.2.3.1 Definition and properties

The *box dimension*, sometimes called capacity dimension (Farmer, 1983) and more frequently fractal dimension, is one of the parameters most frequently used to characterize fractal sets arising in geophysics. Since the box dimension is not more "fractal" than any other, we will use the term box-dimension. It can be measured easily from data, which probably explains its popularity among experimenters. It is defined for a wider class of sets than the

similarity dimension. Given a set S imbedded in a D-dimensional euclidian space, the box-dimension of S is defined by

$$d_B = \lim_{\delta \to 0} \frac{\log N_B(\delta)}{\log(1/\delta)} \qquad (4.2.2)$$

where $N_B(\delta)$ is the minimum number of D-dimensional balls (or cubes) of diameter δ needed to cover S. The box dimension (when it exists) determines the amount of information needed to locate the set within an accuracy δ, i.e. we need only specify the location of $N_B(\delta)$ balls. For a fixed value of δ, $N_B(\delta)$ increases if d_B increases. In that sense $d_B(S_1) > d_B(S_2)$ implies that the set S_1 is "fatter" than the set S_2.

For simple euclidian sets the box dimension obviously equals the topological dimension. By contrast, d_B takes in general *non-integer* values for fractal sets and can exceed the topological dimension. More generally the box-dimension can be verified to have all the properties of fractal dimension mentioned in section 4.2.1, except for (v) which holds only for finite collections of sets. For that reason, Tricot (1973) argues that the box dimension is not a dimension and proposes instead the name *densité logarithmique* (i.e. "logarithmic density"). For the box-dimension, the property (v) reduces to

$$d_B(\mathbf{U} S_i) = \sup_i \{ d_B(S_i) \}, \qquad (4.2.3)$$

where n is finite. Denoting by $N_B(S,\delta)$ the minimum number of boxes of size δ needed to cover a set S, (4.2.3) is derived from the inequality

$$\sup_i N_B(S_i) \le N_B\Big(\mathbf{U}_{i=1}^{n} S_i, \delta\Big) \le \sum_{i=1}^{n} N_B(S_i,\delta),$$

which follows from the possible overlap between the sets S_i (inequality on the right side), as well that property (iv) (left inequality). That (4.2.3) holds only for finite collection of sets is clearly illustrated by the example of rationals. Although each rational number has $d_B = 0$, their collection in the unit interval [0,1] has box-dimension unity. Indeed rationals are dense in the

real numbers, which means that any real number can be approached arbitrarily closely by a rational. If follows that every box (i.e. interval) used to cover the unit interval is filled (i.e contains at least one rational) and consequently $d_B = 1$. Actually, the box-dimension characterizes the *closure of a set*, i.e the set plus its limit points (the closure of a set S is also the smallest closed subset of $\mathbb{R}^n$ containing S). Indeed, it is not possible to cover a set with closed balls without covering also all the limit points of the sets, i.e its closure (Tricot (1973), Falconer (1990)). It follows for example that both rational and irrational numbers have box-dimension unity.

The definition of d_B presupposes the covering of the set with balls. In a numerical experiment, however, it is convenient to cover the set with a *regular grid of cubes*. This method, often called *box-counting*, gives the same value of dimension as the optimal collection of cubes. Indeed if $N_B'(\delta)$ denotes the number of grid cubes containing points then since each cube of the minimal cover is covered by at most 3^D cubes on the grid,

$$N_B(\delta) \leq N'_B(\delta) \leq 3^D \; N_B(\delta).$$

Taking logs then shows that (4.2.2) continues to hold with N_B replaced by $N'_B(\delta)$. The box-dimension is also independent of the shape of the balls used for the covering. More generally, one can show that the box dimension is invariant under metric equivalence. An open ball of radius R centered about a point x being defined by $\rho(x) < R$, a different but equivalent choice of the metric ρ deforms and stretches the ball by finite amounts with no breaking (see Barnsley (1988) for a more detailed presentation of metric equivalence). The invariance of d_B under metric equivalence also implies that a set can be stretched arbitrarily by finite amounts, while keeping the box-counting grid fixed, without changing d_B. In that sense the box-dimension is a "robust" parameter for sets.

It should be noted that sets can be constructed for which d_B does not exist. In such cases, the notion of lim may be replaced by the twin notions of lim sup and lim inf, leading in general

to two different dimensions respectively called upper and lower box (or entropy) dimensions (Mandelbrot, 1983).

4.2.3.2 Exactly self-similar sets

This section focuses on the calculation of d_B for exactly self-similar sets with splitting factor M and scale ratio r. We show that

$$N_B(\delta) = \delta^{-dS}\, P(\log\delta), \tag{4.2.4}$$

where P is a periodic function of period log(1/r). The possibility of prefactor oscillations in the context of turbulence is discussed and the sensitivity of P to the box-counting grid is examined.

Let $N_B(S;\delta)$ denote the minimum number of boxes needed to cover a set S. Suppose that S splits into M identical copies S_i. If the sets S_i are *positively separated* , i.e. S_i and S_j are separated by finite distances $d(S_i,S_j)$ for each (i,j), and if $\delta < \min\{d(S_i,S_j)\}$ then

$$N_B(S;\delta) = M\, N_B(S_i;\delta) \tag{4.2.5}$$

because there is no overlap between the coverings of the S_i's. S_i being a scaled down copy of S with scale ratio r,

$$N_B(S_i;\delta) = N_B(S;\delta/r)$$

and (4.2.5) then becomes

$$N_B(\delta) = M\, N_B(\delta/r), \tag{4.2.6}$$

which is a linear functional equation for $N_B(\delta)$ (the argument S was dropped for simplicity). Denoting $N_B(\delta) = \delta^{-dS}\, P(\log\delta)$, where P will be called the *prefactor*, and replacing in (4.2.6) yields

$$P(\log\delta) = P(\log\delta + \log(1/r)), \tag{4.2.7}$$

which implies that P is a periodic function of period log(1/r). Note that P is also discontinuous since $N_B(\delta)$ is. The general solution of (4 2.6) is therefore given by (4.2 4). Note that while d_B alone does not determine uniquely M and r (see section 4.2.2), they are determined given both d_B and the period. This method for measuring the parameters M and r of an exactly self-similar set does not appear to have been proposed previously.

Iterating (4.2.6) yields the equivalent equation

$$N_B(\lambda_n \delta) = \lambda_n^{-dS} N_B(\delta), \qquad (4.2.8)$$

where $\lambda_n = r^n$ (n = 0, 1, 2, ...). (4.2.8) is the property satisfied by any homogeneous function when the parameter λ_n varies continuously in some range, but here λ_n is restricted to a discrete set of values. In that sense (4.2.8) can be regarded as a *discrete scaling principle*. The possibility of oscillations of the prefactor is related to the intrinsic discreteness of the self-similarity. The effect of this discreteness is "felt" by $N_B(\delta)$ when the ratios δ/δ_0 are not integer powers of r. Conversely the prefactor oscillations are not visible if $N_B(\delta)$ is examined only at scales $\delta_n = r^n \delta_0$, where δ_0 is arbitrary. The existence of oscillations is worth examining in experimental measurements to investigate the possibility of discrete scale ratios in geophysical contexts. Similar oscillations were noticed by Mandelbrot (1983, p. 123) in the context of the geometrical characterization of clusters.

A natural continuous extension of the discrete scaling principle (4.2.8) is

$$F(\lambda \delta) = \lambda^H F(\delta) \qquad (4.2.9)$$

where λ varies continuously in some interval and H is fixed. For a fixed λ the solution of (4.2.9) is $F_\lambda(\delta) = \delta^H P_\lambda(\log\delta)$, where $P_\lambda(x) = P_\lambda(x+\log(\lambda))$, but this solution holds for each λ hence the prefactor must be a constant. The continuous extension of (4.2.8) therefore spoils, in general, the oscillatory behavior of the prefactor. Equations of the type (4 2.9) are

known to apply to various quantities in physics: According to the K41 theory the velocity structure functions in fully developed turbulence satisfy

$$<|\Delta v(\lambda L)|^h> = \lambda^{h/3} <|\Delta v(L)|^h>; \qquad (4.2.10)$$

the root mean square displacement $\Delta X(t)$ of a particle in Brownian motion during a time t satisfies $\Delta X(\lambda t) = \lambda^{1/2} \Delta X(t)$; similar laws appear to hold for rainfall rate increments over a time lag T (Lovejoy, 1985) and radar reflectivities averaged over volumes of size L (Schertzer and Lovejoy, 1987). In the context of turbulence, assuming that (4.2.10) holds for a fixed λ, Smith *et al.* (1986) have suggested that the general solution could be $<|\Delta v(L)|^h> = L^{h/3} P_h(\log\delta)$, where $P_h(x)$ is periodic in x. From this point of view the period of the function P becomes a fundamental parameter of turbulent flows. It is emphasized that the K41 theory predicts a constant prefactor and does not make room for oscillations Nevertheless, oscillations of the prefactor have been observed for $h > 12$ by Anselmet *et al* (1984). If these oscillations are not statistical artefacts, their existence contradicts both the K41 theory and the continuous scaling principle (4.2.10). We will return to this question in chapter 8.

If $N_B(\delta)$ is obtained with a box-counting grid, it is emphasized that (4.2.6) *does not hold* because the S_i's are not in general aligned in the same way with respect to the grid, so that (4.2.5) is not necessarily satisfied. In special cases, the symmetry of the set and a proper choice of the grid position can allow (4.2.5) to be satisfied exactly. This is what happens for example with the triadic Cantor set if a grid line splits the set exactly in the middle. The behavior of the prefactor can be illustrated with the triadic Cantor set: Since $N_B(1) = 1$ and $N_B(\delta) = 2$ when $1/3 \le \delta < 1$, the prefactor $N_B(\delta)\delta^{dB}$ is given by

$$P(0) = 1 \text{ and } P(\log\delta) = 2\, e^{dB \log\delta} \text{ for } 1/3 \le \delta < 1.$$

The prefactor has discontinuities at the scales $\delta_n = r^n$ (n = 0, 1, 2, ...). It is interesting to compare this with a numerically calculated prefactor using box-counting on a grid. An M-piece Cantor set is represented by a string of binary digits indicating the surviving intervals by a 1 and the deleted ones by a 0. Using this convention, the triadic Cantor set (101) and the 3-piece Cantor set (1101) were considered, using 12 and 10 iterations respectively. The smallest construction scale was defined to be 1. The first line of the box-counting grid was positioned on the left edge of the sets and therefore the symmetry of the set (101) was not exploited. The results were plotted in figure 4.4 and 4.5. P(x) is not periodic for several reasons. Firstly, the renormalization equation (4.2.6) no longer holds on a box-counting grid so the measured prefactor is at best approximate. For the set (1101), two of the subsets S_j are not separated and therefore (4.2.6) holds only approximately even if a grid was not used. Secondly, at the smallest scales the set is not fractal and therefore self-similarity is spoiled. Despite the noise contaminating P(x), the periodicity of the discontinuities appears clearly in both cases. For the set (101) large peaks occur at scales $L_n = 3^n$ while for the set (1101) they occur at $L_n = 4^n$, which is consistent with (4.2.7).

This numerical experiment demonstrates that the prefactor functions of $N_B(\delta)$ and $N'_B(\delta)$ (obtained with box-counting) can be very different. In general the prefactor of $N'_B(\delta)$ will not be periodic partly because of the lack of separation of the S_j's and partly because the grid will not be aligned in the same way for each S_j. This appears to be the first discussion of oscillating prefactors and grid effects in the context of box-counting. A better method for measuring periodic prefactors will be examined in chapter 8.

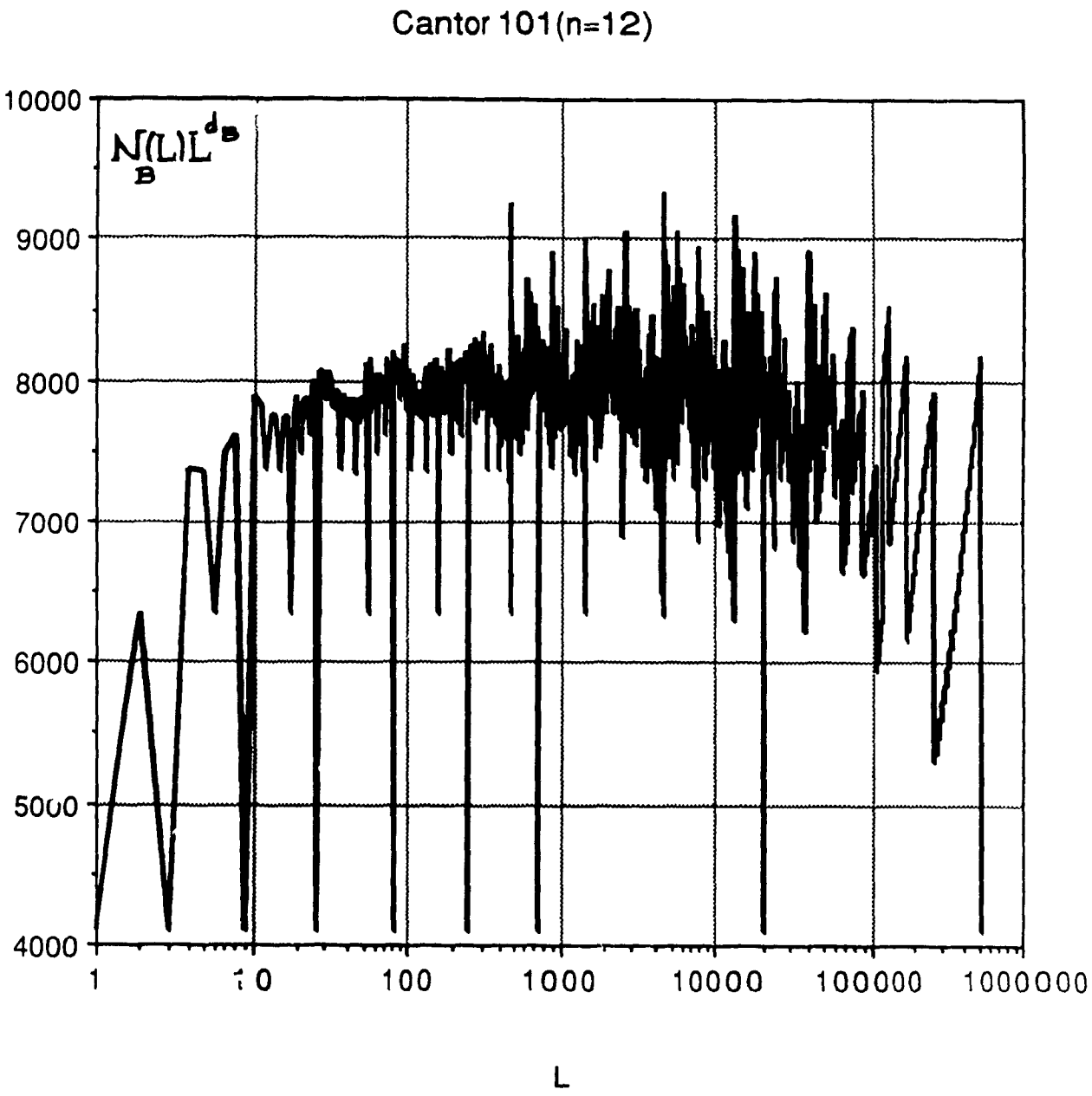

Figure 4.4: Prefactor of $N_B(\delta)$ for the Cantor set (101). Periodic discontinuities at scales 3^n are clearly apparent.

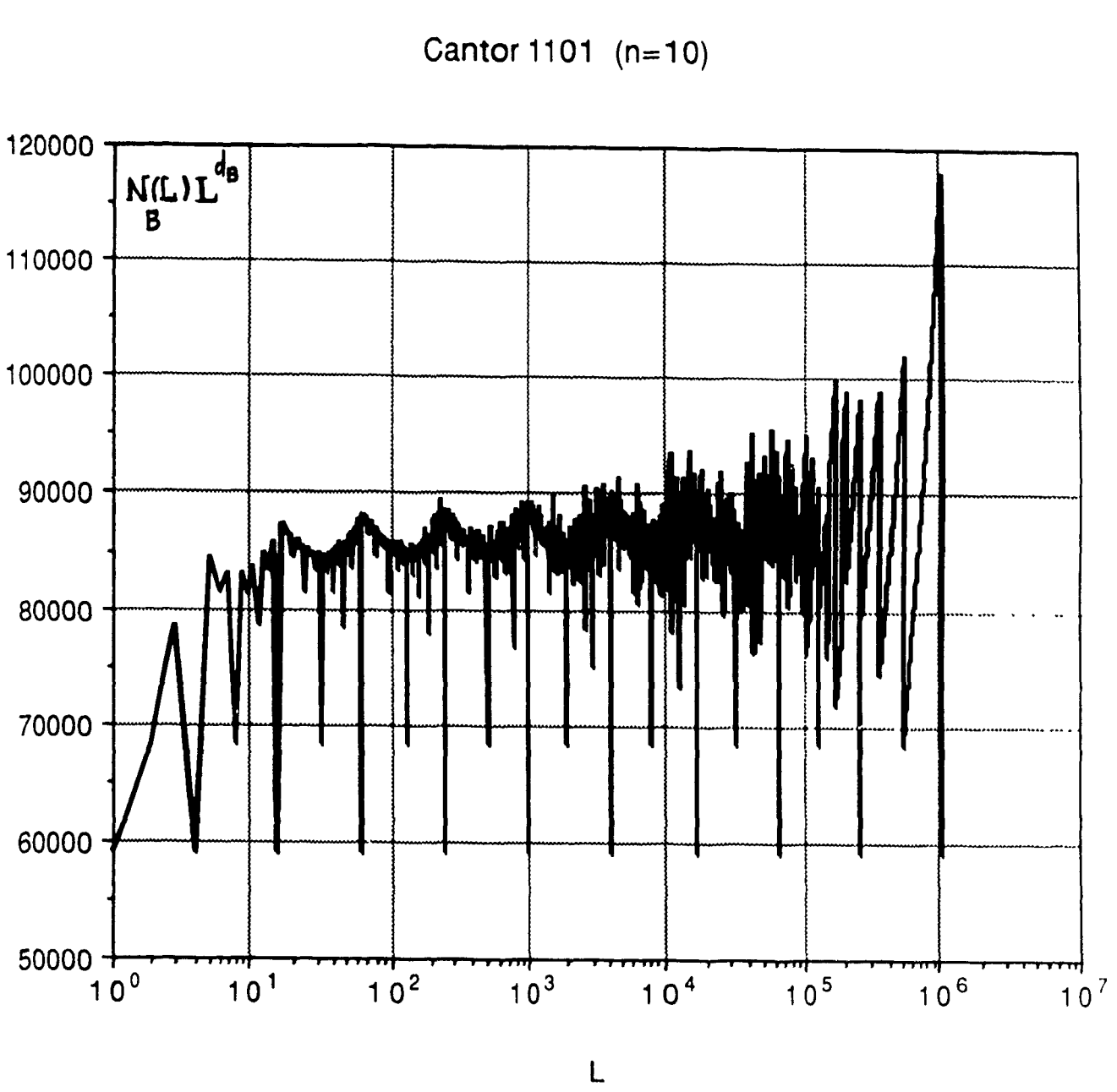

Figure 4.5: Prefactor of $N_B(\delta)$ for the Cantor set (1101). Periodic discontinuities occur at scales 4^n.

4.2.3.3 Multiscale self-similar sets

Multiscale self-similarity is the most natural generalization of exact self-similarity. This scale symmetry has been used successfully, in particular, in the modelling of self-similar measures associated with non-linear dynamical systems (see chapter 5). *A priori*, they appear to be relevant candidates in the modelling of fractal fields. In this section we focus on the calculation of their box-dimension.

A multiscale self-similar set S can be broken into M disjoint copies S_i scaled down by different ratios $r_1, ..., r_M$. Self-similarity directly leads to the renormalization equation

$$N_B(\delta) = \sum_{i=1}^{M} N_B(\delta/r_i) , \qquad (4.2.11)$$

that holds exactly if the sets S_i are positively separated and $\delta < \min d(S_i,S_j)$. Define d_0 to be the real root of

$$\sum_{i=1}^{M} r_i^d = 1. \qquad (4.2.12)$$

d_0 is unique because the function $f(t) = \sum r_i^t$ satisfies $f'(t) < 0$ while $f(0) = M > 1$ and $\lim_{\infty} f = 0$. Denoting $N_B(\delta) = \delta^{-d_0} P(\delta)$, where $P(\delta)$ is the prefactor, and replacing in (4.2.11) yields the prefactor equation

$$P(\delta) = \sum_{i=1}^{M} r_i^{d_0} P(\delta/r_i) . \qquad (4.2.13)$$

The general solution of (4.2.13) is a linear combination of elementary solutions of the form δ^{-d}, with d complex, and is derived in the appendix 4.1. Two cases must distinguished for the general solution of (4.2.11):

(i) **Generic case** : The general solution is

$$N_B(\delta) = \delta^{-d_0} \{ c_0 + R(\delta) \} \qquad (4.2.14)$$

where

$$R(\delta) = \sum_n c(n)\, \delta^{-d_R(n)} \exp(-i\, d_I(n) \log\delta)$$

and $d_R(n) < 0$ for all values of n. It follows that $R(\delta) \to 0$ as $\delta \to 0$ and therefore the prefactor is constant in the limit $\delta \to 0$. If $d_R(n) \approx 0$ for some values of n the oscillations could survive over finite ranges of scale because of the slow damping rate.

(ii) **Special case**: The values of r_j are of the form

$$r_j = r_0^{\,n_j}, \quad j = 1, 2, \ldots, M. \qquad (4.2.15)$$

The general solution becomes

$$N_B(\delta) = \delta^{-d_0} \{ P(\log\delta) + R(\delta) \} \qquad (4.2.16)$$

where $P(x) = P(x + \log(1/r_0))$ and $R(\delta) \to 0$ as $\delta \to 0$.

In both cases, it is clear that $d_B = d_0$. The box dimension of a multiscale self-similar set is therefore always given by the real root of (4.2.12). (4.2.12) can be regarded a generalized definition of the similarity dimension for multiscale self-similar sets because it reduces to (4.2.1) in the special case of equal ratios. By contrast with exactly self-similar sets, the prefactor function does not determine the scale ratios r_i. In the generic case the oscillatory behavior of $P(\delta)$ is spoiled by the introduction of *incommensurate scale ratios* and $P(\delta)$ is constant in the limit $\delta \to 0$. In the special case of commensurate scale ratios, however, a periodic prefactor is recovered in the limit $\delta \to 0$. The period determines r_0 (see 4.2.15) which is an upper bound for the ratios r_i.

As for exactly self-similar sets, d_B does not determine uniquely the splitting factor M and the ratios r_j. For example, squaring (4.2.12) yields

$$\Sigma\Sigma\, (r_i r_j)^d = 1,$$

which shows that a multiscale self-similar set with splitting factor M^2 and scale ratios $r_i r_j$ ($i, j = 1, ..., M$) has the same box-dimension. The same argument can be made by raising (4.2.12) to any integer power.

4.2.4 Hausdorff dimension and self-similar sets

4.2.4.1 Definition and properties

Hausdorff dimension is discussed in this thesis because of its relevance to the multifractal spectrum of a self-similar measure, introduced in chapter 5, which nowadays plays an important role in the modelling of turbulent fields. By contrast with the box-dimension, the Hausdorff dimension d_H exists for all sets. While d_B does not distinguish a set from its closure (e.g. d_B(rationals) = d_B(irrationals)), d_H does. Hausdorff dimension is also a metric concept. To define it, we consider a covering of a set S with sets U_i of variable diameters δ_i. Recall that the diameter δ of a set U is defined by $\delta = \sup\{d(x,y): x, y \in U\}$, where $d(x,y)$ is the Euclidian metric. If $0 < \delta_i \leq \delta$ for each i, $\{U_i\}$ is called a *δ-cover* of S. Given a δ-cover of S, define the outer measure

$$H^d_\delta(S) = \inf \{ \sum_i \delta_i^d \}, \qquad (4.2.17)$$

where the infimum (i.e. greatest lower bound) extends over all possible δ-covers of S (a brief recap on the notions of measure and outer measure is given in section 5.1). $H^d_\delta(S)$ is a decreasing function of δ because the class of permissible covers of S is reduced as δ decreases, and therefore $H^d_\delta(S)$ increases. Now define the d-dimensional Hausdorff outer-measure by

$$H^d(S) = \lim_{\delta \to 0} H^d_\delta(S) \ . \qquad (4.2.18)$$

$H^d(S)$ exists since $H^d_\delta(S)$ increases as δ decreases, but may be (and usually is) zero or infinite. Since $\sum \delta_i^d$ is a decreasing function of d for a fixed cover, the infimum $H^d_\delta(S)$ is also a decreasing function of d. Furthermore, a similar reasoning implies that if $d > t$ then

$$H^d_\delta(S) \leq \delta^{d-t} H^t_\delta(S)$$

Letting $\delta \to 0$ we see that if $H^t(S) < \infty$, then $H^d(S) = 0$ for $d > t$. Also, if $H^d(S) = \infty$ then $H^t(S) = \infty$ for $t < d$. Hence there exists a critical value d_H, called the *Hausdorff dimension*, above which $H^d(S) = 0$ and below which $H^d(S) = \infty$. This divergence rule may be regarded as a generalization of the statement "the length of a surface is infinite, its volume is zero". $H^{d_H}(S)$, called the Hausdorff outer measure of S, may be either 0, ∞, or a finite positive number. d_H and d_B are related in general by

$$0 \leq d_H \leq d_B \leq D, \qquad (4.2\ 19)$$

which follows from the inequality $N_B(\delta;S) \geq H^d_\delta(S)$.

$H^d_\delta(S)$ can equivalently be defined in terms of δ-covers of S by restricted classes of sets, e.g. convex, open or closed sets, and d_H remains unchanged (Falconer, 1985). Hausdorff dimension shares all properties of a fractal dimension (see section 4.2.1). In particular, the property (v) follows directly from the fact that $H^d(S)$ is an outer measure. Indeed

$$\sup_n H^d(S_n) \leq H^d(\mathbf{U} S_n)) \leq \sum_n H^d(S_n),$$

which implies that $d_H(\mathbf{U} S_n) = \sup_n d_H(S_n)$. It follows in particular that the Hausdorff dimension of any countable subset of $\mathbb{R}^D$ is zero, since $d_H = 0$ for each individual point. For example, the Hausdorff dimension of rationals is zero.

The Hausdorff outer-measure can be turned into a measure if one restrict ourselves to Borel sets, i.e. finite or countable unions or intersections of open and closed sets. Any set that can be

constructed using a sequence of countable unions or intersections starting with the open sets or closed sets will certainly be Borel (Falconer, 1990). Multiscale Cantor sets and Koch curves are therefore Borel.

It is worth mentioning that the original definition of fractal sets, introduced by Mandelbrot, was based on the concept of Hausdorff dimension:

> "A fractal is by definition a set for which the Hausdorff dimension d_H strictly exceeds the topological dimension d_T".

This definition was found to be problematic for various reasons, in particular because of the fact that it excludes fractal sets for which d_H and d_T are equal. According to Mandelbrot, the basic purpose of this definition was to distinguish fractal sets from simple euclidian sets for which $d_H = d_T$. In any case, it certainly defines a class of sets that are irregular at all scales, i.e. a class of fractal sets.

In general the practical estimation of d_H is difficult. Its definition is rarely (never?) used as the basis of experimental procedures for the determination of fractal dimensions of physical sets (Barnsley, 1988). However, we shall see an example in chapter 5 where a measure, possibly relevant to turbulence modelling, gives rise to sets for which d_H can be obtained indirectly through measurable scaling exponents. This fact gives some physical credit to the notion of Hausdorff dimension, which may seem a little exotic at first.

4.2.4.2 Self-similar sets.

In this section we compute the Hausdorff dimension of self-similar sets by taking advantage of the scaling symmetry. The limitations of this approach, due to the possibly vanishing value of the Hausdorff outer measure, are highlighted.

Consider a set S that can be broken into M identical disjoint copies S_i scaled down by a common ratio r, i.e. an exactly self-similar set. If the S_i are positively separated and $\delta < \min_{i,j} d(S_i,S_j)$, the lack of overlap implies

$$H^d_\delta(S) = \sum_{i=1}^{M} H^d_\delta(S_i). \tag{4.2.20}$$

Scaling and self-similarity implies that

$$H^d_\delta(S_i) = r^d H^d_{\delta/r}(S), \tag{4.2.21}$$

and therefore (4.2.20) becomes

$$H^d_\delta(S) = M r^d H^d_{\delta/r}(S). \tag{4.2.22}$$

As previously for $N_B(\delta)$, the general solution of (4.2.22) takes the form

$$H^d_\delta(S) = \delta^{d-ds} P_d(\log\delta), \tag{4.2.23}$$

where $d_S = \log M/\log(1/r)$ and $P_d(x) = P_d(x+\log(1/r))$. A periodic prefactor, already encountered in the analysis of box-counting, is again obtained. In the case of a separated multiscale self-similar set, (4.2.22) becomes

$$H^d_\delta(S) = \sum_{i=1}^{M} r_i^d H^d_{\delta/ri}(S), \tag{4.2.24}$$

which is formally identical to the equation (4.2.13) for the prefactor of $N_B(\delta)$ in the case of a multiscale self-similar set. In the generic case of non-commensurate scale ratios r_i the solution of (4.2.24) is therefore

$$H^d_\delta(S) = \delta^{d-d_S} \{ c_0(d) + R_d(\delta) \} \qquad (4.2.25)$$

where $R_d(\delta) \to 0$ as $\delta \to 0$ and d_S is the real root of the characteristic equation (4.2.12).

If the prefactors P_d (in (4.2.23)) or $c_0(d)$ (in (4.2.25)) are non-zero for all values of d, it is clear from (4.2.23) and (4.2.25) that $H^d_\delta(S)$ vanishes in the limit $\delta \to 0$ for $d > d_S$ and diverges for $d < d_S$, and therefore $d_H = d_S$. The possibility $d_H \leq d_S$ is is clearly illustrated by the example of rational numbers in the unit interval. The set of rationals is exactly self-similar (the sum of two rationals is rational and the product of two rationals is also rational. It follows that a unit interval of rationals can split into M identical subintervals of size r = 1/M, each being a copy of the interval scaled down by a factor r). The similarity dimension is therefore 1, while $d_H = 0$ since the rationals form a countable set. Note that if we assume that

$$0 < H^{d_H}(S) < \infty, \qquad (4.2.26)$$

then (4.2.23) and (4.2.25) imply that $d_H = d_S$. Borel sets satisfying (4.2.26) are called *s-sets*, and multiscale Cantor sets and von Koch curves are examples of such sets (Falconer (1990) section 2.2)

The more general case of non-separated but "just touching" self-similar sets, such as the von Koch curve where the subsets share two common points at their edges, can be treated by focusing on Borel sets (see Falconer (1990) and Hutchison (1981) for more details on the separation condition). In this case H^d is a measure and the property $H^d(US_i) = \sum H^q(S_i)$ can be used together with (4.2.21) and (4.2.26) to deduce that $d_H = d_S$. Roughly speaking, s-sets that are "sufficiently separated" satisfy $d_H = d_S$.

4.2.5 Comparison between box and Hausdorff dimension

For the M-piece Cantor set or the M-piece von Koch curve the similarity dimension is defined by $d_S = \log M/\log(1/r)$. For such sets, it was shown that

$$d_S = d_B = d_H$$

For the multiscale Cantor set or the multiscale von Koch curve, the similarity dimension is defined by $\sum_{i=1}^{M} r_i^{dS} = 1$. For these four sets the above equality holds, which is basically a consequence of self-similarity for s-sets.

Consider the set of numbers $S = \{1,1/2,1/3,1/4, ...\}$. This is a first example of non self-similar set and d_S is therefore undefined. For this set $d_H = 0$ because S is countable. The Hausdorff measure is $H^0(S) = \infty$ because the Hausdorff measure of each point is $\delta^0 = 1$, and there is an infinite number of points. The box dimension of S can be obtained with the following argument. If $\delta = 1/n$, we need one box per point except when the distance between consecutive points is smaller than δ. The distance between consecutive points $1/k$ and $1/(k+1)$ exceeds δ when $1/k - 1/(k+1) > 1/n \Rightarrow k(k+1) < n$. For n large, this implies approximately $k < \sqrt{n}$. We will therefore need about $\sqrt{n}$ boxes to cover the interval $[1/\sqrt{n},1]$ The remaining interval $[0,1/\sqrt{n}]$ can be covered by $1/\sqrt{n}$ / $(1/n) = \sqrt{n}$ boxes. The total number of boxes of size $\delta_n = 1/n$ needed to cover S is therefore $N(n) = \sqrt{n} + \sqrt{n} = 2\sqrt{n}$. Hence $N(\delta_n) = 2\ \delta_n^{-1/2}$ and $d_B = 1/2$. As for the case of rationals, the origin of the difference between d_B and d_H is the countability of S.

4.2.6 Multinomial sets

Rationals satisfy $d_S = 1$, $d_B = 1$ while their countability implies $d_H = 0$. It is worth stressing that d_B and d_H can also differ for sets that are not countable as will be shown in the next example. The *multinomial sets* may *a priori* seem a little exotic to the reader, but they will

be shown in chapter 5 to arise naturally in the study of a self-similar measure that might play a role in the modelling of turbulent fields. Each number in the unit interval I=[0,1] has a base M expansion

$$x = \sum_{i=1}^{\infty} \varepsilon_i \frac{1}{M^i},$$

where the ε_i's are integers 0, 1, 2, ..., M-1. This is also written alternately as $x = \varepsilon_1\varepsilon_2....$ Note that if x_n represents the n-term expansion of x then $x \in [x_n, x_n + 1/M^n]$, i.e. there is a 1-1 relation between the n-term expansions and the intervals of length $1/M^n$. Let I' be the collection of reals with a well-defined frequency of occurrence of integers in the base M expansion and let $\xi_r(x)$, r = 0, 1, 2, ..., M-1 be the frequency of occurrence of r. These frequencies satisfy to $0 \le \xi_r \le 1$ and $\sum_{r=0}^{M-1} \xi_r = 1$. According to Eggleston (1949), the *multinomial sets*

$$Z(\xi_0, ..., \xi_{M-1}) = \{ x \in I' : \xi_r(x) = \xi_r, r = 0, ..., M-1 \}$$

have Hausdorff dimension

$$d_H(Z) = - \sum_{r=0}^{M-1} \xi_r \log_M \xi_r . \qquad (4.2.27)$$

Since any open interval contains reals with any desired frequencies ξ_r, Z is dense in the interval and consequently has box dimension unity. Z is non-compact and its closure is the unit interval I. The box and Hausdorff dimensions are consequently distinct.

Z is also an exactly self-similar set. On one hand $\xi_r(x+y_n) = \xi_r(x)$ because only a finite number of digits in the base M expansion is affected by the addition of the truncated expansion y_n. In addition, for any integer n $\xi_r(x/M^n) = \xi_r(x)$ because the division only shifts the digits in the expansion of x, which does not affect ξ_r. It follows from these translational and scaling invariance that the multinomial set can split into M^n identical pieces, copies of the original scaled

down by a factor $1/M^n$. The result $d_S = d_B \neq d_H$ is apparently a consequence of the control of the prefactor on the Hausdorff dimension (see section 4.2.4.2).

(4.2.27) can be made plausible by considering the set of all x with a particular frequency of occurrence for each integer {0, ..., M-1} in the n-term expansion, i.e. by considering the sequence of sets

$$Z_n(\xi_0, ..., \xi_{M-1}) = \{ x \in I' : \xi_r(x_n) = R_n(\xi_r), r = 0, ..., M-1 \},$$

where $R_n(\xi_r)$ denotes the rational of the form p/n closest to ξ_r. For fixed ξ_r, S_n contains

$$N_n = \frac{n!}{(n\xi_0)! \ ... \ (n\xi_{M-1})!}$$

intervals of length $1/M^n$. Since $\log n! = n \log n - n + 1/2 \log n + O(1)$ according to Stirling's formula, we get

$$\ln(N_n) = n \log n - n + \frac{1}{2} \log n - \sum_{k=0}^{M-1} \{ n\xi_k \log(n\xi_k) - n\xi_k + \frac{1}{2} \log(n\xi_k) \} + O(1)$$

$$= - n \sum_{k=0}^{M-1} \xi_k \log \xi_k - \frac{(M-1)}{2} \log n + O(1)$$

and since $\delta_n = 1/M^n$ then

$$N_n = C \ \delta_n^{-D} | \log_M \delta_n |^{-(M-1)/2},$$

where D is given by (4.2.27). It is emphasized that D characterizes the entire sequence of sets and is not the box dimension of any of the individual sets. Since this sequence of sets approaches Z as $n \to \infty$, it is not necessarily surprising that D is is the Hausdorff dimension of Z.

Chapter V

MULTIFRACTAL MEASURES IN GEOPHYSICS

Les cascades dansaient là-bas
comme de blancs chevaux fougueux,
La crinière pleine d'écume et d'arcs-en-ciel

Mais, patatras, au bord du précipice
Les voilà tombés sur leurs jambes de devant
Cassées, oh, blanches jambes.

Et ils sont morts au pied du rocher.
Désormais dans leurs yeux éteints
Se reflète le ciel, glacé

Les cascades, Ismaïl Kadare

Multifractal measures have been used to describe many geophysical fields, such as radar reflectivity fields generated by showers, cloud fields (Schertzer and Lovejoy, 1984, 35, 87, 89) and the energy dissipation field in turbulent flows (Yaglom (1966), Mandelbrot (1974), Sreenivasan *et al.* (1988), Meneveau *et al.* (1987a-b-c, 1990a-b), Novikov (1990), Schertzer and Lovejoy (1984, 85, 87, 89)). Such measures also model the invariant probability measure of some non-linear dynamical systems in the chaotic regime (Hentschel and Procaccia (1983), Halsey *et al.* (1986)). In addition, a formalism similar to the multifractal formulation has been proposed to explain the scaling of the velocity field in fully developed turbulence (appendix of Frisch and Parisi, 1983). The multifractal description appears to be a possible junction point for the fields of turbulence, non-linear dynamics and statistical mechanics. In this chapter we propose a turbulence-oriented presentation of the concept of multifractal measure.

We start with the notion of measure and discuss its relevance to remote sensing and turbulence measurements where resolution limits and averaging are ubiquitous. Next comes a study of the multinomial measure, an example that has been used in various applications and that leads naturally to the general properties attached to the concept of multifractal measure.

Given the subtleties inherent to this field, as well that the frequent misconceptions that they still generate, we give a fairly detailed treatment. The originality of this presentation is the use of a formalism that allows both sets and measures (either deterministic or random) to be treated in a same unified framework based on scale renormalization. In the context of measures, our study of prefactor oscillations is unusual and relatively new. Our considerations about correlations in multifractal also involve several original elements. The goal of this chapter is to propose a classification of cascade models and to determine to what extent the multifractal characterization allows different cascade models to be distinguished.

5.1 BASIC CONSIDERATIONS

Any positive integrable scalar field $\rho(x)$, e.g. the mass density at point x can be used to construct a measure. The mass $\mu(S)$ contained in a volume S,

$$\mu(S) = \int_{x \in S} \rho(x)\, dV,$$

is a simple example of measure. Generally speaking a *measure* μ associates a non-negative number $\mu(S)$ to subsets S contained in the embedding space $\mathbb{R}^n$ (the subsets S form a family F called a sigma-field, i.e. F is closed under complementation and under countable unions). μ satisfies $\mu(\varnothing) = 0$ for the empty set and

$$\mu\left(\bigcup_{j=1}^{\infty} S_j\right) = \sum_{j=1}^{\infty} \mu(S_j) \qquad (5.1.1)$$

for every countable sequence of disjoint subsets of F. It follows that μ is an increasing set function, i.e.

$$S' \supset S \Rightarrow \mu(S) \leq \mu(S') \ . \qquad (5.1.2)$$

Outer measures, used for example in the definition of the Hausdorff dimension (see chapter 4), are essentially measures with the property 5.1.1 weakened to subadditivity. The measures

examined in this section are probability measures which means that if S is the support of μ, then $\mu(S) = 1$ (the support of a measure is the union of all the open sets G such that $\mu(G) \neq 0$).

The use of measures rather than densities to describe geophysical fields is motivated by the limited resolution and the intrinsic irregularity of measured fields. The density function cannot be determined unless the natural inner scale of the field is resolved, which is rarely the case. Measurements rather provide averages over intervals, areas or volumes which can be naturally interpreted as measures (if they are non-negative). These averages provide what we call a *coarse-grained* description of the measure. The idealized fractal fields used to model irregular fields, such as the energy dissipation rate in turbulent flows do not have well defined densities, i.e their densities are *singular*. This is one of the characteristic properties of multifractal measures, which are consequently described in terms of the scaling properties of coarse-grained quantities.

5.2 AN EXACTLY SELF-SIMILAR MEASURE: THE MULTINOMIAL MEASURE

5.2.1 Definition

Let the unit interval [0,1] be divided into M pieces of equal sizes, each being assigned a measure w_i, i=0, ..., M-1, where $\sum w_i = 1$. Suppose next that the process is repeated by dividing each interval into M subintervals and assigning the j^{th} subinterval of the i^{th} interval a measure $w_i w_j$. After n steps the construction process generates M^n subintervals of size $\delta_n = 1/M^n$, of the form $I_n(i) = [x_i, x_i + \delta_n]$ where $x_i = i\ \delta_n$, $i = 0, ..., M^n - 1$. The number of intervals $I_n(i)$ with measure $w_0^{k_0} ... w_{M-1}^{k_{M-1}}$, where $k_0 + ... + k_{M-1} = n$, is

$$N(k_0, ..., k_{M-1}) = \frac{n!}{k_0! ... k_{M-1}!} \quad ,$$

which is the coefficient of $x_0^{k_0} ... x_{M-1}^{k_{M-1}}$ in the multinomial expansion of $(x_0 + ... + x_{M-1})^n$. The measure derives its name from this property.

The multinomial measure is obtained when the construction process is repeated *ad infinitum*. If all the weights w_i are non-zero the support of the measure is S = [0,1]. If only M_e weights are non-zero the measure is supported by an M_e-piece Cantor set. Notice that the process conserves exactly the total measure at each stage in the sense that if $I_n(i)$ has a given measure after n construction steps, the subsequent steps will not change this measure. A cascade process with these properties of conservation was called *microcanonical* or *conservative* by Mandelbrot (1974).

This measure is *exactly self-similar* in the following sense. Consider one of the $I_n(i)$ and assume that the measure of any subinterval of $I_n(i)$ has been normalized by $\mu\{I_n(i)\}$ (the normalized measure $\mu'\{I\}$ of any subinterval I of $I_n(i)$ is defined by $\mu'\{I\} = \mu\{I\}/\mu\{I_n(i)\}$). It appears that μ' is a scaled down copy of the original measure supported by the shorter interval $I_n(i)$. Roughly speaking, properly normalized pieces of this probability measure are scaled down copies of the original measure. This characteristic property is the basis of the renormalization equations that will be used to analyze this measure. An illustration of the binomial measure (M=2), obtained with the weights w_1=0.3 and w_2=0.7, is given in figure 5.1.

5.2.2 Pointwise scaling and singularities

In this section the multinomial measure is shown to be singular in the sense that its density does not exist everywhere. For a regular measure in a D-dimensional space, the measure $\mu_x(\delta)$ of a ball centered about a point x is proportional to δ^D in the limit $\delta \to 0$ and the *average density*, defined by $\rho_x(\delta) = \mu_x(\delta)/\delta^D$, converges for each x as $\delta \to 0$. By contrast for a singular measure there are points for which $\rho_x(\delta)$ diverges as $\delta \to 0$. For the multinomial measure, we will show that the divergence is due to a *local scaling property*, i.e. $\mu_x(\delta) \sim \delta^{\alpha(x)}$ as $\delta \to 0$, where in general $\alpha(x) \neq D$.

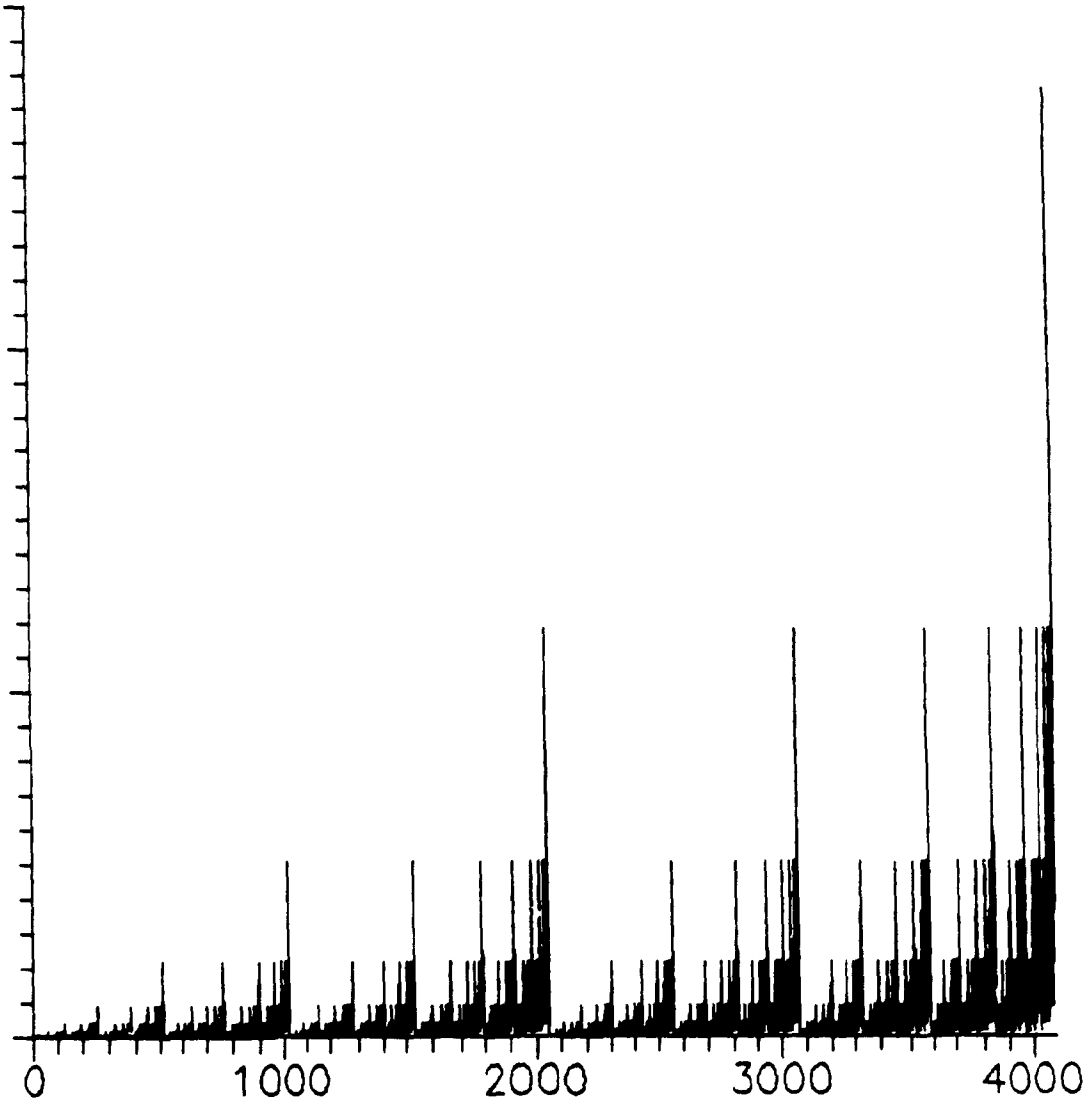

Figure 5.1: A picture of the binomial measure, coarse-grained at the scale $1/2^{12}$, obtained with the weights $w_1=0.3$ and $w_2=0.7$. As will be shown later, these weights reproduce accurately the scaling properties of $\int_0^L (\partial v/\partial x)^2 dx$, where $v(x)$ is the longitudinal velocity in a fully turbulent flow. Random generalizations of the binomial measure will be shown to provide more realistic models of $(\partial v/\partial x)^2$.

The set of values $\mu\{I_n(i)\}$, i = 0, ..., M-1, provides a possible coarse-grained description of the multinomial measure. Using the notation of section 4.2.6, where x_n represents the n term base-M expansion of x and $I_n(x) = [x_n, x_n + \delta_n]$,

$$\mu\{I_n(x)\} = w_0^{k_0(x)} \ldots w_M^{k_{M-1}(x)} \quad , (\sum k_i(x) = n)$$

where $k_i(x)$ is the number of times the digit i occurs in the n term expansion of x. Denoting by $\xi_{r,n}(x)$ the fraction k_r/n of r's in the first n terms of the base M expansion of x, this can be rewritten in the form

$$\mu\{I_n(x)\} = (w_1^{\xi_{0,n}(x)} \ldots w_M^{\xi_{M-1,n}(x)})^n .$$

Using $\delta_n = 1/M^n$ leads to

$$\mu\{I_n(x)\} = \delta_n^{\alpha_n(x)} \quad \text{where} \quad \alpha_n(x) = - \sum_{r=0}^{M-1} \xi_{r,n}(x) \log_M w_1.$$

If the fractions $\xi_r(x)$ exist (i.e. $x \in I'$, see section 4.2.6) then $\xi_{r,n}(x) \to \xi_r(x)$ as $n \to \infty$ and $\alpha_n(x) \to \alpha(x)$, where

$$\alpha(x) = - \sum_{r=0}^{M-1} \xi_r(x) \log_M w_1. \qquad (5.2.1)$$

The measure therefore scales at x and $\alpha(x)$ is called the *pointwise scaling exponent* of μ at x. In the special case M = 2, $\alpha(x)$ takes the form

$$\alpha(x) = - \{ \xi_0(x) \log_M(w_0) + (1-\xi_0(x)) \log_M(1-w_0) \}.$$

By contrast with a regular measure for which $\alpha(x) = D$ for all x, the multinomial measure has a continuous spectrum of pointwise scaling exponents.

Generally speaking, given any measure μ defined on a D-dimensional euclidian space the pointwise scaling exponent $\alpha(x)$ at point x is

$$\alpha(x) = \lim_{\delta \to 0} \frac{\log \mu(B_\delta(x))}{\log \delta} \qquad (5.2.2)$$

if it exists, where $B_\delta(x)$ denote a D-dimensional ball of radius δ centered about x. Notice that $\alpha(x)$ is non-negative since μ is an increasing set function (property (5.1.2)). Pointwise scaling exponents have also been called pointwise dimensions (Farmer, 1983), cluster dimensions (Feder, 1988) or singularity strengths (Halsey *et al.*, 1986). For the multinomial measure, the average probability density defined above becomes

$$\rho(x,\delta) = \delta^{\alpha(x) - D},$$

and therefore $\rho(x,\delta) \to 0$ if $\alpha(x) > D$ and diverges if $0 \le \alpha(x) < D$. The multinomial measure is therefore singular on the set $\{x \in I' : 0 \le \alpha(x) < D\}$. Notice that these singularities are not Dirac distributions because they carry a zero measure: Indeed $\alpha(x) > 0$ therefore $\mu\{B_\delta(x)\} \to 0$ as $\delta \to 0$.

The multinomial measure gives rise in general to a continuous range of pointwise scaling exponents (if the weights w_j are different). By contrast some singular measures are characterized by a single pointwise scaling exponent, i.e. $\alpha(x)$ is constant everywhere on the support. These measures are sometimes called *fractally homogeneous* (a term introduced by Mandelbrot) and are among the simplest singular measures. A simple example of fractally homogeneous measure is the special case of the multinomial measure obtained when all the M_c non-zero weights are equal to $w = 1/M_c$ (figure 5.2). If $M_c = M = 1/r$ the measure is uniform and regular and $\alpha(x) = 1$ for all x. If $M_c < 1/r$ the support S of the measure is the M_c-piece Cantor set and (5.2.1) yields $\alpha(x) = d_S$ everywhere on S.

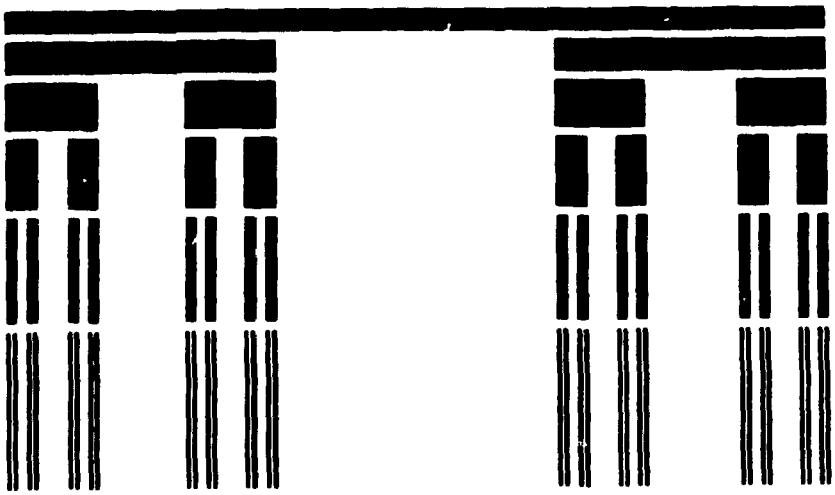

Figure 5.2: Triadic Cantor measure. Starting with a unit mass spread uniformly on the unit interval, the mass is split in two and uniformly distributed on two subintervals of length 1/3. The same process is then repeated iteratively on each subinterval. The height of the bars in the n^{th} stage is proportional to the average density. The pointwise scaling exponent on the support is $\alpha = \log 2/\log 3$ and equals the box dimension of the support.

5.2.3 Generating function and mass exponents

Singular measures are usually characterized by the scaling properties of coarse-grained quantities such as the *generating function*. Consider a measure μ defined on a D-dimensional euclidian space and a cover of the support S of μ with cubes (or balls) of size δ. If $\mu_i(\delta)$ denotes the probability measure of the i^{th} cube, the generating function $\chi_q(\delta)$ is defined for any real number q by

$$\chi_q(\delta) = \inf \sum_i (\mu_i(\delta))^q \qquad (5.2.3)$$

where the infimum extends over all the possible covers of S. The introduction of the infimum is usually neglected in the literature, but is necessary for $\chi_q(\delta)$ to be uniquely defined. In practice $\chi_q(\delta)$ is estimated by using a regular box-counting grid. $\chi_q(\delta)$ decreases monotonically with increasing q. Indeed for a given covering $\Sigma[\mu_i(\delta)]^q$ decreases if q increases and so does the infimum.

We shall now show that the exact self-similarity of the multinomial measure (see section 5.2.1) leads to a renormalization equation for $\chi_q(\delta)$. Denoting by $\chi_q(\delta;S)$ the generating function of a measure supported by a set S, then

$$\chi_q(\delta;S) = \sum_{i=1}^{M} \chi_q(\delta;S_i)$$

where the sets S_i are the scaled down supports of the M weighted copies of the measure μ. As for fractal sets with $N_B(\delta)$, this equality holds exactly if the S_j are positively separated and $\delta < \min\{d(S_i, S_j)\}$. The measure defined on S_j is a scaled down copy of the whole measure, but multiplied by w_j, which implies

$$\chi_q(\delta;S_i) = w_i^q \, \chi_q(\delta/r;S).$$

Consequently

$$\chi_q(\delta;S) = (\sum_{i=1}^{M} w_i^q)\, \chi_q(\delta/r;S) \qquad (5.2.4)$$

(5.2.4) is formally identical to the renormalization equation (4.2.6) for $N_B(\delta)$ in the case of an exactly self-similar set. The general solution is therefore

$$\chi_q(\delta) = \delta^{\tau(q)}\, P_q(\log\delta) \qquad (5.2.5)$$

where

$$\tau(q) = -\frac{\log\sum_{i=1}^{M} w_i^q}{\log(1/r)} \qquad (5.2.6)$$

and $P_q(x) = P_q(x+\log(1/r))$. The generating function therefore scales with δ and a periodic prefactor is obtained, revealing the scale ratio of the measure. $\tau(q)$ is called the *order-q mass exponent* of the measure.

For more general measures $\tau(q)$ is defined by the limit

$$\tau(q) = \lim_{\delta \to 0} \frac{\log \chi_q(\delta)}{\log\delta}. \qquad (5.2.7)$$

It is emphasized that $\tau(q)$ is always a *concave* function of q, i.e. $\tau''(q) \leq 0$ (more details on the properties of τ will be given in section 5.2.6.1). Measures for which $\tau(q)$ exists and is finite for any real q will be called *scaling measures*. So far, the multifractal formalism has been applied mostly to scaling measures, or to measures for which $\chi_q(\delta)$ scales in some limited range of exponents q (Fourcade and Tremblay, 1987). The mass exponents are related to the "generalized dimensions" D(q) of Hentschel and Procaccia (1983) by $\tau(q) = D(q)\,(q-1)$. The finiteness of $\tau(q)$ implies that $\chi_q(\delta) \sim P_q(\delta)\, \delta^{\tau(q)}$ as $\delta \to 0$, where $P_q(\delta)$ satisfies $\log(P_q(\delta))/\log(\delta) \to 0$ as $\delta \to 0$. It is emphasized that in general the prefactor $P_q(\delta)$ is sensitive to the box-counting grid used in the estimation of $\chi_q(\delta)$. This problem has already

been encountered in the estimation of the prefactor of $N_B(\delta)$ for exactly self-similar sets. The originality of the above treatment lies in the exact renormalization equations derived from a general statement of exact self-similarity for measures, as well that in prefactor considerations for the generating function.

5.2.4 The density of singularities and the multifractal spectrum

Another equivalent way of characterizing the measure is to examine the frequency distribution of the values of $\mu(\delta)$ as a function of δ. Define the *singularity strength* $\alpha(\delta)$ of a box of measure $\mu(\delta)$ by

$$\mu(\delta) = \delta^{\alpha(\delta)}. \tag{5.2.8}$$

It is emphasized that $\alpha(\delta)$ is distinct from the pointwise scaling exponent $\alpha(x)$ since $\alpha(\delta)$ is defined for finite values of δ, while $\alpha(x)$ is defined at point x. Define the number of boxes of size δ and measure $\delta^{\alpha(\delta)}$ with $\alpha < \alpha(\delta) < \alpha + d\alpha$ as $n(\delta,\alpha)d\alpha$, where $n(\delta,\alpha)$ is called the *density of singularities*. $n(\delta,\alpha)$ characterizes the frequency distribution of $\mu(\delta)$. In general, for any measure, the generating function and the density of singularities are related by

$$\chi_q(\delta) = \int_0^\infty n(\delta,\alpha)\, \delta^{\alpha q}\, d\alpha. \tag{5.2.9}$$

(5.2.9) can be rewritten in the form

$$\chi_q(\delta) = \int_0^\infty n(\delta,\alpha)\, e^{-s\alpha}\, d\alpha,$$

where $s = -q \log\delta > 0$ for $q > 0$ and $\delta < 1$. $\chi_q(\delta)$ is therefore the Laplace transform of $n(\delta,\alpha)$. The inverse transform yields, after the change of variable $s = -q \log\delta$,

$$n(\delta,\alpha) = \frac{|\log\delta|}{2\pi i} \int_{\gamma-i\infty}^{\gamma+i\infty} \delta^{-\alpha q}\, \chi_q(\delta)\, dq \tag{5.2.10}$$

Using the pair (5.2.9)-(5.2.10), $\chi_q(\delta)$ and $n(\delta,\alpha)$ can be obtained directly from each other, and in that sense both characterizations are equivalent.

For the multinomial measure or any self-similar measure, (5.2.10) and (5.2.5) lead to

$$n(\delta,\alpha) = \frac{|\log\delta|}{2\pi i} \int_{\gamma-i\infty}^{\gamma+i\infty} \delta^{-\alpha q + \tau(q)} P_q(\log\delta)\, dq. \qquad (5.2.11)$$

(5.2.11) also holds for any scaling measure but P_q is not periodic in general. It is emphasized that $\chi_q(\delta)$ scales exactly with δ (within an oscillating prefactor), while $n(\delta,\alpha)$ is a continuous superposition of scaling terms. Nevertheless, asymptotic scaling for $n(\delta,\alpha)$ is recovered in the limit $\delta \to 0$. Indeed, as $\delta \to 0$ the value of q that maximizes $-\alpha q + \tau(q)$ makes the main contribution to the integral and the saddle point method (see Wong (1989) or Bender and Orszag (1978)) yields the asymptotic expression

$$n(\delta,\alpha) \sim \frac{|\log\delta|}{2\pi i}\, i\, \delta^{\max\{-\alpha q+\tau(q)\}} P_{q_0}(\log\delta) \sqrt{\frac{2\pi}{|\tau''(q_0)\log\delta|}}$$

where $q_0(\alpha)$ is defined implicitly by $\tau'(q_0(\alpha)) = \alpha$. Using

$$\max_q\{-\alpha q + \tau(q)\} = -\min_q\{\alpha q - \tau(q)\}$$

and denoting

$$f(\alpha) = \min_q\{\alpha q - \tau(q)\} \iff \tau(q) = \min_q\{\alpha q - f(\alpha)\}, \qquad (5.2.12)$$

$n(\delta,\alpha)$ takes the final asymptotic form

$$n(\delta,\alpha) \sim \delta^{-f(\alpha)} P_{q_0}(\log\delta) \sqrt{\frac{|f''(\alpha)\log\delta|}{2\pi}}\,, \qquad (5.2.13a)$$

where the identity $\tau''(q_0(\alpha)) = 1/f''(\alpha)$, which follows from the definition (5.2.12), was used. (see section 5.2.6 for more details). According to (5.2.13a), the dependence of $n(\delta, \alpha)$ on δ as $\delta \to 0$ is mainly ruled by the function $f(\alpha)$, usually called the *multifractal spectrum* of the measure, for reasons that will be exposed in the next section. As seen from (5.2.12), $f(\alpha)$ is the Legendre transform of τ. The interpretation of the twin relations (5.2.12) is the following. As $\delta \to 0$ the generating function, and consequently the mass exponents $\tau(q)$, are uniquely determined by the values of the coarse-grained measure equal to $\delta^{\alpha_0(q)}$, where $\alpha_0(q)$ is defined implicitly by $f'(\alpha_0(q)) = q$. The contribution of the other values of the measure is negligible in the limit $\delta \to 0$.

The above derivation of the density of singularities, based on the Laplace transform, is more deductive than the standard presentation (Halsey *et al.* (1986), Hentschel and Procaccia (1983)). Indeed, the approach presented in the literature is to show that a density of singularities of the form $\delta^{-f(\alpha)}$, where f is *assumed* to be concave (i.e. $f''(\alpha) \leq 0$), is consistent with a generating function of the form $\delta^{\tau(q)}$ when Laplace's method (see Wong (1989) or Bender and Orszag (1978)) is applied to the integral 5.2.9 in the limit $\delta \to 0$:

$$\chi_q(\delta) = \int_0^\infty \rho(\alpha)\, \delta^{\alpha q - f(\alpha)} \sim \delta^{\min_\alpha [\alpha q - f(\alpha)]} = \delta^{\tau(q)} \qquad (5.2.13b)$$

as $\delta \to 0$. By contrast, the general transforms (5.2.9)-(5.2.10) allow to deduce the density of singularities $n(\delta,\alpha)$ directly from the generating function. One advantage of this presentation is that the concavity of $f(\alpha)$ does not need to be assumed, it is derived: As long that $\tau(q)$ is a smooth function, the concavity of f follows from the concavity of τ via (5.2.12) because the Legendre transform conserves concavity. This inversion method, originally developed for probability densities by Fourcade and Tremblay (1987), was applied here to the generating function in a deterministic context.

It is emphasized that the Legendre transform (5.2.13b) can take different forms. Suppose for example that α is restricted to a finite interval $D_f = [\alpha_-,\alpha_+]$ and that f is finite at the boundaries of D_f. In this case the minimum of $\alpha q - f(\alpha)$ is not necessarily inside D_f. Indeed, the equation $f'(\alpha) = q$ does not have a solution in D_f for all q if $f'(\alpha)$ is not infinite at the boundaries of D_f. If $f'(\alpha)$ is finite everywhere in D_f the minimum occurs inside D_f if $q \in [q_-, q_+]$ where $q_- = f'(\alpha_+)$ and $q_+ = f'(\alpha_-)$. For $q \notin [q_-, q_+]$ the minimum occurs at one of the endpoints of D_f. The Legendre transform of f therefore takes two different forms:

(i) $q \in [q_-, q_+]$: $f'(\alpha) = q$ has a solution in D_f and therefore

$$\tau(q) = \alpha_0(q)q - f(\alpha_0(q)), \text{ where } f'(\alpha_0(q)) = q. \tag{5.2.13c}$$

(ii) $q \notin [q_-, q_+]$: $f'(\alpha) = q$ does not have a solution in D_f when $q \notin [q_-, q_+]$. If $q > 0$ the minimum of $\alpha q - f(\alpha)$ is in α_- while for $q < 0$ it is in α_+. It follows that

$$\tau(q) = \alpha_- q - f(\alpha_-) \text{ for } q > q_+$$
and
$$\tau(q) = \alpha_+ q - f(\alpha_+) \text{ for } q < q_- \tag{5.2.13d}$$

i.e. τ is *exactly linear* when $q \notin [q_-, q_+]$. In the case where $f'(\alpha)$ is infinite at the boundaries of D_f, while f remains finite, τ can be shown to be *asymptotically linear* in the large |q| limit. In this case we obtain a behavior similar to the multinomial measure, i.e.

$$\tau(q) \sim \alpha_{\mp} q - f(\alpha_{\mp}) \text{ as } q \to \pm\infty.$$

This result about the asymptotic behavior of τ as $|q| \to \infty$ is derived in the appendix 5.1 and appears to be original.

5.2.5 Interpretation of the multifractal spectrum

In this section, it is shown that for the multinomial measure $f(\alpha)$ has a geometrical interpretation in terms of the Hausdorff dimension of sets supporting the measure. This interpretation is the basis of the terminology "multifractal measure". Our treatment is based on Mandelbrot (1988). The pointwise scaling exponents $\alpha(x)$ (section 5.2.2) allow a natural decomposition of the support of the measure in terms of the α-singular sets $S(\alpha) = \{x: \alpha(x) = \alpha\}$, defined by a fixed value of the singularity strength. Each $S(\alpha)$ is formed of a union of multinomial sets $Z(\xi_0, ..., \xi_{M-1})$ (see section 4.2.6) of Hausdorff dimension

$$d_H(Z) = - \sum_{r=0}^{M-1} \xi_r \log_M(\xi_r).$$

Indeed $\alpha(x)$, given by (5.2.1), can also be regarded as a function $\alpha_Z(\xi_0, ..., \xi_{M-1})$ of the fractions ξ_i, and therefore a given singularity strength is associated with sets of various Hausdorff dimensions. More precisely

$$S(\alpha) = \bigcup_{\alpha_Z(\xi_0,...,\xi_{M-1}) = \alpha} Z(\xi_0, ..., \xi_{M-1}). \qquad (5.2.14)$$

As $\delta \to 0$, $n(\delta,\alpha)$ should be mainly determined by the subset $Z(\xi_0, ..., \xi_{M-1})$ of $S(\alpha)$ having the largest Hausdorff dimension $d_{H_{max}}(\alpha)$, i.e. by the "fattest" subset denoted by Z_α.

$d_{Hmax}(\alpha)$ can be obtained by maximizing the dimension function $d_H(\xi_0, ..., \xi_{M-1})$ given by (4.2.27) with respect to the ξ_i subject to the constraints $g_1 = \Sigma\xi_i - 1 = 0$ and $g_2 = \alpha_Z(\xi_0, ..., \xi_{M-1}) - \alpha = 0$. Maximizing $d_H - Q\, g_1 + P\, g_2$, where Q and P are two Lagrange multipliers, leads to $\xi_i = e^{-1}\, M^{-P}\, w_i^Q$. The first constraint then yields

$$e^{-1}\, M^{-P} \Sigma w_i^Q = 1 \Rightarrow \xi_i = \frac{w_i^Q}{\Sigma w_i^Q} .$$

The second constraint gives

$$\alpha = - \frac{\sum w_i^Q \log_M(w_i)}{\sum w_i^Q} = \frac{\partial T(Q)}{\partial Q} \quad \text{where} \quad T(Q) = - \log_M(\Sigma w_i^Q), \qquad (5.2.15)$$

which determines implicitly the multiplier $Q(\alpha)$. The maximum Hausdorff dimension becomes

$$d_{Hmax}(\alpha) = - \sum \frac{w_i^Q}{\sum w_i^Q} \log_M\left(\frac{w_i^Q}{\sum w_i^Q}\right) = - \frac{\Sigma w_i^Q \{Q \log_M(w_i) - \log_M(\Sigma w_i^Q)\}}{\Sigma w_i^Q} = Q \frac{\partial T}{\partial Q} - T.$$

$d_{Hmax}(\alpha)$ is therefore the Legendre transform of $T(Q)$, i.e.

$$d_{Hmax}(\alpha) = \min_Q \{ \alpha Q - \tau(Q) \} \qquad (5.2.16)$$

It is noticed that $\tau(q) = T(q)$, where T is given by (5.2.15). It follows that

$$d_{Hmax}(\alpha) = f(\alpha) \quad . \qquad (5.2.17)$$

The multifractal spectrum therefore reveals the Hausdorff dimension of the Z_α sets of the multinomial measure. The result (5.2.17) is based on Eggleston theorem about the Hausdorff dimension of the multinomial sets on the interval [0,1]. It is emphasized that in general (5.2.17) does not hold for any scaling measure. In the analysis of turbulent fields a test of this assumption would require a direct measurement of the dimensions of these sets. It is stressed that each Z_α is a multinomial set and consequently is dense on the unit interval. Their box dimension is therefore 1 for any α. If some weights vanish the support S of the measure is the M_e-piece Cantor set, where M_e is the number of non-vanishing weights, Z_α is replaced by $Z_\alpha \cap S$ and $f(\alpha)|_{max} = d_B(S) = d_H(S)$.

In the special case of fractal homogeneity (i.e. equal weights w_i) the mass exponents reduce to $\tau(q) = d_S(q-1)$. $f(\alpha)$ is defined only for the values of α for which $\tau'(q) = \alpha$ has a solution, i.e. for $\alpha_0 = d_S$ where $f(\alpha_0) = d_S$. This homogeneous measure, characterized by a single dimension d_S, is sometimes called *monofractal* by opposition to multifractal.

5.2.6 Properties of the functions $\tau(q)$ and $f(\alpha)$

For any scaling measure, τ and its Legendre transform $f(\alpha)$ have a few general properties that will now be derived and illustrated with the multinomial measure. $\tau(q)$ and $f(\alpha)$ were plotted in figure 5.3 and 5.4, summarizing the main results of the next two sub-sections.

5.2.6.1 Mass exponents

The properties of $\tau(q)$ are inherited from the properties of $T(q,\delta) = \log(\chi_q(\delta))/\log\delta$ because $\tau(q) = \lim_{\delta \to 0} T(q,\delta)$. The main properties of $\tau(q)$ are:

(i) $\tau(q) > 0$ for $q > 1$, $\tau(q) < 0$ for $q < 1$, $\tau(1) = 0$,

(ii) $\tau' \geq 0$,

(iii) $\tau''(q) \leq 0$,

(iv) $\tau(0) = -d_B(S)$.

(i) follows from $\chi_1(\delta) = 1$, that holds for a probability measure, and $\partial\chi_q(\delta)/\partial q \leq 0$. (ii) follows from

$$\partial T/\partial q = \frac{\partial\chi_q(\delta)/\partial q}{\chi_q(\delta)\,\log\delta} \geq 0,$$

where $\chi_q(\delta) > 0$ and $\partial\chi_q(\delta)/\partial q \leq 0$. (iii) is the result of a classical theorem of probability theory (Feller, 1966). For the property (iv), $\tau(0) = -d_B(S)$ follows from $\chi_0(\delta) = N_B(\delta)$, where S is the support of the measure.

Consider for example the function $\tau(q)$ for the multinomial measure. If w_- and w_+ denote the minimum and maximum values of the weights w_i while $n_- \geq 1$ and $n_+ \geq 1$ are the number of weights respectively equal to w_- and w_+, then from (5.2.6)

$$\tau(q) \sim -\frac{\log(n_+ w_+^q)}{\log(1/r)} \text{ as } q \to +\infty \quad \text{and} \quad \tau(q) \sim -\frac{\log(n_- w_-^q)}{\log(1/r)} \text{ as } q \to -\infty$$

and $\tau(q)$ is seen to have linear asymptotes with slopes $-\log(w_{\pm})/\log(1/r)$ as $q \to \pm\infty$ respectively.

5.2.6.2 Multifractal spectrum

We shall assume here that τ' exists and is strictly positive ($\tau' > 0$) for all q. The definition (5.2.12) then leads to

$$f(\alpha) = \alpha\, q_0(\alpha) - \tau(q_0(\alpha)) \qquad (5.2.18)$$

where

$$\tau'(q_0(\alpha)) = \alpha. \qquad (5.2.19)$$

It follows from (5.2.19) that the domain of definition of f is $D_f = [\tau'(\infty), \tau'(-\infty)] \equiv [\alpha_-, \alpha_+]$ (the concavity of τ implies that $\tau'(\infty) \leq \tau'(-\infty)$). It is emphasized that two regions of the $f(\alpha)$ curve can be distinguished: The range $\alpha < D$ (D is the topological dimension of the embedding space) characterizes the singularities of the measure ($\mu(\delta)/\delta^D \approx \delta^{\alpha-D} \to \infty$ as $\delta \to 0$) while the range $\alpha \geq D$ corresponds to non-singular behavior ($\mu(\delta)/\delta^D \leq 0$ as $\delta \to 0$). The assumption $\tau' > 0$ implies that (5.2.19) has a unique solution $q_0(\alpha)$ for each $\alpha \in D_f$, and $q_0(\alpha)$ varies in $\mathbb{R}$ when α varies in D_f. The main properties of the multifractal spectrum can be derived from the above two equations:

(i) $f''(\alpha) \leq 0$,

(ii) f has a unique maximum at $\alpha_* = \tau'(0)$ and $f(\alpha_*) = d_B(S)$,

(iii) $f(\alpha) \leq \alpha$,

(iv) $f(\alpha_{\mp}) = \lim_{q \to \pm\infty} q\,\tau'(q) - \tau(q)$,

(v) $\lim_{\alpha_{\pm}} f' = {}_{\mp}\infty$,

Differentiating (5.2.18) twice yields $f''(\alpha) = q_0'(\alpha)$ and differentiating (5.2.19) yields $q_0'(\alpha) = 1/\tau''(q_0(\alpha))$, therefore $f''(\alpha) = 1/\tau''(q_0(\alpha))$ and $\tau'' \leq 0$ implies (i). Therefore f has a unique maximum in $\alpha = \alpha_*$ where $f'(\alpha_*) = q_0(\alpha_*) = 0$, and (ii) follows from (5.2.18)

and $\tau(0) = -d_B(S)$. The third property follows from Young's inequality: For any $(\alpha, q) \in D_f \times \mathbb{R}$, $\alpha\, q - \tau(q) \geq f(\alpha)$ which follows from the definition of f. But $\tau(q) \geq 0$ for $q \geq 1$ hence for any $q \geq 1$ and $\alpha \in D_f$ we have $\alpha\, q - f(\alpha) \geq 0$, and (iii) then follows from $q \geq 1$. (iv) follows directly from (5.2.18), (5.2.19) and $q_0(\alpha) \in \mathbb{R}$ while (v) follows from $f'(\alpha) = q_0(\alpha)$.

Some of these results will now be illustrated with the multinomial measure. The boundaries of D_f are given by

$$\alpha_- = -\frac{\log(w_+)}{\log(1/r)} \quad \text{and} \quad \alpha_+ = -\frac{\log(w_-)}{\log(1/r)}$$

and (ii) implies

$$\alpha_* = -\frac{1}{M_e} \sum_{w_i \neq 0} \frac{\log(w_i)}{\log(1/r)} \quad \text{and} \quad f(\alpha_*) = \frac{\log M_e}{\log(1/r)}$$

where M_e is the number of non-zero weights w_i. With (5.2.6) , (iv) leads to

$$f(\alpha_\pm) = \frac{\log(n_\mp)}{\log(1/r)} \geq 0$$

and therefore $f(\alpha) \geq 0$ everywhere.

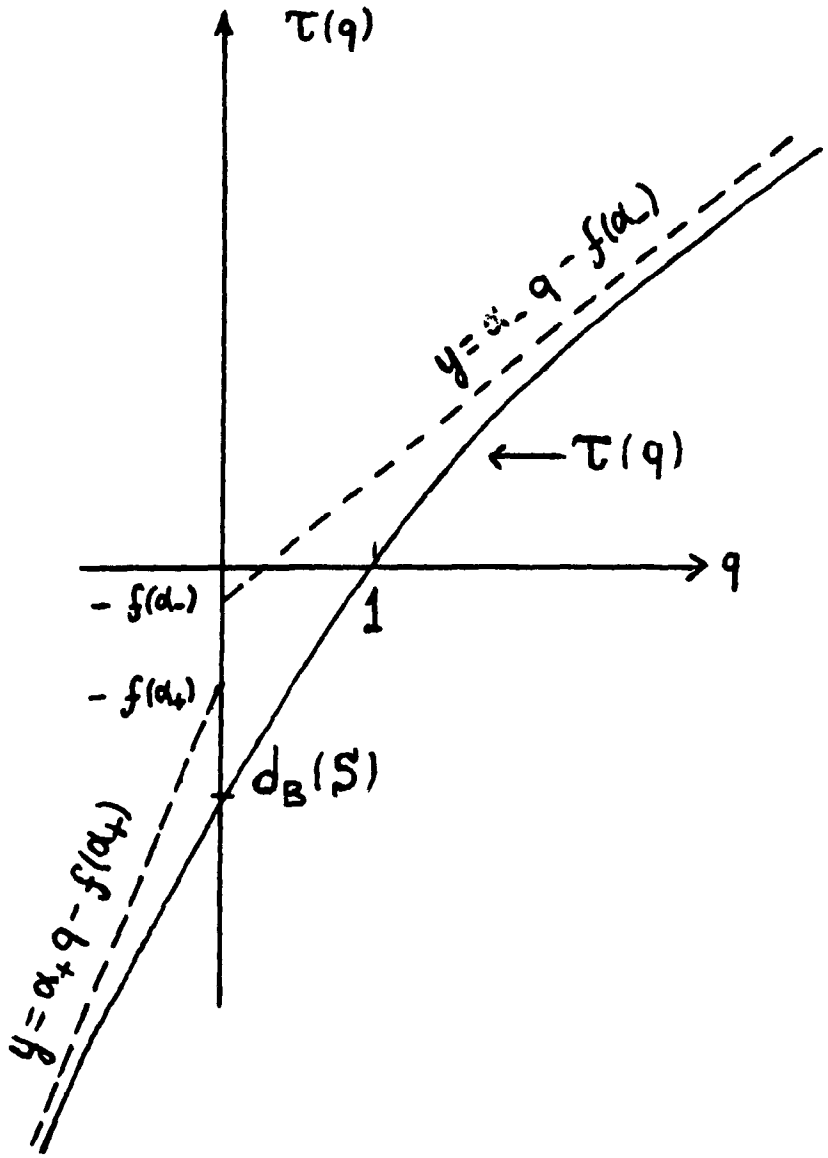

Figure 5.3: The function τ(q) for a deterministic scaling measure. For the multinomial measure

$$d_B(S) = \frac{\log M_e}{\log(1/r)},$$

$$\alpha_- = -\log(w_+)/\log(1/r), \qquad \alpha_+ = -\log(w_-)/\log(1/r),$$

$$f(\alpha_-) = \log(n_+)/\log(1/r), \qquad f(\alpha_+) = \log(n_-)/\log(1/r)$$

where $w_\pm$ are the maximum and minimum values of the weights w_i, M_e is the number of non-zero weights, n_+ and n_- the number of weights equal respectively to w_+ and w_-, and r the scale ratio of the cascade.

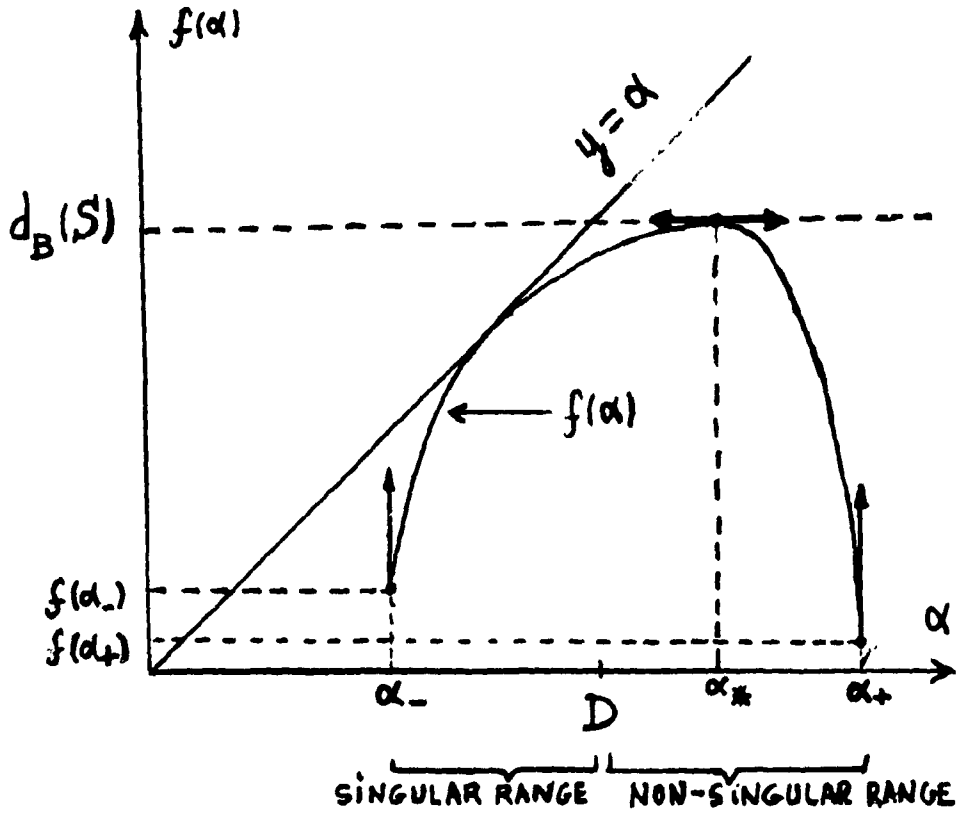

Figure 5.4: The function f(α) for a deterministic scaling measure. For the multinomial measure,

$$\alpha_* = -\frac{1}{M_e} \sum_{w_i \neq 0} \log(w_i)/\log(1/r).$$

See figure 5.3 for the values of the other parameters.

5.2.7 Non-concave multifractal spectrum

So far, we have defined scaling measures by the scaling behavior of their generating function. Alternately, scaling measures can be defined directly via the scaling behavior of their density of singularities. In this case we emphasize that $f(\alpha)$ is *not necessarily concave*. For example, the sum of two scaling measures with concave multifractal spectra $f_1(\alpha)$ and $f_2(\alpha)$ yields a total density of singularity $n(\delta) \sim \delta^{-f_1(\alpha)} + \delta^{-f_2(\alpha)}$ if the supports of the two measures are separated (the prefactors of each density of singularity are not written for simplicity). In the limit $\delta \to 0$ we get $n(\delta) \sim \delta^{-f(\alpha)}$ where $f(\alpha) = \max\{f_1(\alpha), f_2(\alpha)\}$, which is not a concave function in general (see figure 5.4b). In this case the generating function is $\chi_q(\delta) = \delta^{\tau_1(q)} + \delta^{\tau_2(q)} \sim \delta^{\min\{\tau_1(q), \tau_1(q)\}}$ as $\delta \to 0$ and therefore $\tau(q) = \min\{\tau_1(q), \tau_2(q)\}$. Even if $f(\alpha)$ is not concave the corresponding $\tau(q)$ remains concave (τ is *always* concave) but exhibits in general discontinuities in its derivative at the intersection points of τ_1 and τ_2 (see figure 5.4b).

In this example we chose τ_1 and τ_2 so that they cross only in $q = 1$ and $f'(\alpha)$ is infinite at the boundaries of the domain of definitions of f_1 and f_2. This intersection point defines two critical values of α, namely $\alpha_1 = \tau'_1(1)$ and $\alpha_2 = \tau'_2(1)$. Since $f(\alpha) = q\tau'(q) - \tau(q)$ where $\tau'(q) = \alpha$ and $f'(q) = \alpha$, using $q = 1$ yields

$$\begin{cases} \alpha_1 = \tau'_1(1),\ \alpha_2 = \tau'_2(1) \\ f'(\alpha_1) = f'(\alpha_2) = 1 \\ f(\alpha_1) = \alpha_1,\ f(\alpha_2) = \alpha_2. \end{cases} \qquad (5.2.20)$$

The non-concave part of $f(\alpha)$, in the range $\alpha_1 \le \alpha \le \alpha_2$, does not contribute to the generating function in the limit $\delta \to 0$. Indeed, we will now show that the following truncated density of singularities (see figure 5.4b)

$$n(\delta,\alpha) = \delta^{-f_1(\alpha)}\,[1 - \theta(\alpha - \alpha_1)] + \delta^{-f_2(\alpha)}\,\theta(\alpha - \alpha_2) \qquad (5.2.21)$$

yields the correct $\chi_q(\delta)$ as $\delta \to 0$ (θ is the Heaviside function: $\theta(x) = 1$ for $x \geq 1$ and $\theta(x) = 0$ elsewhere). The first term of (5.2.21) on the right hand side makes the following contribution to $\chi_q(\delta)$:

$$I_1(\delta) = \int_{-\infty}^{\alpha_1} \delta^{\alpha q - f_1(\alpha)} \, d\alpha.$$

If $q > f_1'(\alpha_1) = 1$ the minimum of $\alpha q - f_1(\alpha)$ lies in the range $\alpha < \alpha_1$, while for $q < 1$ it is in α_1. Hence, using (5.2.13c&d) yields

$$I_1(\delta) \sim \delta^{\tau_1(q)} \, \theta(q - 1) + \delta^{\alpha_1 q - f_1(\alpha)} \, (1 - \theta(q - 1))$$

as $\delta \to 0$. A similar result $I_2(\delta)$ is obtained from the second term of (5.2.21). Adding I_1 and I_2, using (5.2.20) and factorizing yields

$$\chi_q(\delta) \sim [\delta^{\tau_1(q)} + \delta^{\tau'_2(1)(q - 1)}] \, \theta(q - 1) + [\delta^{\tau_2(q)} + \delta^{\tau'_1(1)(q - 1)}] \, (1 - \theta(q - 1)).$$

But we see from figure 5.4b that

$$\begin{cases} \tau_1(q) < \tau_2'(1)(q - 1) \text{ for } q > 1 \\ \tau_2(q) < \tau_1'(1)(q - 1) \text{ for } q < 1 \end{cases}$$

and therefore

$$\chi_q(\delta) \sim \delta^{\tau_1(q)} \, \theta(q - 1) + \delta^{\tau_2(q)} \, (1 - \theta(q - 1)),$$

which is the exact asymptotic form of $\chi_q(\delta)$ as $\delta \to 0$.

We conclude that different $f(\alpha)$ spectra can share the same mass exponent function $\tau(q)$, i.e. τ does not define uniquely the multifractal spectrum. The relation $\tau(q)$-$f(\alpha)$ is one-to-one when $\tau(q)$ is smooth, i.e. differentiable everywhere, which is the case studied by most authors. The possibility of a non-concave $f(\alpha)$ for scaling measures does not appear to have been noticed previously.

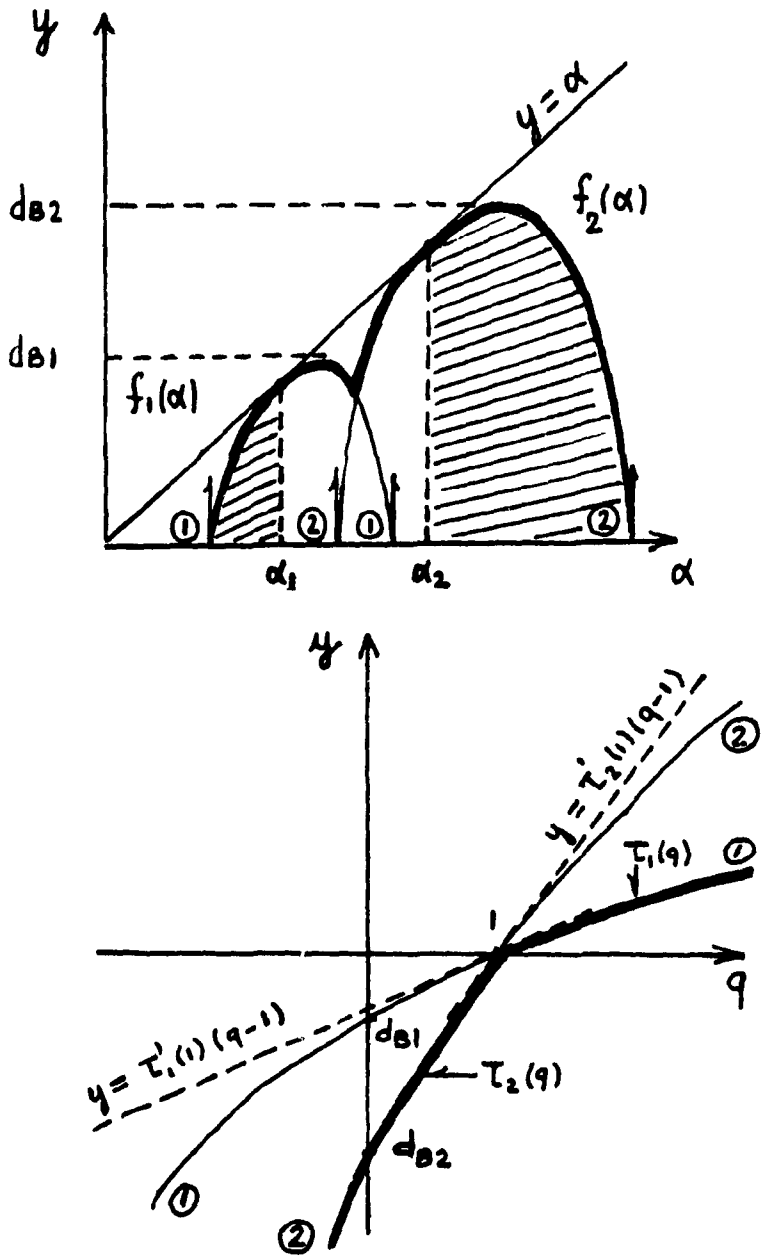

Figure 5.4b: Top: The two multifractal spectra f_1 and f_2 of the measures μ_1 and μ_2 are plotted on the same graph. The darker curve $f(\alpha) = \max\{f_1(\alpha), f_2(\alpha)\}$ is the resulting spectrum for the total measure $\mu = \mu_1 + \mu_2$ when the supports of μ_1 and μ_2 are separated. The hatched area indicates the part of $f(\alpha)$ that contributes effectively to the generating function in the limit $\delta \to 0$. The non-convex part of f, between α_1 and α_2, does not contribute to $\chi_q(\delta)$ as $\delta \to 0$. Bottom: The two mass exponent functions τ_1 and τ_2 of μ_1 and μ_2 are plotted on the same graph. The darker curve is the resulting spectrum $\tau(q)$ for the total measure. $\tau(q)$ is concave but is not differentiable in $q = 1$.

5.3 Multiscale self-similar measures

5.3.1 Definition

A natural generalization of exact self-similarity for measures is *multiscale self-similarity*, where the pieces generated at each construction step are allowed to have different sizes. Such measures have been used in particular by Hentschel and Procaccia (1983) as a model of the invariant probability measure associated with a non-linear chaotic dynamical system. In this context, the measure is defined through the motion of a point in space: Given for example a discrete-time orbit $\{x_i\}$, i=1, 2, ... where $x_i \in \mathbb{R}^D$, the space is divided in cubes of size δ and the probability measure of a given cube is defined to be the fraction of time spent by x_i in the cube. They showed that multiscale self-similarity was flexible enough to account for the scaling properties of the generating function for some dynamical systems.

For a multiscale self-similar measure the support S is composed of M disjoint copies S_i scaled down by different ratios $r_1, r_2, ..., r_M$. By definition, the normalized measure defined on each S_i (see section 5.2.1) is self-similar to the full measure. For example, the *multiscale Cantor measure* (figure 5.5) is constructed by replacing a unit cube of probability measure 1 by M disjoint subcubes of sizes $r_1 \leq ... \leq r_M \leq 1$ and measures $w_1, \ldots, w_M$, the total measure being conserved. This process is then repeated *ad infinitum* on each subcube: Each cube of size l_i and measure m_i is replaced by M subcubes of sizes $r_1 l_i \leq \ldots \leq r_M l_i$ and measures $w_1 m_i, ..., w_M m_i$. The special case of equal scale ratios corresponds to the exactly self-similar multinomial measure.

A multiscale self-similar measure also gives rise to a spectrum of pointwise scaling exponents, which can be shown by considering an expansion adapted to this model. The position of a point of the support of this measure can be determined by the sequence $n_1 n_2 \ldots$ where n_i is the label of the set S_i chosen at level i of construction. One may consider the set of

Figure 5.5: A two scale Cantor measure with r_1=0.25, r_2=0.4, w_1=0.6, w_2=0.4. The height of the bars at the n^{th} stage is proportional to the average density $\rho_i=\mu_i/\delta_i$, where μ_i is the measure of the segment of length δ_i.

points I' for which the fractions n_i/n converge as $n \to \infty$. For any point in I' the pointwise scaling exponent exists and takes the same form than the one obtained for the multinomial measure.

5.3.2 Generating function, mass exponents and multifractal spectrum

The generating function satisfies the renormalization equation

$$\chi_q(\delta) = \sum_{i=1}^{M} w_i^q \, \chi_q(\delta/r_i), \tag{5.3.1}$$

a direct generalization of (5.2.4). Let us define $\tau_0(q)$ to be the real root of

$$\sum_{i=1}^{M} w_i^q \; r_i^{-\tau(q)} = 1. \tag{5.3.2}$$

$\tau_0(q)$ exists and is unique because $\partial\tau_0(q)/\partial q > 0$, which can be checked by differentiating (5.3.2) and using the constraints $0 < w_i < 1$ and $0 < r_i < 1$. Substituting $\chi_q(\delta) = \delta^{\tau_0(q)} P_q(\delta)$ in (5.3.1) leads to the prefactor equation

$$P_q(\delta) = \sum_{i=1}^{M} w_i^q \, r_i^{-\tau_0(q)} \, P_q(\delta/r_i), \tag{5.3.3}$$

which is in a form identical to the prefactor equation of $N_B(\delta)$ in the case of a multiscale self-similar set. Using the results of the appendix 4.1, the generic solution of (5.3.1) becomes

$$\chi_q(\delta) = \delta^{\tau_0(q)} \{ c_0 + R_q(\delta) \}, \tag{5.3.4}$$

where $R_q(\delta) \to 0$ as $\delta \to 0$, and therefore the prefactor of $\chi_q(\delta)$ is constant in the limit $\delta \to 0$. The mass exponents of a multiscale self-similar measure is therefore $\tau_0(q)$, the real root of (5.3.2). The introduction of incommensurate scale ratios r_i is found to spoil the periodic oscillations of the prefactor of the generating function, as for $N_B(\delta)$ with multiscale self-similar

sets. The density of singularities is obtained from $\chi_q(\delta)$ with the transform (5.2.10) and the saddle point method implies that $f(\alpha)$ is the Legendre transform of $\tau_0(q)$. This treatment has the originality of showing clearly the analogies between the renormalization equations satisfied by $N_B(\delta)$ and $\chi_q(\delta)$ for multiscale self-similar sets and measures respectively.

5.4 GENERALIZATION TO RANDOM MEASURES

5.4.1 Generating function and multifractal spectrum

Randomness is an essential ingredient of turbulent fields in general, and of the energy cascade process in particular. In this section we generalize the concepts of generating function and multifractal spectrum to random measures in a way that allows the renormalization arguments to be extended directly to random self-similar measures. Consider a statistical ensemble of measures sharing the same support of topological dimension D (e.g. a line segment). We define the generating function $\chi^*_q(\delta)$ of this random measure by

$$\chi^*_q(\delta) = < \chi_q(\delta) >, \tag{5.4.1}$$

where $\chi_q(\delta)$ is computed on each realization. It follows from (5.4.1) that

$$\chi^*_q(\delta) = \delta^{-D} < (\mu(\delta))^q > \tag{5.4.2}$$

if the random measure is spatially homogeneous. Pursuing the analogy with deterministic measures, the generalized mass exponents $\tau^*(q)$ are defined by

$$\tau^*(q) = \lim_{\delta \to 0} \log(\chi^*_q(\delta))/\log\delta. \tag{5.4.3}$$

Using (5.4.2) yields

$$\tau^*(q) = -D + \lim_{\delta \to 0} \frac{\log <(\mu(\delta))^q>}{\log\delta}. \tag{5.4.4}$$

A random measure for which $\tau^*(q)$ exists and is finite for all q will be called a *random scaling measure*. The singularity strength $\alpha(\delta)$ is now a random variable parametrized by δ, defined implicitly by

$$\mu(\delta) = \delta^{\alpha(\delta)}. \tag{5.4.5}$$

If $g(\alpha,\delta)$ denotes the probability density of $\alpha(\delta)$, then the generalized density of singularities is

$$n^*(\delta,\alpha) = \delta^{-D}\, g(\alpha,\delta) \tag{5.4.6}$$

As in the deterministic case, $\chi^*_q(\delta)$ and $n^*(\delta,\alpha)$ are related by the pair of integral transforms (5.2.9) and (5.2.10). In the limit $\delta \to 0$, it follows from the saddle point method that

$$n^*(\delta,\alpha) \sim P^*(\delta,\alpha)\, \delta^{-f^*(\alpha)},$$

where $\log(P^*(\delta,\alpha))/\log\delta \to 0$, and where the generalized multifractal spectrum is given by

$$f^*(\alpha) = \min_q\{\alpha q - \tau^*(q)\}, \tag{5.4.7}$$

i.e. $f^*(\alpha)$ is the Legendre transform of $\tau^*(q)$. The general properties of τ^* and f^* (section 5.2.6) remain unchanged except for a few exceptions: Firstly, the constraint $\tau^{*\prime\prime}(q) \le 0$ does not prevent τ from being negative for q large enough; secondly, $f^*(\alpha)$ no longer needs to be positive. Indeed the Legendre transform of a function satisfying $\tau'' \le 0$ is not, in general, positive definite. Fourcade and Tremblay (1987) claimed that a negative range for $f^*(\alpha)$ appears to be possible only in the context of random measures.

Remark 1: The scaling of a random measure is sometimes studied (Mandelbrot (1974), Schertzer and Lovejoy (1985)) in terms of an *average density* $\rho(\delta) = \mu(\delta)/\delta^D$ and the singularity strength γ is given by $\rho(\delta) = \delta^{-\gamma}$. Scaling exponents are then defined by

$$K(q) = -\lim_{\delta \to 0} \frac{\log\langle(\rho(\delta))^q\rangle}{\log\delta} \tag{5.4.8a}$$

and the density of singularity takes the form $n(\delta, \gamma) = \delta^{C(\gamma)}$ where

$$C(\gamma) = \max_q\{\gamma q - K(q)\} \tag{5.4.8b}$$

It follows from (5.4.8a) that $\tau^*(q)$ and $K(q)$ are related by

$$\tau^*(q) = D\,(q - 1) - K(q). \qquad (5.4.9a)$$

γ and the function $C(\gamma)$ are related to α and $f(\alpha)$ by

$$\gamma = D - \alpha \quad \text{and} \quad C(\gamma) = D - f(\alpha), \qquad (5.4.9b)$$

which follows from (5.4.8b). $C(\gamma)$ is then called the *codimension function*. (5.48a-b) are essentially the definitions used in section 3.3.3 for the energy dissipation field in one of our formulations of the 3rd Kolmogorov hypothesis.

Remark 2: The idea of using scaling probability densities to obtain multiscaling moments has been used in turbulence by Frisch and Parisi (appendix of Frisch 1983) to explain the nonlinear scaling exponents of the velocity structure functions $\langle(\Delta v(L))^h\rangle$ for $h \geq 4$, as observed by Anselmet *et al.* (1984). They suggested that the probability density of α, defined implicitly by $\Delta v(L) = L^\alpha$, was of the form $\rho(\alpha)\, L^{C(\alpha)}$. It follows that

$$\langle(\Delta v(L))^h\rangle = \int \rho(\alpha)\, L^{\alpha h - C(\alpha)}\, d\alpha \sim L^{\zeta(h)}$$

as $L \to 0$, where $\zeta(h) = \min_\alpha\{\alpha h - C(\alpha)\}$. It should be noted that neither $\Delta v(L)$ nor $|\Delta v(L)|$ define a measure. In this context α is interpreted as a kind of statistical Holder exponent for the velocity field (see chapter 2 for a discussion of Holder exponent). The geometrical interpretation of $C(\alpha)$ remains unclear.

5.4.2 The random multinomial measure (microcanonical case)

In this section the concept of self-similarity is extended to random measures, and we show how the previous renormalization equations for the generating function can be generalized to the stochastic case. The possibility of a negative $f^*(\alpha)$ for random measures is examined. We start with a simple example: The random multinomial measure. The difference between the deterministic and the random multinomial measure is that the weights used in the construction are not rigidly fixed, they are random variables W_i. The variables W_i at different stages of construction are assumed to be independent. The total weight of a segment (or a square or a cube...) is exactly conserved in the construction, i.e.

$$\sum_{i=1}^{M} W_i = 1, \tag{5.4.10}$$

which implies that the variables W_i at a same stage of construction are correlated. Random cascade processes with this property of conservation were called *microcanonical* or *conservative* by Mandelbrot (1974). The constraint (5.4.10) implies $W_i \leq 1$ and $\langle W \rangle = 1/M$. A realization of a random binomial measure is given in figure 5.6.

The renormalization argument used in the deterministic case can be generalized to this random measure. The support S of a realization of the random measure splits into M subsets S_j that are statistically self-similar to S, but scaled down by a factor r. For the generating function, the statistical self-similarity of the measure is expressed by

$$\chi_q(\delta;S_i) \stackrel{d}{=} W_i^q \; \chi_q(\delta/r;S), \tag{5.4.11}$$

where " $\stackrel{d}{=}$ " denotes the equality in probability distribution, and where W_i and $\chi_q(\delta;S)$ are statistically independent. If the sets S_j are separated and if $\delta < \min d(S_i,S_j)$, then

$$\chi_q(\delta;S) = \sum_{i=1}^{M} \chi_q(\delta;S_i), \tag{5.4.12}$$

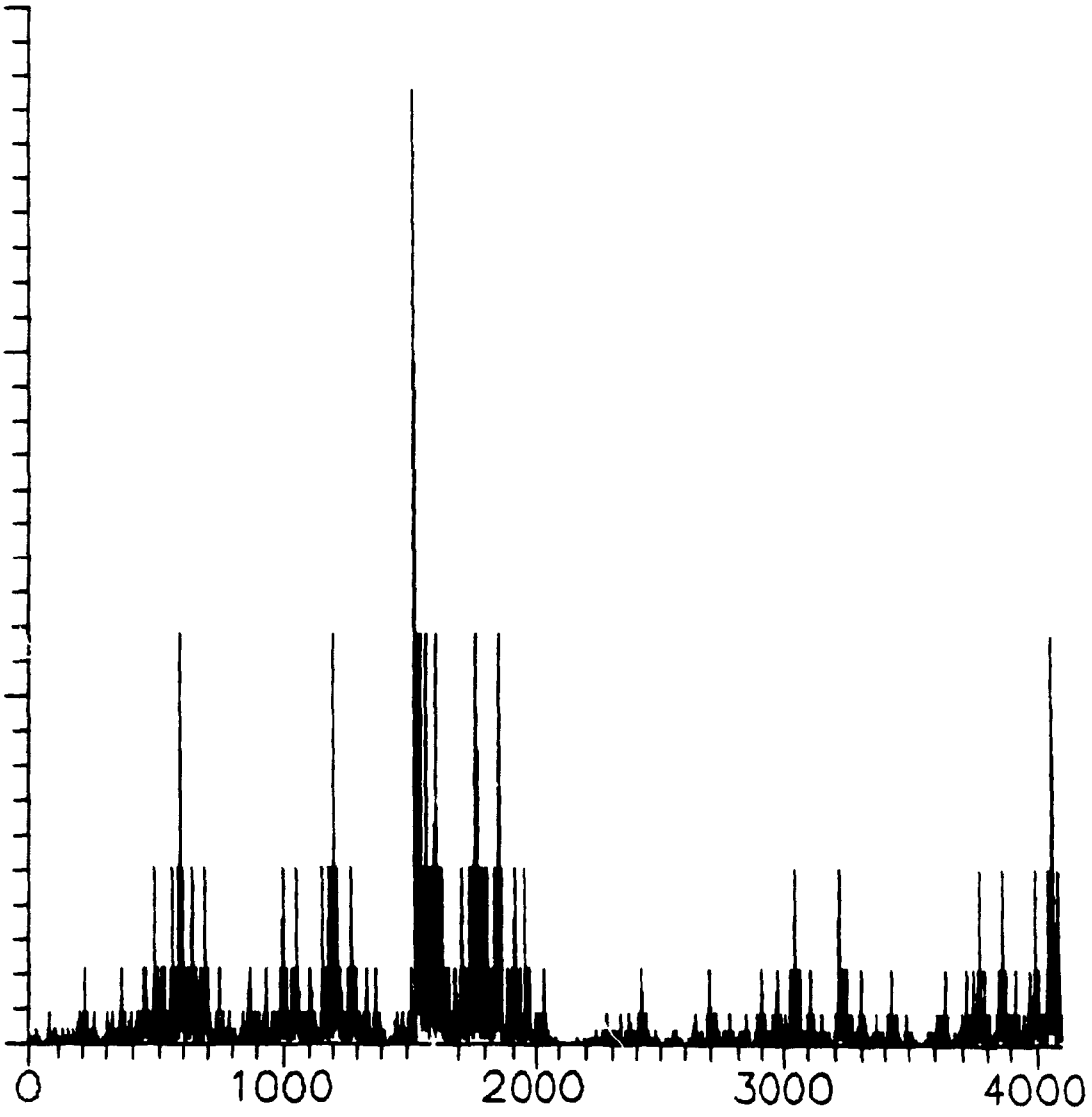

Figure 5.6: A random binomial measure with $w_1 = 0.3$ and $w_2 = 0.7$, coarse-grained at scale $1/2^{12}$. At each cascade step the location (left or right) of the weights is chosen randomly with equal probability.

Using (5.4.11), it follows from (5.4.12) that

$$\chi_q(\delta;S) \stackrel{d}{=} \sum_{i=1}^{M} W_i^q \, \chi_q(\delta/r;S)|_i, \tag{5.4.13}$$

where the variables $\chi_q(\delta/r;S)|_i$ are independent and identically distributed. A statistical averaging on (5.4.13) yields (the argument S is dropped for simplicity)

$$\chi^*_q(\delta) = M \langle W^q \rangle \, \chi^*_q(\delta/r). \tag{5.4.14}$$

The general solution of (5.4.14) is

$$\chi^*_q(\delta_n) = \delta_r^{\tau^*(q)} P_q(\log\delta) \quad \text{where} \quad \tau^*(q) = - d_S - \frac{\log\langle W^q \rangle}{\log(1/r)}, \tag{5.4.15}$$

with $d_S = \log(M)/\log(1/r)$ and $P_q(\log\delta+\log(1/r)) = P_q(\log\delta)$. Periodic oscillations of the prefactor are therefore also obtained in the stochastic case. The renormalization equation (5.4.14) can be directly generalized to the case of a multiscale random measure. Some specific values of $\tau^*(q)$ are

$$\tau^*(0) = - d_S - \frac{\log(1 - p_0)}{\log(1/r)} \quad \text{and} \quad \tau^*(1) = 1 - d_S,$$

where $p_0 = \text{Prob}\{W = 0\}$. The unique maximum of f^* occurs in

$$\alpha_* = \tau^{*\prime}(0) = - \frac{1}{1-p_0} \left\langle \frac{\log W}{\log(1/r)} \right\rangle \quad \text{and} \quad f^*(\alpha_*) = - \tau^*(0) = d_S + \frac{\log(1-p_0)}{\log(1/r)}$$

In this model the weights W_i are random but their positions are constrained by a rigid grid. In a more general model these positions could be chosen randomly at each cascade step, thus removing the artificial "grid-effect". As long that the randomly positioned daughter subsegments remain contained in their mother segment, the renormalization equation (5.4.14) still holds and consequently the prefactor may still oscillate. Therefore the oscillations are not

necessarily produced by the rigidity of the splitting grid, but are rather due to the existence of privileged scale ratios.

It will now be shown that $f^*(\alpha)$ can be negative for the random multinomial measure. Assume for example that W has a discrete and bounded probability distribution, with w_- and w_+ denoting the minimum and maximum values of W. $\tau^*(q)$ becomes

$$\tau^*(q) = - d_S - \log\{\sum_{i=1}^{m} p_i w_i^q \}/\log(1/r),$$

where $p_i = \text{Prob}\{W = w_i\}$. If p_+ and p_- denote the probabilities corresponding to w_+ and w_- respectively, then

$$\tau^*(q) \sim - \log(p_+ w_+^q)/\log(1/r) \text{ as } q \to +\infty \text{ and } \tau^*(q) \sim - \log(p_- w_-^q)/\log(1/r) \text{ as } q \to -\infty.$$

The limit values of f, obtained with the limits (iv) (section 5.2.6.2), are

$$f^*(\alpha_+) = d_S + \log(p_-)/\log(1/r) \quad \text{and} \quad f^*(\alpha_-) = d_S + \log(p_+)/\log(1/r) \qquad (5.4.16)$$

and are therefore negative if p_- or $p_+ < (1/r)^{d_S}$ respectively. Notice that negative dimensions corresponds to *decaying* singularity strengths: Indeed the number of values of $\alpha(\delta)$ with $\alpha < \alpha(\delta) < \alpha+d\alpha$ is proportional to $\delta^{-f^*(\alpha)}$ (within a logarithmic correction) and therefore goes to zero as $\delta \to 0$ when $f^*(\alpha) < 0$. It also follows that $f^*(\alpha)$ cannot be interpreted as a Hausdorff dimension in the negative range since fractal dimensions are always positive. This example illustrates the fact that $f^*(\alpha)$ does not have in general an interpretation in terms of dimension.

5.4.3 The random multinomial measure (canonical case)

In addition to the possible emergence of a negative range for $f^*(\alpha)$, randomness also brings the possibility of divergent generating functions and unusual behaviors of the mass exponents, e.g. $\tau^*(q) < 0$ for $q > 0$. This can be illustrated with the *canonical* random multinomial measure, obtained from the previous model by replacing the constraint of exact conservation (5.4.10) by a condition of conservation on the average:

$$< \sum_{i=1}^{M} W_i > = 1 \Rightarrow < W > = 1/M. \qquad (5.4.17)$$

By contrast with the previous model, the weights are independent of each other at a given level of construction. In addition, they are no longer constrained by $W_i \leq 1$, i=1, ..., M, which makes room for larger values of the multiplicative factors W_i. The weaker constraint (5.4.17) of conservation on the average implies that the total measure of a realization obtained after an infinite number of cascade steps is no longer unity, but is rather a random variable. Hence the canonical process does not generate a probability measure. The renormalization equation (5.4.14) and its solution (5.4.15) still hold. However a complication arises from the non-conservation of the measure: The measure $\mu_n(\delta)$ obtained after n steps of construction is affected in general by the cascade steps arising at scales smaller than δ, and one must worry about the convergence of $<(\mu_n(\delta))^q>$ as $n \to \infty$. When large tail probability densities are used for W, we shall now see that the periodic prefactor of $\chi^*_q(\delta_n)$ in (5.4.15) may diverge for some q in the limit $n \to \infty$.

For reasons of symmetry, the initial measure given to [0,1] at the beginning of the construction will be made random and equal to W (this slight departure from Mandelbrot's convention (1974), where the initial measure is unity, brings significant simplifications later on). Denoting by $\mu(\delta_n)$ the measure of an interval of size $\delta_n = r^n$, it is seen that

$$< (\mu(\delta_n))^q > = <W^q>^n <(\mu(\delta_0))^q> = \delta_n^{\tau^*(q)+D} <(\mu(\delta_0))^q> , \qquad (5.4.18)$$

where $\mu(\delta_0)$ is the order-q moment of the total measure generated by the fully constructed cascade process (figure 5.7 for a graphical explanation of (5.4.18)). In the microcanonical case, the exact conservation of the measure implies trivially that $\mu(\delta_0) = 1$. In the canonical model, however, two alternatives arise:

(i) $<(\mu(\delta_0))^q>$ is finite for all q,

(ii) $<(\mu(\delta_0))^q>$ diverges when $q > q_c \geq 1$.

In the first case, $<(\mu(\delta_0))^q>$ becomes independent of the construction inner scale η as $\eta \to 0$ (or equivalently of the number of cascade steps n) and the scaling of the generating function is not affected by the factor $<(\mu(\delta_0))^q>$. In the second case however, $<(\mu(\delta_0))^q>$ keeps a strong dependence on η as $\eta \to 0$. This dependence changes the scaling of $\chi^*_q(\delta_n)$ and results in the divergence of $<(\mu(\delta_0))^q>$.

This phenomenon of divergence of moments, first examined by Mandelbrot (1974), arises when the field is very intermittent. Cascade steps at large scale allow the determination of the low order moments of $\mu(\delta)$, while high order moments - representative of rare fluctuations - are essentially determined by cascade steps arising at scales smaller than δ. The origin of the divergence can be briefly explained as follows. If μ_n denotes the measure obtained after n steps of construction then $\mu_n(\delta_0)$ is the total measure of the field constructed down to scale δ_n. The multiplicative structure of the field implies

$$\mu_{n+1}(\delta_0) \stackrel{d}{=} W \sum_{i=1}^{M} \mu_{n,i}(\delta_0) \quad \text{with} \quad \mu_0(\delta_0) = W \quad \text{and} \quad n = 0, 1, 2 \ldots \qquad (5.4.19)$$

where " $\stackrel{d}{=}$ " denotes an equality in probability distribution, and where $\mu_{n,i}(\delta_0)$ and

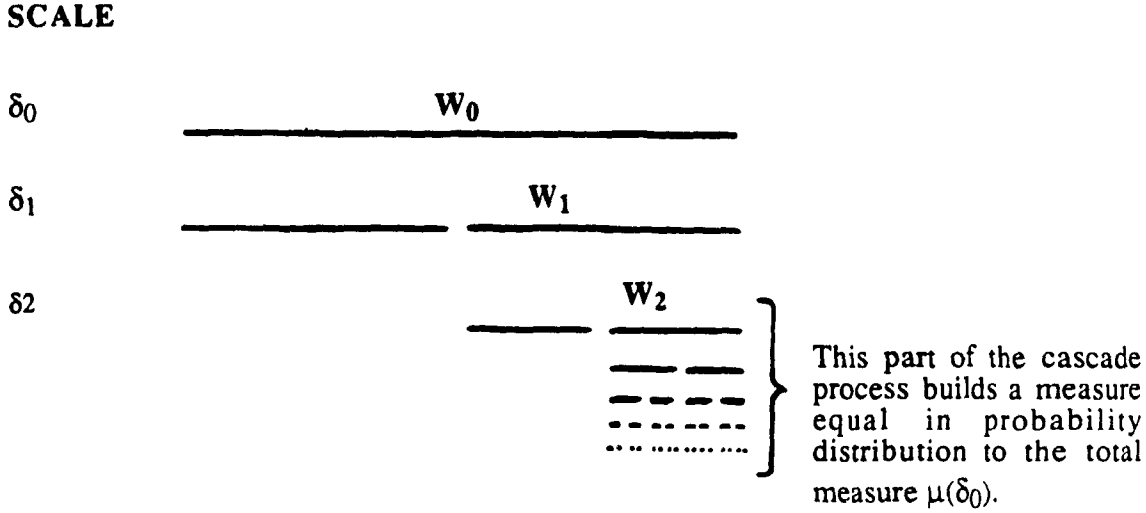

Hence

$$\mu(\delta_2) \stackrel{d}{=} W_0 W_1 \mu(\delta_0)$$

where "$\stackrel{d}{=}$" denotes the equality in probability distribution and where the random variables W_0, W_1 and $\mu(\delta_0)$ are independent. Raising to the power q and averaging yields

$$\langle(\mu(\delta_2))^q\rangle = \langle W^q\rangle^2 \langle(\mu(\delta_0))^2\rangle,$$

a special case of the general result (5.4.18).

Figure 5.7: Graphical explanation of the relation (5.4.18) in the special case of a 1-D cascade with splitting factor M = 2.

W are independent statistically (see figure 5.8 for a graphical explanation of (5.4.19)). Using $\langle W \rangle = 1/M$ (see (5.4.17)), (5.4.19) implies that

$$\langle \mu_{n+1}(\delta_0) \rangle = \langle \mu_n(\delta_0) \rangle = \langle \mu_0(\delta_0) \rangle = 1/M,$$

i.e. the random series $\{\mu_n(\delta_0)\}$ is a *martingale*. A recurrence relation for $\langle (\mu_n(\delta_0))^q \rangle$ can be derived from (5.4.19) by raising both sides to an integer power q and averaging:

$$\langle (\mu_{n+1}(\delta_0))^q \rangle = \langle W^q \rangle \langle \{ \sum_{i=1}^{M} \mu_{n,i}(\delta_0) \}^q \rangle \quad . \tag{5.4.20}$$

In the special case q = 2, (5.4.20) becomes (making use of the independence of the $\mu_{n,i}(\delta_0)$)

$$\langle (\mu_{n+1}(\delta_0))^2 \rangle = \langle W^2 \rangle \{ M \langle (\mu_n(\delta_0))^2 \rangle + 1 - 1/M^2 \}$$

and therefore $\langle (\mu_n(\delta_0))^2 \rangle$ diverges as $n \to \infty$ if $\langle W^2 \rangle M > 1 \iff \langle W^2 \rangle > 1/M$. More generally, Mandelbrot conjectured that divergence happens for $q > 1$ if and only if

$$\langle W^q \rangle > 1/M, \tag{5.4.21}$$

which defines a divergence range $q > q_c > 1$, where q_c is defined by $\langle W^{q_c} \rangle = 1/M$. This result was proved rigorously by Kahane and Peyrière (1976). Using (5.4.9) and (5.4.15), (5.4.21) is equivalent to

$$\tau^*(q) < 0 \qquad \text{or} \qquad K(q) > D(q - 1), \tag{5.4.22}$$

When W has a discrete probability distribution, it was shown that $\tau^*(q) > 0$ for $q > 1$ and therefore divergence of moments does not occur. For more general unbounded distributions however, (5.4.22) may be satisfied in the range $q > q_c$, where $q_c > 1$ is defined by $\tau^*(q_c) = 0$.

One cascade steps ($n = 1$, $\delta_1 = 1/2$)

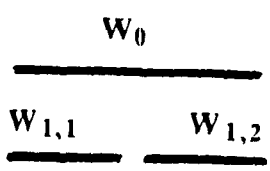

=> Total measure $\equiv \mu_1(\delta_0)$

Two cascade steps ($n = 2$, $\delta_2 = (1/2)^2$)

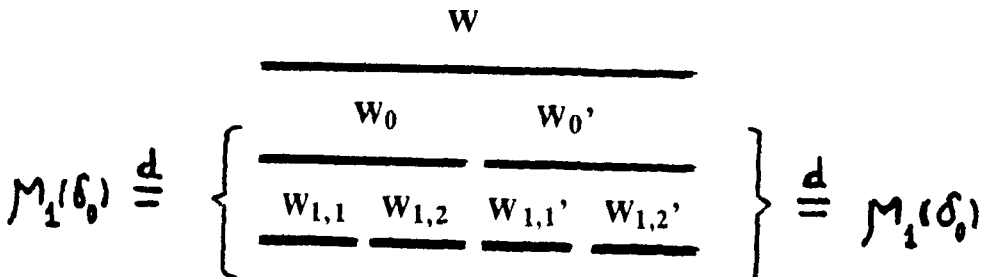

=> Total measure $\equiv \mu_2(\delta_0)$

$= W \{\mu_{1,1}(\delta_0) + \mu_{1,2}(\delta_0)\}$

where $\mu_{1,1}(\delta_0)$ and $\mu_{1,2}(\delta_0)$ are independent and identically distributed. This a special case of the general relation (5.4.19).

Figure 5.8: A graphical explanation of the recurrence relation (5.4.19) in the special case of a one dimensional cascade with splitting factor M = 2.

In the divergent case it is interesting to examine the asymptotic expression of $<(\mu_n(\delta))^q>$ in the limit of large but finite n. As seen from (5.4.20), for an integer $q > q_c$

$$<(\mu_n(\delta_0))^q> \sim k(q)\,(M<W^q>)^n \tag{5.4.23}$$

as $n\to\infty$, where k(q) is a constant. With $r^n = \eta/\delta$ and (5.4.15), where η is the inner construction scale of the cascade process, this becomes

$$<(\mu_n(\delta_0))^q> \sim k(q)\,(\eta/\delta)^{\tau^*(q)}. \tag{5.4.24}$$

$\tau^*(q) < 0$ for $q > q_c$ and therefore $<(\mu_n(\delta_0))^q>\to\infty$ as $\eta\to 0$ as expected. (5.4.18) finally leads to

$$\begin{cases} q < q_c,\ <(\mu(\delta))^q> \sim \delta^{\tau^*(q)+D}\,<(\mu(\delta_0))^q> \\ q > q_c,\ <(\mu(\delta))^q> \sim k(q)\,\delta^{\tau^*(q)+D}\,(\eta/\delta)^{\tau^*(q)} = k(q)\,\delta^D\,\eta^{\tau^*(q)} \end{cases} \tag{5.4.25}$$

as $\eta\to 0$. In terms of the average density $\rho(\delta) = \mu(\delta)/\delta^D$, (5.4.25) becomes

$$\begin{cases} q < q_c,\ <(\rho(\delta))^q> \sim \delta^{\tau^*(q) - D(q-1)}<(\mu(\delta_0))^q> \\ q > q_c,\ <(\rho(\delta))^q> \sim k(q)\,\delta^{-D(q-1)}\,\eta^{\tau^*(q)} \end{cases} \tag{5.4 26}$$

as $\eta\to 0$. For the generating function, (5.4.2) implies

$$\begin{cases} q < q_c,\ \chi^*_q(\delta) \sim \delta^{\tau^*(q)}\,<(\mu(\delta_0))^q> \\ q > q_c,\ \chi^*_q(\delta) \sim k(q)\,\eta^{\tau^*(q)} \end{cases} \tag{5.4.27}$$

as $\eta\to 0$. We conclude that divergence of moments leads to a breakdown of the scaling dependence of $\chi^*_q(\delta)$ on δ, i.e. *the effective mass exponent ($\neq\tau^*$) vanishes for large enough q* As will be shown in chapter 6 this behavior is not observed for the energy dissipation field in fluids. (5.4.27) suggests that the limit measure is composed of a multifractal measure - that determines low order moments - plus a finite set of isolated intense spikes that determine entirely high order moments. Indeed, if the spikes are isolated then varying δ does not change

$\mu(\delta)$ and therefore $\chi^*_q(\delta)$ remains constant, as shown by (5.4.27). The possibility of decomposing a divergent measure in two parts does not appear to have been emphasized previously.

Our presentation of canonical cascade processes is simpler than the original Mandelbrot (1974) exposition because of our different convention about the measure given to the initial unit interval. In particular the recurrence relation (5.4.19) is simpler than Mandelbrot's equivalent equation, which involves M different weights W_i instead of a single one. Notice that for *q integer* (5.4.20) can be developed and averaged using a multinomial expansion, which leads to a non-linear system of equations for the moments $<(\mu_n(\delta_0))^q>$. For example, in the special case M = 2 we obtain

$$Y^q(n+1) = <W^q> \sum_{k=0}^{q} \binom{q}{k} Y^k(n)\, Y^{q-k}(n), \quad q = 2, 3, \ldots$$

where $Y^q(n) \equiv <(\mu_n(\delta_0))^q>$. A numerical iteration of this system allows an accurate and computationally efficient determination of $<(\mu_n(\delta_0))^q>$. We present this possibility as an attractive complement to the computationally expensive Monte-Carlo methods sometimes used to study canonical multiplicative cascades (Lavallée, 1990). It should be noticed that this system can also be used to check the validity of the asymptotic form (5.4.23).

5.5 CORRELATIONS IN SCALING MEASURES

5.5.1 Brief review

The complete characterization of a random field f(x) requires in general the specification of the n-point probability distributions of $\{f(x_1), ..., f(x_n)\}$ for all values of $(x_1, .., x_n)$ and for all n (Monin and Yaglom, 1975). So far, the scaling properties of a measure have been characterized by the scaling exponents of the generating function or of $<[\mu(\delta)]^q>$ for random measures. Since $\mu(\delta)$ involves several points of the field generating the measure, the mass exponents contain some information about the n-point probability distributions, but the extent to which $\tau(q)$ (or equivalently $f(\alpha)$) characterizes the field still remains unclear. In this section we review briefly previous work on related questions (Cates and Deutsch (1987), Siebesma and Pietronero (1988), Meneveau and Chhabra (1990), Lee and Halsey (1990)).

In order to go beyond the multifractal characterization Cates and Deutsch (1987) proposed to consider several boxes simultaneously in order to take into account the correlations between their measures. The simplest choice is to consider pairs of boxes. Denoting by $\mu_{\mathbf{x}}(\eta)$ the measure of a box of size η centered about a point $\mathbf{x}$, and by $\mathbf{r}$ a lag vector, they defined the correlation function

$$C_\eta(p, q; \mathbf{r}) = < (\mu_{\mathbf{x}}(\eta))^p (\mu_{\mathbf{x}+\mathbf{r}}(\eta))^q >. \qquad (5.5.1)$$

For single scale isotropic random multinomial measures the independence of the multiplicative factors allows the decomposition

$$C_\eta(p, q; r) = < (\mu_{\mathbf{x}}(r))^p (\mu_{\mathbf{x}+\mathbf{r}}(r))^q > <(\mu_{\mathbf{x}}(\eta)/\mu_{\mathbf{x}}(r))^p> <(\mu_{\mathbf{x}+\mathbf{r}}(\eta)/\mu_{\mathbf{x}+\mathbf{r}}(r))^q>,$$

where $r = |\mathbf{r}|$. Using the usual multiscaling $<(\mu_{\mathbf{x}}(\eta)/\mu_{\mathbf{x}}(r))^p> = k(p)\,(\eta/r)^{\tau(p)+D}$ yields

$$C_\eta(p, q; r) = k(p)\,k(q)\,C_r(p, q; r)\,(\eta/r)^{\tau(p)+D}\,(\eta/r)^{\tau(q)+D}, \qquad (5.5.2)$$

where $C_r(p, q; r) = < (\mu_x(r))^p (\mu_{x+r}(r))^q >$. So far, the main issue discussed in the literature has been the calculation of $C_r(p, q; r)$ for simple models. The first attempt was made by Cates and Deutsch who simply made the approximation $\mu_x(r) \approx \mu_{x+r}(r)$. Using $<(\mu_x(r))^p> = k(p)\ (r/L_0)^{\tau(p)+D}$, where L_0 is the outer scale of the multiplicative process, they consequently obtained

$$C_r(p, q; r) = k(p+q)\ (r/L_0)^{\tau(p+q)+D}, \qquad (5.5.3)$$

Replacing (5.5.3) in (5.5.2) yields

$$C_\eta(p, q; r) = k(p)\, k(q)\, k(p+q)\ (\eta/L_0)^{\tau(p+q)+D}\ (\eta/r)^{\tau(p)+\tau(q)-\tau(p+q)+D}, \qquad (5.5.4)$$

that implies that the scaling of the correlation function is entirely determined by the scaling of single boxes, i.e. by the function τ. From now on we shall refer to (5.5.3) as the Cates and Deutsch scaling (in short, CD-scaling).

Later on Siebesma and Pietronero (1988) showed on a special case of deterministic 3-weight multinomial measure that the assumption $\mu_x(r) \approx \mu_{x+r}(r)$ was untenable but that the correct scaling exponent $\tau(p+q) + D$ of $C_r(p, q; r)$ was nevertheless obtained using this assumption. Finally Meneveau and Chhabra (1990) and Lee and Halsey (1990) showed that some combinations of p and q can emphasize the difference between $\mu_x(r)$ and $\mu_{x+r}(r)$ and consequently break the CD scaling in some regions of the (p,q) plane. We will return in section 5.5.4 on the CD-scaling breakdown.

5.5.2 Extended CD-scaling for separated self-similar measures

In this section our goal is to show that an extended form of CD scaling can be derived rigorously for any deterministic or random *separated* self-similar measure using renormalization arguments. The more general case of a non-separated random self-similar measure will be

examined in section 5.5.4 with a specific example. For deterministic measures we define the *correlation generating function*

$$\phi_{p,q}(\delta,r) = \inf \sum_i [\mu_{x_i}(\delta)]^p \mu_{x_i+r}(\delta)]^q, \qquad (5.5.5)$$

where the infimum is taken over all the covers of the support of the measure by boxes of size δ. We restrict ourselves to the special case where $r = n\delta$, i.e. r is related to the coarse-graining resolution δ. For one dimensional measures, this restricted correlation generating function is approximated by

$$\Phi^{(n)}_{p,q}(\delta) \equiv \phi_{p,q}(\delta,n\delta) = \sum_i [\mu_i(\delta)]^p \mu_{i+n}(\delta)]^q, \qquad (5.5.6)$$

where $\mu_i(\delta)$ and $\mu_{i+n}(\delta)$ are the measures of two boxes separated by a distance $n\delta$. Our choice $r = n\delta$ is motivated by the fact that $\Phi^{(n)}_{p,q}(\delta)$ is a *natural scale invariant quantity for self-similar measures.* This property allows to use renormalization equations in a simple and natural way. Note that the quantity $C_r(p, q; r)$ defined above for random measures corresponds to the special case n = 1, i.e. $\langle\Phi^{(1)}_{p,q}(\delta)\rangle = (L_0/\delta)^D C_\delta(p, q; \delta)$.

Consider a deterministic multiscale self-similar measure, with support $S = S_1 U ... U S_M$, where the sets S_j are self-similar to S. Following the steps of section 5.2.3, and assuming that $n\delta < \min d(S_i,S_j)$, the self-similarity of the measure leads to the renormalization equation

$$\Phi^{(n)}_{p,q}(\delta) = \sum_j w_j^{p+q} \Phi^{(n)}_{p,q}(\delta/r_j)$$

and the trial solution δ^t yields the characteristic equation

$$\sum_j w_j^{p+q} r_j^{-t} = 1.$$

Therefore

$$\Phi^{(n)}_{p,q}(\delta) = \delta^{t(n,p,q)} (c + R(\delta))$$

where $R(\delta)\to 0$ as $\delta\to 0$ and

$$t(n,p,q) = \tau(p+q). \tag{5.5.7}$$

(5.5.7) generalizes the CD scaling that corresponds to the special case n = 1. We emphasize that (5.5.7) holds for all (n, p, q), i.e. the possibility of CD scaling breakdown noted by Meneveau and Chhabra for space filling measures does not occur for separated self-similar measures.

Suppose now that the weights W_j are random but that the scale ratios r_j are fixed. The self-similarity of the measure then implies

$$\Phi^{(n)}_{p,q}(\delta) \overset{d}{=} \sum_j W_j^{p+q}\, \Phi^{(n)}_{p,q}(\delta/r_j)|_j, \tag{5.5.8}$$

where " $\overset{d}{=}$ " denotes the equality in probability distribution, and where the random variables $\Phi^{(n)}_{p,q}(\delta/r_j)|_j$ are independent of the W_j. An ensemble average on (5.5.8) yields

$$\langle\Phi^{(n)}_{p,q}(\delta)\rangle = \langle W^{p+q}\rangle \sum_j \langle\Phi^{(n)}_{p,q}(\delta/r_j)\rangle$$

and the trial solution δ^t leads to the characteristic equation

$$1 = \langle W^{p+q}\rangle \sum_{j=1}^{M} r_j^{-t(n,p,q)}, \tag{5.5.9}$$

which defines t(n,p,q) implicitly. On the other hand the renormalization equation for $\chi_q(\delta)$ with the same random measure is

$$\langle\chi_q(\delta)\rangle = \langle W^q\rangle \sum_i^{M} \langle\chi_q(\delta/r_j)\rangle,$$

which leads to the characteristic equation

$$1 = \langle W^q\rangle \sum_{j=1}^{M} r_j^{-\tau(q)}. \tag{5.5.10}$$

Comparing (5.5.9) and (5.5.10) leads again to (5.5.7) and therefore the extended CD scaling also holds for all (n,p,q) in the random separated case. This result appears to be original.

5.5.3 Constraints on correlations due to single-box scaling

We now return to the more general problem of determining to what extent the only assumption of single box scaling, i.e.

$$<[\mu(\delta)]^q> = c(q)\,\delta^{\gamma(q)},\ \gamma(q) = \tau(q) + D, \tag{5.5.11}$$

restricts the scaling of $<(\mu_i(\delta))^p(\mu_{i+n}(\delta))^q>$, where $\mu_i(\delta)$ and $\mu_{i+n}(\delta)$ are the measures of boxes separated by a distance $n\delta$. Consider a one dimensional scaling measure. An interval of size 2δ and measure $\mu(2\delta)$ can always be split in two adjacent and disjoint intervals of size δ and measures $\mu_1(\delta)$ and $\mu_2(\delta)$ and therefore

$$\mu(2\delta) = \mu_1(\delta) + \mu_2(\delta). \tag{5.5.12}$$

Squaring (5.5.11) and averaging gives

$$<\mu_1(\delta)\mu_2(\delta)> = 1/2\ <(\mu(2\delta))^2> - <(\mu(\delta))^2>$$

if the measure is spatially homogeneous. (5.5.11) then yields

$$<\mu_1(\delta)\mu_2(\delta)> = c_1\ \delta^{\gamma(2)}, \tag{5.5.12a}$$

where $c_1 = c(2)\,(2^{\gamma(2)-1} - 1)$. $<\mu_1(\delta)\mu_2(\delta)>$ is therefore *entirely determined* by (5.5.11) Similarly, raising (5.5.12) to the power 3 and averaging yields

$$<(\mu_1(\delta))^2\mu_2(\delta)> = 1/6\ <(\mu(2\delta))^3> - 1/3\ <(\mu(\delta))^3> \propto \delta^{\gamma(3)} \tag{5.5.12b}$$

Raising (5.5.12) to the powers 4 and 5 and averaging yields

$$6\ <(\mu_1(\delta)\mu_2(\delta))^2> + 8\ <(\mu_1(\delta))^3\mu_2(\delta)> \propto \delta^{\gamma(4)} \tag{5.5.12c}$$

$$10 \langle(\mu_1(\delta)(\mu_2(\delta))^4\rangle + 20 \langle(\mu_1(\delta))^3(\mu_2(\delta))^2\rangle \propto \delta^{\gamma(5)}.$$

Hence for powers greater than 3 we find that the splitting procedure and the single box scaling (5.5.11) no longer determines uniquely the quantities $\langle(\mu_i(\delta))^p(\mu_{i+1}(\delta))^q\rangle$ but rather determines linear combinations of them.

Alternatively we may divide an interval of length 3δ in three subintervals of length δ so that

$$\mu(3\delta) = \mu_1(\delta) + \mu_2(\delta) + \mu_3(\delta). \tag{5.5.13}$$

Squaring and averaging (5.5.13) then yields

$$\langle\mu^2(3\delta)\rangle = 3 \langle\mu^2(\delta)\rangle + 4 \langle\mu_1(\delta)\mu_2(\delta)\rangle + 2 \langle\mu_1(\delta)\mu_3(\delta)\rangle$$

and using (5.5.11) and (5.5.12a) leads to

$$\langle\mu_1(\delta)\mu_3(\delta)\rangle \propto \delta^{\gamma(2)}. \tag{5.5.13a}$$

Raising (5.5.13) to the power 3, averaging and using (5.5.11), (5.5.12a) and (5.5.12b) implies

$$\langle\mu_1(\delta)(\mu_3(\delta))^2\rangle \propto \delta^{\gamma(3)} \tag{5.5.13b}$$

Raising (5.5.13) to higher powers leads to relations of the type (5.5.12c) that do not determine directly the correlations. More generally an interval could be split into n subinterval and the same method implies

$$\langle\mu_i(\delta)\mu_{i+n}(\delta)\rangle \propto \delta^{\gamma(2)} \quad \text{and} \quad \langle\mu_i(\delta)(\mu_{i+n}(\delta))^2\rangle \propto \delta^{\gamma(3)} \tag{5.5.14}$$

for $n = 1, 2, 3, \ldots$.

In conclusion, our splitting procedure implies that low order integer correlations are forced to satisfy the constraint (5.5.7), while higher order correlations obey weaker constraints of the type (5.5.12c) which are consistent but not necessarily equivalent to (5.5.7). These weaker

constraints might therefore make room for different scaling behaviors (i.e. non CD-scaling) of the correlations $<(\mu_i(\delta))^p(\mu_{i+1}(\delta))^q>$. An example of this behavior will be given in the next section.

5.5.4 Correlations in random microcanonical multinomial measures

The calculation of $<(\mu_i(\delta))^p(\mu_{i+1}(\delta))^q>$ is more delicate for non-separated self-similar measures. Some exact results have been obtained for a deterministic single scale and three-weight measure (Siebesma and Pietronero, 1988) and for a single scale measure using two weights, restricted to two values, with random positions (Lee and Halsey (1990) and Meneveau and Chhabra (1990)). In this section we give an exact 1-D calculation of the correlations for a more general family of random single-scale microcanonical multinomial measures, using M weights having arbitrary probability distributions.

The scale ratio of this multiplicative process is $r = 1/M$. There are M^n disjoint intervals of size $\delta_n = r^n$ and the order-1 correlation generating function is

$$\Phi^{(1)}_{p,q}(\delta_n) = \sum_{i=1}^{M^n-1} [\mu_i(\delta_n)]^p[\mu_{i+1}(\delta_n)]^q. \qquad (5.5.15)$$

We can write

$$\Phi^{(1)}_{p,q}(\delta_{n+1}) = \sum_{i=1}^{M^n} \sum_{j=1}^{M-1} [\mu_i(\delta_n)W_{i,j}]^p[\mu_i(\delta_n)W_{i,j+1}]^q + \sum_{i=1}^{M^n-1} [\mu_i(\delta_n)W_i]^p[\mu_{i+1}(\delta_n)W_{i+1}]^q, \qquad (5.5.16)$$

where W_i and W_{i+1} denote random weights belonging to different and adjacent mother eddies of size δ_n, while $W_{i,j}$ and $W_{i,j+1}$ denote adjacent weights belonging to the same i^{th} mother eddy of size δ_n (see figure 5.9 for a graphical explanation of (5.5.16)). W_i and W_{i+1} are therefore independent random variables while $W_{i,j}$ and $W_{i,j+1}$ are correlated by the microcanonical constraint $\sum_{j=1}^{M} W_{i,j} = 1$ for all i. Taking an ensemble average on (5.5.16) yields

$$\langle \Phi^{(1)}_{p,q}(\delta_{n+1}) \rangle = \langle W^p \rangle \langle W^q \rangle \langle \Phi^{(1)}_{p,q}(\delta_n) \rangle + (M-1) \langle W^p_{i,j} W^q_{i,j+1} \rangle \langle \chi_{p+q}(\delta_n) \rangle,$$

where $\chi_q(\delta_n)$ is the order-q generating function of the measure given by $\langle \chi_q(\delta_n) \rangle = (M \langle W^q \rangle)^n$ in this case (see (5.4.14) section 5.4.2). Introducing the simplifying notation $\phi_n \equiv \langle \Phi^{(1)}_{p,q}(\delta_{n+1}) \rangle$, the above equation reduces to

$$\phi_{n+1} = b\, \phi_n + A\, c^n, \tag{5.5.17a}$$

where

$$\begin{cases} b = \langle W^p \rangle \langle W^q \rangle \\ A = (M-1) \langle W^p_{i,j} W^q_{i,j+1} \rangle \\ c = M \langle W^{p+q} \rangle \end{cases} \tag{5.5.17b}$$

and

$$\phi_1 = \Big\langle \sum_{i=1}^{M-1} W^p_i W^q_{i+1} \Big\rangle = (M-1) \langle W^p_{i,j} W^q_{i,j+1} \rangle = A.$$

The general solution of (5.5.17a) using the initial condition $\phi_1 = A$ is

$$\phi_n = A \frac{c^n - b^n}{c - b}, \tag{5.5.18}$$

where $\delta_n = r^n$. If $c > b$ then $\phi_n \sim k\, c^n$ as $n \to \infty$ (or equivalently $\delta_n \to 0$) and therefore CD scaling is recovered ($k = A/(c - b)$). However if $c < b$ then $\phi_n \sim -k\, b^n$ and another scaling exponent is obtained. Expressed in terms of δ, we get

$$\langle \Phi^{(1)}_{p,q}(\delta) \rangle \sim \delta^{\gamma_D(p,q)} \quad \text{as } \delta \to 0, \tag{5.5.19}$$

where

$$\gamma_D(p,q) = \begin{cases} \tau(p+q) & \text{if } c > b, \text{ i.e. CD-scaling} \\ \tau(p)+\tau(q)+2 & \text{if } c < b, \text{ i.e. non CD-scaling} \end{cases}.$$

This example shows that CD-scaling is not necessarily obeyed for all (p, q), a general result that was already suggested by the argument of section 5.5.3.

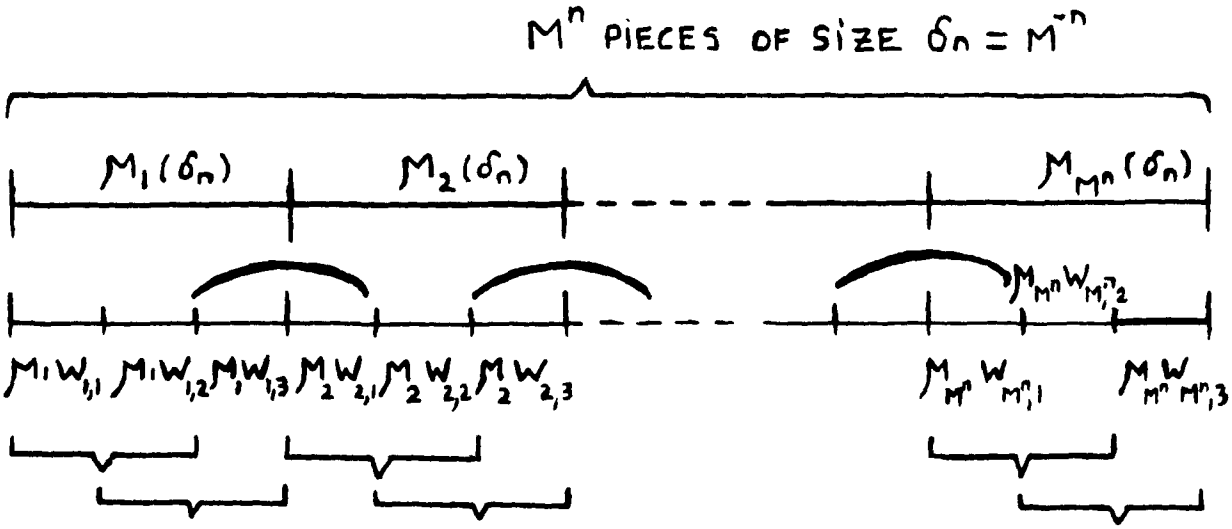

Figure 5.9: Graphical explanation of the relation (5.5.16) in the special case M = 3. The brackets ⌣ indicates the pairs of intervals of size δ_{n+1} involved in the first summation of (5.5.16), while the brackets ⌢ indicates the pairs involved in the second summation.

The conditions $c > b$ and $c < b$ define two regions of the (p, q) plane. The frontier between these regions is defined by $c = d$, which implies (using (5.5.17b)) that $\langle W^p \rangle \langle W^q \rangle = M \langle W^{p+q} \rangle$. Using $\langle W^q \rangle = M^{-\tau(q)-1}$, which follows from (5.4.15) with $d_S = 1$, yields

$$\tau(p+q) - \tau(q) - \tau(q) - 2 = 0, \tag{5.5.20}$$

which is the equation of the frontier between the two scaling domains. For a measure with a $\tau(q)$ similar the field $(\partial u/\partial x)^2$ as measured in locally isotropic turbulence, e.g. the binomial measure with weights $w_1 = 0.3$ and $w_2 = 0.7$, these domains are illustrated in figure 5.10. We emphasize that this is the first derivation of $\langle \Phi^{(1)}_{p,q}(\delta_n) \rangle$ for general random multinomial measures and that our derivation of the recurrence relation (5.5.17a) appears to be simpler than previous derivations, involving "tedious counting and algebra" (Lee and Halsey, 1990). We also stress that our argument does not seem to be directly generalizable to multiscale scaling measures.

It should be noted that the multinomial measure is not spatially homogeneous. Although $\langle (\mu_i(\delta_n))^q \rangle$ is independent of the position i of the interval, the correlations $\langle (\mu_i(\delta))^p (\mu_{i+1}(\delta))^q \rangle$ depend on i because they "remember" the tree structure of the cascade process. It follows that $\langle (\mu_i(\delta))^p (\mu_{i+1}(\delta))^q \rangle$ cannot be deduced directly from $\langle \Phi^{(1)}_{p,q}(\delta_n) \rangle$, which rather gives the ensemble average of a spatial average since $\langle \Phi^{(1)}_{p,q}(\delta_n) \rangle = (L_0/\delta) \langle \langle (\mu_i(\delta))^p (\mu_{i+1}(\delta))^q \rangle_S \rangle$, where $\langle ... \rangle_S$ denotes a spatial average and L_0 is the outer scale.

Remark: The quantities $\langle W^p_{i,j} W^q_{i,j+1} \rangle$ defined in (5.5.17b) can be obtained using the microcanonical constraint. For example, in the simple case $M = 2$ the microcanonical constraint implies that $W_2 = 1 - W_1$ and therefore $\langle W^p_{i,j} W^q_{i,j+1} \rangle = \langle W^p (1 - W)^q \rangle$

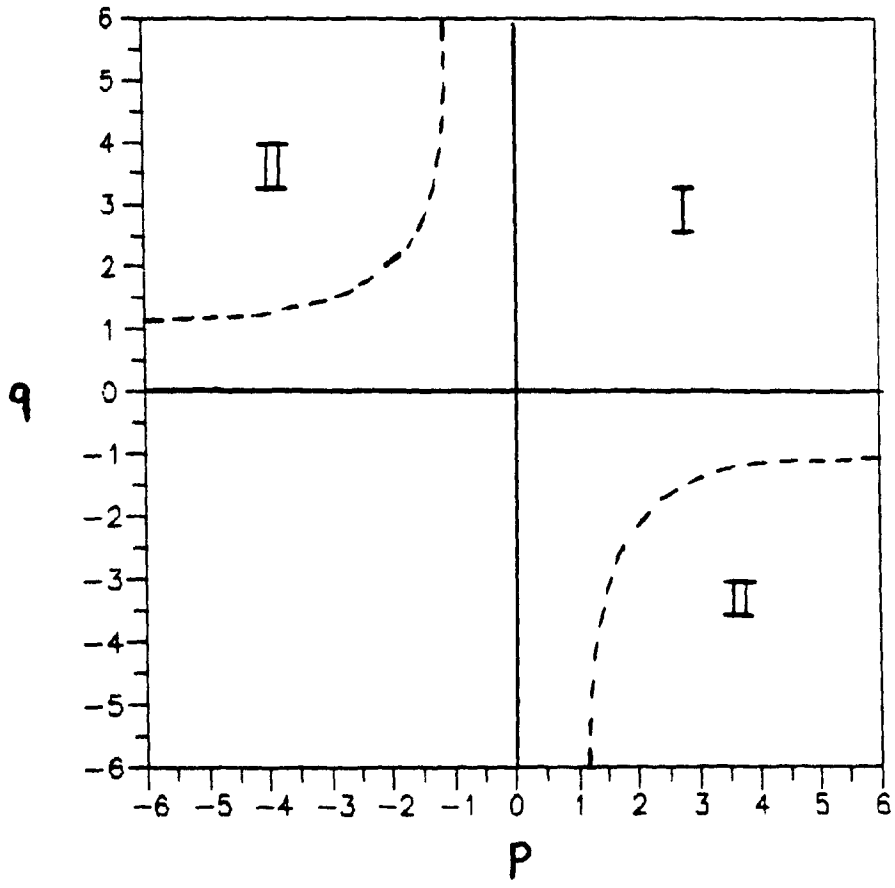

Figure 5.10: Illustration of the two scaling domains of multinomial measures with a $\tau(q)$ similar to real turbulent flows. (I) denotes the CD-scaling region while (II) denotes the non CD-scaling region and the dashed lines separate the two regions.

5.5.5 Implications for data analysis

In the absence of more information about the general connection between the scaling exponents of $<(\mu_i(\delta))^p(\mu_{i+1}(\delta))^q>$ and $<(\mu_i(\delta))^p>$, we will regard the two scaling domains of figure 5.10, as well that the corresponding scaling exponents $\gamma_D(p, q)$, as characteristic of single scale multinomial measures sharing their $\tau(q)$ function with the energy dissipation field in real turbulent flows. From this standpoint, the verification on real data of these scaling regimes provides a new way of testing multiplicative cascade models. In chapter 6 the first experimental study of these scaling regimes will be presented. Some tests of the extended CD-scaling (5.5.7) will also be performed.

5.6 GENERAL CONSIDERATIONS ABOUT THE COMPARISON OF CASCADE MODELS WITH REAL TURBULENT FIELDS

A priori, one may think that the measures studied so far are too artificial to be considered as realistic models for any geophysical field. Cascade models look like toy models inspired from some rather cloudy phenomenology. For some simple non-linear dynamical systems, e.g quadratic maps (Halsey *et al.*, 1986) it is known theoretically that the invariant probability measure can be described by a multiscale Cantor measure. By contrast, in turbulence one must recognize that the discrete splitting of eddies characteristic of cascade models has not so far received a rigorous basis and that little is known about the limitations of these models. Nevertheless, these simplistic models reproduce many of the scaling properties of real measures and in fact, it can be surprisingly difficult to develop tests allowing these models to be distinguished from natural fields. Comparing real natural fields with cascade models is an exercise that develops our ability to describe more accurately turbulent flows. As argued by Mandelbrot, the limitations of our skills to predict the behavior of turbulent fluids may be mainly due to our inability to produce efficient and intuitive mathematical descriptions of irregular fields.

Some of the singular measures introduced in this chapter may be appropriate candidates for the modelling of the energy cascade process. Various generalizations of discrete scale cascade models are possible (see for example Kraichnan, 1974), and it becomes quickly confusing to make a choice in this jungle of models. One of our goals is to try to narrow down a little the spectrum of all the *a priori* possible models of the energy dissipation field. We shall therefore propose a tentative classification of random cascade models. A first dichotomy is provided by the alternative between microcanonical and canonical models, i.e. between exact conservation of the energy flux and conservation on the average. More refined dichotomies involve the details of the model. From the simplest to the most general, the following models are examples of

possible alternatives (recall that M denotes the number of daughter eddies generated by a mother eddy, r_j a scale ratio, and W_j a random weight):

1) **Single scale models**: The scale ratio r is fixed.
   - M fixed, W_j random (= multinomial measures)
   - M random, W_j fixed
   - M random, W_j random

2) **Multiscale models**: Several scale ratios r_j are used, which may be fixed or random.
   - M fixed, W_j fixed
   - M fixed, W_j random
   - M random, W_j fixed
   - M random, W_j random.

All these models generate non-uniform singular measures, and further generalizations are possible when the positions of the daughter eddies are made random, as long that they remain disjoint and contained in their mother eddy. In addition, Schertzer and Lovejoy (1987) have shown that multiscaling measures could also be constructed without using any discrete scheme (this is the notion of *continuous cascades*). With a little imagination, the above list could be made much longer.

The mass exponents $\tau(q)$ only provide a partial characterization of a scaling measure. Unfortunately, these exponents are usually not constraining enough to allow different cascade models to be distinguished. If one considers for example the scaling of the measure associated to the field $(\partial u/\partial x)^2$ in a fully turbulent flow, it turns out (Meneveau and Sreenivasan, 1987a) that the simplest deterministic two-weights binomial measure can reproduce the $\tau(q)$ measured in turbulent flows with a good accuracy. Using a more complex model, involving for example a larger number of weights or else several different scale ratios, introduces more parameters and therefore leads to an even better fit to the measured $\tau(q)$. $\tau(q)$ is therefore rather insensitive to the various alternatives of cascade models presented above, a difficulty that was noticed in

particular by Chhabra *et al.* (1989). From a more fundamental point of view, Feigenbaum (1987) showed that different scaling measures can share an identical function τ and in that sense the characterization of a measure by τ is *degenerate*. Let us illustrate this possibility by following Feigenbaum example. Consider a deterministic multiplicative measure with $r = 1/2$ where four weights w_1, w_2, w_3 and w_4 are used (see figure 5.11 for the construction rule). We shall consider the two measures of figure 5.11 simultaneously and denote their generating functions by $\chi^1_q(\delta)$ (starting the construction with w_1 and w_2) and $\chi^2_q(\delta)$ (starting with w_3 and w_4). Writing a renormalization equation for each of these measures yields

$$\begin{cases} \chi^1_q(\delta) = w_1^q\ \chi^1_q(\delta/r) + w_2^q\ \chi^2_q(\delta/r) \\ \chi^2_q(\delta) = w_3^q\ \chi^1_q(\delta/r) + w_4^q\ \chi^2_q(\delta/r) \end{cases} \tag{5.6.1}$$

which is a linear system of renormalization equations. Introducing the array $\mathbf{X}(n) = (\chi^1_q(r^n), \chi^2_q(r^n))$, the system (5.6.1) can be rewritten in the form $\mathbf{X}(n+1) = M\,\mathbf{X}(n)$, where

$$M = \begin{pmatrix} w_1^q & w_2^q \\ w_3^q & w_4^q \end{pmatrix} \tag{5.6.2}$$

The general solution of (5.6.1) is of the form

$$\mathbf{X}(n) = a\,\lambda_+^n\,\mathbf{V}_+ + b\,\lambda_-^n\,\mathbf{V}_- \tag{5.6.3}$$

where λ_+ and λ_- are the eigenvalues of M ($\lambda_+ > \lambda_-$) and ($\mathbf{V}_+$, $\mathbf{V}_-$) the corresponding eigenvectors (a and b are constants). As $n\to\infty$ (5.6.3) yields $X_1(n) \sim k\,\lambda_+^n$ where k is a constant. Using $\delta_n = r^n$ this also implies that $\chi^1_q(\delta) \sim \delta^{\tau(q)}$ as $\delta\to 0$ where

$$\tau(q) = -\frac{\log\lambda_+(q)}{\log(1/r)} \text{ and } \lambda_+(q) = \frac{w_1^q+w_4^q}{2} + \left[\frac{w_1^q-w_4^q}{2} + (w_2w_3)^q\right]^{1/2}. \tag{5.6.4}$$

It is seen from (5.6.4) that different measures sharing the same product w_2w_3 will share the same $\tau(q)$.

Characterizations going beyond the usual $\tau(q)$-$f(\alpha)$ functions are therefore needed. The study of correlations in multifractals is an alternative that will be investigated in chapter 6. A second alternative is the possibility of periodic prefactors. Such oscillations reveal the underlying scale ratio of the cascade. Their observation in turbulent flows would therefore support the use of single scale multinomial measures in the modelling of the energy dissipation field (Novikov, 1990, Smith *et al.*, 1986). This issue will be examined in chapter 8. Another testing method of multiplicative processes could be based on the central limit theorem. As argued in chapter 3, our weaker formulation of the third hypothesis suggests that the moments of $\log(\varepsilon(\delta))$ can be estimated using the gaussian approximation. This possibility will be examined in chapter 7.

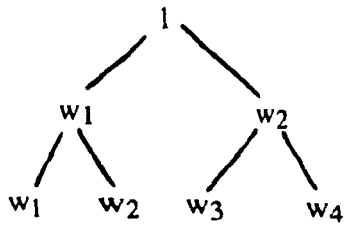

etc ...

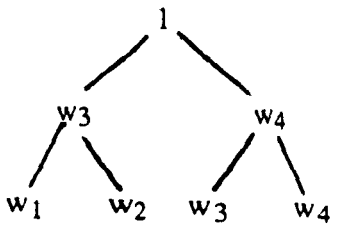

etc ...

Figure 5.11: Two examples of deterministic measures constructed with r = 1/2 using four different weights in the construction. The weights satisfy $w_1+w_2=1$ and $w_3+w_4=1$ The above trees show in which order the multiplicative factors are chosen in the construction of the measures.

Chapter VI

PRELIMINARY DATA ANALYSIS AND SCALING STUDIES

Less is known about the fine scale of turbulence—for example, the scale of 1 mm in the atmosphere—than about the structure of atomic nuclei. Lack of basic knowledge about turbulence is holding back progress in fields as diverse as cosmology, meteorology, aeronautics and biomechanics. Understanding the hierarchically organized complexity of turbulence may well provide a paradigm for understanding a variety of problems at the frontiers of physics research

Uriel Frisch and Steven A. Orszag (1990)

Our purpose being to compare cascade models to the energy dissipation field in real turbulent fluids, we chose to collect data sets in the atmospheric surface layer at a height of four meters with a hot wire anemometer. Relatively wide scaling ranges can be obtained easily in the atmosphere and at this height only a large wind tunnel could provide similar scaling ranges. Wide scaling ranges are useful to measure scaling exponents but they also bring other difficulties. For example, it becomes difficult to distinguish non-stationarity from scaling effects which are responsible for correlations over large distances. This problem is unavoidable for measurements in flows at high Reynolds number and scaling ranges comparable to the sample size can be obtained.

In order to convince ourselves that we were dealing with an appropriate data set, we reproduced in this chapter some key classical analysis. These include the $k^{-5/3}$ energy spectrum, the power spectrum of $(\partial v/\partial x)^2$, velocity structure functions and the generating function associated to the field $(\partial v/\partial x)^2$. Our results are compared with the results of other experimenters. In the case of the generating function, we clarify the interpretation of some earlier work on the subject. We also present the first results about the scaling of the correlation generating function for the energy dissipation field.

6.1 DATA ACQUISITION

We consider measurements of the air speed on a windy day above a flat and open grass field in the spring time (in the direction of the mean wind, the closest trees were at least 500 meters away on both sides). A pole was used to support a hot film probe at a height of about 4 meters, and the longitudinal component of the velocity was measured (i.e. in the direction of the mean wind). The mean velocity at the hot-wire location during the data acquisition was about 8 m/s. A T.S.I. anemometer (model 1054) was used with a hot film probe of length 1.5 mm and diameter 0.15 mm. The typical upper frequency response of this probe in air is 250 kHz, while the anemometer itself is limited to an upper frequency of 10 kHz (this limit is essentially due to the frequercy response of the amplifiers involved in the linearization circuit). The analog output of the anemometer was digitized at 20 kHz, without using any analog filtering, with a 12 bit digital-to-analog converter and stored on the hard disk of an A.T. personal computer. A 5 minute sample was recorded, i.e. 6×10^6 points. Everywhere in the following chapter time intervals have been converted into spatial lags using the frozen turbulence hypothesis, i.e. $\Delta x = U \Delta t$, where U is the mean wind speed. Using this conversion, the data set is 2.4 km long and one point every 0.4 mm was recorded. We shall see that the electronic noise added to the velocity signal reduces this maximum resolution to about 1/3 cm.

The Reynolds number based on the mean flow at a 4 meters height is

$$R_e = \frac{U\,L}{\nu_{air}} = \frac{8 \times 4}{1.5 \times 10^{-5}} = 2.13 \times 10^6.$$

The *turbulent* (or *local*) Reynolds number is defined here by

$$R_e(L) = \frac{\langle \Delta u(L)]^2 \rangle^{1/2}\, L}{\nu_{air}} = \frac{1 \times 4}{1.5 \times 10^{-5}} = 2.67 \times 10^5$$

for L = 4 meters (it will be shown in section 6.3 that $\langle \Delta u(L)]^2 \rangle^{1/2} \approx 1$ m/s in the horizontal direction). It is recognized in the literature that inertial range behaviors and $k^{-5/3}$ energy spectra

are observable when R_e typically exceeds 10^4. Our Reynolds number is therefore about 200 times larger than this lower limit. In order to study larger scales more accurately, a longer 30 minute sample was also recorded in the same conditions immediately after the 5 minutes sample, but with a 300 Hz sampling frequency.

6.2 SPECTRA AND PREPROCESSING

6.2.1 Energy and dissipation spectra

The whole sample was split in about 180 disjoint slices of 13 meters. The energy spectrum of each slice was obtained with a F.F.T. and these spectra were averaged. The resulting energy spectrum is plotted on a log-log scale in figure 6.1. An almost perfect power law is obtained in the range [0.1m,13m]. The slope measured in this range with a logarithmic linear regression is 1.73, i.e. about 4% larger than the $5/3 \approx 1.67$ predicted by the K41 theory. This slight excess is consistent with the theories accounting for the effect of intermittency on the energy spectrum. A clear dissipation range is observed in the range [10cm,1cm]. The noise floor is reached for scales smaller than 0.5 cm, which corresponds approximately to a 2 kHz frequency. The energy spectrum of the longer 30 minutes sample is plotted in figure 6.2. A line of slope -5/3 is given for reference. A departure from $k^{-5/3}$ occurs for scales larger than 10 meters. The larger variability of E(k) is due to a smaller amount of averaging for this sample. It is also noticed that the variability of E(k) increases with k. This suggests a breakdown of the K41 theory that rather implies $\langle (E(k))^2 \rangle - (\langle E(k) \rangle)^2 \rangle^{1/2} \propto k^{-5/3}$, i.e. that leads to a decreasing variability as k increases.

Before doing any further analysis with the data, frequencies higher than 2 kHz were digitally filtered out. For illustration, a sample of the unfiltered signal is displayed next to the filtered signal in figure 6.3, and a picture of the filtered velocity field over a wider range of scales is given in figure 6.4. The filtration is absolutely crucial for the estimation of the

derivative $\partial u/\partial x$, as well that for the scaling properties of the field $(\partial u/\partial x)^2$. The dissipation spectrum $E_d(f)$, defined so that

$$\langle(\partial u/\partial x)^2\rangle = \int_0^\infty E_d(f)\, df,$$

where $f = k/2\pi$, is useful to determine the accuracy of our estimate of $\langle(\partial u/\partial x)^2\rangle$. Note that $E_d(f) = f^2\, E(f)$, where $E(f)$ is the velocity energy spectrum. $E_d(f)$ was displayed in figure 6.5 in the area-preserving representation $E_d(f)f$ versus $\log(f)$ (Since that $E_d(f)df = E_d(f)f\, d(\ln(f))$, the area under the graph $E_d(f)df$ versus $\log(f)$ is proportional to $\langle(\partial u/\partial x)^2\rangle$). The bulk of the contribution to $\langle(\partial u/\partial x)^2\rangle$ comes from scales smaller than 1 meter, and in the inertial range $E_d(f) \sim f^2\, f^{-5/3} = f^{1/3}$. The bell-shaped curve is spoiled by noise for scales smaller than 1 cm. Assuming an exponential decay of the energy spectrum in the unresolved part of the dissipation range, one concludes that an error of at most 10% is made on $\langle(\partial u/\partial x)^2\rangle$, and consequently also for each value of $\partial u/\partial x$.

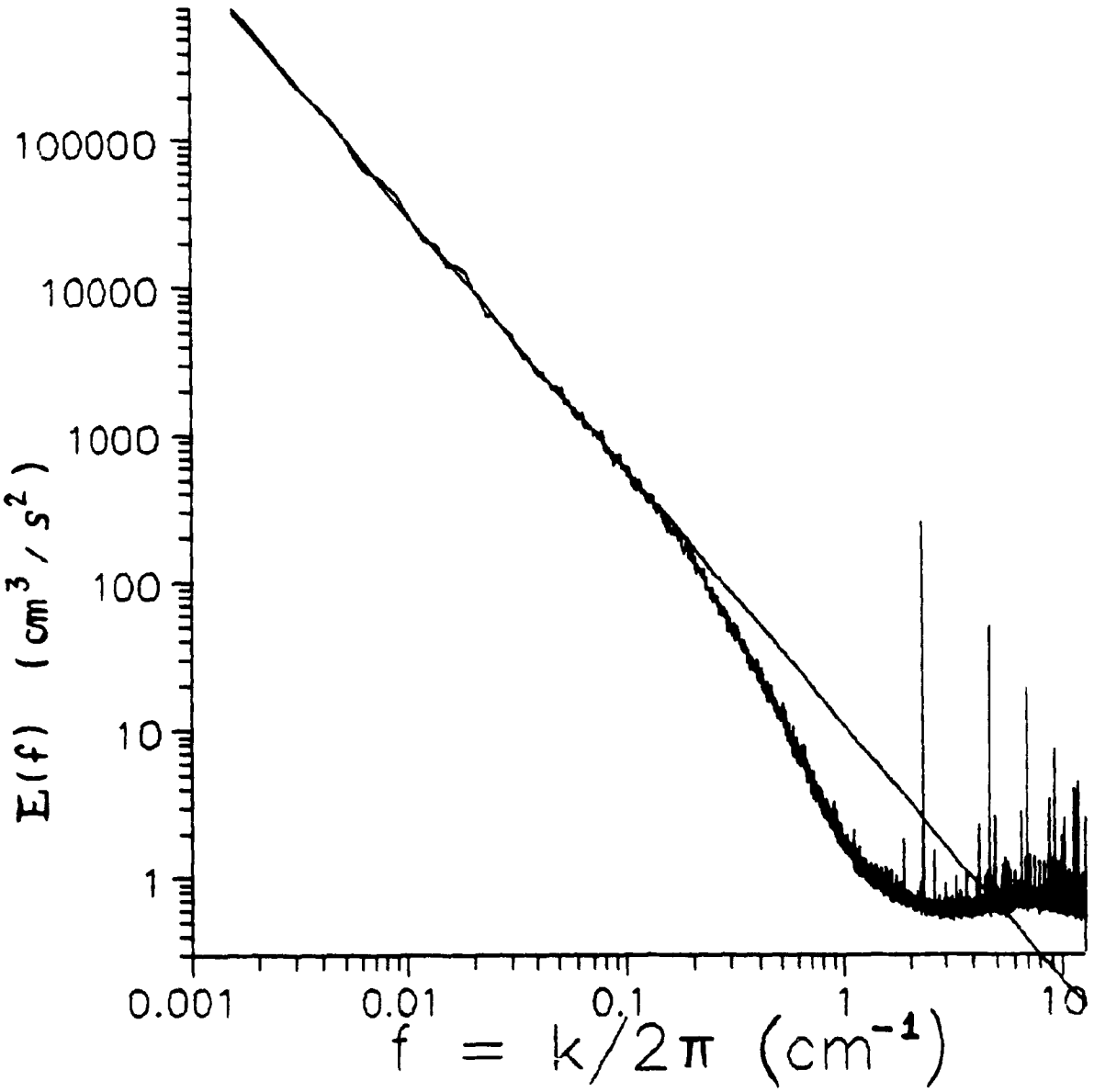

Figure 6.1: Energy spectrum of the velocity field, obtained by averaging the spectra of 180 samples of 13 meters. The exponent of the power law (straight line fitted with a linear regression) is -1.73, i.e. about 4% larger than the 5/3 predicted by the K41 theory. Notice that this slight positive correction to the exponent 5/3 is consistent with the intermittency correction due to intermittency predicted in particular by the β-model. The noise floor is reached for scales smaller than 1/2 cm. The dissipation range starts for scales smaller than $1/0.2 \approx 5$ cm. The beginning of the dissipation range typically occurs around about 60 times the kolmogorov dissipation scale η, therefore $\eta \approx 1$ mm.

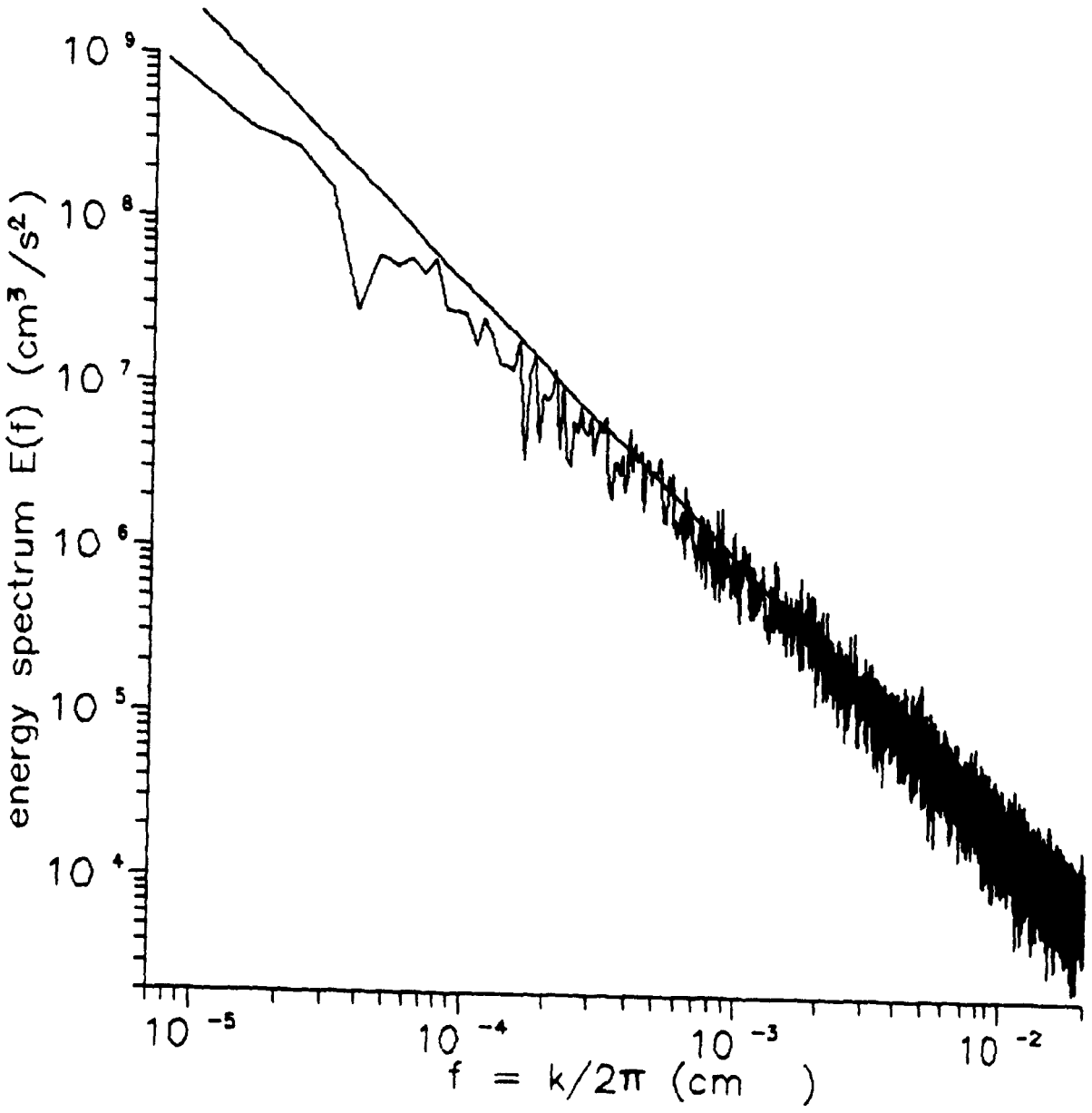

Figure 6.2: Energy spectrum of the velocity field obtained with the longer 1/2 hour sample This longer sample allows to resolve more accurately larger scales. It is seen that a slow but clear departure from the $k^{-5/3}$ spectrum (the straight line) occurs for scales larger than 10 meters.

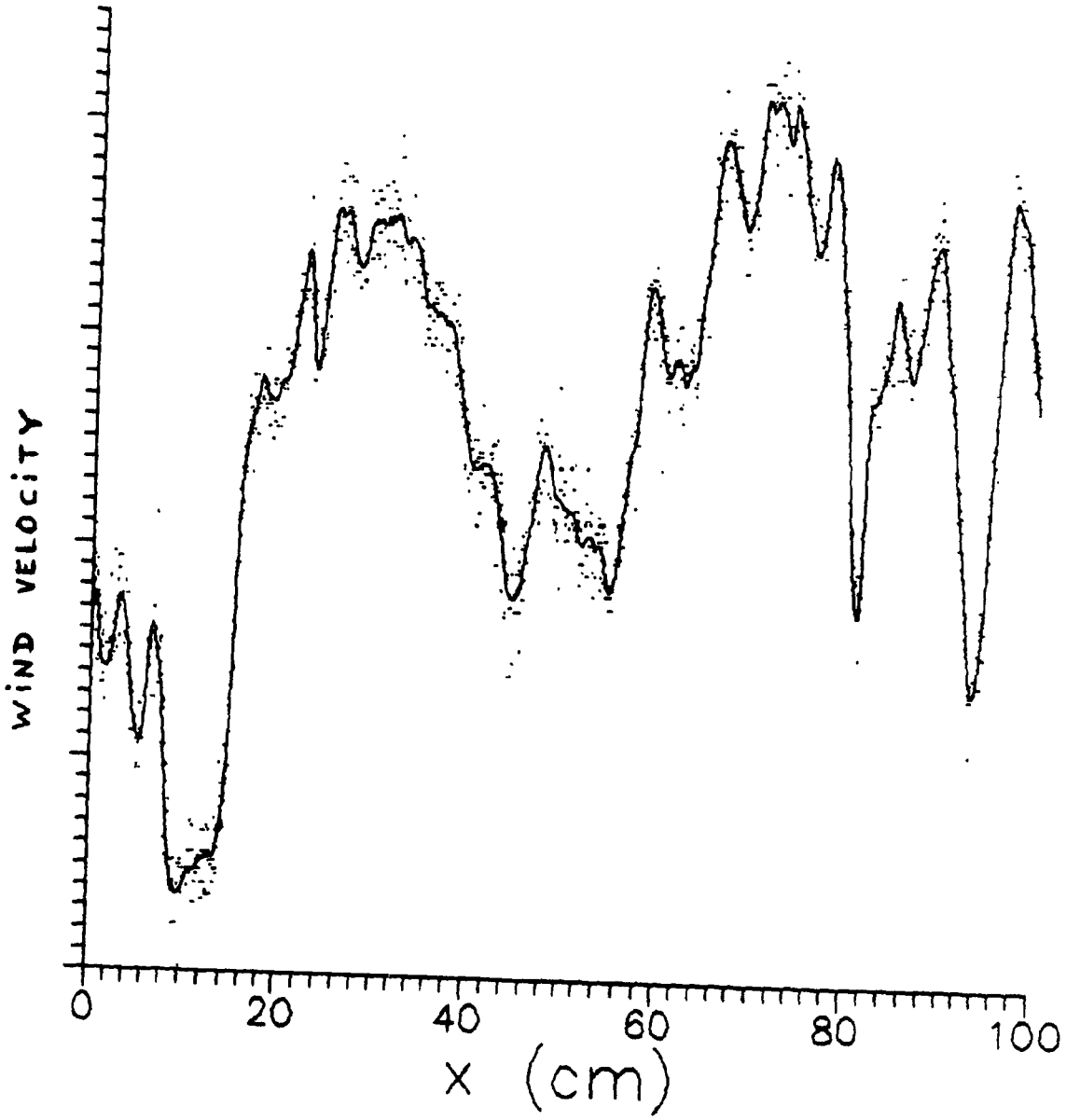

Figure 6.3: A picture of the raw velocity signal (the cloud of dots) together with the filtered signal (the solid line).

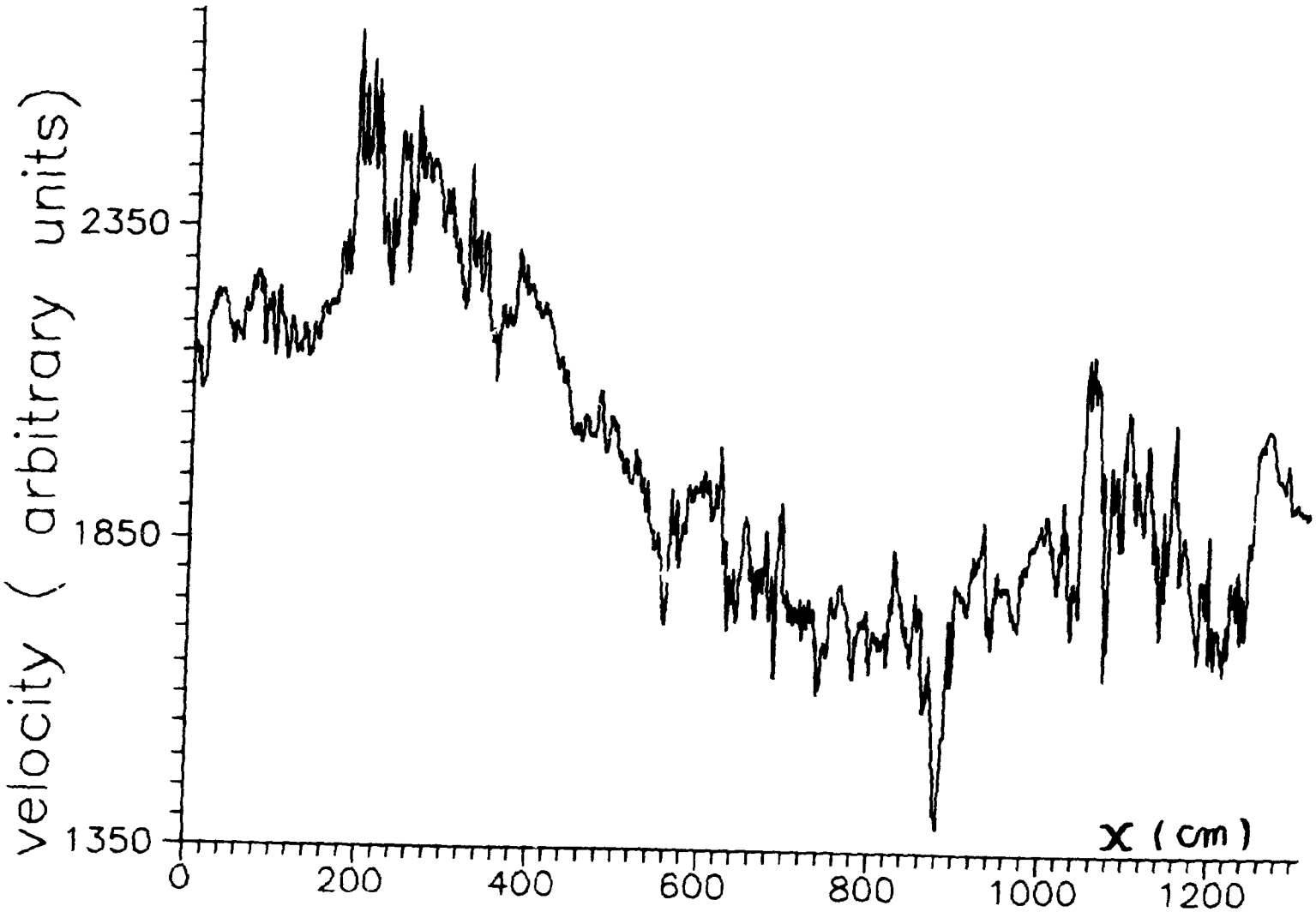

Figure 6.4: A larger scale view of the filtered velocity signal, showing clearly the abrupt velocity changes characteristic of the motion in the inertial range. In the context of the 1941 Kolmogorov theory, this function is not differentiable because $\Delta v(L) \sim L^{1/3}$ and therefore $\Delta v(L)/L \sim L^{-2/3}$ diverges as $L \to 0$.

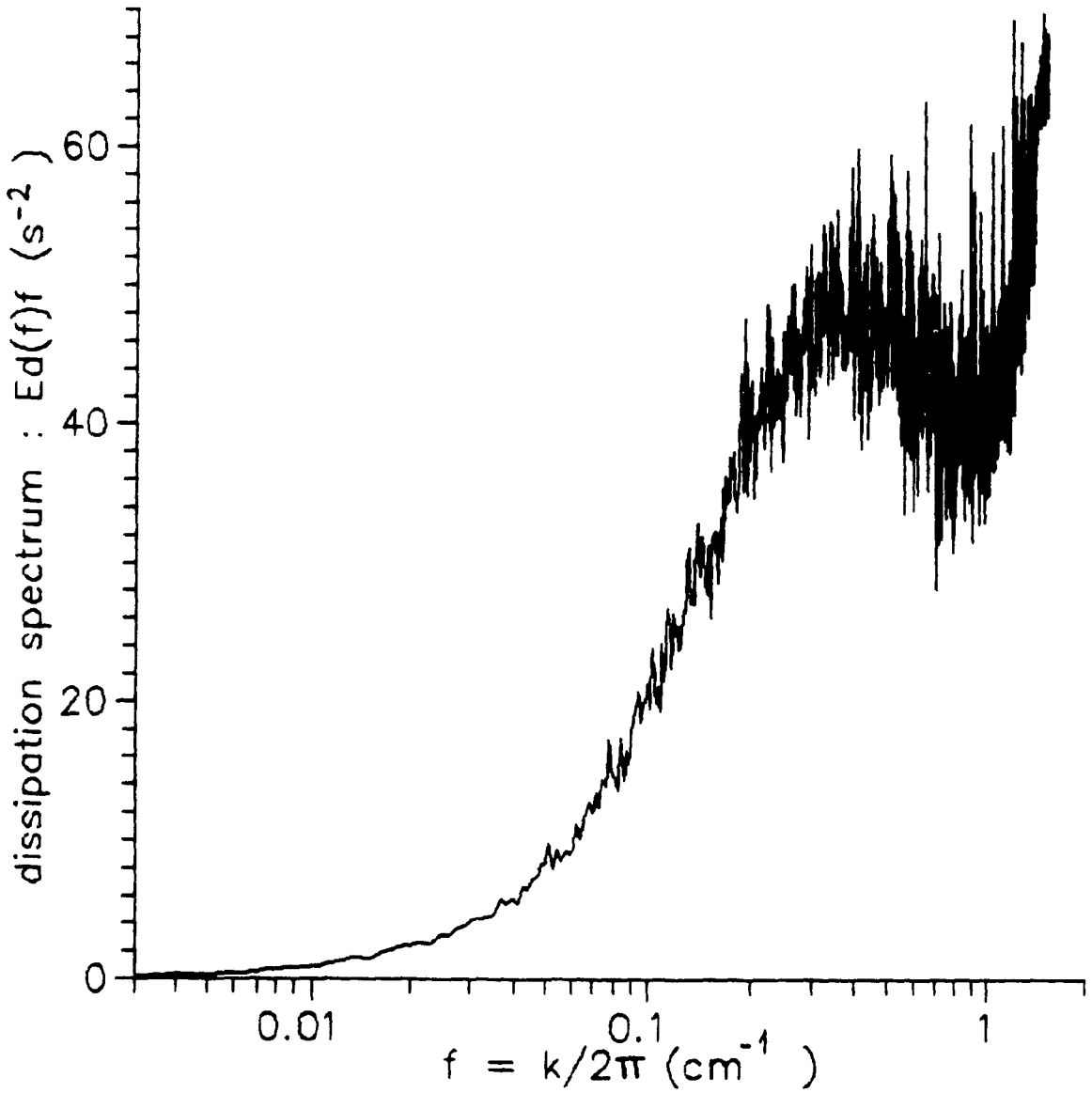

Figure 6.5: Dissipation spectrum obtained with the unfiltered velocity signal. The area under this curve is proportional to $\langle(\partial u/\partial x)^2\rangle$. The main contribution to $\langle(\partial u/\partial x)^2\rangle$ comes from scales smaller than 1 meter. For $f > 0.8$ cm^{-1} the spectrum is ruined by the noise. The fall-off being exponential in the dissipation range, at least 50% of the value of $\langle(\partial u/\partial x)^2\rangle$ is being resolved. We therefore expect the relative error on each value of $(\partial u/\partial x)^2$ to be smaller than 50%.

6.2.2 Power spectrum of $(\partial u/\partial x)^2$

The field $(\partial u/\partial x)^2$, obtained by differentiating the filtered velocity signal (using finite differences to approximate the derivative), is displayed in figure 6.6. A zoom on the first 100 cm of the figure 6.6 is given in figure 6.7. The singular nature of this measure is striking, and the intuitive resemblance of this field to an artificial discrete scale cascade model is obvious. The power spectrum of $(\partial u/\partial x)^2$, obtained by averaging 180 spectra, is displayed in figure 6.8. An approximate power law is obtained for scales larger than 1 cm The slope of the straight line drawn in figure 6.8 is -0.7. Results reported by other experimenters (Monin and Yaglom (1974), section 25.3) yield an exponent lying in the range [0.5,0.7], which is consistent with this result. Note that the power spectrum of the field generated by a discrete scale cascade model with a finite number of cascade steps is also proportional to k^{-s}, where $0 < s < 1$ (Monin and Yaglom (1974), section 25.3).

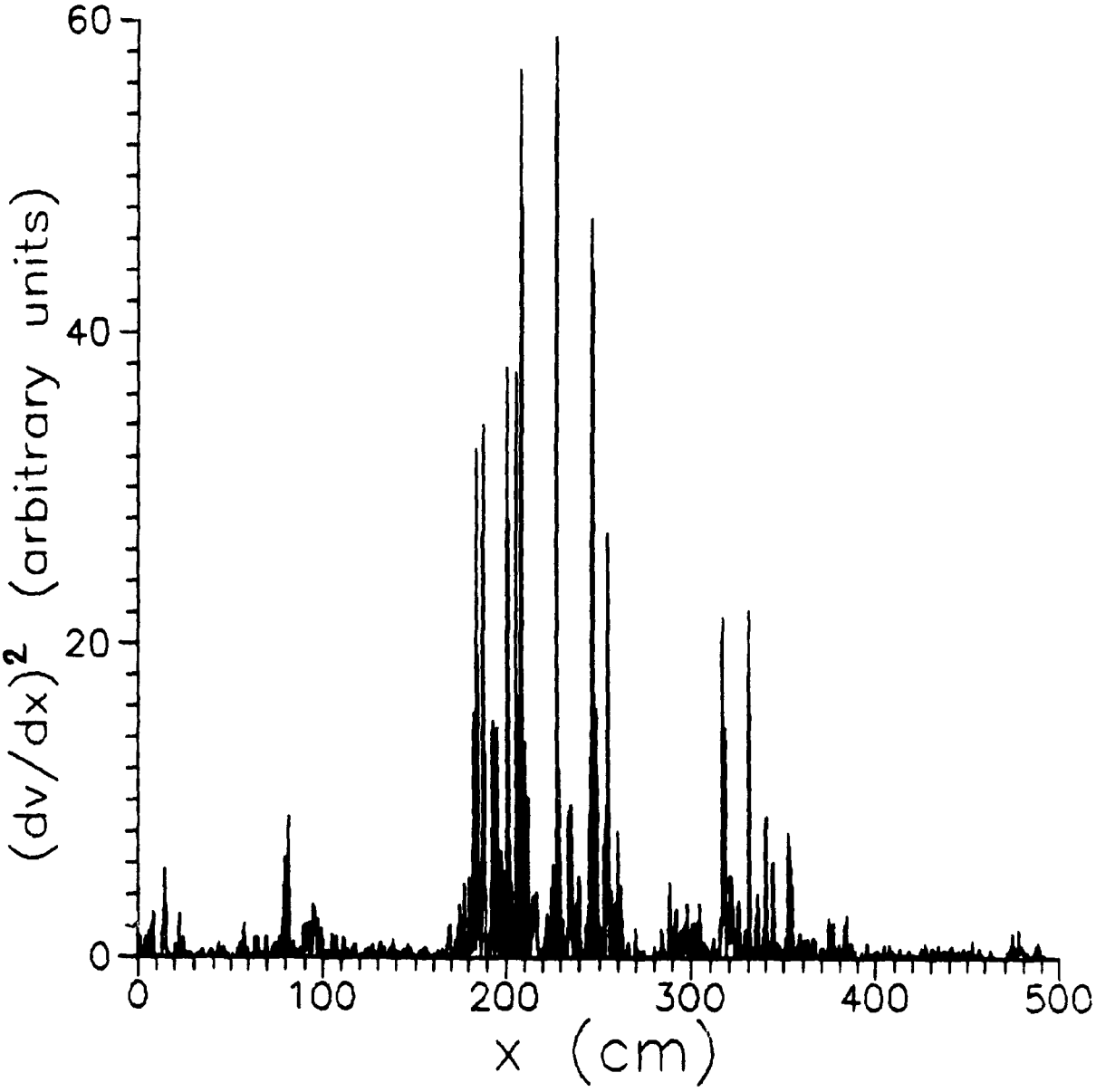

Figure 6.6: A picture of the field $(\partial u/\partial x)^2$ obtained by finite differences on the filtered velocity field. The singular nature of the dissipation field is striking. Regions of high intensity corresponds to regions of high vorticity in the fluid. The concentration of the regions of high vorticity on a sparse set is due to the stretching of vortex tubes characteristic of fully developed turbulence.

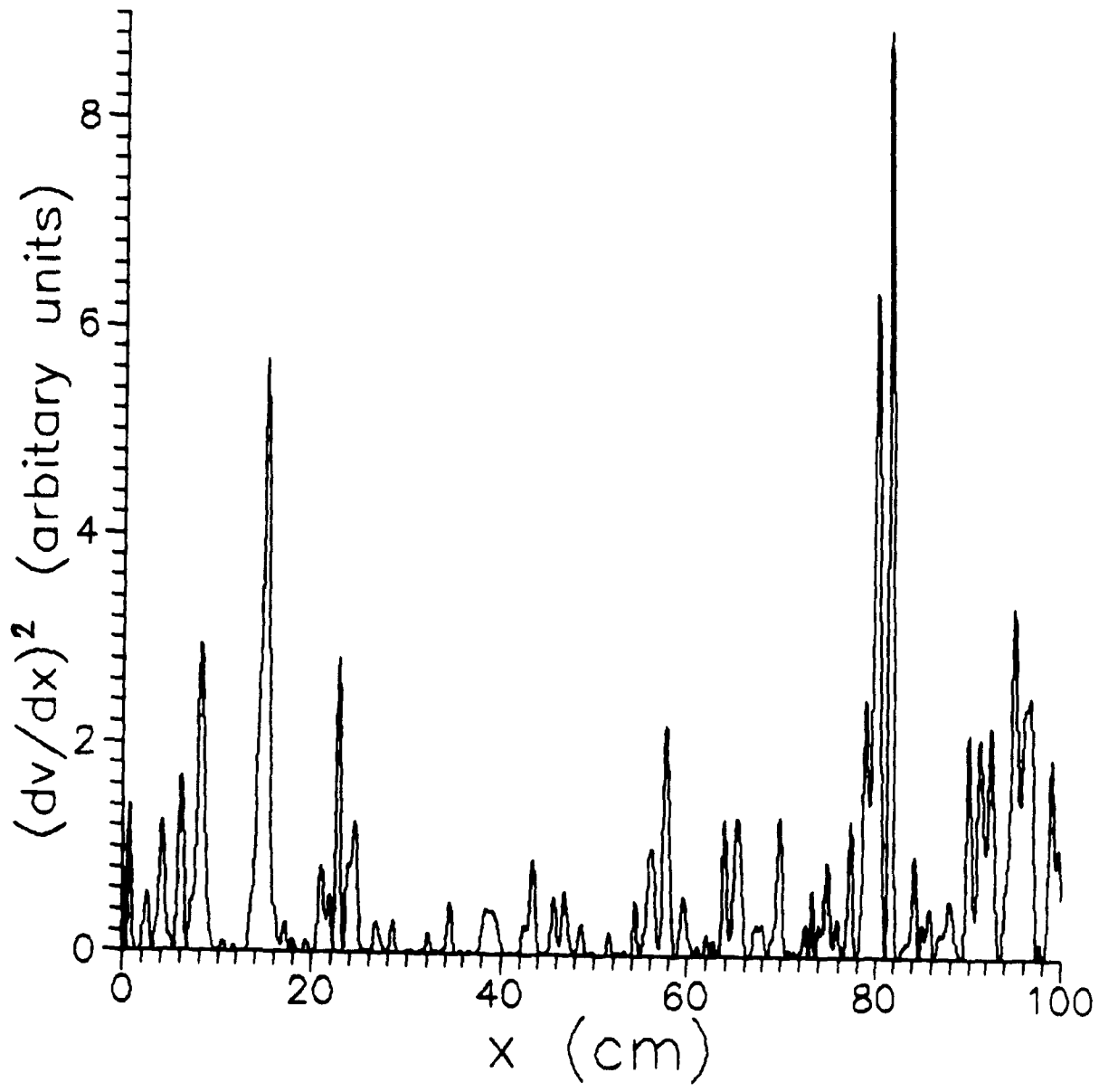

Figure 6.7: A zoom on the first meter of figure 6.6.

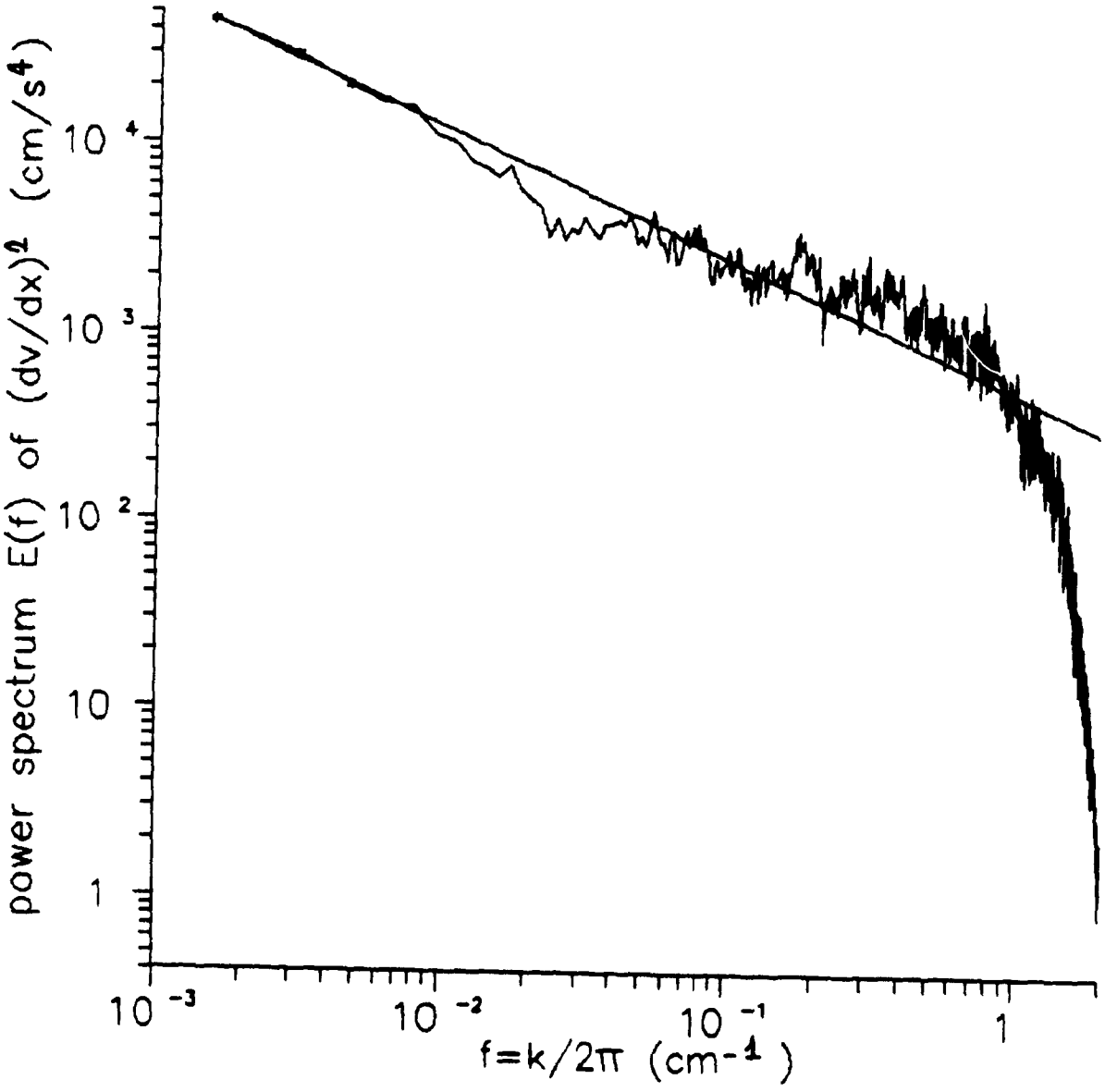

Figure 6.8: The power spectrum of $(\partial u/\partial x)^2$ is plausibly approximated by a power law with an exponent $s \approx -0.7$ (straight solid line), which is consistent with the results of earlier experimenters, who got $-0.7 \leq s \leq -0.5$.

6.3 VELOCITY STRUCTURE FUNCTIONS

In order to check the 2/3 law, the velocity structure function

$$D_2(L) = <(\Delta v(L))^2>^{1/2}$$

was plotted in figure 6.9. According to the K41 theory, $D_2(L) \sim L^{1/3}$. Besides, a $k^{-5/3}$ energy spectrum implies, by Fourier transformation, that $D_2(L) \sim L^{1/3}$ holds. A short scaling range appears to occur between 10 cm and 2 m. In that range a linear regression yields a slope of 0.34, very close to the predicted 1/3.

A priori one may be surprised to get such a short scaling range for $D_2(L)$, where at the same time a $k^{-5/3}$ energy is obtained over a wider range of scales. Results of other experimenters in comparable conditions have been similar (see for example Van Atta and Chen, 1970). For low altitudes in the surface layer (< 20 m), the scaling range is short and $D_2(L)$ becomes quickly smaller than the predicted $L^{1/3}$ at large scales; two decades of scaling range can be obtained if the altitude exceeds 30 meters. The best verifications of the K41 theory have always been obtained with energy spectra. In general, the connection between the power spectrum and the autocorrelation function implies that $D_2(L)$ and the energy spectrum E(k) are related by (Monin and Yaglom (1975) section 13.1)

$$(D_2(L))^2 = 2 \int_0^\infty \sin^2(kL/2)\, E(k)\, dk. \qquad (6.3.1)$$

Given that E(k) decays rapidly like $k^{-5/3}$, the main contribution to $D_2(L)$ comes from the first interval where $\sin(kl/2) = 1$, i.e. from the wave number satisfying $kL/2 = \pi/2$. Using $k = 2\pi/\lambda$ this corresponds to scales $\lambda = 2L$. A range of scales around 2L therefore make the main contribution to $D_2(L)$. A breakdown of the $k^{-5/3}$ energy spectrum for $\lambda > 10$ m, as

observed in figure 6.2, might therefore correspond to a breakdown of the scaling of $D_2(L)$ at scales smaller than 10 meters.

The indication of the length of the isotropic inertial range from a one dimensional time series remains an open question. In our case the $k^{-5/3}$ energy spectrum holds perfectly for 10 cm < λ < 10 m, and remains relatively close to $k^{-5/3}$ at larger scales. Van Atta and Park, 1971) also observed, at comparable altitudes, a good $k^{-5/3}$ over wide range of scales. At a 4 meters altitude large scales cannot be isotropic and therefore the energy spectrum is not a sensitive indicator of the scale at which isotropy breaks down. Van Atta and Park (1971), observing a sharp change in behavior of $<(\Delta v(L))^3>$ at a scale comparable to the altitude, have suggested that this structure function may be a more sensitive indicator of isotropy. In general however the scaling of the order h structure function breaks down gradually at large scales. The width of the scaling range is also observed to shrink as h increases.

Higher order structure functions $<|\Delta v(L)|^h>$ were measured for h = 1, 2, ... 18. The normalized quantities

$$D_h(L) = <|\Delta v(L)|^h>^{1/h} \sim L^{\zeta(h)/h}$$

were plotted in figure 6.10 and 6.11. For $1 \le h \le 6$ a fairly good power law is obtained between 10 and 100 cm (the first 4 points on the graph), and $\zeta(h)$ was measured in that range The power law is especially good when h=3 and $\zeta(3) = 1.01$, a good agreement with the exact result $\zeta(3) = 1$ for isotropic flows (see chapter 2). For $7 < h < 18$, a plausible but limited power law is obtained between 20 cm and 150 cm (from the second to the fifth point), and that range was used to measure $\zeta(h)$ with a linear regression. The resulting function $\zeta(h)$ was plotted in figure 6.12, together with the results of Anselmet *et al.* (1984, results of jet turbulence in table 2 for the highest Reynolds number). The straight line is the prediction of the K41 theory. Both results agree well for $h \le 4$ and are fairly consistent for $h > 4$. Our $\zeta(h)$ starts showing a significant departure from the K41 prediction for $h \ge 5$. Beyond this limit

$\zeta(h)$ becomes more or less linear, with a slope of about 0.2. This interesting result will be examined in more details in the next chapter.

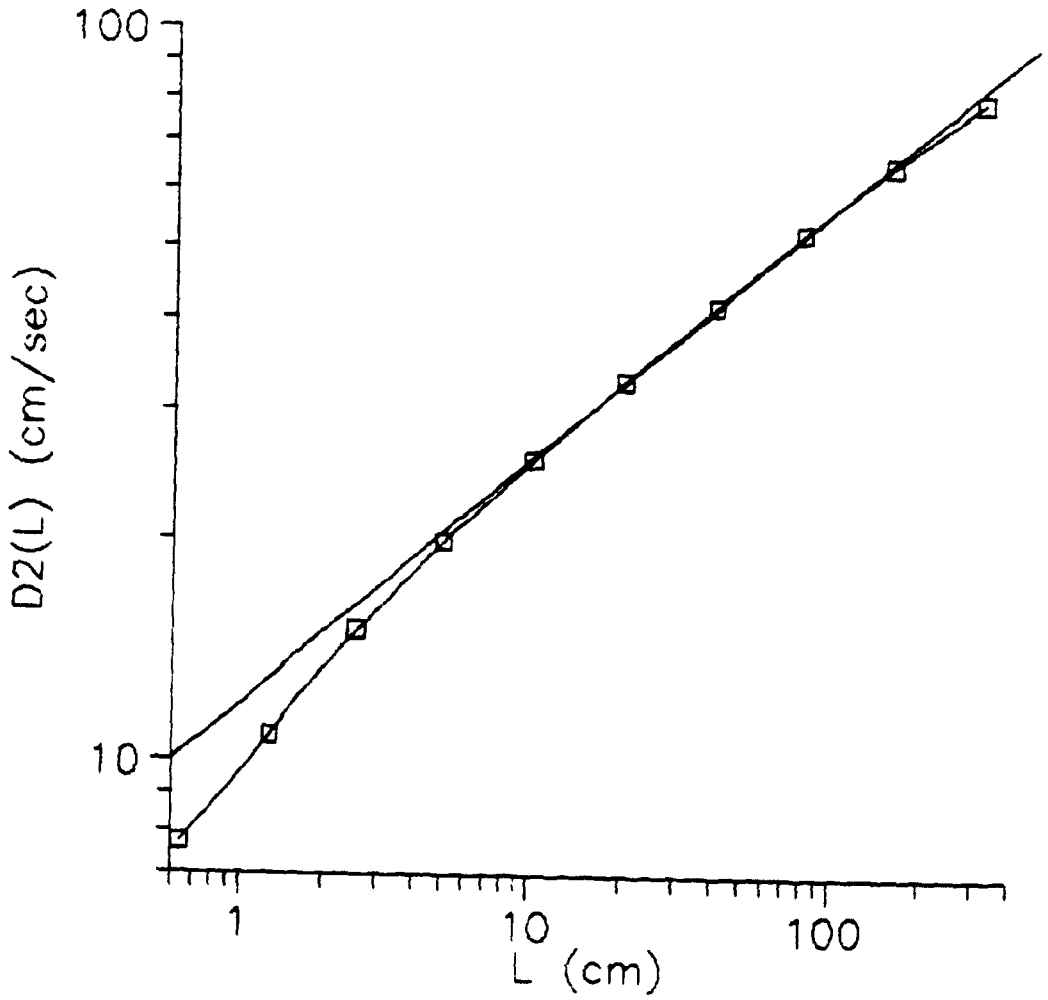

Figure 6.9: Second order velocity structure function $D_2(L) = [<(\Delta v(L))^2>]^{1/2}$. The solid line is a power law with exponent 0.34, in good agreement with the 1/3 predicted by the K41 theory. Notice that the short scaling range extends from 10 cm to 2 m.

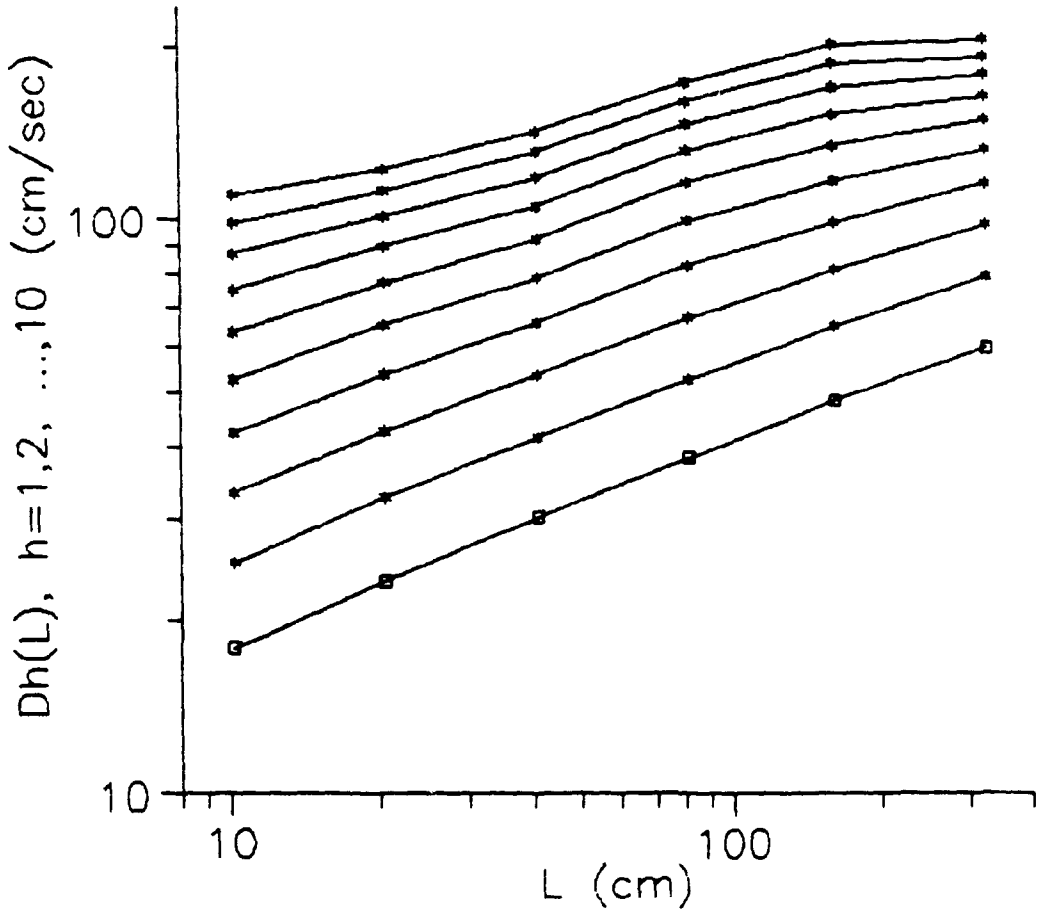

Figure 6.10: Velocity structure functions $D_h(L) = \langle|\Delta v(L)|^h\rangle^{1/h}$ for h=1, 2, , 10, from bottom to top respectively. The scaling is fairly good for the first 4 points, between 10 cm and 2 m. It is especially good for the third order structure function, a result consistent with the fact that both the original and the refined similarity theories make the same prediction $\langle|\Delta v(L)|^3\rangle \sim L$ for h = 3.

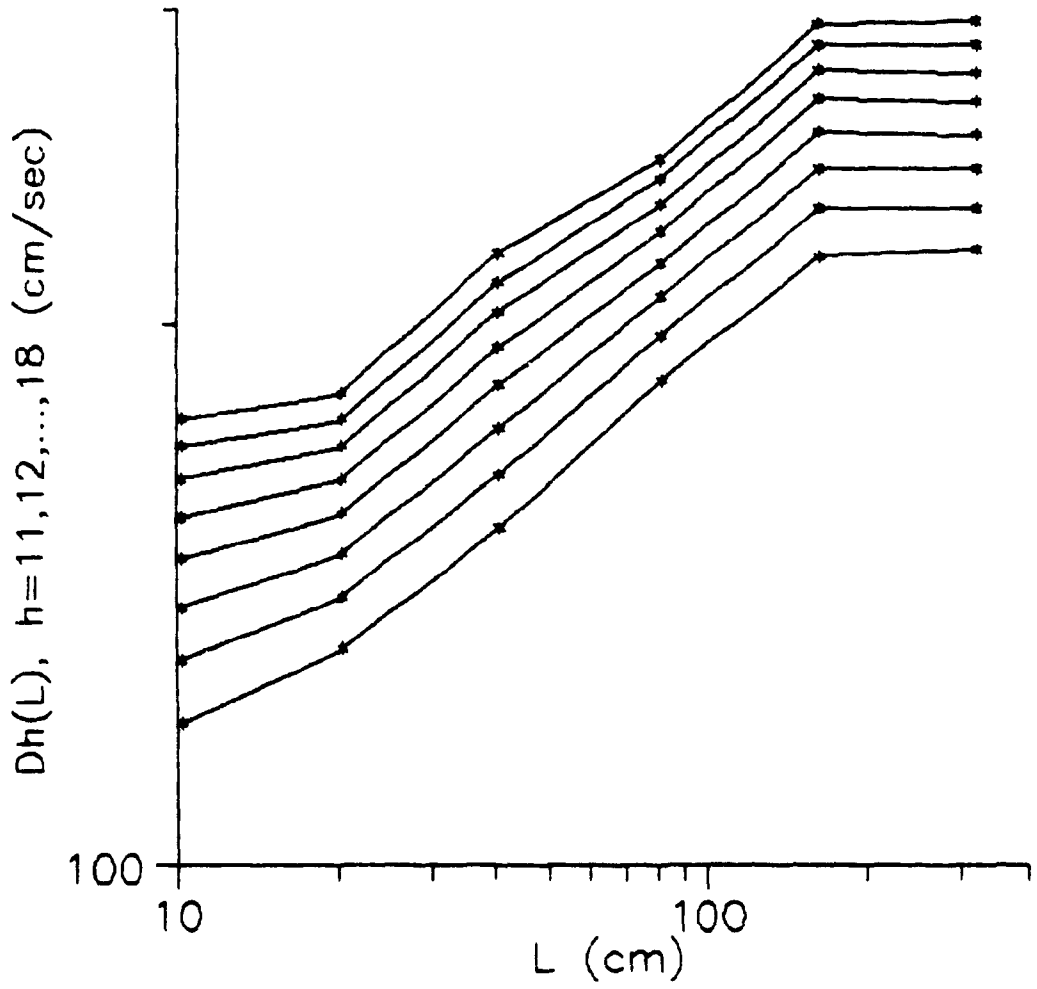

Figure 6.11: Velocity structure functions $D_h(L) = \langle|\Delta v(L)|^h\rangle^{1/h}$ for h=11, 12, ..., 18, from bottom to top respectively. The scaling exponents were measured by fitting a power through the points 2 to 5 (counted from left to right), where the scaling is fairly good. It is emphasized that the estimation errors are larger on high order moments.

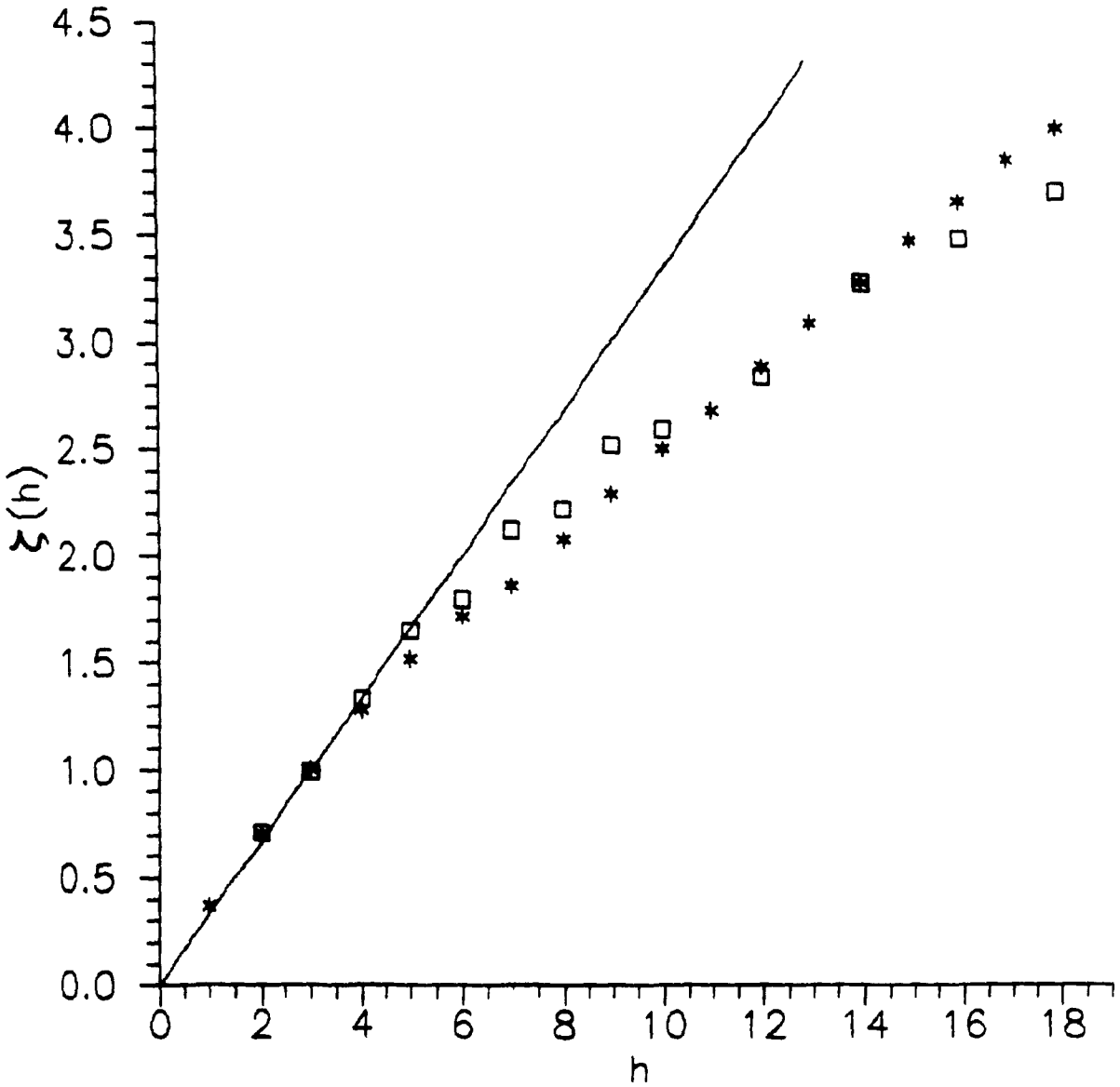

Figure 6.12: A comparison between the $\zeta(h)$ measured by Anselmet et al. (squares) and our measurements (stars). The agreement is perfect for $h \leq 4$ and fair at larger h. Notice that on our measurements $\zeta(h)$ appears to be straight at large h. This straight line is accurately fitted by $\zeta(h) = 0.195h + 0.548$. The solid line is the prediction of the Kolmogorov 1941 theory, i.e. $\zeta(h) = h/3$.

6.4 GENERATING FUNCTION OF $(\partial u/\partial x)^2$

The sample was split in 24 disjoint slices of 100 meters. The generating functions $\chi_q(\delta)$ were computed on each slice and averaged. The normalized quantities

$$Z_q(\delta) = (<\chi_q(\delta)>)^{1/(q-1)} \sim \delta^{D(q)}, \text{ where } D(q) = \tau(q)/(q-1), \qquad (6.4.1)$$

were considered for q=-10.5,-9.5, ..., 10.5. $Z_q(q)$ is displayed for q = -10 in figure 6.13. A good scaling is obtained between 10 cm and 100 meters. This behavior is representative of the range $-10.5 < q < 1.5$. $Z_q(q)$ is displayed for q = 3.5 and 10.5 in figures 6.14 and 6.15 respectively. Their behavior is representative of the range $q \geq 2.5$: $Z_q(\delta)$ is a little irregular but a power law remains a plausible representation of the data, since $Z_q(\delta)$ does not exhibit a constant curvature. The D(q)'s were measured with a linear regression in the range $10 \text{ cm} < \delta < 100 \text{ m}$, and the mass exponents were obtained with (6.4.1). $\tau(q)$, plotted in figure 6.16, exhibits two linear asymptotes in the limits $|q| \to \infty$, exactly like the multinomial measure (see section 5.2.6).

We shall next study the convergence of $\tau(q)$ as a function of the sample size. The quantity $Z_q(\delta)$ was calculated successively with 1/8, 1/4, 1/2 and the totality of the sample. In each case the resulting $\tau(q)$ was plotted in figure 6.16. For $q > 0$, $\tau(q)$ appears to be well defined. This convergence suggests that $\alpha(\delta)$ has a lower bound α_- where f is finite (see section 5.2.4). By contrast, for $q < -1$ the function $\tau(q)$ changes with the sample size but remains linear asymptotically. The asymptotic slope decreases with increasing sample size, which means that the mass exponents in the range $q < -1$ are less reliable. We say that the scaling is *spurious* when the exponents have not converged. This appears to be the first evidence of spurious scaling for the energy dissipation field. Spurious scaling effects have been described and illustrated with numerical experiments by Lavallée *et al.* (1990).

The $\tau(q)$ obtained by Meneveau and Sreenivasan (1987a) were fairly accurately fitted by a microcanonical binomial measure with weights 0.7 and 0.3. For a binomial measure, $\tau(q)$ has linear asymptotes at infinity with slopes

$$s_+ = -\frac{\log(w_-)}{\log 2} \text{ for } q > 0 \quad \text{and} \quad s_- = -\frac{\log(w_+)}{\log 2} \text{ for } q < 0. \qquad (6.4.4)$$

For our data, the asymptotes obtained with the whole sample are accurately fitted by

$$\tau(q) \sim 0.482\, q - 0.048 \text{ for } q \to \infty \text{ and } \tau(q) \sim 1.42\, q - 0.0375 \text{ for } q \to -\infty.$$

Using the values 0.482 and 1.42 for s_- and s_+ respectively, (6.4.4) yields

$$w_- = 0.716 \quad \text{and} \quad w_+ = 0.374,$$

which is close to the Meneveau and Sreenivasan results. Notice that $w_- + w_+ = 1.09$, i.e the microcanonical constraint $\sum w_i = 1$ is almost respected. The function

$$\tau(q) = -\log_2\{ (0.716)^q + (0.374)^q \}$$

was also plotted in figure 6.16 and obviously gives an excellent fit to the data.

It is emphasized that our method for measuring $\tau(q)$ is different, and more simple, than the method previously used by Meneveau and Sreenivasan (1987b, 1987c) In their analysis, different realizations of the field were treated like deterministic measures and the $\tau(q)$ were measured on each sample. They discarded some samples because of the lack of scaling Other samples did scale but produced different D(q) curves, and they chose to average the D(q)'s to get the final result. Averaging the D(q)'s is equivalent to averaging $\log(\chi_q(\delta))$ This averaging is not consistent with the properties of random scaling measures because $\chi_q(\delta)$ is the scale invariant quantity, not $\log(\chi_q(\delta))$. By contrast, we averaged $\mu^q(\delta)$ over a sample as large as possible because the field $(\partial u/\partial x)^2$ was regarded as a random field In preliminary analyses we

noticed that relatively small samples did exhibit some scaling with apparently random values of D(q). Our larger data set (5 minutes of recording, in comparison with 30 seconds for Meneveau and Sreenivasan, for similar air flows) allowed to show that this problem disappears for large enough samples for which $\tau(q)$ becomes well defined (at least for $q > 0$!). Actually, for our data set the minimum sample size needed to get a reasonable convergence of the $\tau(q)$'s was about 30 seconds, which may explain the difficulties encountered by Meneveau and Sreenivasan since their maximum sample size was also 30 seconds. For large enough samples a good scaling is observed and the variations of D(q) as measured on small samples are more simply interpreted as natural randomness.

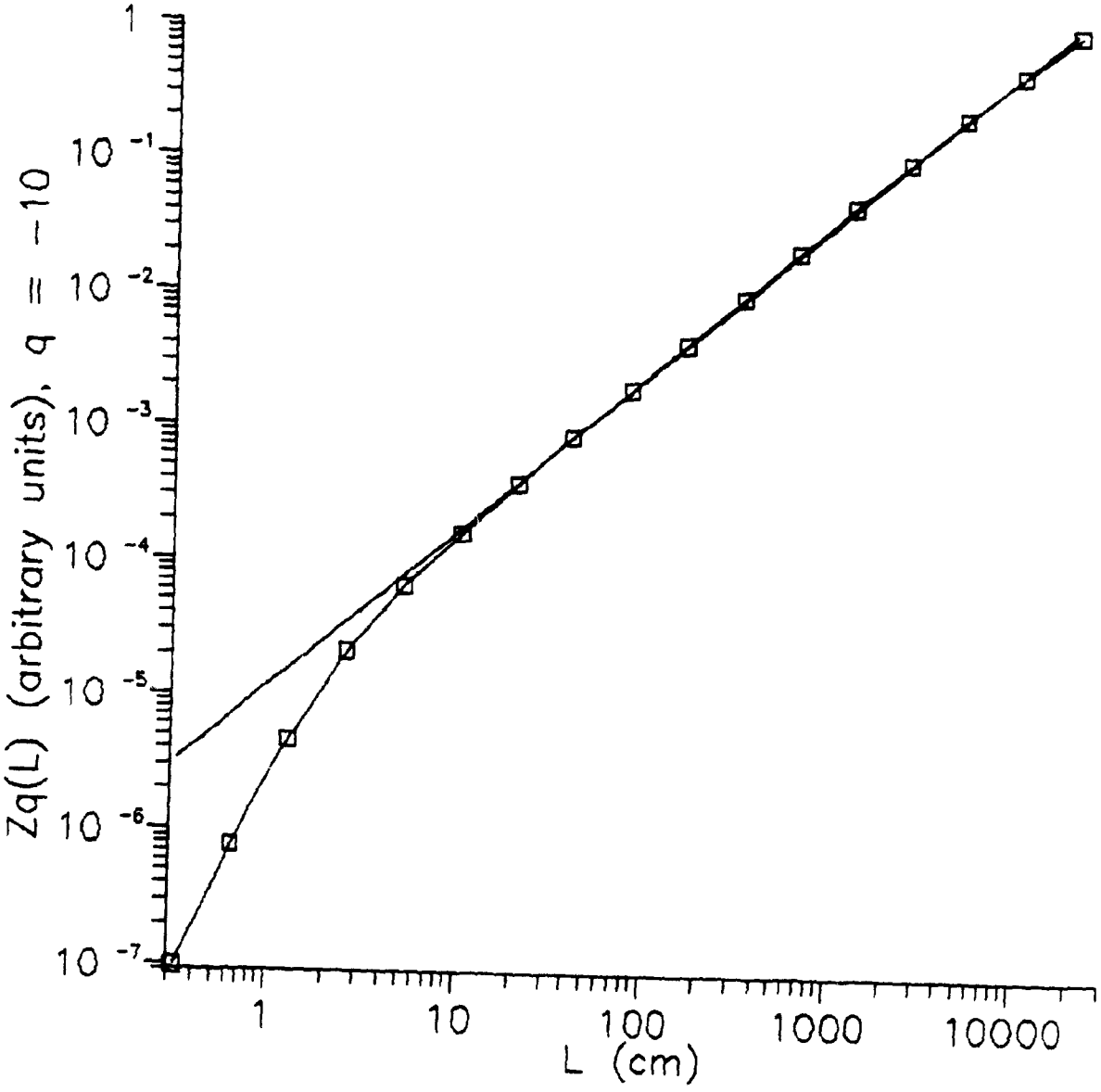

Figure 6.13: A plot of the normalized generating function $Z_q(\delta) = (\chi^*_q(\delta))^{1/(q-1)} \sim \delta^{D(q)}$, where $D(q) = \tau(q)/(q-1)$, for $q = -10$. The scaling is good up to scales of 100 meters and may even extend to larger scales. Huge scaling ranges have also been observed by Meneveau and Sreenivasan (1987b,1987c). This behavior is representative of the range $-10.5 < q < 1.5$

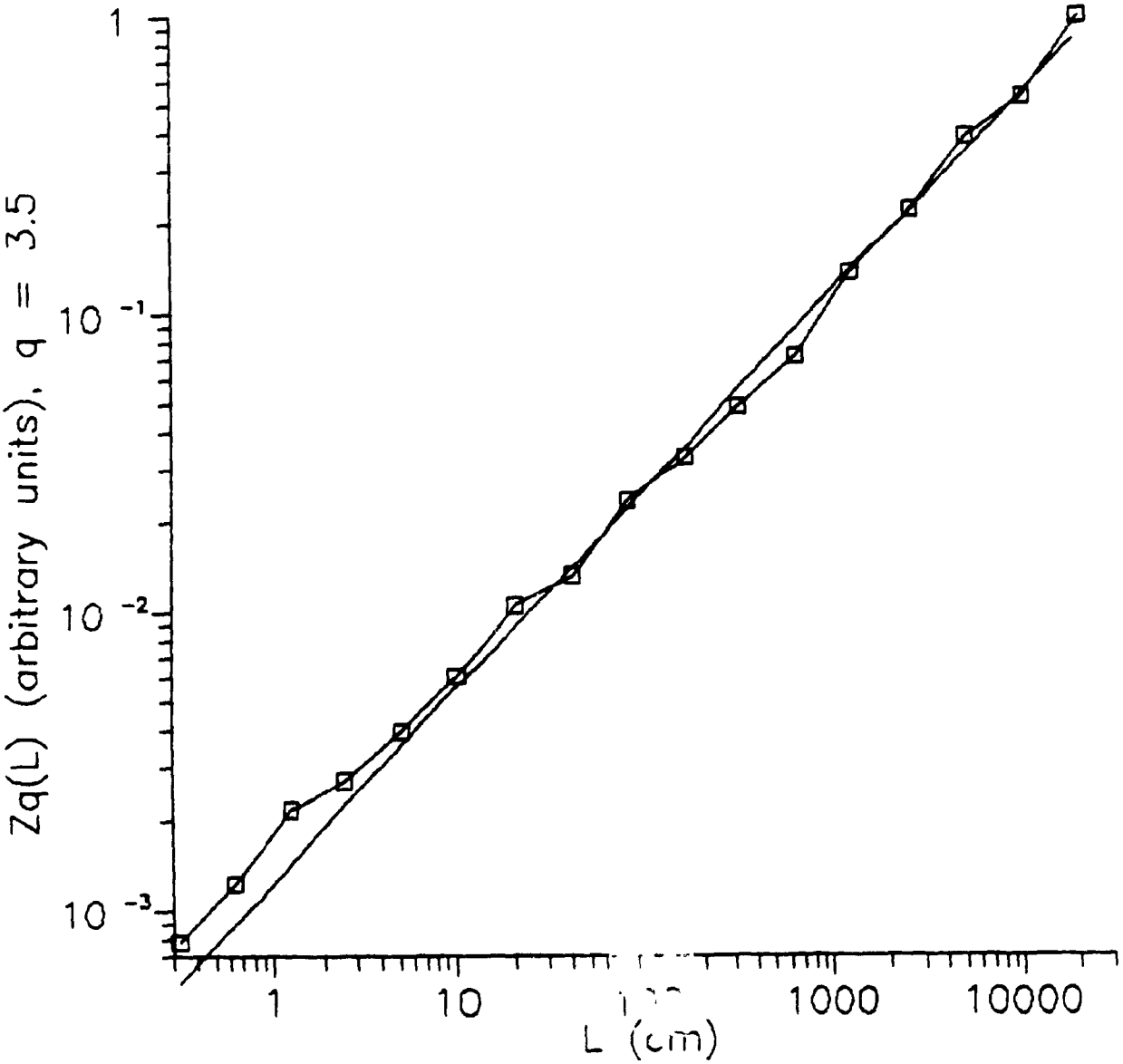

Figure 6.14: A plot of the normalized generating function $Z_q(\delta)$ for q = 3.5. Although a little irregular, $Z_q(\delta)$ is well described by a power law. Indeed $Z_q(\delta)$ does not have a constant curvature but rather wiggles around a power law. This behavior is representative of the range $q \geq 2.5$. Again, the scaling range is very large with respect to the height of the probe from the ground (about 4 meters).

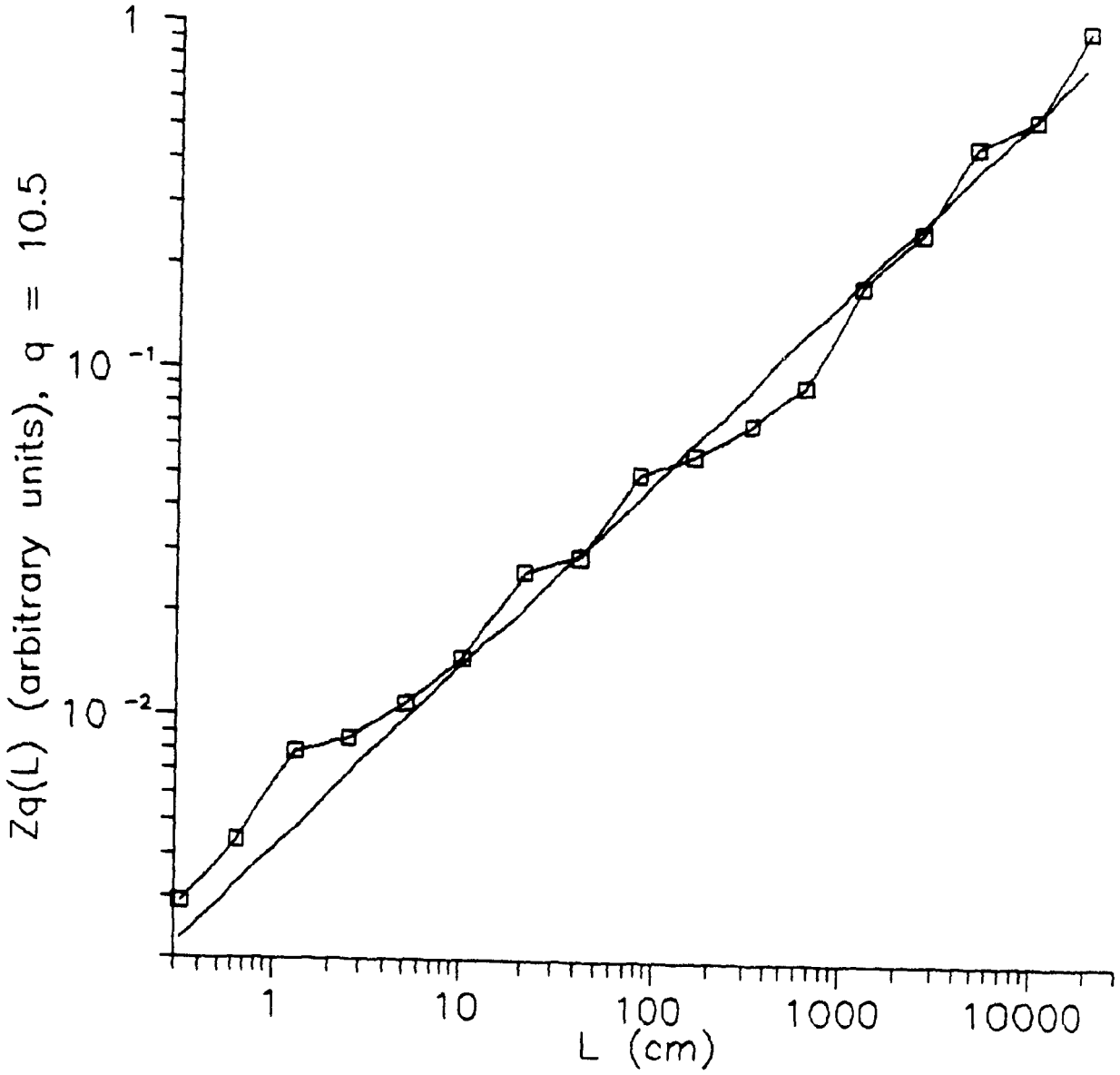

Figure 6.15: Normalized generating function $Z_q(\delta)$ for q = 10.5 The amplitude of the oscillation around the power law increases as q increases.

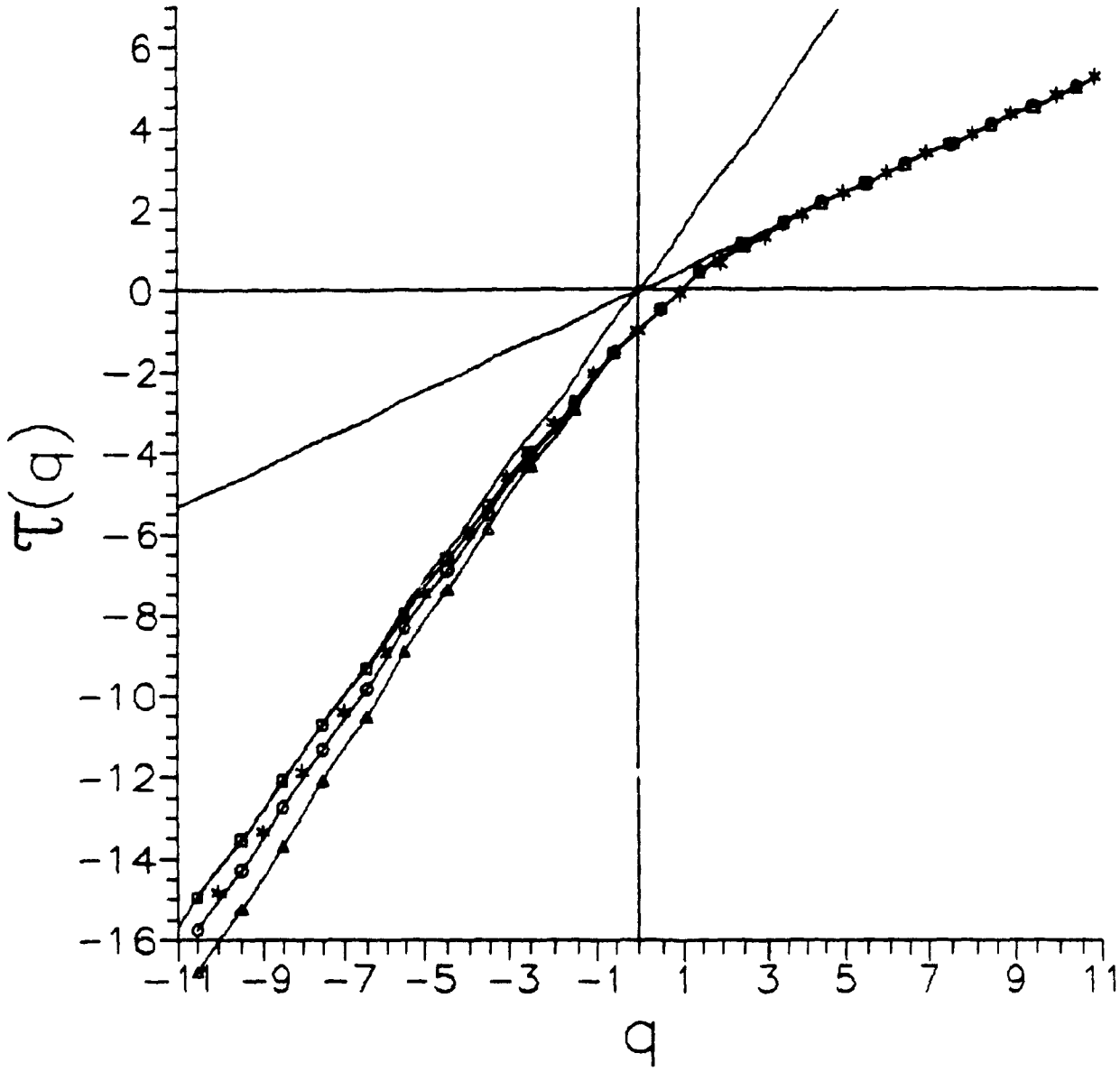

Figure 6.16: Mass exponents measured from the data. 3 curves are displayed: The first one (squares) was obtained by averaging $Z_q(L)$ on the whole sample. The second curve (circles) was obtained by averaging on 1/2 or 1/4 of the sample (the same result was obtained), and the last curve (triangles) was obtained with 1/8 of the sample. The stars are points on the function $\tau(q) = -\log_2(0.716^q + 0.358^q)$, which fits the data very well. For $q > 0$ the mass exponents converge rapidly. By contrast, for $q < 0$ the exponents $\tau(q)$ increase when $Z_q(L)$ is averaged over a larger sample. This phenomenon occurs for $q < -1.5$ and therefore the mass exponents in that range do not appear to be reliable.

6.5 CORRELATION GENERATING FUNCTION OF $(\partial u/\partial x)^2$

Let us now consider the correlation generating function of this measure Consider the quantity

$$W_q(\delta) = (<\Phi^{(1)}_{q/2,q/2}(\delta)>)^{1/(q-1)}, \qquad (6.4.5)$$

where $\Phi^{(1)}_{q,q}(\delta) = \sum [\mu_i(\delta)\mu_{i+1}(\delta)]^q$. This is a special case of the correlation generating function $\Phi^{(n)}_{p,q}(\delta)$ (section 5.5) where p = q and n = 1, i.e. adjacent boxes. For multinomial measures CL-scaling holds on the line p = q (see figure 6.22), i.e

$$W_q(\delta) \sim \delta^{D(q)}, \text{ where } D(q) = \tau(q)/(q-1). \qquad (6.4.6)$$

The fact that $W_q(\delta)$ and $Z_q(\delta)$ scale with the same exponent is regarded as a characteristic property of multinomial measures (see section 5.5.5) The quantities $\Phi^{(1)}_{q,q}(\delta)$ were computed on each 100 meters subsample and were then averaged over all the subsamples to obtain $W_q(\delta)$ For $q < 0$, a good scaling (similar to figure 6.13) was obtained For $q > 0$, $W_q(\delta)$ also scales over the whole range of scales but again irregular departures from a power law are visible (figure 6.17). The scaling exponents $\tau(q)$ obtained with the whole sample with $Z_q(\delta)$ (single-box generating function) and $W_q(\delta)$ (double-box generating function) were plotted on the same graph in figure 6.18. The agreement is good. The largest differences (at most 10%) are obtained for $q > 0$ and are explained by the error induced by the oscillating power laws Within these small errors we conclude that the correlation constraint (5.5.7) is well obeyed for n = 1, i.e. for adjacent boxes.

In order to see if the constraint (5.5.7) was satisfied for $n > 1$ the quantities $<\mu^q(\delta)>$ and $<[\mu_i(\delta)\mu_{i+n\delta}(\delta)]^{q/2}>$ where plotted on normalized scales for n = 1, 2, 3 and 4 with q fixed For a separated multinomial measure we expect these quantities to scale like $\delta^{\tau(q)+D}$. Figure 6.19 displays the results obtained with q = 2. Notice that in this case the constraint (5.5.7) is

necessarily satisfied because it is implied by single box scaling (see (5.5.12a), section 5.5.3), and therefore we expect to get $<\mu_i(\delta)\mu_{i+n\delta}(\delta)> \propto \delta^{\tau(2)+1}$ for all n, where $\tau(2) \approx 0.79$. The variations of the measured exponent are small and the agreement with (5.5.12a) is therefore good, as expected. Figure 6.20 displays the results obtained with $q = -2$. According to section 5.5.3 this case does not satisfy (5.5.7) trivially. The agreement is good and even better than in the above trivial case where the agreement should in principle be perfect. Similar results were obtained in the range $-5 < q < -1$. Figure 6.21 displays the results obtained with $q = 5$. The scaling is not as good than in the previous cases. The prefactor irregularities imply relatively large errors on the fitted exponents. Within these errors the agreement with (5.5.7) remains plausible. Similar results were obtained in the range $3 \leq q < 5$ but the scaling was found to be a little better.

In order to see if the energy dissipation field exhibits a scaling transition comparable to non-separated multinomial measures (see section 5.5.4), we chose to examine the scaling of $<(\mu_i(\delta))^p(\mu_{i+1}(\delta))^q>$ along the line $q = -2p$ (see figure 6.22). It should be recalled that, according to (5.5.19), the scaling expected for such measures is

$$<(\mu_i(\delta))^p(\mu_{i+1}(\delta))^q> \sim \delta^{A(p,q)} \quad \text{as } \delta \to 0, \tag{6.4.7}$$

where

$$A(p,q) = \begin{cases} \tau(p+q)+1 & \text{(CD-scaling domain)} \\ \tau(p)+\tau(q)+3 & \text{(non CD-scaling domain)} \end{cases}.$$

For $p < 2$ along the line $q = -2p$ the multinomial model obeys CD-scaling, while for $p > 2$ a scaling transition ruled by (6.4.7) occurs. In figure 6.23 we plotted on the same graph $<(\mu_i(\delta))^p(\mu_{i+1}(\delta))^{-2p}>$ and $<(\mu_i(\delta))^{-p}>$ for $p = 1/2, 1, 3/2, 2, 5/2$, as obtained from the dissipation field. In the CD-scaling domain these quantities are expected to scale with the same exponent. It is noticed that the two-box products are power laws at large scale only while the single box moments scale over the whole range. For $q < 2$ the exponents $A(p,-2p)$ and $\tau(-p)+1$ are about equal, i.e. CD-scaling is well obeyed. However, for $q \geq 2$ the exponents

$A(p,-2p)$ and $\tau(-p)+1$ start to exhibit significant differences and therefore a scaling transition occurs. In order to see if the scaling transition was consistent with (6.4.7), we plotted on the same graph (figure 6.24) the exponents $A(p,-2p)$, $\tau(-p)+1$ and the prediction (6.4.7) for non CD-scaling, i.e. $\tau(p)+\tau(-2p)+3$. Taking the estimation errors into account, we conclude that a scaling transition is indeed taking place but that the exponents $A(p,-2p)$ are different from $\tau(p)+\tau(-2p)+3$, which is the prediction of the multinomial model.

These results are interesting for at least three reasons: Firstly, CD-scaling is well obeyed on the line $p = q$ which is consistent with the multinomial model; secondly, the scaling transition predicted in the model actually occurs in the dissipation field; thirdly, the exponents $A(p,q)$ do not match the exponents of the model in the non CD-scaling domain (and maybe also elsewhere), which allows to distinguish the energy dissipation field from single scale cascades. From a more general viewpoint, this suggests that the functions $A(p,q)$ defined above may not be everywhere related in a simple manner to $\tau(q)$, in which case they would provide a more complete description of a scaling field that goes beyond the multifractal characterization. The failure of the single scale multinomial model to account for the scaling of correlations might suggest that more general models, such as multiscale cascades, may be more adequate for the energy cascade process.

Remark: It is noticed (figure 6.17) that the prefactor of $W_q(\delta)$ appears to be periodic in $\log\delta$. This is observed for all $q > 3$, and three minimums occur at scales approximately equal to 1.3 cm, 82 cm and 5240 cm. The ratios 82/1.3 and 5240/82 are 63 and 64 respectively, which suggest that the scale ratio $r \approx 64$ plays a special role. Oscillations of that kind have been regularly observed in measurements of high order velocity structure functions in turbulent flows (e.g. Van Atta and Park (1971), Anselmet *et al* (1984)), with a period consistent with a scale ratio of about 60. The temptation is to interpret them as log-periodic oscillations analogous, in some sense, to the prefactor oscillations of $N_B(\delta)$ for exactly self-similar sets. However, a more convincing result would require the observation of more than two periods,

which is a problem when the scale ratio is so large. It also remains to be shown that these oscillations are not statistical artefacts. On the other hand, the field $(\partial u/\partial x)^2$ is necessarily anisotropic at these scales (because of the 4 meters altitude) and the effect of anisotropy is poorly understood. The origin of these oscillations therefore remains unclear. A more detailed investigation of prefactor oscillations in the context of self-similar sets and measures will be proposed in chapter 8.

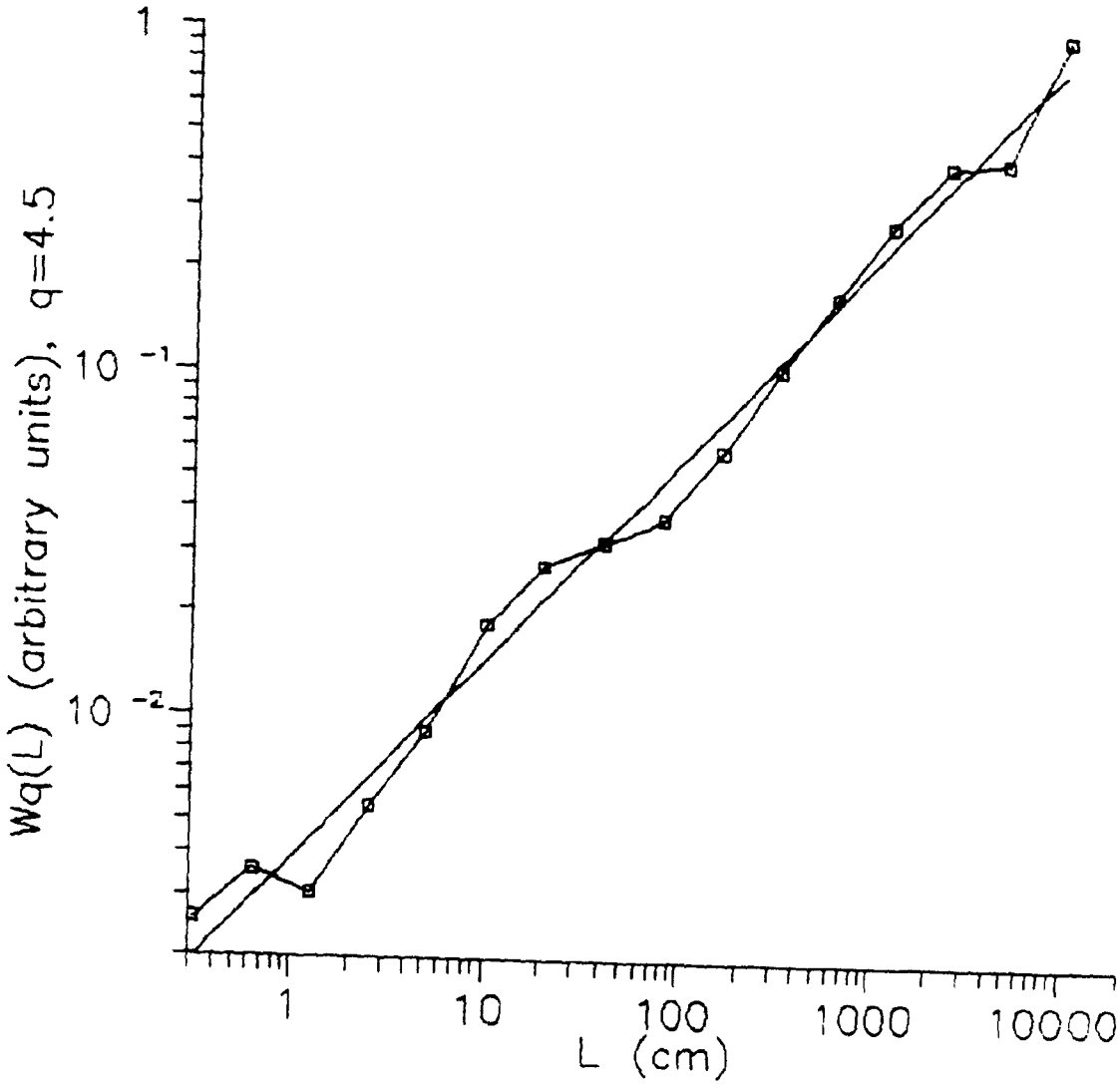

Figure 6.17: $W_q(\delta)$ versus δ on a log-log scale, for $q = 4.5$. The curve oscillates periodically around a power law. This behavior is representative of $q > 0$ The amplitude of the oscillations is observed to increase with q.

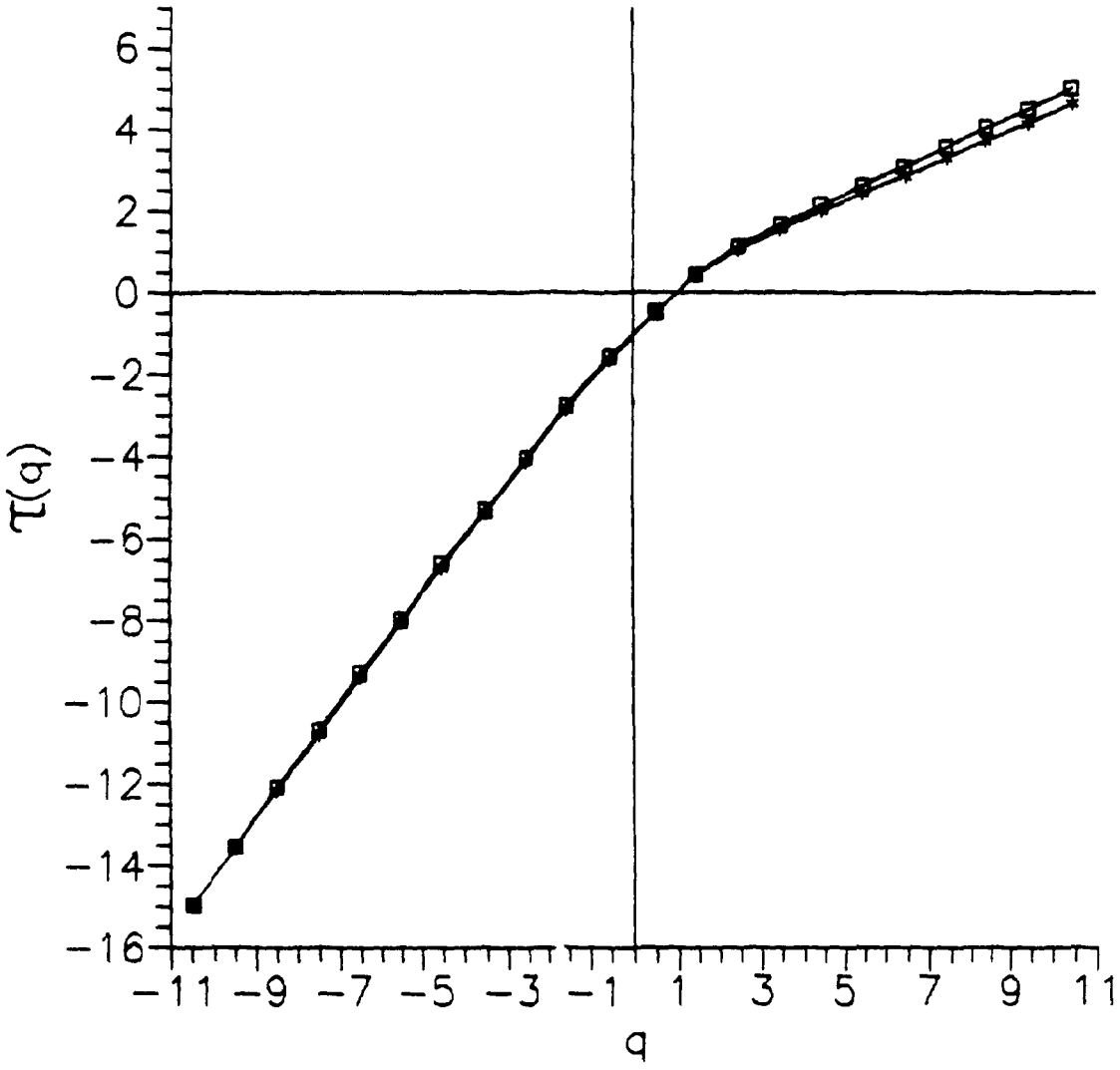

Figure 6.18: Exponents $\tau(q)$ (squares) and $t(q/2)$ (stars) as measured with the one-box and two-boxes generating functions on the energy dissipation field. Within the experimental errors (less than 10%), which are maximum for $q > 0$ because of the oscillations of $W_q(\delta)$, both functions are identical. As proved in section 5.5, these exponents are equal for random microcaconical multiscale measures.

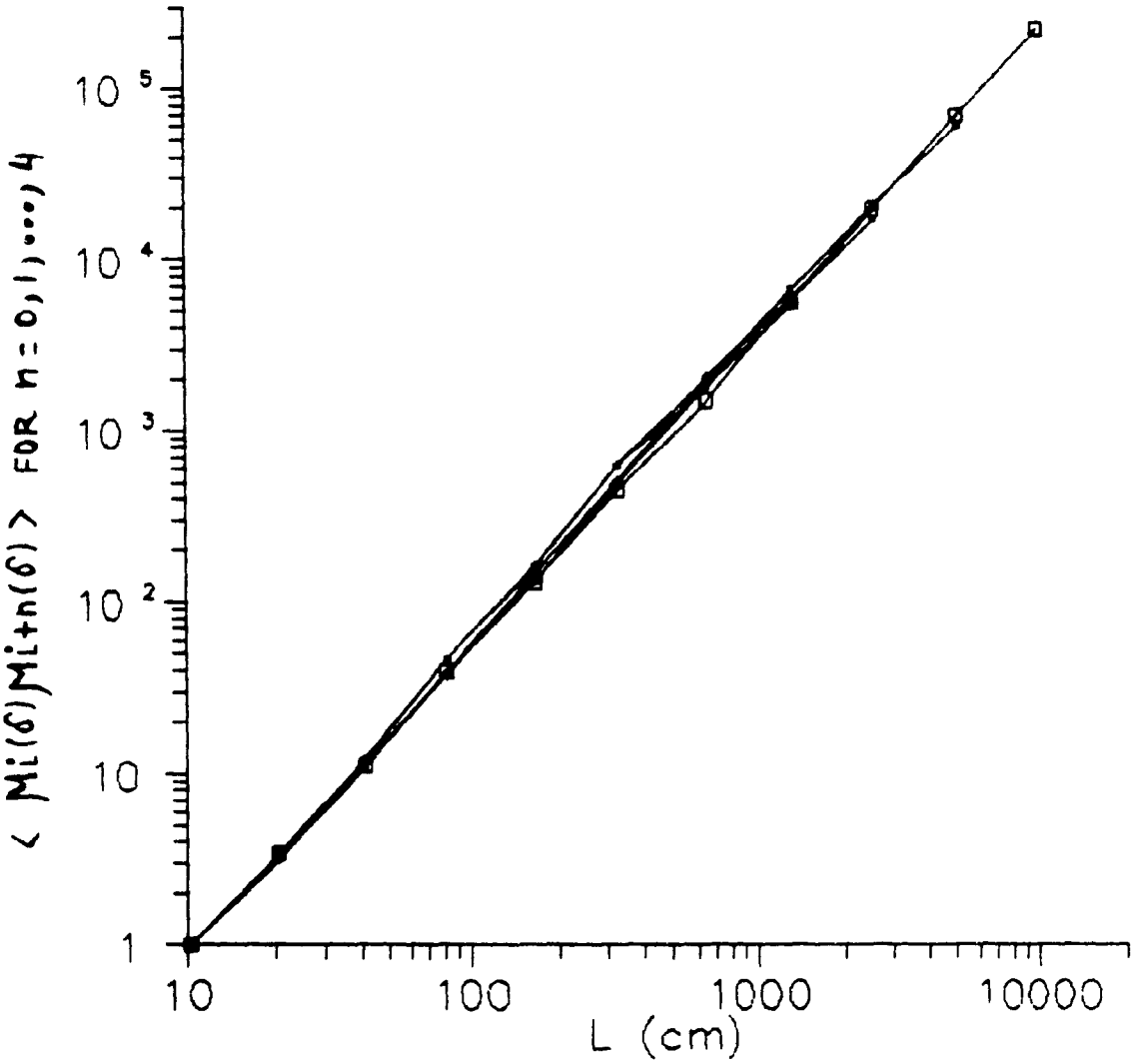

Figure 6.19: $<\mu^2(\delta)>$ (squares) and $<\mu_i(\delta)\mu_{i+n\delta}(\delta)>$ (other symbols) where plotted on normalized scales for n = 1, 2, 3 and 4 For any scaling measure we expect all these quantities to scale like $\delta^{\tau(2)+D}$, where $\tau(2) \approx 0.79$ The exponents obtained by fitting power laws to these curves are (after subtracting 1) 0.80, 0.83, 0 85, 0 86 (±0 05) for n = 1, 2, 3, 4 respectively. The agreement is therefore good, as expected for q = 2

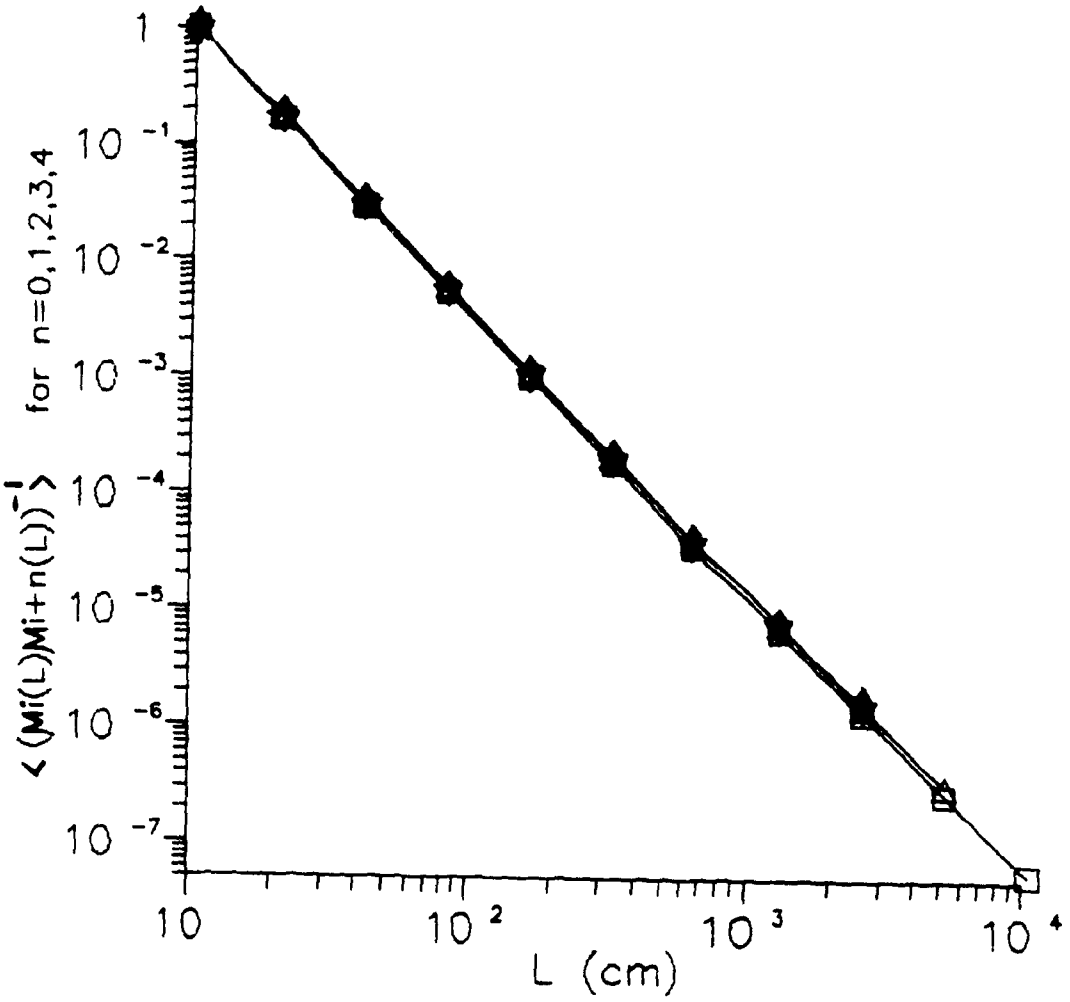

Figure 6.20: $\langle[\mu_i(\delta)\mu_{i+n\delta}(\delta)]^{-1}\rangle$ for n = 1, 2, 3, 4 and $\langle\mu^{-2}(\delta)\rangle$ on normalized scales. The exponent fitted using linear regressions do not vary by more than 1%. The agreement between the scaling exponents is therefore good.

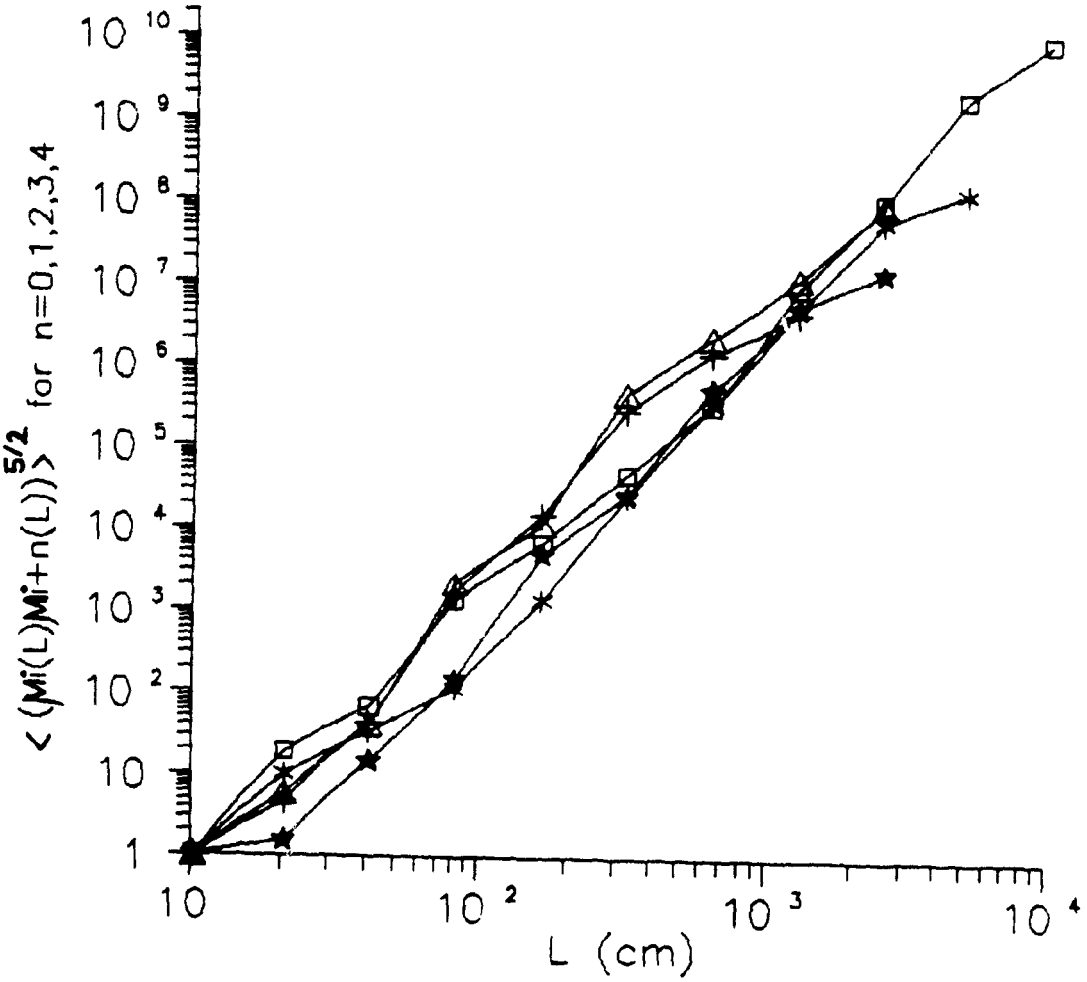

Figure 6.21: $<[\mu_i(\delta)\mu_{i+n\delta}(\delta)]^{5/2}>$ for n = 1, 2, 3, 4 and $<\mu^5(\delta)>$ (symbol □) on normalized scales. n = 1: ✱ , n = 2: ☆ , n = 3. Δ , n = 4: + . The scaling is not as impressive. Within the errors due to the prefactor irregularities the agreement betwen the fitted exponents remains plausible. Notice that the agreement is a little better for n = 1 and 2 than for n = 3 and 4.

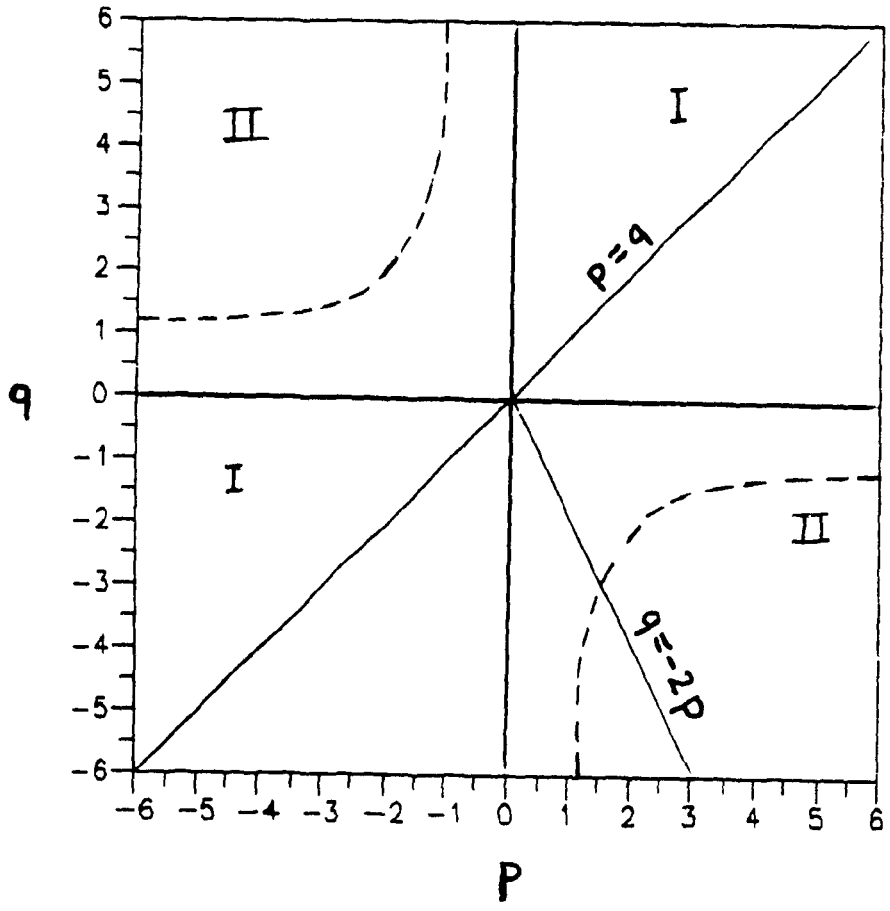

Figure 6.22: A graph of the CD-scaling domain (I) and the non-CD scaling domain (II) for multinomial measures with mass exponents similar to the energy dissipation field (the dashed lines separate the two regions). The correlations $<(\mu_i(\delta))^p(\mu_{i+1}(\delta))^q>$ were examined along the lines p = q, that lies in region I, and along the line q = -2p, that crosses both regions.

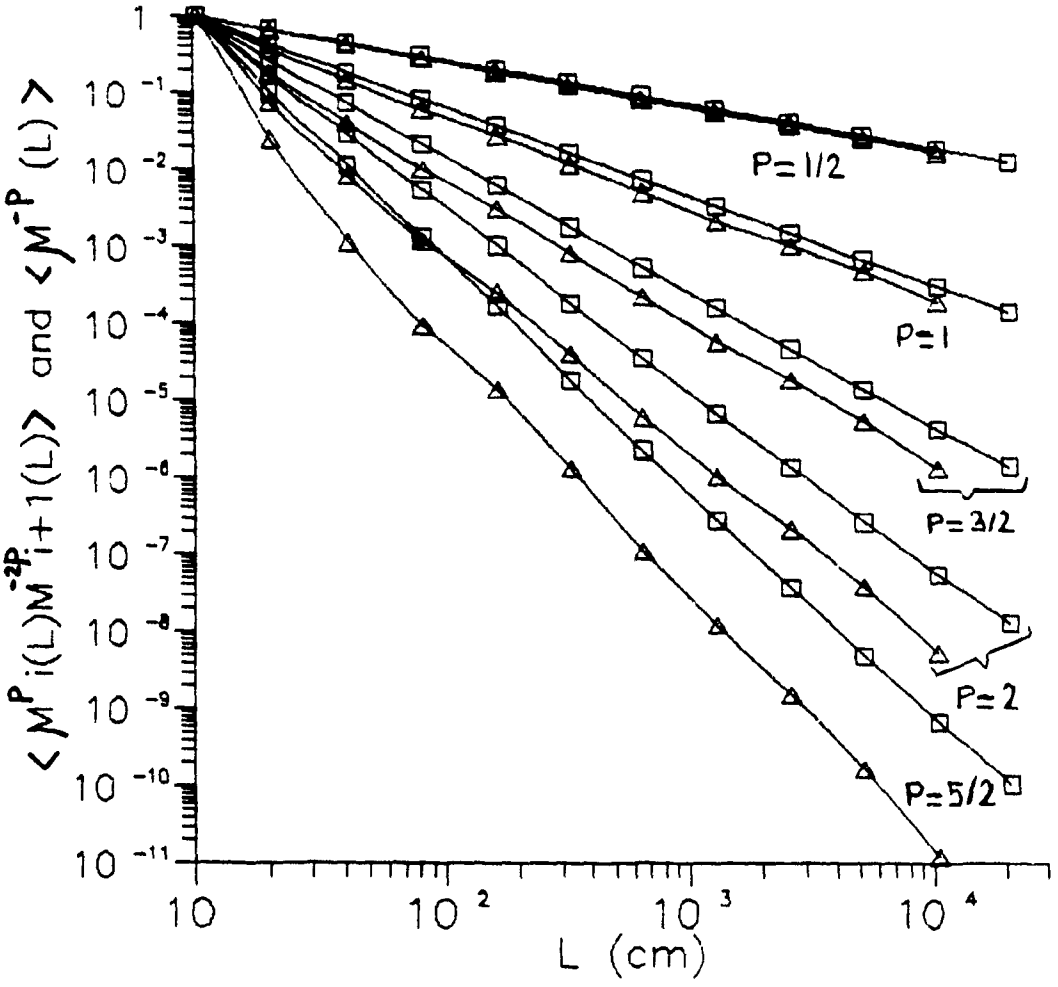

Figure 6.23: A graph of $<(\mu_i(\delta))^{-p}>$ (squares) and $<(\mu_i(\delta))^{p}(\mu_{i+1}(\delta))^{-2p}>$ (triangles) on normalized scales for p = 1/2, 1, 3/2, 2, 5/2 (from top to bottom) Both moments scale with similar exponents at large scale for $p < 2$, which is consistent with the CD-scaling of the multinomial model in this region. Significant differences between the scaling exponents are visible for $p \geq 2$, which means that a scaling transition is taking place This is also qualitatively consistent with the multinomial model.

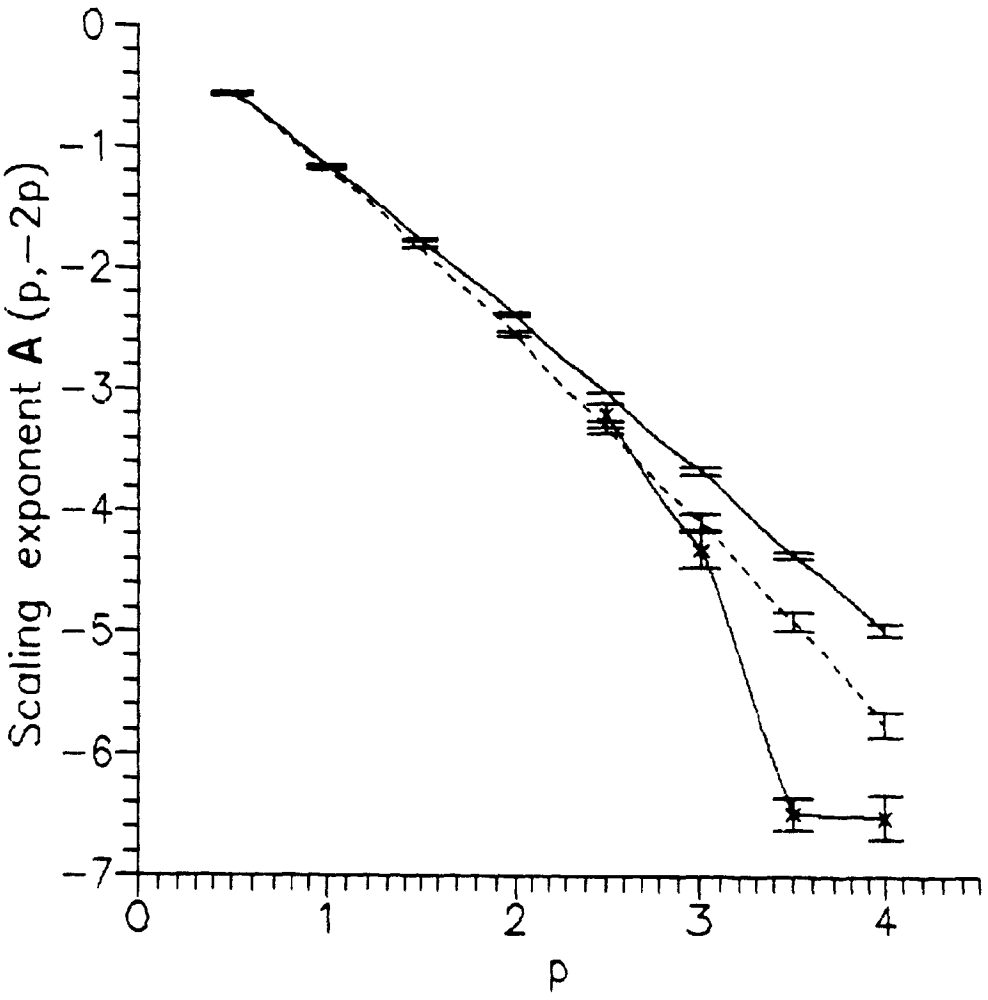

Figure 6.24: Three curves are plotted on this graph: The scaling exponents $\tau($ $\cdot 1$ (solid line) of $<(\mu_i(\delta))^{-p}>$, the scaling exponents A(p,-2p) of $<(\mu_i(\delta))^{p}(\mu_{i+1}(\delta))^{-2p}>$ (dashed line) and the exponents $A(p,-2p) = \tau(p)+\tau(-2p)+3$ (solid line with crosses) predicted by the multinomial model in the non CD-scaling domain (here $p \geq 2$). CD-scaling is well obeyed for $p < 2$ but a scaling transition takes place for $p \geq 2$. Taking the error bars into account, it is seen that significant differences between $\tau(p)+\tau(-2p)+3$ and A(p,-2p) occur for p = 3 5 and p = 4

Chapter VII

EXPERIMENTAL INVESTIGATIONS OF SOME TURBULENCE THEORIES

Le vent ramassa, le tourbillon dispersa

Turc saying

In this chapter three different aspects of turbulence theory are examined. In the first part 7.1, the cause of the breakdown of the Kolmogorov scaling law $\langle(\Delta v(L))^h\rangle \propto L^{h/3}$ at large h is examined. In the second part 7.2, a simple and possibly new experimental evidence of the existence of a spatially localized energy cascade is given and the idea of a fractal velocity field formed of "bursts nested into bursts" is shown to be supported. In the third part 7.3, we investigate the validity of the alternate (and weaker) form of the third hypothesis proposed in section 3.3.3.

7.1 TESTING SIMPLE SCALING IN THE VELOCITY FIELD

Let us focus on the implications of the 1941 Kolmogorov theory on the probability distribution of $|\Delta v(L)|$. The prediction $\langle|\Delta v(L)|^h\rangle \propto L^{h/3}$ leads to

$$\langle|\Delta v(\lambda L)|^h\rangle = \lambda^{h/3} \langle|\Delta v(L)|^h\rangle. \tag{7.1}$$

If (7.1) holds for all h then

$$|\Delta v(\lambda L)| \stackrel{d}{=} \lambda^{h/3} |\Delta v(L)|, \tag{7.2}$$

where "$\stackrel{d}{=}$" denotes the equality in probability distribution. (7.2) implies that the cumulative probability distribution of $|\Delta v(L)|$ has the form

$$\text{Prob}\{\, |\Delta v(L)| > u \,\} = \phi(u/u_*(L)), \tag{7.3}$$

where ϕ is an unknown function and $u_*(L) = L^H$ with $H = 1/3$. The K41 theory suggests the dimensional normalization $u_*(L) = (\varepsilon_0 L)^{1/3}$, but in the following we shall only make use of the proportionality assumption $u_*(L) \propto L^{1/3}$. (7.2) also implies that the probability density $\rho_L(x)$ of $|\Delta v(L)|$ takes the form

$$\rho_L(x) = \rho_1(x/L^H)\ L^{-H} \qquad (7.4)$$

where ρ_1 is an unknown function.

In order to see to what extent simple scaling is obeyed by the velocity field, the probability distributions (7.3) of $|\Delta v(L)|$ for L = 10, 20, 40 and 80 cm, obtained from the whole data set, were plotted in figure 7.1. Such plots were used in particular by Lovejoy (1985) and Lovejoy and Schertzer (1986) to show simple scaling in the rain field, the temperature field and the velocity field. In this representation, the simple scaling (7.3) implies that the horizontal spacings between these curves are equal at any height. Indeed if u_{n+1} and u_n denote the values of dv at a fixed probability level for scales L and λL respectively, then $\phi(u/L^H)$ is constant if $u_{n+1} = \lambda^H u_n$, i.e. if $\log(u_{n+1}) - \log(u_n) = H \log\lambda$. This condition is respected fairly accurately. The spacing between these curves can be used to deduce the scaling exponent H. Indeed, these curves cross a horizontal line at values dv_i (i=1, ..., 4) such that $H = \log(dv_{i+1}/dv_i)/\log(2)$. Looking for example at the probability level 5×10^{-3}, it is found that $dv_1 = 98.94$, $dv_2 = 123.94$, $dv_3 = 155.26$, $dv_4 = 194.48$ (in cm/sec). Using these values and the above formula yields $H \approx 0.325$, in good agreement with the Kolmogorov 1/3.

A more direct way of emphasizing simple scaling is to plot Prob{ $|\Delta v(L)| > u$ } versus $u/u_*(L)$, as suggested by (7.3). In this representation the distributions obtained with different lags L should fall on top of each other if simple scaling holds. This was done in figure 7.2 and the superposition of the various curves is convincing. Notice the differences in the tails are larger than elsewhere on the distribution. In this log-log representation an asymptotically

hyperbolic distribution would exhibit linear tails. One rather observe a constant curvature on each of these curves. The hypothesis of Schertzer and Lovejoy (see chapter 2) is therefore not strongly supported.

The simple scaling of the probability densities can also be examined by first constructing histograms of the values of $|\Delta v(L)|$ using bins with width $\Delta v_i(L) = \Delta v_i^* L^H$ for each L. The bins of these histograms fall on top of each other when the velocity differences are normalized by L^H, providing normalized histograms suitable for statistical tests. Average probability densities $p_L(x)$ are next calculated for each bin. If $p_L(x)L^H$ is plotted versus x/L^H the curves obtained for different values of L should be superposed if simple scaling holds, as implied by (7.4). This was done in figure 7.3. A fairly good agreement is obtained. The relative difference between the different normalized densities is about 25% around 30 $cm^{2/3}/sec$ and reaches 100% in the tail. The error associated with the simple scaling approximation is therefore worse in the tails.

The differences between the normalized histograms were examined using a χ^2 statistical test. The statistics used to test the null hypothesis that two histograms come from the same probability distribution is

$$\chi^2 = \sum_{j=1}^{N_{bins}} \frac{(N_1(j) - N_2(j))^2}{N_1(j) + N_2(j)},$$

where N_{bins} is the number of bins in the histograms and $N_i(j)$ denotes the number of counts in the j^{th} bin of the i^{th} histogram (Press *et al.*, 1986, section 13.5). An equal number of velocity differences $\Delta v(L)$ was sampled for each lag L. χ^2 is then expected to be distributed as a χ^2 random variable with $\nu = N_{nbins} - 1$ degrees of freedom. Using this test the differences between the various pairs of histograms were found to be statistically significant: Typically, we obtained $\chi^2/\nu \approx 200$ which leads to $\text{Prob}\{\chi^2/\nu \geq 200\} \approx 0$ and therefore the null hypothesis is strongly rejected. The reject is strong because our sample contains a relatively large number

of points, namely 735000. It follows that the frequencies estimated in each bin are fairly accurate and consequently the small differences observed around 20 $cm^{2/3}/sec$ in figure 7.3 are significant, and in fact more significant statistically than the larger errors in the extreme tails where the bins are less populated and the frequencies consequently less accurate. It is interesting to see that the main contribution to the statistical error comes from events having a 3% probability of occurrence, i.e. from the tails of the distributions (Figure 7.4).

We conclude that *simple scaling is rejected on a strict statistical basis*. Simple scaling is nevertheless satisfied sufficiently accurately for low values of $|\Delta v(L)|$ to yield $\langle|\Delta v(L)|^h\rangle \propto L^{h/3}$ for $h < 5$, but the differences between the tails of the probability densities are sufficiently large to break the linear behavior of $\zeta(h)$. We emphasize that our use of a χ^2 test on suitably normalized histograms to check the validity of simple scaling appears to be original. One advantage of this procedure for testing simple scaling over the verification of $\zeta(h) = hH$ is that $\langle|\Delta v(L)|^h\rangle$ does not need to be measured accurately for high values of h. Our results essentially support one of the conclusions of Anselmet *et al.* (1984), i.e. the velocity field does not satisfy simple scaling. The Frisch hypothesis of broken stretching symmetry in turbulent flows is therefore supported by these results, while the alternate hypothesis of simple scaling appears to be invalid. This study therefore resolves the controversy stated in chapter 2.

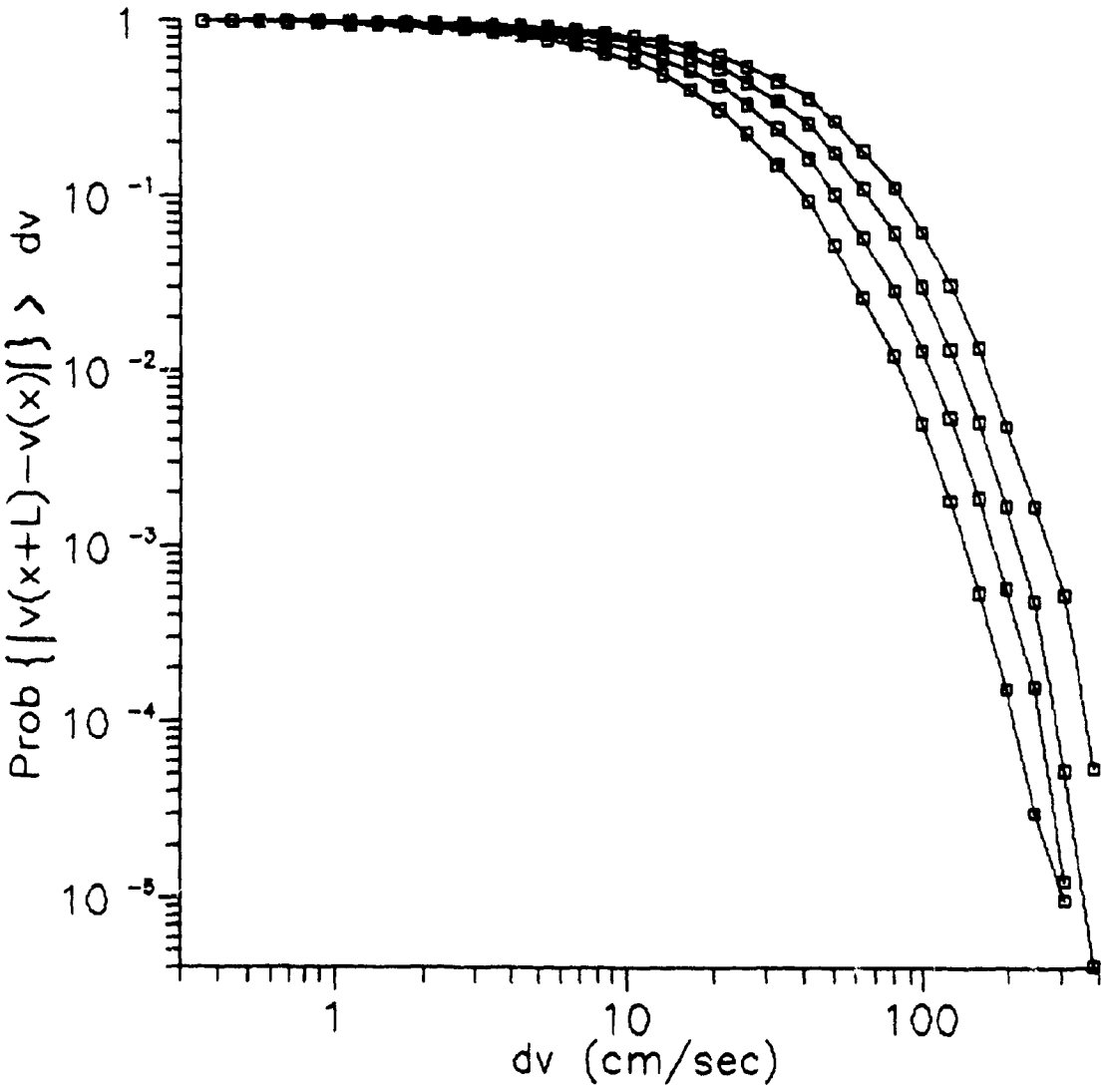

Figure 7.1: Cumulative probability distribution of $|\Delta v(L)|$ for L=10, 20, 40 and 80 cm (from left to right respectively). The constant horizontal spacing between these curves indicates that simple scaling is satisfied.

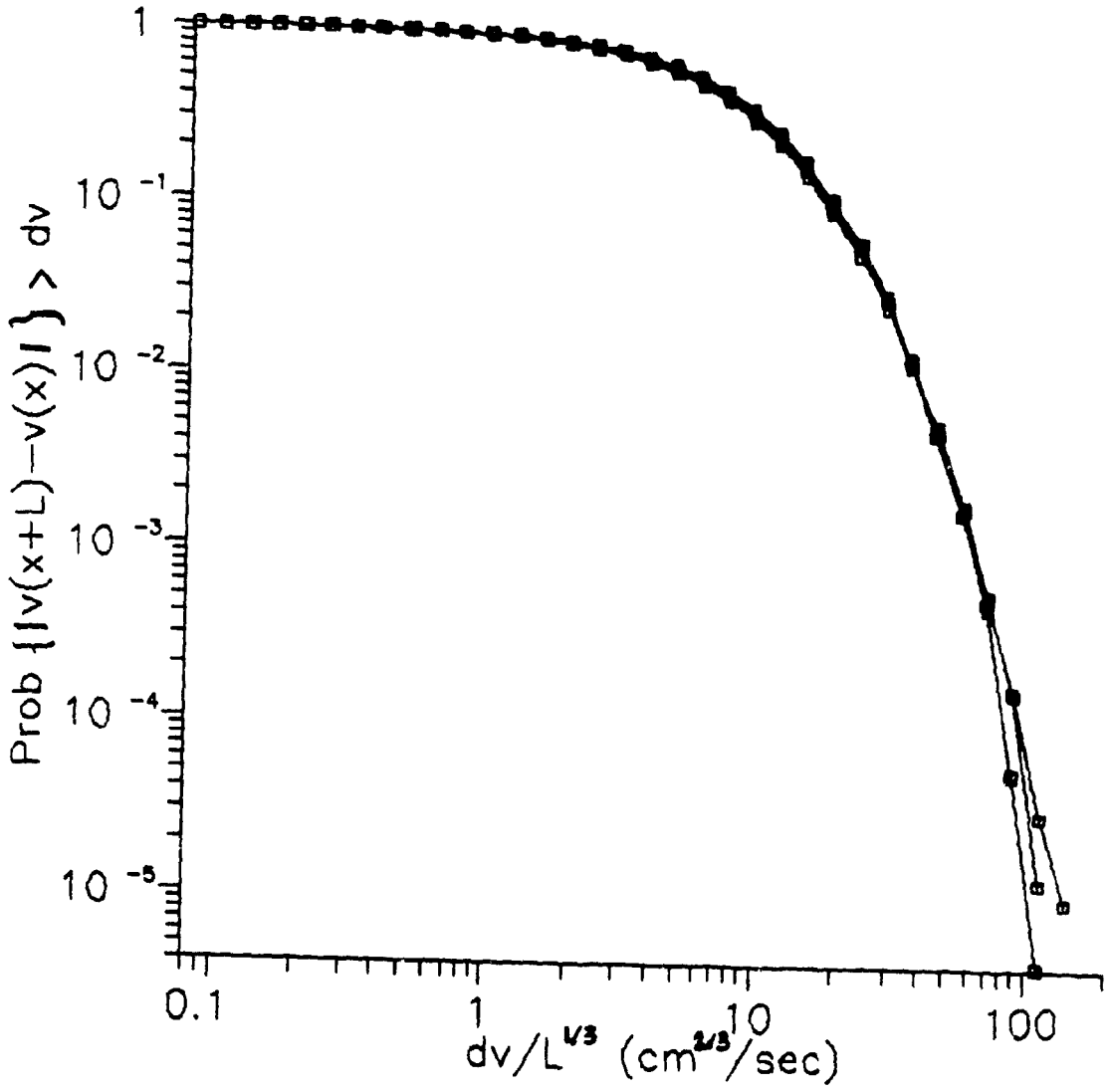

Figure 7.2: Cumulative probability distribution of $|\Delta v(L)|$ for L=10, 20, 40 and 80 cm on normalized scales. In this representation the curves should fall on top of each other if simple scaling holds. The differences are worse in the tails of the distributions.

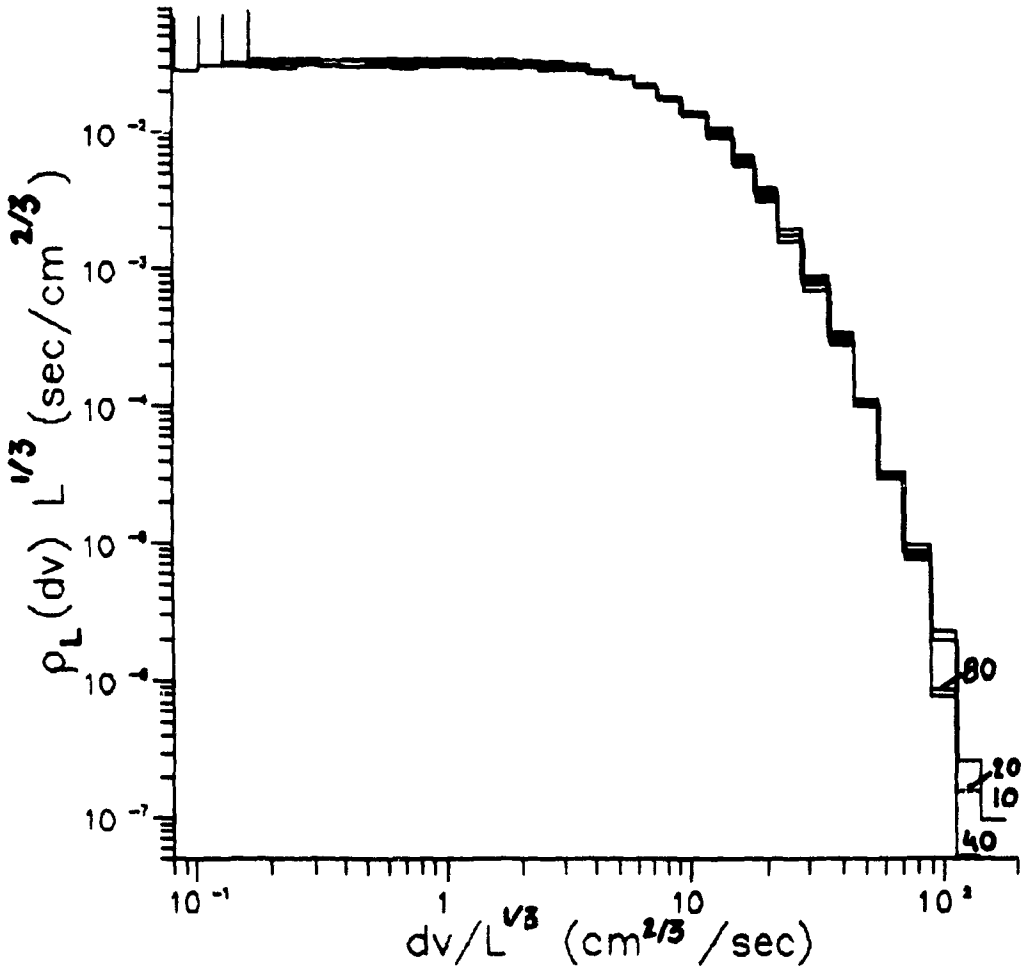

Figure 7.3: Probability densities of $\Delta v(L)|$ for L=10, 20, 40 and 80 cm on normalized scales. In this representation the curves should fall on top of each other if simple scaling holds. The differences are about 25% around 30 $cm^{2/3}/sec$ and reach 100% in the tails. The curves corresponding to different values of L are indexed with L (cm) in the tails.

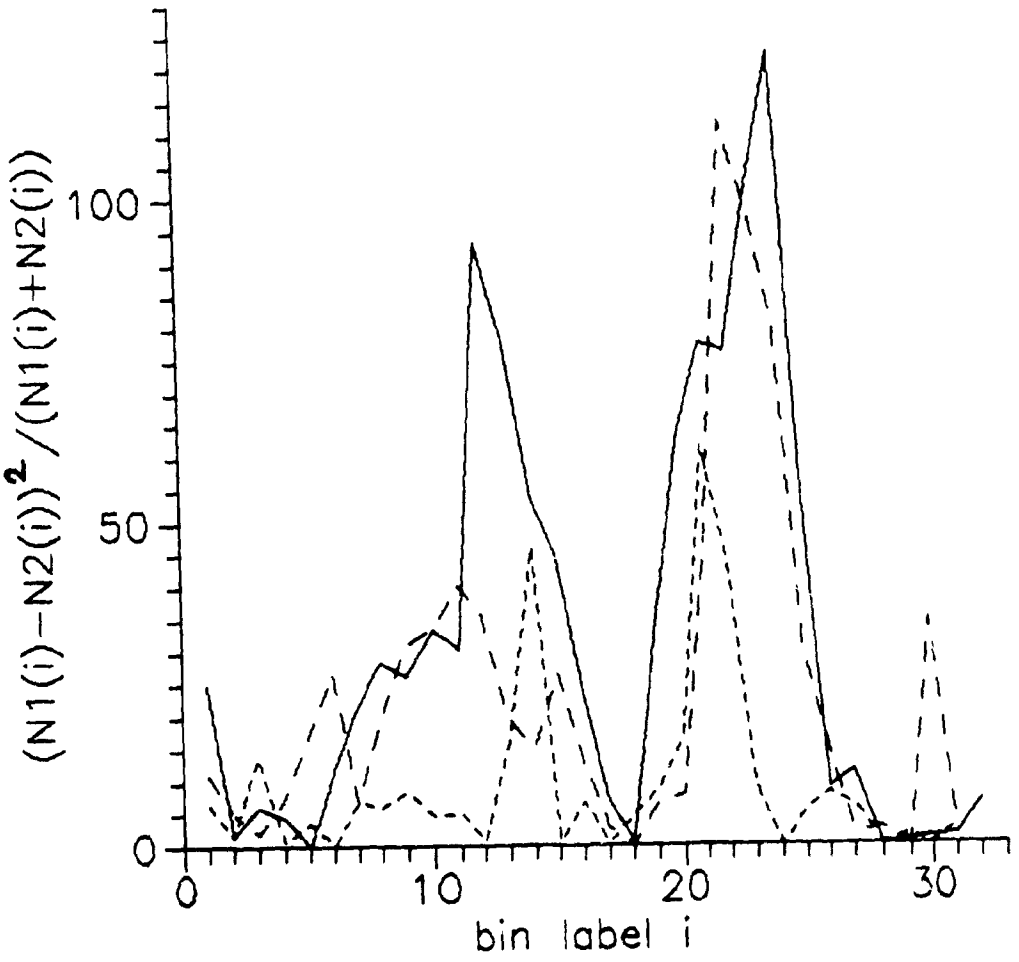

Figure 7.4: Contribution of each bin to the χ^2 statistics. The labels are associated to the bins shown by the staircase densities in figure 7.3. The three curves corresponds to tests performed on different pairs of histograms, i.e. to different pairs of lags. The main contributions to the statistical error comes from the range 20-25, and significant contributions also come from the range 8-16. The peak of the contributions comes approximately from the 23^{th} bin which corresponds to $dv/L^{1/3} \approx 30$ $cm^{2/3}/sec$ in figure 7.2, i.e. to probabilities of occurrence of 3%. The statistical error therefore comes mainly from the tails of the distributions.

7.2 EVIDENCE SUPPORTING A SPATIALLY LOCALIZED ENERGY CASCADE

The self-similar nature of a turbulent velocity field is often pictured using the idea of "bursts nested into bursts". This geometrical assumption of self-similarity is implicit to the phenomenology of the energy cascade in Kolmogorov theories, and explicit in some quantitative models of intermittency, such as the Frisch-Sulem-Nelkin β-model (in short F.S.N. β-model) or the Novikov "pulse-in-pulse" model (section 2.4.3) Apparently, no direct experimental evidence of the existence of structures inside of structures has been given (Kadanoff, 1990). Our aim in this section is to try to see qualitatively to what extent this fractal idea is supported by the observations

In early measurements of high-passed velocity signals, such as those of Sandborn (1959), intermittency was observed in frequency bands corresponding to the inertial range. It seems that the study of spatial correlations between these bands, that would reveal to what extent small scale energy bursts "grow" on nearby larger scales energy bursts, was neglected We therefore propose here to consider several bands simultaneously. In the spirit of the F.S.N β-model, a series of digital filters keeping only the scales in the intervals $[L_0, L_0/2]$, $[L_0/2, L_0/4]$, .., $[L_0/2^n, L_0/2^{n+1}]$ was applied to the velocity field, and all these filtered signals were plotted on top of each other in figure 7.5 and 7.6, using normalized units. Our procedure somewhat differs from the F.S.N. β-model, where three dimensional frequency bands are considered, because we are restricted to one dimensional samples A large 105 meter sample was used in figure 7.5 in order to give a broad view of the intermittency in the inertial range In order to focus on the dissipation range intermittency, a shorter 28 meters sample was considered in figure 7.6.

In both figures the characteristic intermittent behavior of the filtered signal is recognized The intermittency exists both in the inertial range (10 cm to 10 m) and the dissipation range (1 cm to 10 cm). The activity pockets in each band are not "dead" or "alive", as assumed in

the F.S.N β-model, but are rather weak or intense, which is due to the relatively large widths of the bands. Indeed it is usually observed that the intermittency of the filtered signal increases (e.g. higher kurtosis) if the filtration bandwidth decreases. The pockets of activity are usually at the same location in each band. Some (rare) exceptions can be found, where the energy in the small scales is small, even though larger scales at the same spatial location exhibit bursts of activity. The hypothesis of bursts of energy at various scales nested into each other is therefore essentially confirmed. The fact that the signals in different bands are strongly correlated is consistent with a cascade that occurs locally in real space, as postulated in the 1962 Kolmogorov-Obukhov refined similarity theory. We don't regard these correlations as especially surprising, precisely because we expect a large scale energy burst to "contaminate" all the scales of the velocity field through the cascade process. Nevertheless, this may be the first attempt of a direct experimental verification of the self-similar structure of intermittency.

These observations support a qualitative cascade phenomenology, but unfortunately they do not lead unambiguously to more quantitative models. The F.S.N β-model is an attempt to derive some quantitative results, e.g. the correction to the $k^{-5/3}$ energy spectrum, but it remains too close to the crude observations to lead much beyond a purely qualitative description.

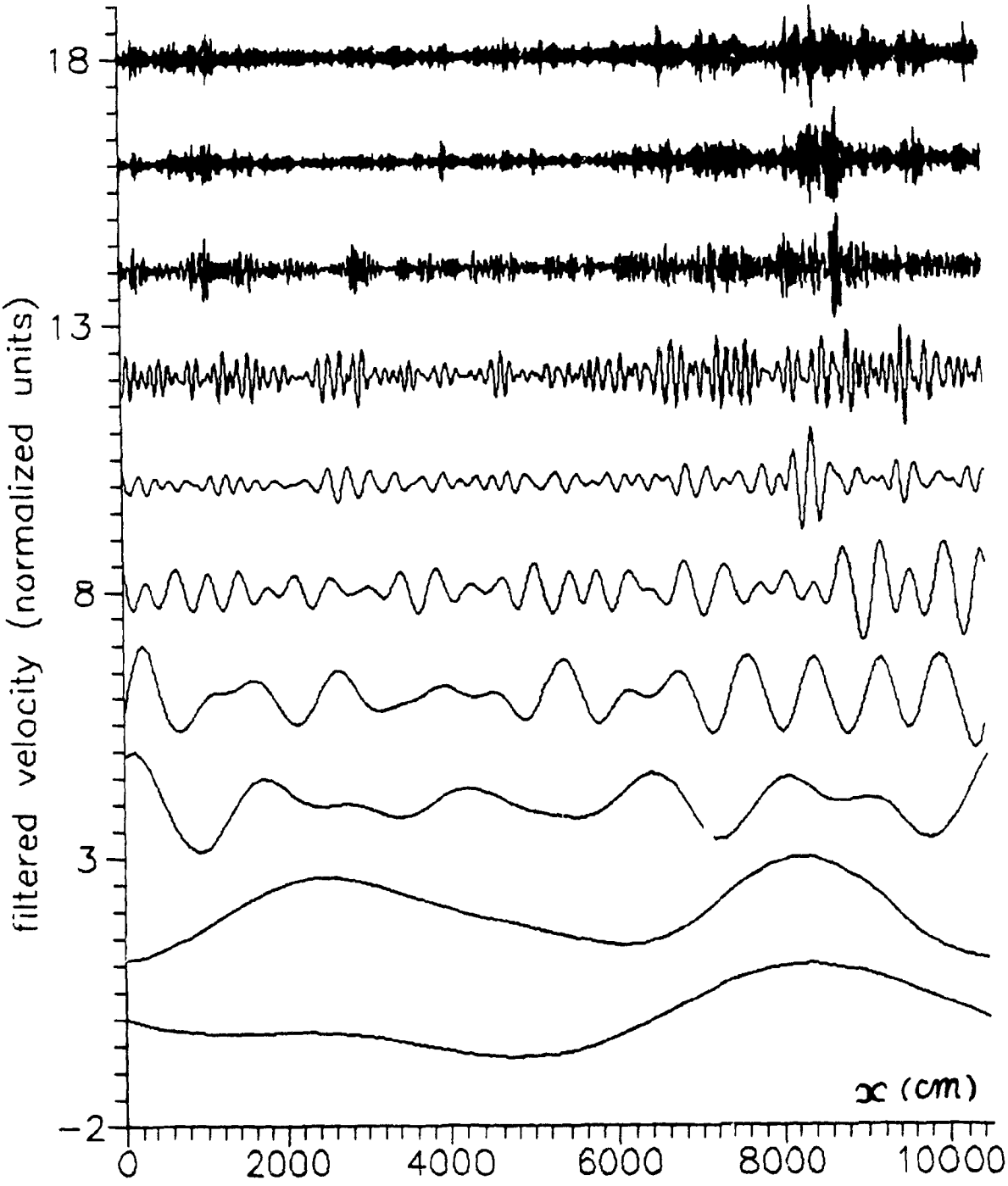

Figure 7.5: This graphs shows the velocity field digitally filtered in 10 different wavelengths bands, namely [52m, 105m], [26m, 52m], [13m, 26m], ..., [10cm, 20cm] (from bottom to top). The first 7 bands, starting from the top, corresponds to wavelengths smaller than 13 meters and are therefore related to the inertial range. The bursts of activity are strongly correlated from band to band, which is consistent with Landau's idea of an energy cascade that occurs locally in real space.

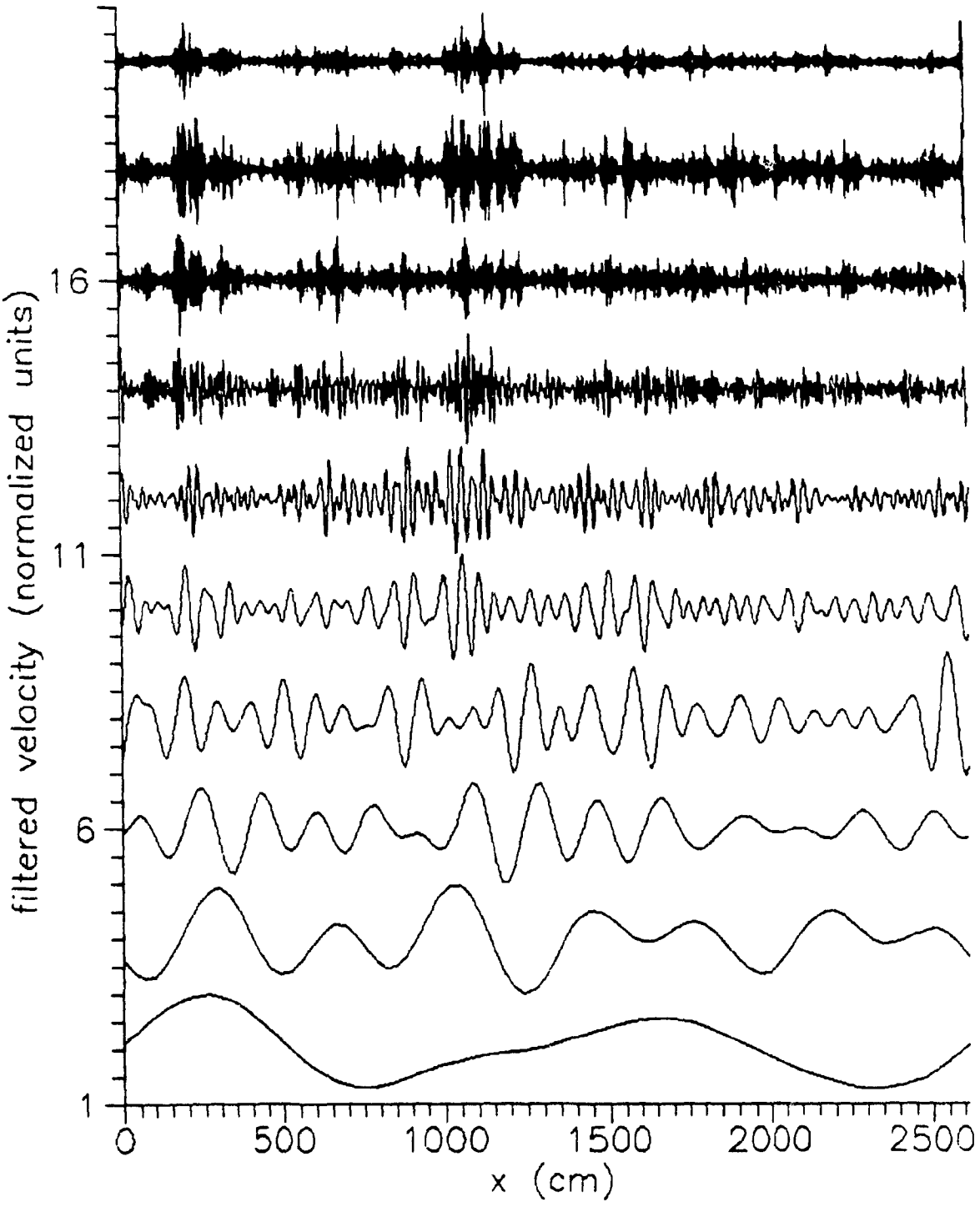

Figure 7.6: This graphs shows the velocity field digitally filtered in 10 different wavelengths bands, namely [6.6m, 13m], [3.3m, 6.6m], [1.6m, 0.8m], ..., [5cm,10cm], [2cm 5cm], [1cm, 2cm] (from bottom to top). The first 3 bands, starting from the top, corresponds to wavelengths smaller than 10 cm and are therefore related to the dissipation range. The other bands are in the inertial range. Intermittency is clearly visible in the dissipation range as well that in the inertial range.

7.3 TEST OF A WEAKER FORM OF THE THIRD KOLMOGOROV HYPOTHESIS

In section 3.3.3 it was argued on the basis of the properties of multiplicative processes that the moments of $\log(\varepsilon(L))$ may be calculated using the gaussian approximation even if the lognormal approximation was untenable for the calculation of the moments of $\varepsilon(L)$. In this section we shall try to verify this hypothesis with the energy dissipation field (recall that $\varepsilon(L)$ denotes the energy dissipation rate field averaged over a length scale L).

The moments of a centered gaussian $N(0,\sigma^2)$ are given by

$$\langle N^q \rangle = (q-1)!!\ \sigma^q \tag{7.3.1}$$

for q even. It follows that

$$R_0(q) = \frac{\langle N^q \rangle}{\langle N^2 \rangle^{q/2}} = (q-1)!! \tag{7.3.2}$$

for q even. Introducing the centered quantity $V(L) = \log\varepsilon(L) - \langle \log\varepsilon(L) \rangle$ we define the ratio

$$R(L,q) = \frac{\langle V(L)^q \rangle}{\langle V(L)^2 \rangle^{q/2}} . \tag{7.3.3}$$

If our new form of the third hypothesis is valid the ratio $R(L,q)/R_0(q)$ should be unity for $q = 2, 4, 6, \ldots$ and for L small enough. This ratio was plotted in figure 7.7 as a function of q for each L. The agreement with $R(L,q)/R_0(q) = 1$ is really good for $L < 2$ meters since the error does not exceed 15% for $q \leq 10$. A random scatter around the gaussian value is observed. We regard this result as a reasonable evidence for support of multiplicative processes. It also provides indirect support for the hypothesis of finite variance required for the

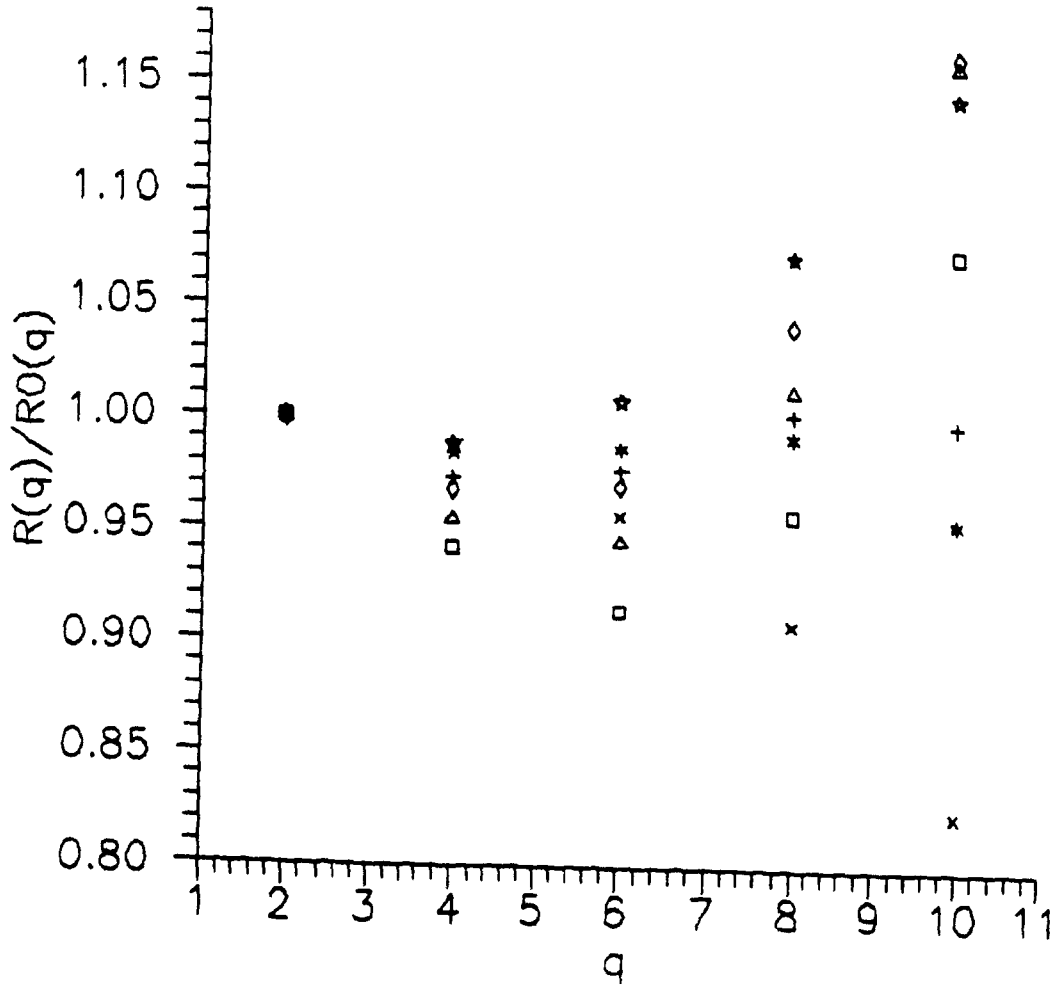

Figure 7.7: $R(L,q)/R_0(q)$ for each L. □ = 10 cm, △ = 20 cm, ◇ = 40 cm, ☆ = 80 cm, + = 160 cm, × = 320 cm, ✱ = 640 cm. We observe a random scatter around the gaussian unity value.

central limit theorem to apply. It seems that the validity of the gaussian approximation for the calculation of the moments of $\log(\varepsilon(L))$ was never emphasized and verified experimentally before this study.

Chapter VIII

COMPARING THE ENERGY DISSIPATION FIELD WITH SINGLE SCALE CASCADE MODELS: SEARCH FOR A PRIVILEGED SCALE RATIO

De loin, la montagne paraît lisse; de près, elle est rugueuse

Indian saying

In this chapter we shall consider some of the simplest cascade models, namely those involving a single scale ratio, and focus on their characteristic properties. In a study of deterministic single scale Cantor sets, Smith *et al.* (1986) pointed out that a unique scale ratio gives rise to periodic oscillations of the prefactor of the correlation function C(L) (to be defined below) and that the period reveals the scale ratio. On this basis and by using a fractal model of turbulence they claimed that oscillations may also be observed for velocity structure functions measured in natural flows. For single-scale measures, we have shown in chapter 5 that the generating function exhibits a periodic prefactor. The same observation was made by Novikov (1990) using a slightly different approach to the modelling of the energy dissipation field, e.g. the "pulse-in-pulse" model (section 2.4.3), where the energy dissipation field has a power spectrum of the form $k^{-1+\mu}\,\phi(\log(k))$ $(0 < \mu < 1)$, where ϕ is periodic with a period determined a scale ratio. As shown in chapter 4 and 5 such periodic prefactors arise in single scale renormalization equations. They are therefore expected for multiscaling systems having a physically distinguished scale ratio. If prefactor oscillations could be observed in natural flows their period would reveal a privileged scale ratio characteristic of turbulence.

Our first goal in this chapter is to determine whether such prefactor oscillations actually exist in random models. Indeed the existence of such oscillations is only suggested by periodicity statements of the type $f(x) = f(x+T)$ which might possibly mean that f is simply constant. These prefactors have not been calculated either analytically or numerically in random models

(Novikov, 1990) and it is interesting to study the effect of randomness. If oscillations exist the second step is to see if they are sufficiently wide in amplitude to be easily observable. The last step will be to see if similar oscillations can be obtained in real turbulent flows.

It should be recalled that for exactly self-similar sets the periodicity of the prefactor of $N_B(\delta)$ is usually spoiled by the use of a box-counting grid (section 4.2.3.2), and therefore another method is needed to measure prefactors for sets. Various definitions of the correlation function have been proposed in the context of dynamical systems. In section 8.1 we extend these definitions for arbitrary sets and measures. These new quantities have the advantage of allowing an accurate estimation of periodic prefactors. In section 8.2 these methods are first tested on artificial random sets and measures and next applied to the energy dissipation field as measured in the atmospheric surface layer. A first numerical attempt to obtain the periodic spectral prefactor of the Novikov "pulse in pulse" model is made in specific cases

8.1 MEASURING PERIODIC PREFACTORS FOR SETS AND MEASURES

8.1.1 Correlation functions for sets

Given a sequence of points $\{x_i, i = 1, ..., N\}$, usually generated by a dynamical system, the *correlation function* (Grassberger and Procaccia, 1983) is defined by

$$C(\delta) = \lim_{N\to\infty} N^{-2} \sum_{i=1}^{N} N_i(\delta) , \qquad (8.1.1)$$

where $N_i(\delta)$ denotes the number of points inside a ball $B(\delta,x_i)$ of diameter δ centered about x_i. In this context the ratio $N_i(\delta)/N$, interpreted to be the fraction of time spent by the point in $B(\delta,x_i)$, is expected to be finite in the limit $N\to\infty$. $C(\delta)$ is the average of these time fractions and is also finite. The *correlation dimension* ν of the infinite sequence $\{x_i\}$ is defined by

$$\nu = \lim_{\delta\to 0} \frac{\log\{C(\delta)\}}{\log\delta} . \qquad (8.1.2)$$

Note that $C(\delta)$ is defined for infinite sequences but is not necessarily defined for sets. Indeed, given a set a rule is required to enumerate the points and C(L) depends on this rule.

A natural way of "making points" with a set is to coarse-grain it by box-counting at resolution ε. The *correlation function* is then given by

$$C(\delta,\varepsilon) = \frac{1}{(N_B(\varepsilon))^2} \sum_{i=1}^{N_B(\varepsilon)} N_i(\delta,\varepsilon) , \qquad (8.1.3)$$

where $N_i(\delta,\varepsilon)$ is the number of filled boxes of size ε ($\varepsilon << \delta$) inside a ball of diameter δ centered on the i^{th} filled box, and $N_B(\varepsilon)$ is the total number of boxes of size ε needed to cover the set. In general $0 \le C(\delta,\varepsilon) \le 1$ because $0 \le N_i(\delta,\varepsilon) \le N_B(\varepsilon)$ for any i. For some sets, the limit $C(\delta) = \lim_{\varepsilon \to 0} C(\delta,\varepsilon) \ge 0$ may exist and be non-zero. Consider for example a *homogeneous fractal*, i.e. a set S such that any non-empty subset S_i satisfies $d_B(S_i) = d_B(S)$ (in other words, the box dimension of any piece of the set is the same). For such a set $N_i(\delta,\varepsilon) \sim (\varepsilon/\delta)^{-d_B}$ as $\varepsilon \to 0$ and since $N_B(\varepsilon) \sim \varepsilon^{-d_B}$ it follows that $N_i(\delta,\varepsilon)/N_B(\varepsilon) \sim \delta^{d_B}$ as $\varepsilon \to 0$ and therefore

$$C(\delta,\varepsilon) \sim \delta^{d_B} \text{ as } \varepsilon \to 0.$$

The definition (8.1.1) was used by Smith *et al.* (1986) for sets containing a finite number of points. Our expression (8.1.3), which applies to any set, appears to be original.

In a numerical experiment, where an ε-grid is used to coarse-grain the set, $C(\delta,\varepsilon)$ depends on the position of the grid. By contrast with $N_B(\delta)$, where a different grid is used for each δ, no δ-grid is involved in the calculation of $C(\delta,\varepsilon)$. As we shall see, this improvement allows to recover a convincingly periodic prefactor for exactly self-similar sets.

8.1.2 Calculation of $C(\delta,\varepsilon)$ for exactly self-similar sets

Consider an exactly self-similar set S where the copies S_j are positively separated, and denote by $C(\delta,\varepsilon;S)$ the correlation function associated to S. The S_j are identical, hence if $\delta < \min d(S_i,S_j)$ then

$$C(\delta,\varepsilon;S) = \frac{M}{[N_B(\varepsilon;S)]^2} \sum_{k=1}^{N_B(\varepsilon;S_j)} N_k(\delta,\varepsilon) \qquad (8.1.4)$$

where the sum runs over all the boxes covering one of the S_j. (8.1.4) can be rewritten in the form

$$C(\delta,\varepsilon;S) = M \left[\frac{N_B(\varepsilon;S_j)}{N_B(\varepsilon;S)}\right]^2 C(\delta,\varepsilon;S_j). \qquad (8.1.5)$$

For an exactly self-similar set with ratio r, $N_B(\varepsilon;S) = M\, N_B(\varepsilon;S_j)$ and self-similarity implies

$$C(\delta, \varepsilon; S_j) = C(\delta/r, \varepsilon/r; S),$$

therefore (8.1.5) becomes

$$C(\delta, \varepsilon; S) = M^{-1}\, C(\delta/r, \varepsilon/r; S), \qquad (8.1.6)$$

which becomes

$$C(\delta) = M^{-1}\, C(\delta/r), \qquad (8.1.7)$$

as $\varepsilon \to 0$ if the limit exists. Consequently

$$C(\delta) = \delta^{d_S}\, P(\log\delta), \qquad (8.1.8)$$

where $P(\log\delta) = P(\log\delta+\log(1/r))$. Numerical experiments performed by Smith *et al.* (1986) have demonstrated the existence of oscillations for P with M-piece Cantor sets. This periodicity is very clear in comparison with the results obtained in chapter 4 with box-counting. The

details of these oscillations can be used to characterize the properties of the set other than the dimension. For example sets sharing the same dimension, such as the Cantor sets (101) and (101010001), can be distinguished by comparing their prefactors.

For illustration, a numerical experiment was performed on the triadic Cantor set (101). 10 cascade steps were done and C(L) was plotted in figure 8.1. The slope of the line is $d_S = \log 2/\log 3$, and regular oscillations are visible. At small scales, the set is not self-similar and therefore the periodicity is spoiled (the smallest scale is defined to be unity). In figure 8.2, the prefactor $P(\delta) = \delta^{-d_S} C(\delta)$ is plotted versus $\log\delta$. The minimum of the periodic function occurs approximately at scales 100, 100x3, ..., 100×3^n, which reveals that the splitting factor of the set is $r = 1/3$. A zoom on P(L) is given in figure 8.3.

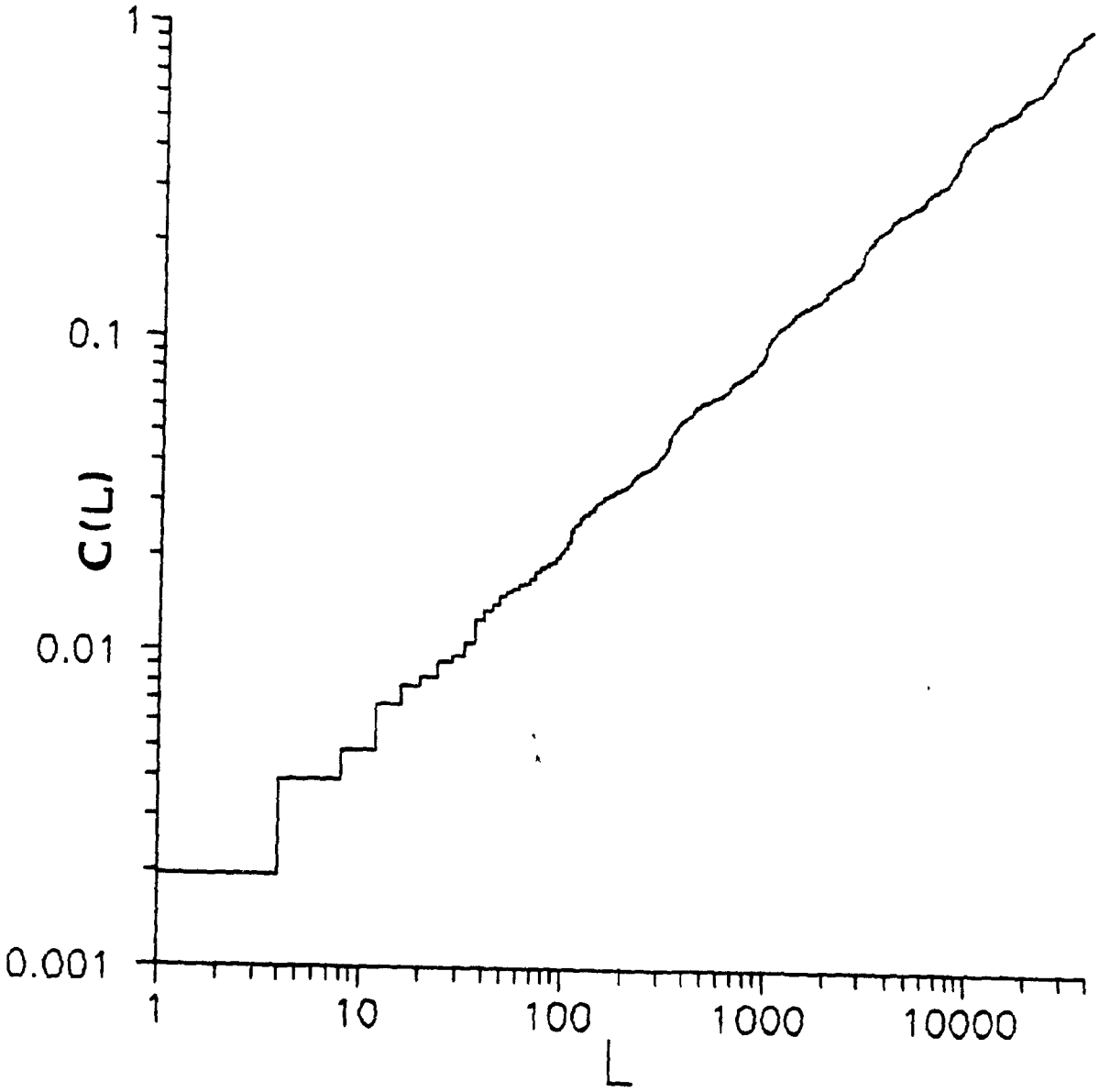

Figure 8.1: C (L) for the triadic Cantor set (101). The slope of the line is log2/log3, the dimension of the set. Periodic oscillations are visible, except at small scales, where self-similarity is spoiled by the finite inner scale.

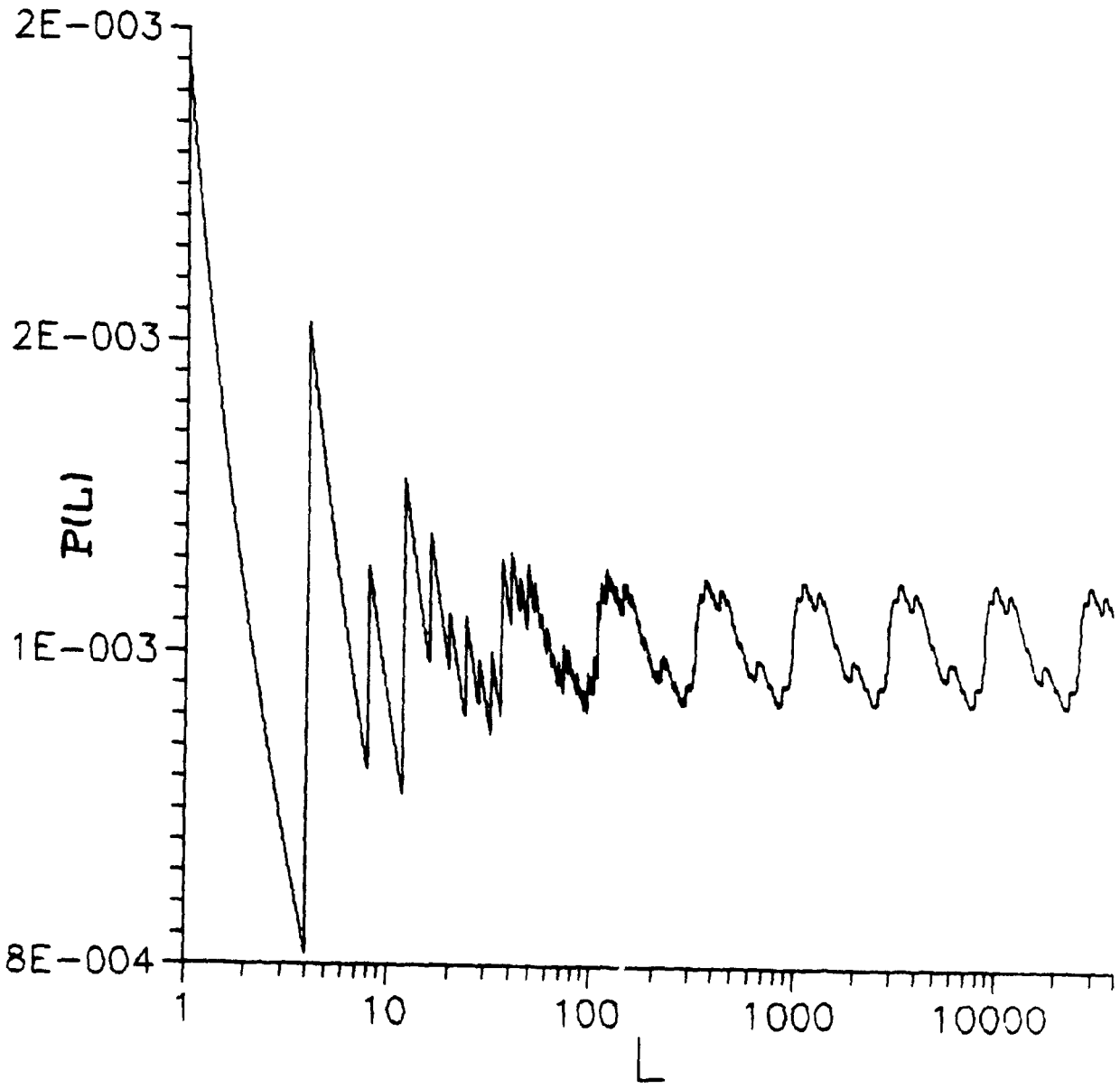

Figure 8.2: Prefactor P (L) = δ^{-dS} C (L) for the triadic Cantor set (101). The minimum of the periodic function occurs approximately at scales 100, 3x100, ..., 3^nx100, which indicates that the scale ratio of the set is r = 1/3

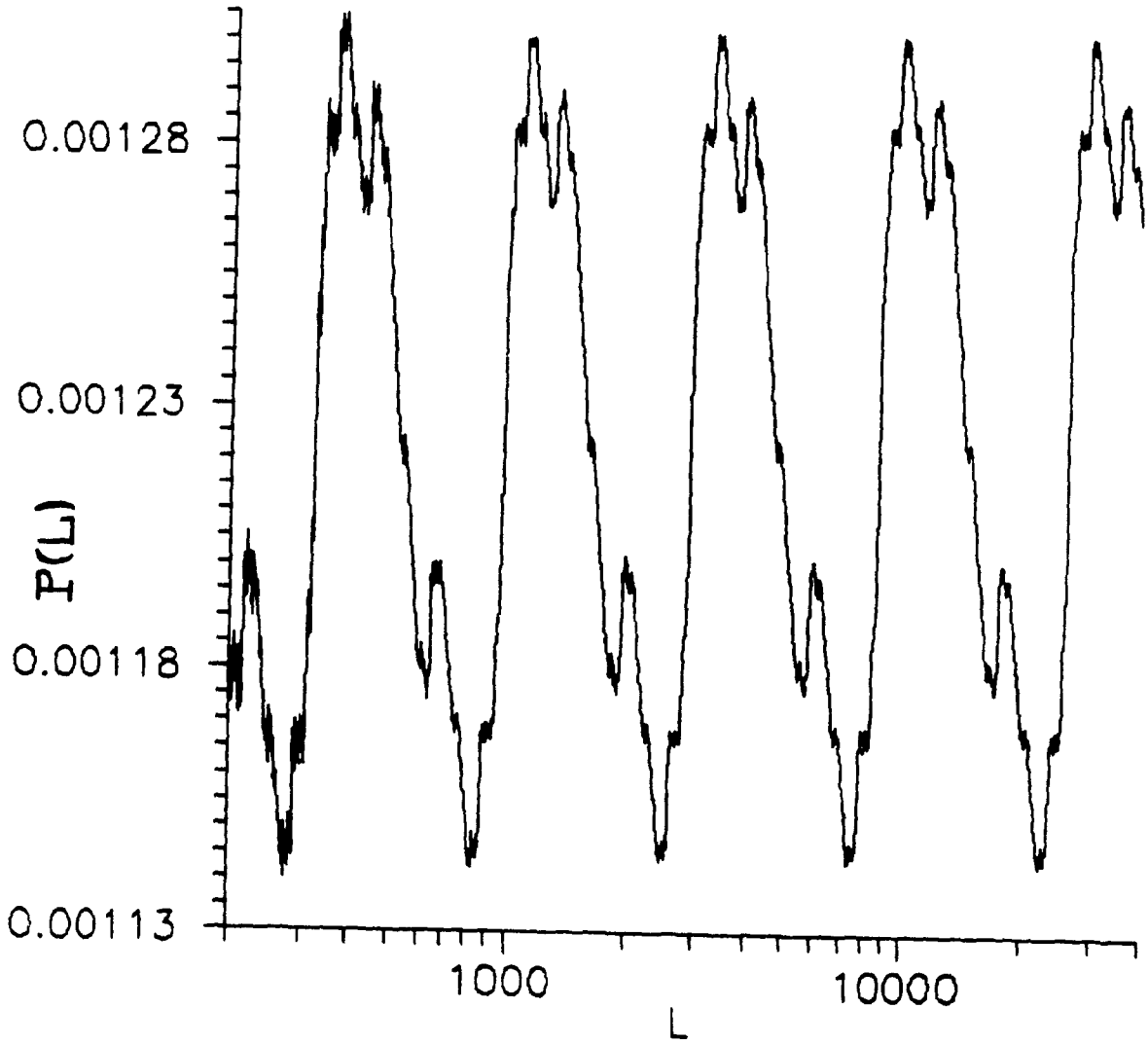

Figure 8.3: Zoom on the function P(L) of the Cantor set (101) (i.e. zoom on figure 8.2).

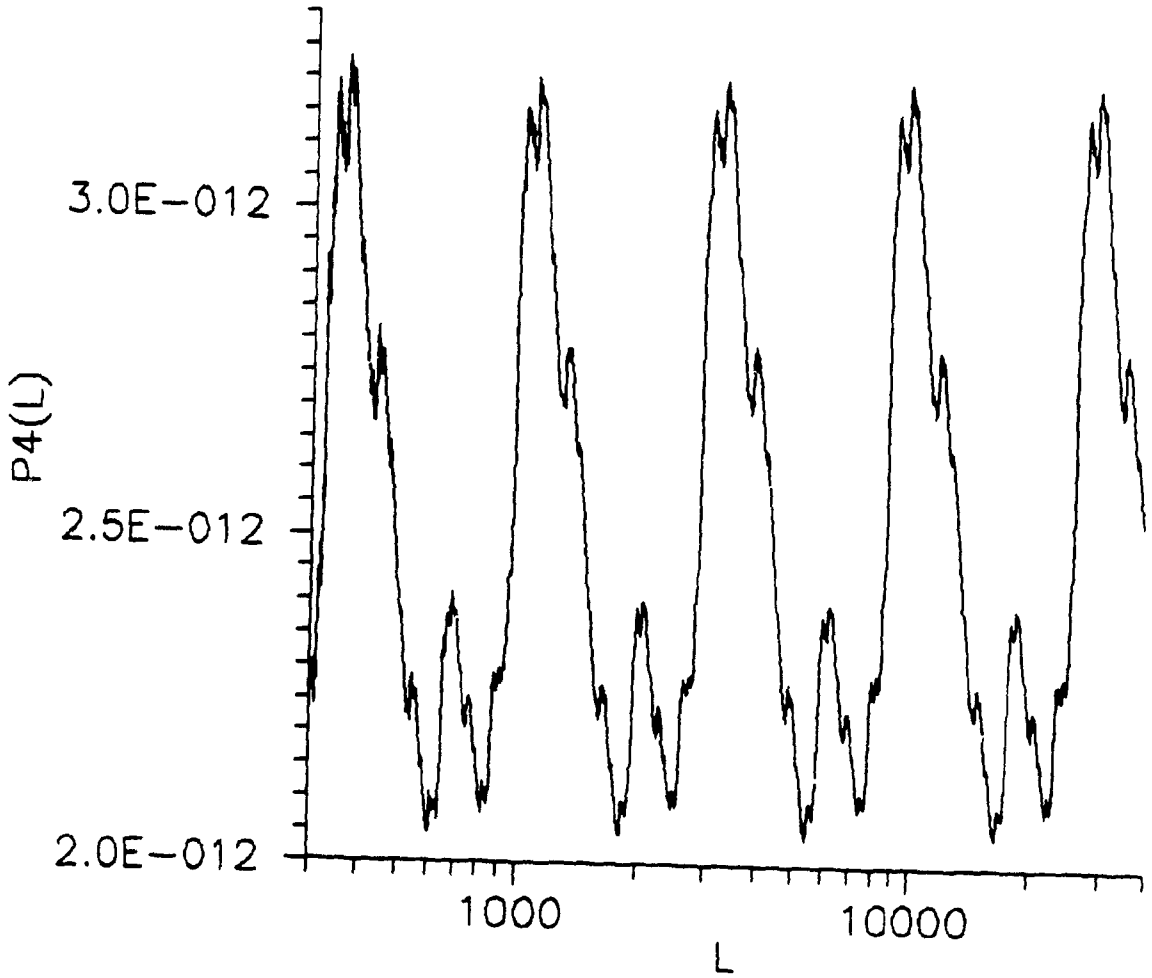

Figure 8.4: Zoom on the function $P_4(L)$ of the Cantor set (101). The set was constructed with 10 cascade steps

8.1.3 Generalization of the correlation function for sets and measures

We propose here a generalization of the correlation function (8.1.3) that leads to a more complete characterization of the set. We define the *order-q correlation function* by

$$C_q(\delta,\varepsilon) = \frac{1}{[N_B(\varepsilon)]^{q+1}} \sum_{i=1}^{N_B(\varepsilon)} [N_i(\delta,\varepsilon)]^q , \qquad (8.1.9)$$

normalized so that $0 \le C_q(\delta,\varepsilon) \le 1$. For exactly self-similar sets, the renormalization argument of section 8.1.2 leads to

$$C_q(\delta) = M^{-q}\, C_q(\delta/r), \qquad (8.1.10)$$

and therefore

$$C_q(\delta) = \delta^{d_S q}\, P_q(\log\delta),$$

where $P_q(\log\delta) = P_q(\log\delta+\log(1/r))$. The order-q correlation function therefore leads to a continuous family of periodic prefactors P_q, instead of a single one. In figure 8.4 the prefactor $P_4(L)$ obtained numerically with the Cantor set 101 constructed with 10 cascade steps is plotted. Obviously $P_4(L) \neq P_1(L)$ and therefore higher order prefactors reveal additional information about the set.

As already mentioned above, the prefactor of the generating function $\chi_q(\delta)$ is also spoiled by the use of a box-counting grid. For separated and self-similar measures, the measurement of the periodic prefactor therefore requires a new tool. We propose here a natural generalization of (8.1.9) for measures. Define the *order-q correlation function of a measure* μ by

$$\Omega_q(\delta,\varepsilon) = \frac{1}{N_B(\varepsilon)} \sum_{i=1}^{N_B(\varepsilon)} [\mu_i(\delta,\varepsilon)]^q, \qquad (8.1.11)$$

where $N_B(\varepsilon)$ is the number of boxes of size ε needed to cover the support of μ and $\mu_i(\delta,\varepsilon)$ is the measure of a ball of radius $\delta > \varepsilon$ centered about the i^{th} filled box of size ε $\Omega_q(\delta,\varepsilon)$ satisfies $0 \le \Omega_q(\delta,\varepsilon) \le 1$ because $0 \le \mu_i(\delta,\varepsilon) \le 1$. For a separated exactly self-similar measure supported by $S = \bigcup S_j$, where the S_j's are scaled down copies of S, the correlation function satisfies

$$\Omega_q(\delta,\varepsilon;S) = \frac{1}{M} \sum_{j=1}^{M} \Omega_q(\delta,\varepsilon;S_j), \tag{8.1.12}$$

where $\Omega_q(\delta,\varepsilon;S)$ denotes the correlation function restricted to a support S. The self-similarity of the measure implies

$$\Omega_q(\delta,\varepsilon;S_j) = w_j^q \; \Omega_q(\delta/r,\varepsilon/r;S), \tag{8.1.13}$$

where r is the scale ratio of the measure and w_j the weight corresponding to S_j. Replacing (8.1.13) in (8.1.12) yields the renormalization equation

$$\Omega_q(\delta,\varepsilon;S) = \frac{1}{M} \left[\sum_{j=1}^{M} w_j^q\right] \; \Omega_q(\delta/r,\varepsilon/r;S). \tag{8.1.14}$$

For some measures the limit $\Omega_q(\delta;S) = \lim_{\varepsilon \to 0} \Omega_q(\delta,\varepsilon;S)$ may exist and be non-zero. In that case (8.1.14) becomes (the argument S is dropped for simplicity)

$$\Omega_q(\delta) = \frac{1}{M} \left[\sum_{j=1}^{M} w_j^q\right] \; \Omega_q(\delta/r) \tag{8.1.15}$$

and yields

$$\Omega_q(\delta) = \delta^{\tau(q) + d_S} \; P_q(\log\delta) \tag{8.1.16}$$

where $d_S = \log M/\log(1/r)$, $\tau(q)$ is the usual mass exponent function of μ and $P_q(x) = P_q(x+\log(1/r))$. This "grid insensitive" method, that allows both the mass exponents and the prefactor to be measured accurately as long that $\delta >> \varepsilon$, appears to be original.

8.2 STUDY OF PREFACTOR OSCILLATIONS IN SINGLE SCALE CANTOR SETS, SINGLE SCALE MEASURES AND TURBULENCE

8.2.1 Effect of the separation condition on the oscillations

In section 8.1.2 it was shown that the renormalization equation satisfied by the correlation function C(L) for an exactly self-similar sets S holds exactly only when the subsets S_j composing S are separated. In the case of non-separated S_j's, the renormalization equation $C_q(L) = M^{-q} C_q(L/r)$ may still hold asymptotically in the limit $\delta \to 0$ if the S_j's do not overlap too much. We shall now examine the prefactor of a non-separated Cantor set. It is noted that the numerical experiments of Smith *et al.* (1986) involved only separated Cantor sets.

The correlation function C(L) for the sets 1101 and 1110 were obtained numerically using eight cascade steps in the construction, and the prefactors were plotted in figure 8.5 (in this chapter, the size L of each set was defined to be 1). The Cantor set 1110 is separated, because the set 1110 equals the set 110110110000, which is formed of three separated subsets. However the set 1101 is not separated, since the set 1101 equals the set 1101110100001101, which is again formed of three non-separated subsets. The separated 3-piece Cantor set 1110 exhibits a very regular periodic prefactor. By contrast, the non-separated set 1101 exhibits a less regular prefactor. Oscillations are visible but the periodicity is broken at large scales. At small scales the prefactor appears to become periodic asymptotically. The function C(L) obtained with the set 1101 was plotted in figure 8.6. It is emphasized that in this representation the oscillations are almost imperceptible. Only a large magnification of the prefactor allows to discover oscillations in this apparently straight line.

We conclude that when the separation condition is not satisfied the periodicity of the prefactor is spoiled at large scales and therefore the scale interval where oscillations could be observed shrinks. This may be the first illustration of the effect on the prefactor of the lack of separation of the S_j's for exactly self-similar sets.

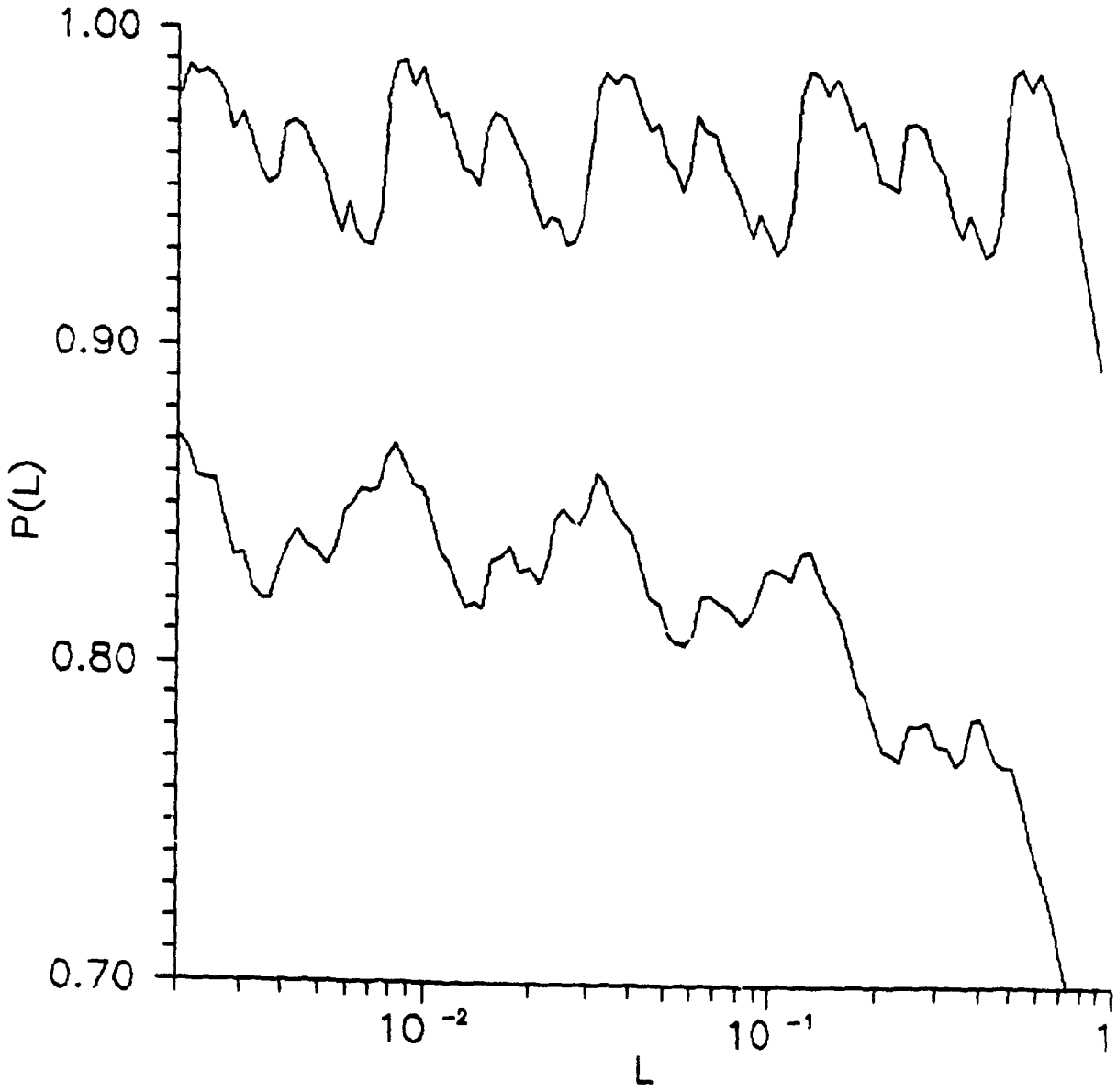

Figure 8.5: Prefactors of the sets 1110 (top) and 1101 (below). The set 1101 is not separated and periodicity is broken at large scales.

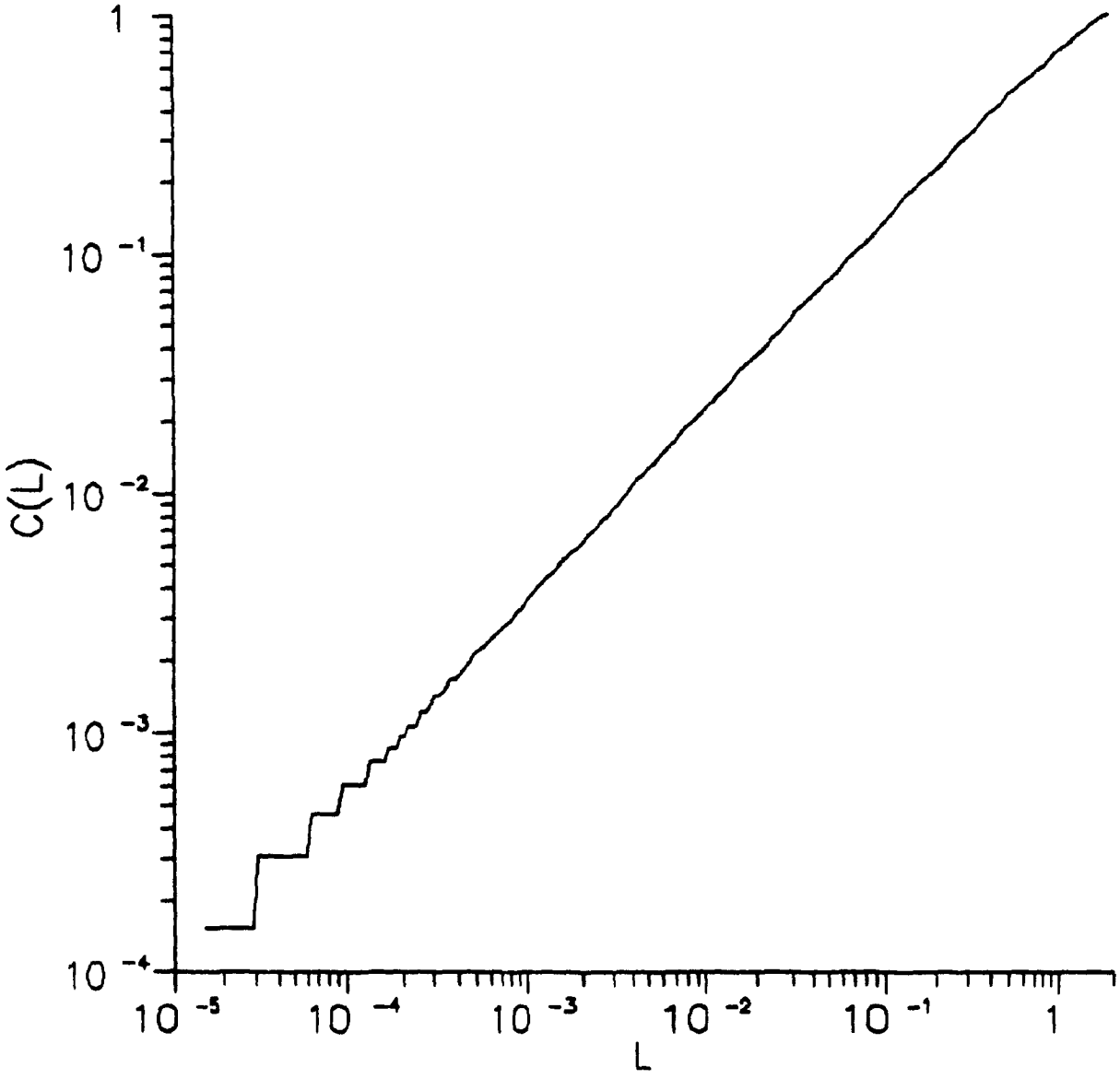

Figure 8.6: C(L) for the Cantor set 1101. The ratio of the amplitude of the oscillation to the mean prefactor is about 7% and the oscillation is almost invisible.

8.2.2 Effect of randomness on the oscillations

Besides the separation condition, another factor may contribute to ruin the oscillations of the prefactor: Randomness. A realistic model of the energy dissipation field must involve randomness. Consider for example a random M-piece Cantor set, i.e. an M-piece Cantor set where the positions of the pieces are chosen randomly at each cascade step. For such sets the renormalization equation for $C_q(L)$ becomes

$$C_q(L) \stackrel{d}{=} M^{-q}\, C_q(L/r), \tag{8.2.1}$$

where "$\stackrel{d}{=}$" denotes an equality in probability distribution. It follows that

$$\langle C_q(L)\rangle = M^{-q} \langle C_q(L/r)\rangle \tag{8.2.2}$$

and therefore

$$\langle C_q(L)\rangle = L^{d_S q}\, P_q(\log L), \tag{8.2.3}$$

where $P_q(x) = P_q(x+\log(1/r))$ (the usual restrictions in connection with the separation condition also apply to this probabilistic case). A similar argument can be made about the renormalization of the correlation function for measures, which is obtained by averaging (8.1.15):

$$\langle \Omega_q(\delta)\rangle = \langle W^q\rangle \langle \Omega_q(\delta/r)\rangle \Rightarrow \langle \Omega_q(\delta)\rangle = \delta^{\tau^*(q)+d_S}\, P_q(\log\delta), \tag{8.2.4}$$

where $\tau^*(q) = -d_S - \log\langle W^q\rangle/\log(1/r)$ and $P_q(x) = P_q(x+\log(1/r))$. A periodic prefactor is therefore also obtained for averaged correlation functions, either for sets or measures. For a random Cantor set, the prefactor of $C_q(L)$ may oscillate for a given realization. The problem is to determine whether these oscillations remain "in phase" for different realizations, in which case the oscillations may survive the averaging of several realizations, or if the oscillations are out of phase and therefore produce a constant prefactor once averaged.

We shall now consider three examples. Let us first consider a separated random Cantor set, where the sequences 1010 and 0101 are chosen randomly with equal probability at each construction step. For any realization, the two subsets composing the whole set are separated, and therefore the renormalization equation (8.2.2) holds exactly. The prefactors $P_1(L)$ obtained with two different realizations were plotted in figure 8.7 (the sets were constructed using 8 cascade steps). For each realization the prefactor oscillates periodically, and the oscillations are in phase. It follows that <C(L)> also has an oscillating prefactor. Oscillations are observed in each realization because these sets remain fairly regular, despite their randomness.

The second example is a triadic Cantor set where the sequences 101, 110 and 011 are chosen randomly with probabilities 0.8, 0.1 and 0.1 respectively. A larger weight has been given to the set 101 in order to enhance oscillations. The prefactors computed on two realizations of this set have been plotted in figure 8.8. 7 cascade steps have been used in the construction of the sets. Although irregular, the prefactors of both realizations oscillate approximately in phase, and therefore the prefactor of <C(L)> should also oscillate. In figure 8.9 the prefactor of <C(L)>, obtained by averaging 200 such realisations, is displayed. A periodic oscillation is obtained and the fall-off at large scale is due to the fact that most realizations are formed of non-separated subsets.

In a third example we considered the triadic Cantor set where the sequences 101, 110 and 011 are chosen with equal probability, which makes the set more irregular. In figure 8.10 the prefactors of three realizations (7 cascade steps) are plotted. No obvious periodicity is visible. In order to determine if the prefactor of <C(L)> oscillates 1000 such realizations were averaged. The prefactor of <C(L)> did not exhibit periodicity and the irregularities of the prefactor were found to be very small (the ratio of their amplitude to the mean prefactor was about 2%). In order to see if the prefactor oscillations could be enhanced for higher order correlation functions, the prefactors of $C_1(L)$, $C_5(L)$ and $C_{10}(L)$ were obtained for a realization and plotted

together in figure 8.11. This graph clearly suggests that the amplitude of the prefactor oscillations are enhanced by raising the order of the correlation function. In figure 8.12 the prefactor $P_{10}(L)$ obtained by averaging 250 realizations of $C_{10}(L)$ is displayed. An oscillation with a period corresponding to a scale ratio 1/3 is clearly visible. The periodicity is altered by statistical errors and by the effect of the lack of separation.

We conclude that the oscillations of the prefactor of $<C_q(L)>$ can be difficult to observe in random self-similar sets. High values of q help emphasizing the oscillations but a lot of averaging is often required to obtain a reasonable evidence for periodic behavior. It seems that the oscillations are never completely destroyed by randomness. Nevertheless it would appear that more "irregular" sets produce oscillations smaller in amplitude and consequently more difficult to observe. These conclusions were also found to apply to the correlation function defined for measures, as verified with numerical experiments on deterministic and random single scale multinomial measures (see figure 8.13)

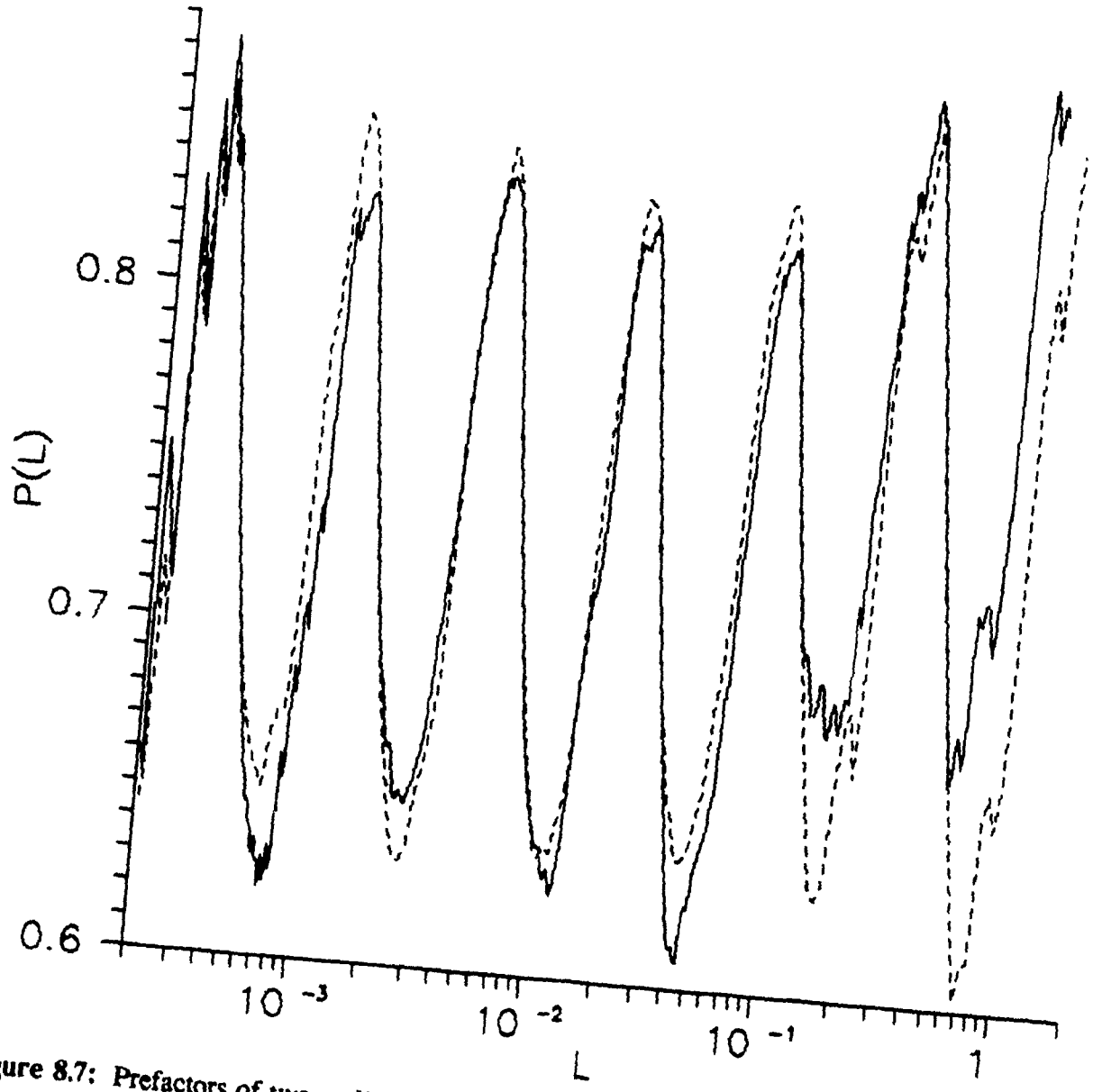

Figure 8.7: Prefactors of two realizations of the random set constructed with the sequences 1010 and 0101, chosen randomly with equal probability. The oscillations remain in phase for each realization (the solid line is one realization, and the dashed line is the other realization).

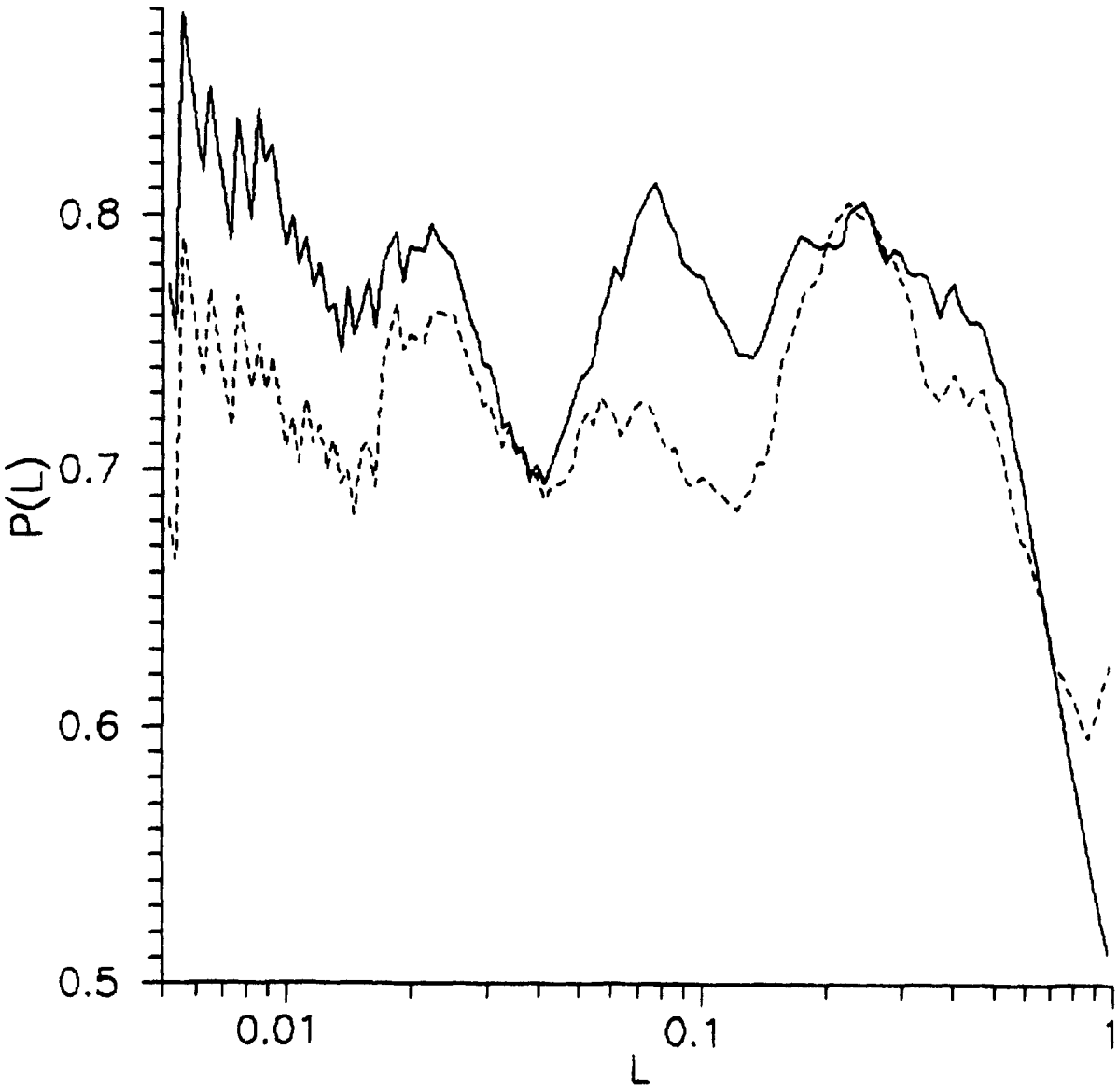

Figure 8.8: prefactors of two realizations of the random set where the sequences 101, 110 and 011 are chosen randomly with probabilities 0.8, 0.1 and 0.1 respectively.

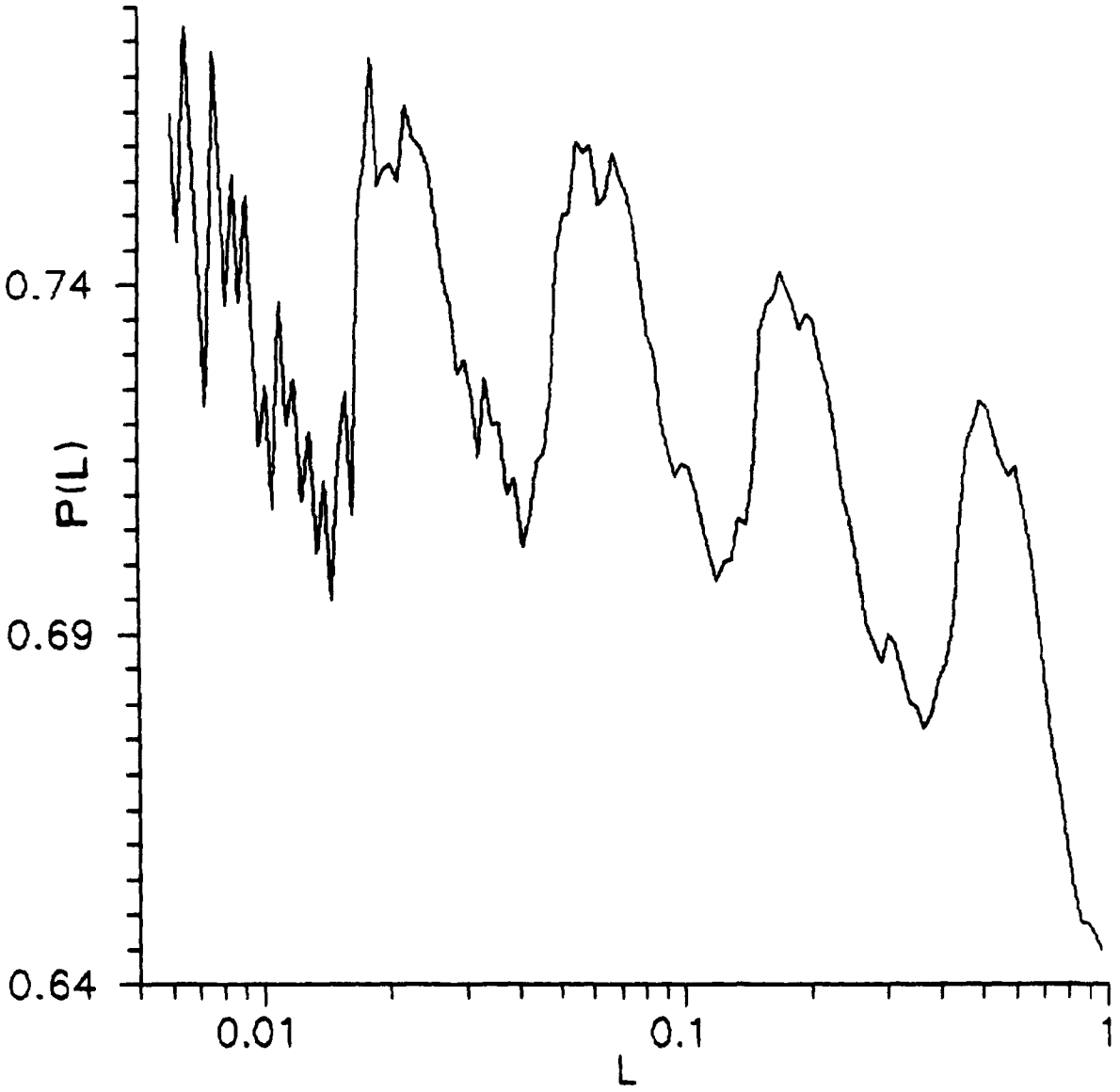

Figure 8.9: Prefactor of <C(L)> averaged over 200 realizations of the random Cantor set where the sequences 101, 110 and 011 are chosen randomly with probabilities 0.8, 0.1 and 0.1 respectively.

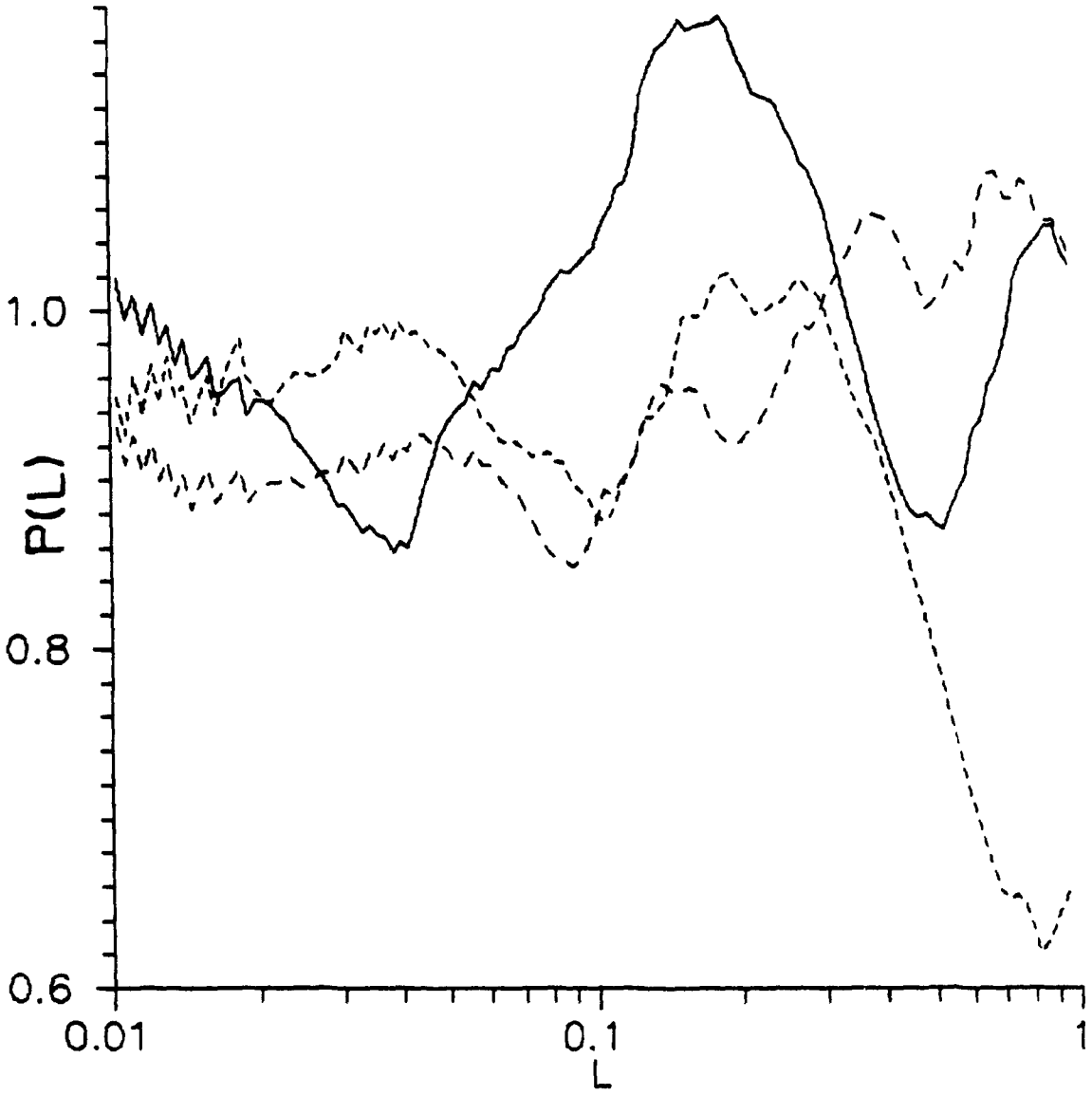

Figure 8.10: Prefactors of 3 realizations of the random Cantor set where the sequences 101, 110 and 011 are chosen randomly with equal probabilities.

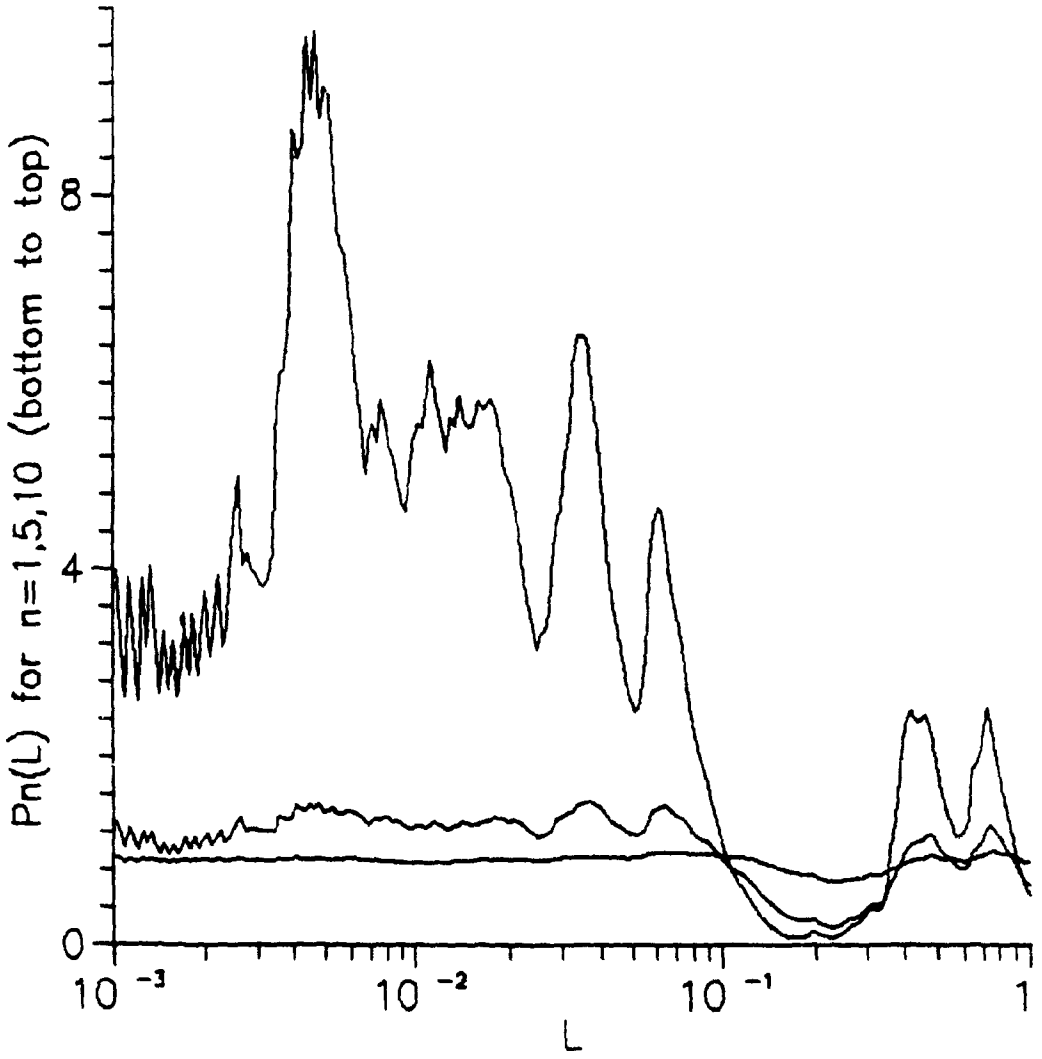

Figure 8.11: Prefactors of $C_1(L)$, $C_5(L)$ and $C_{10}(L)$ (from bottom to top respectively) of a realization of the random set where the sequences 110, 101 and 011 are chosen with equal probabilities. This graph clearly suggests that the amplitude of the prefactor oscillations are enhanced by raising the order of the correlation function.

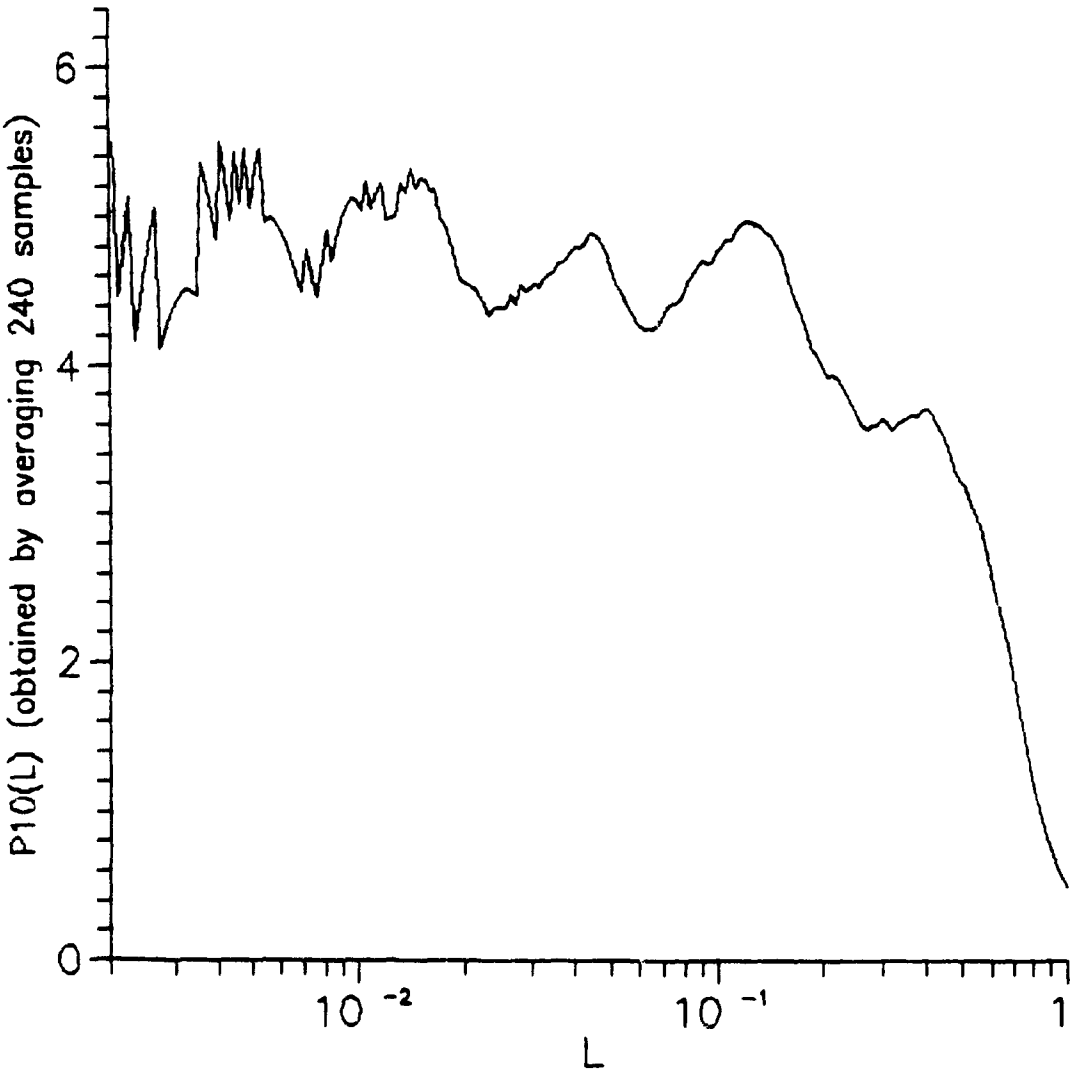

Figure 8.12: $P_{10}(L)$ obtained by averaging 250 realizations of $C_{10}(L)$ obtained with the random sets where the sequences 110, 101 and 011 are chosen with equal probabilities. An oscillation with a period corresponding to a scale ratio 1/3 is clearly visible. The periodicity is altered by statistical errors and by the effect of the lack of separation. The sets were constructed using nine cascade steps.

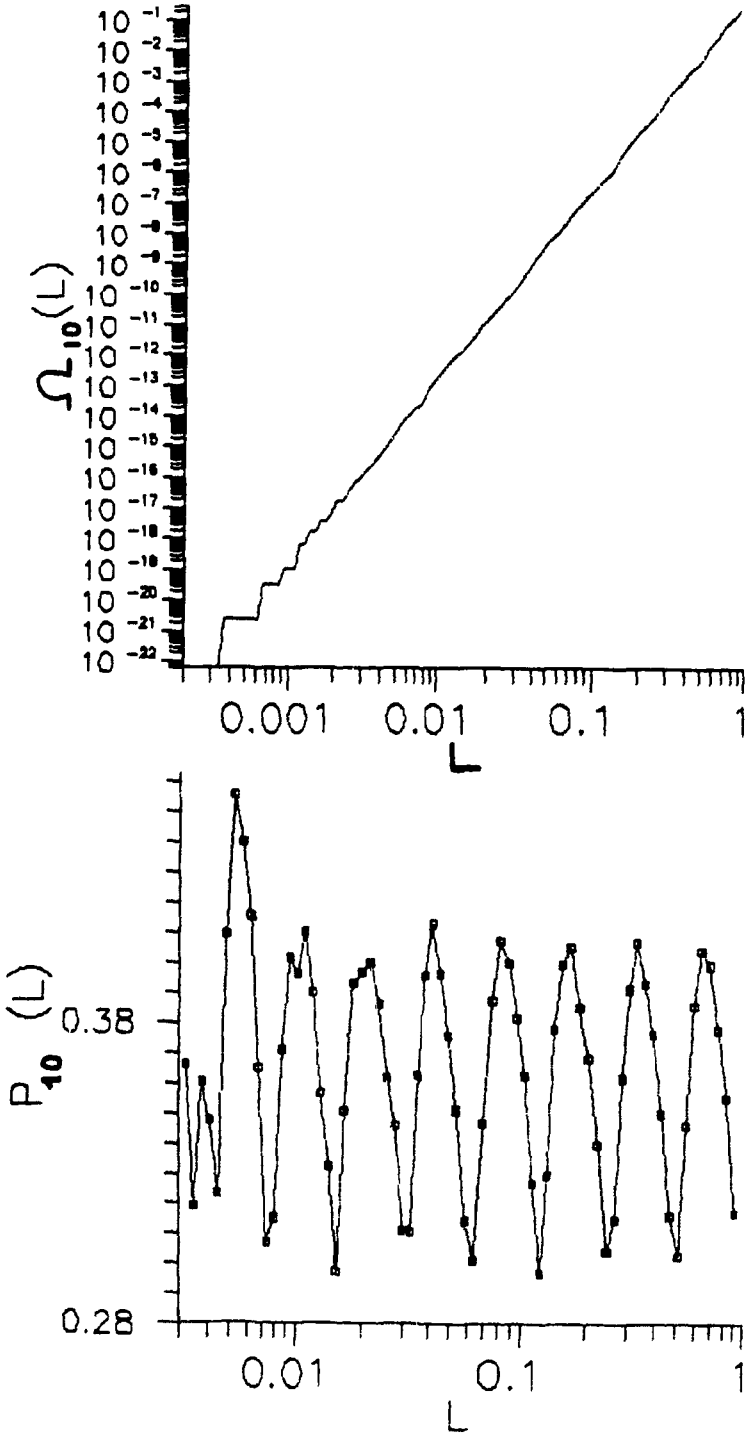

Figure 8.13: Top: The correlation function $\Omega_{10}(L)$ obtained with the deterministic binomial measure using weights $w_1 = 0.3$ and $w_2 = 0.7$ and 12 cascade steps. Bottom: The prefactor of $\Omega_{10}(L)$ exhibits periodic oscillations corresponding to a scale ratio $r = 1/2$.

8.2.3 Numerical experiment with the Novikov "pulse-in-pulse" model

In this section we examine a numerical experiment performed with the Novikov "pulse-in-pulse" model (section 2.4.3). This is an attempt to determine to what extent the oscillations of the power spectrum are easily observable. The construction of the model involves a Poisson process governing the large scale structure of the dissipation field and a cascade process determining its fractal self-similar structure. In order to focus on the scaling range of the power spectrum we constructed a model that did not involve the Poisson process ingredient. Starting with a point centered at $x = 0$ the fractal set determining the energy dissipation function $\varepsilon_s(x)$ was directly constructed around this point The pulse shape was chosen to be $I(x) = a/(\pi(x^2+a^2))$. θ was chosen to be uniformly distributed between -1/2 and 1/2 with $m = 2$, $\beta = 1/3$ and $\lambda_1 = 1$. It follows that the spectrum has the form $E(k) = k^{-\gamma} P(\log k)$ where $\gamma = \log 2/\log 3 \approx 0.6309$ and $P(\log k) = P(\log k + \log(1/3))$. The exponent γ is therefore comparable with the γ measured in turbulent flows that lies between 0.5 and 0.7. Eight cascade steps were performed in the construction of the model. For illustration two realizations of this model with $a = 1/2$ and $a = 1/6$ are given in figures 8.14 and 8.15 respectively.

$\varepsilon_s(x)$ was sampled with a resolution high enough for the power spectrum to exhibit a beginning of fall-off at high frequencies. The prefactor $E(k)\, k^{\gamma}$ of a typical power spectrum obtained from a single realization with $a = 1/6$ is shown in figure 8.16 Using the same vertical scale the prefactors obtained by averaging 10 and 500 realizations are shown in figure 8.17. A tiny oscillation is perceptible and a zoom reveals a rough periodicity with $\beta \approx 1/3$ consistent with the theoretical prediction. The prefactor oscillation therefore exists in this model, i.e. the prefactor is not constant. The ratio of the amplitude of the oscillation to the mean prefactor is about 20% which means that an accuracy on the spectrum of at least 5% is required to observe the oscillation. In our results with atmospheric data (figure 6.8) the noise

level on $E_\varepsilon(k)$ (the power spectrum of $(\partial u/\partial x)^2$) was at least 50% and was therefore too large to observe such a small oscillation.

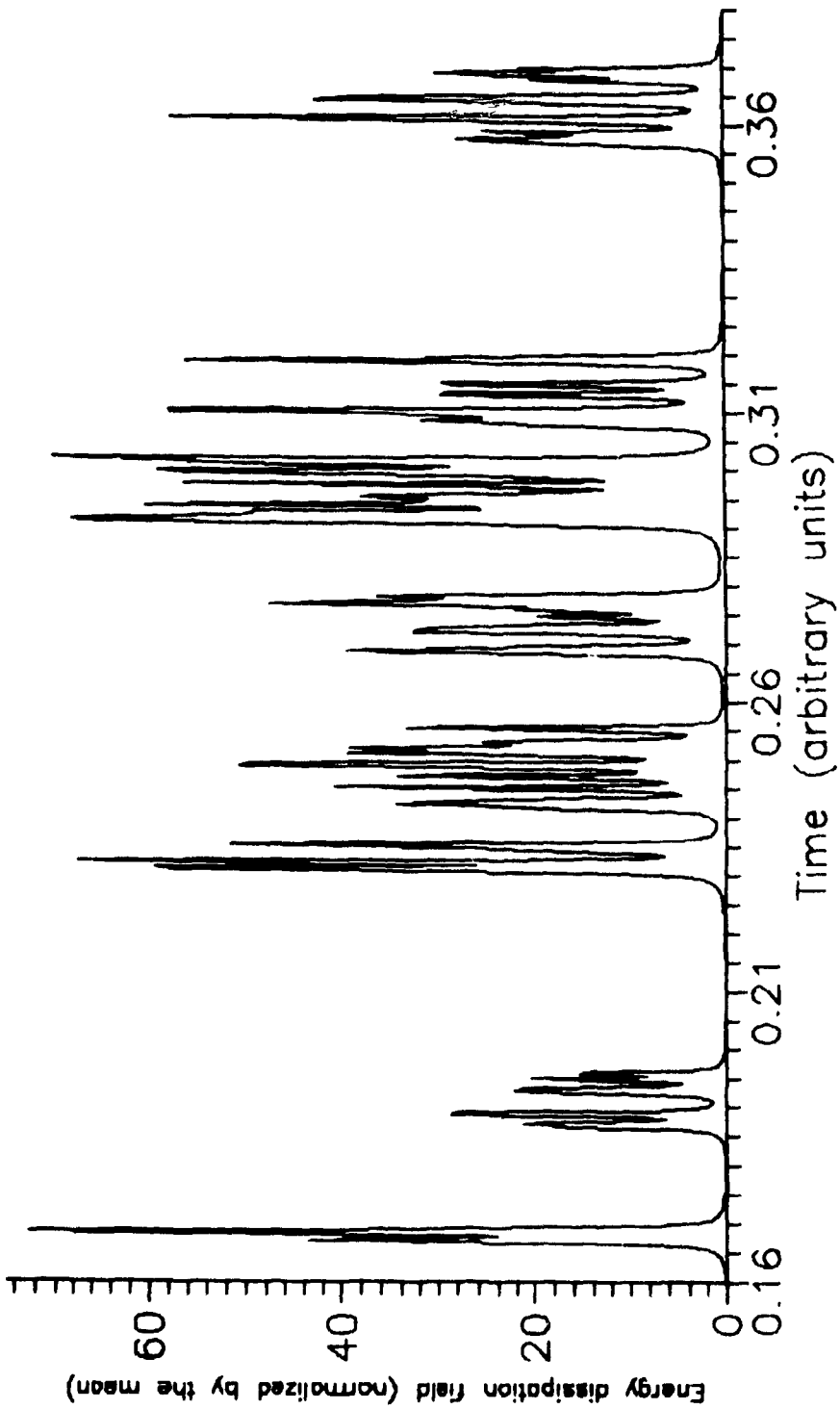

Figure 8.14: A realization of the Novikov model as defined in the text obtained with a = 1/2.

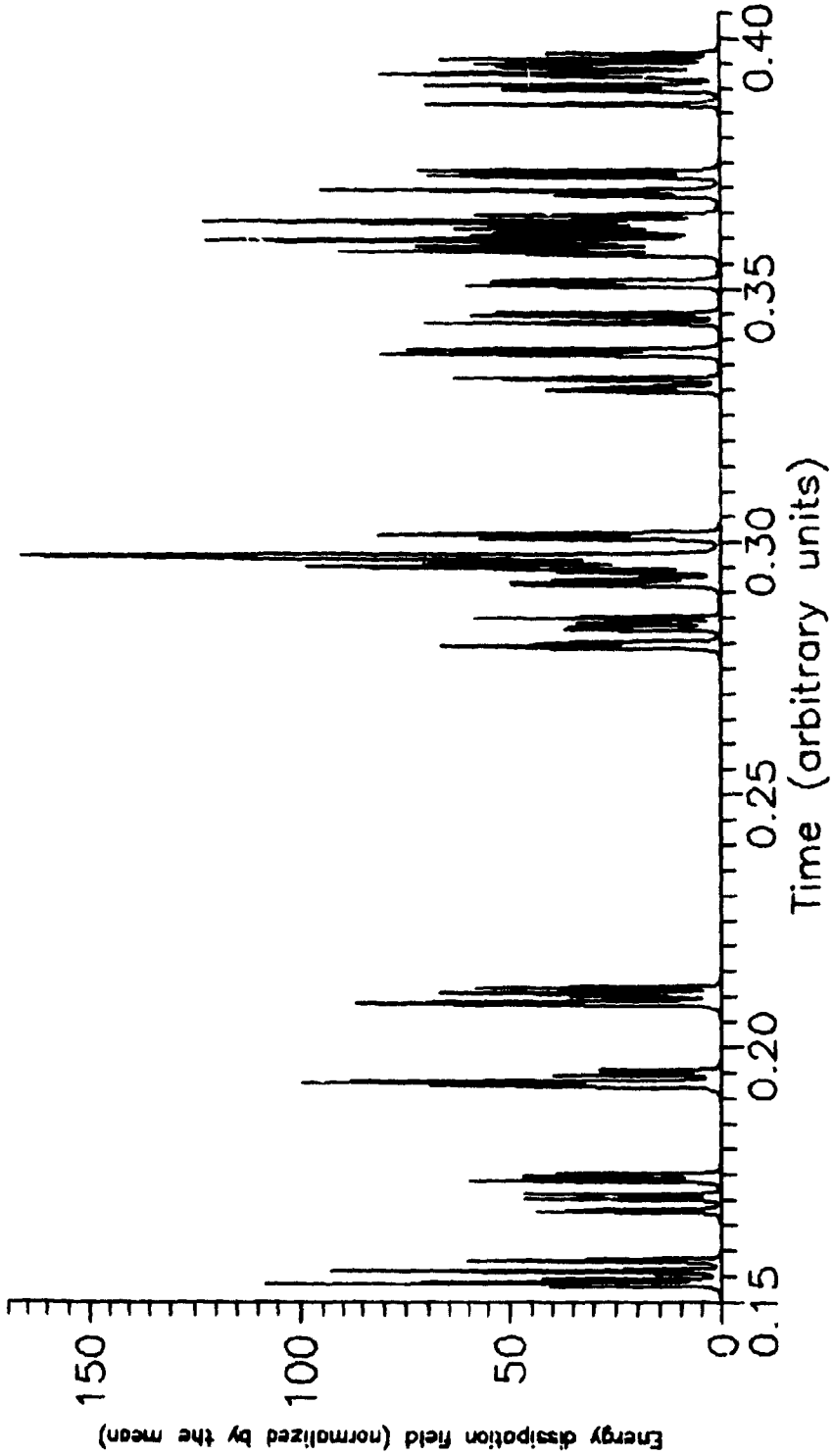

Figure 8.15: A realization of the Novikov model as defined in the text obtained with a = 1/6.

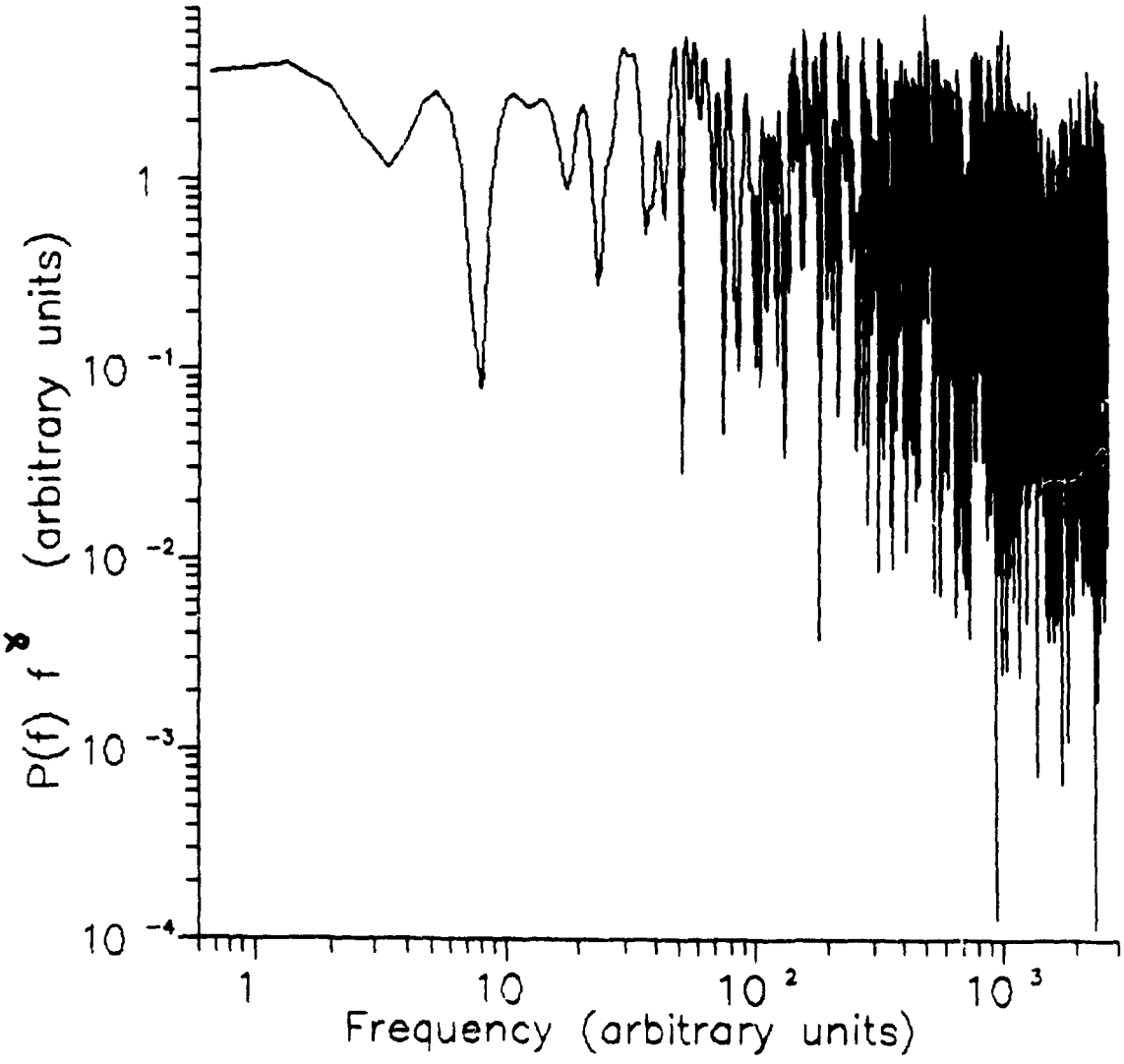

Figure 8.16: Prefactor $E(k)\,k^{\gamma}$ of a typical power spectrum obtained from the Novikov model with a single realization using a = 1/6.

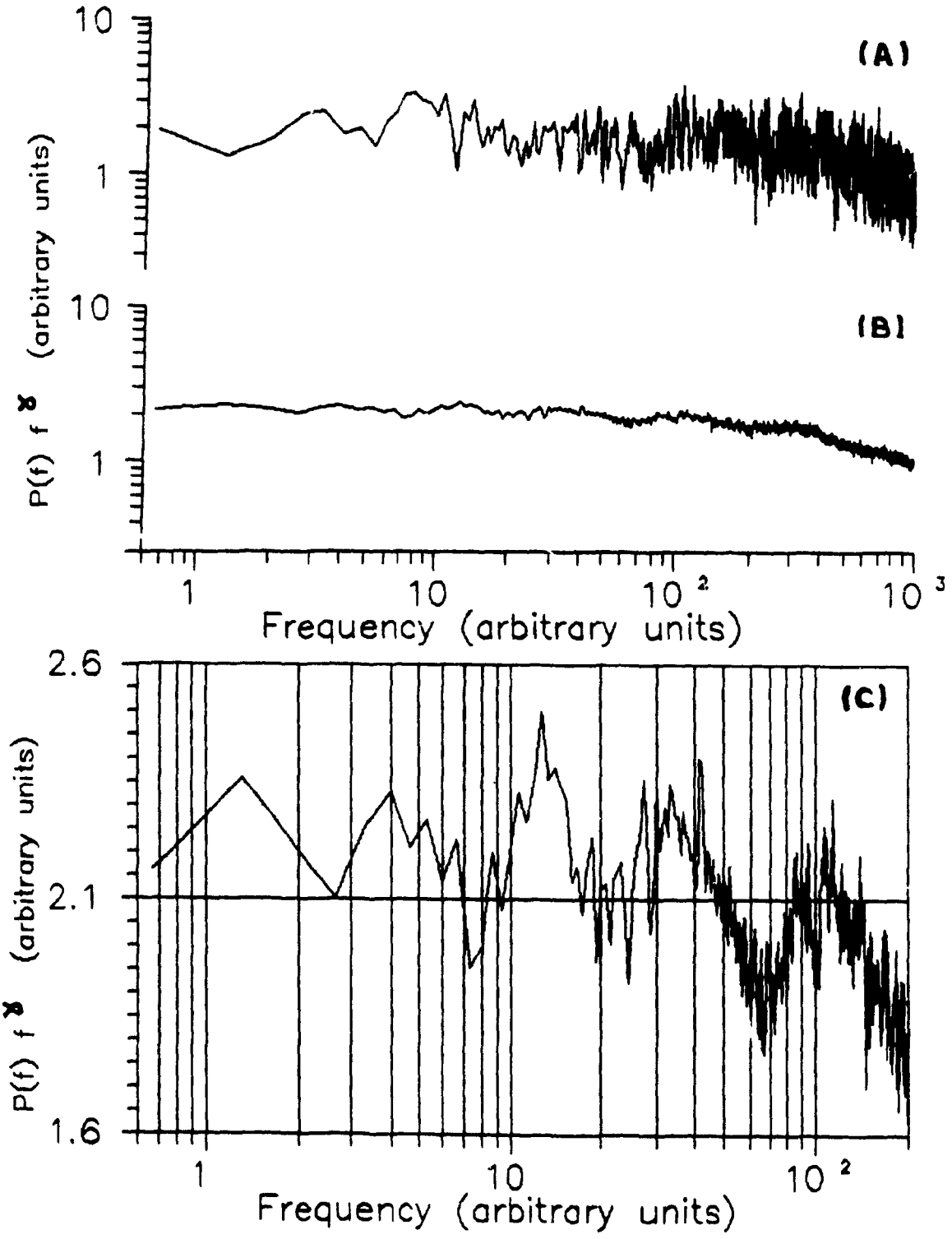

Figure 8.17: Prefactor $E(k)\,k^{\gamma}$ of the power spectrum obtained from the Novikov model using a = 1/6 and by averaging over **a)** 10 realizations **b)** 500 realizations. In **c)** a zoom is made on the prefactor of **b)**.

8.2.4 Experimental results with the energy dissipation field

The measure associated with the field $(\partial u/\partial x)^2$ was shown in chapter 6 to have scaling properties for scales larger than 10 cm. We are comparing this measure with a cascade process, and therefore the inner scale of this hypothetical process should be 10 cm. A graph of the values of the measures of 10 cm intervals is displayed in figure 8.18. Obviously all the intervals have a non-zero measure, and therefore the support of the energy dissipation field is the whole line. The function $C_q(L)$ therefore takes a trivial value. A non-trivial set could be obtained for example by focusing on threshold sets, i.e. sets composed of the union of all the 10 cm intervals having a non-negligible measure. However, for a space-filling multinomial measure the sets obtained with this truncation are not Cantor sets in general. In order to apply directly the methods introduced above to detect prefactor oscillations, it is therefore more suitable to study the measure with the correlation function $\Omega_q(L)$.

It has been emphasized previously that the prefactor oscillations can be very tiny. One must therefore worry about the accuracy of the "wiggles" obtained from a power law before giving them any credit. In figure 8.19 the correlation function $\Omega_2(L)$ obtained with a coarse-graining scale of 10 cm is displayed. The results obtained by averaging on the whole sample, and then on the first and second halves, are given. The differences between these curves show that $\Omega_2(L)$ has not converged yet. However, the scaling exponents are almost identical (within 1%) and therefore there may be some hope that the prefactor oscillations can be detected. In order to see if any systematic variations occur in the prefactors, we extracted a prefactor function from each half-sample, as well that from the whole sample, with the following procedure. Firstly, the scaling exponent γ defined by $[<\Omega_q(L)>]^{1/q} \sim L^{\gamma}$ was obtained using a linear regression; secondly, a prefactor function $P_q(L) = [<\Omega_q(L)>]^{1/q} L^{-\gamma}$ was calculated and normalized by $P_q(L_{min})$, where L_{min} is the smallest scale of the scaling range.

The results obtained for $q = 2$ and $q = -1$ are shown in figure 8.20. In both cases systematic oscillations are visible. Indeed, the prefactors obtained with different samples (i.e. the first and second halves) have their up and downs at the same scales. We therefore conclude that these oscillations are not statistical artefacts, even if they are not very accurate. The prefactors are not measured accurately enough to establish periodicity. Nevertheless, they have their up and downs fairly regularly. A clear change in behavior occurs between the ranges $L \leq 3$ m and $L > 3$ m, which is not necessarily surprising since the altitude is about 4 meters. In the range $L \leq 3$ m, two large oscillations suggest a periodicity corresponding to $r \approx 1/2$. In the range $L > 3$ m, at least four oscillations (smaller in amplitude and period) occur with an approximate periodicity corresponding to $r \approx 1/1.5$. The change in behavior between the two ranges of scale implies that the prefactor cannot be periodic over the whole scaling range. It should be noted that for larger values of $|q|$ we found that the estimation errors on the prefactors, as judged from the variations between the first and second half-sample, were too large for conclusive results to be obtained.

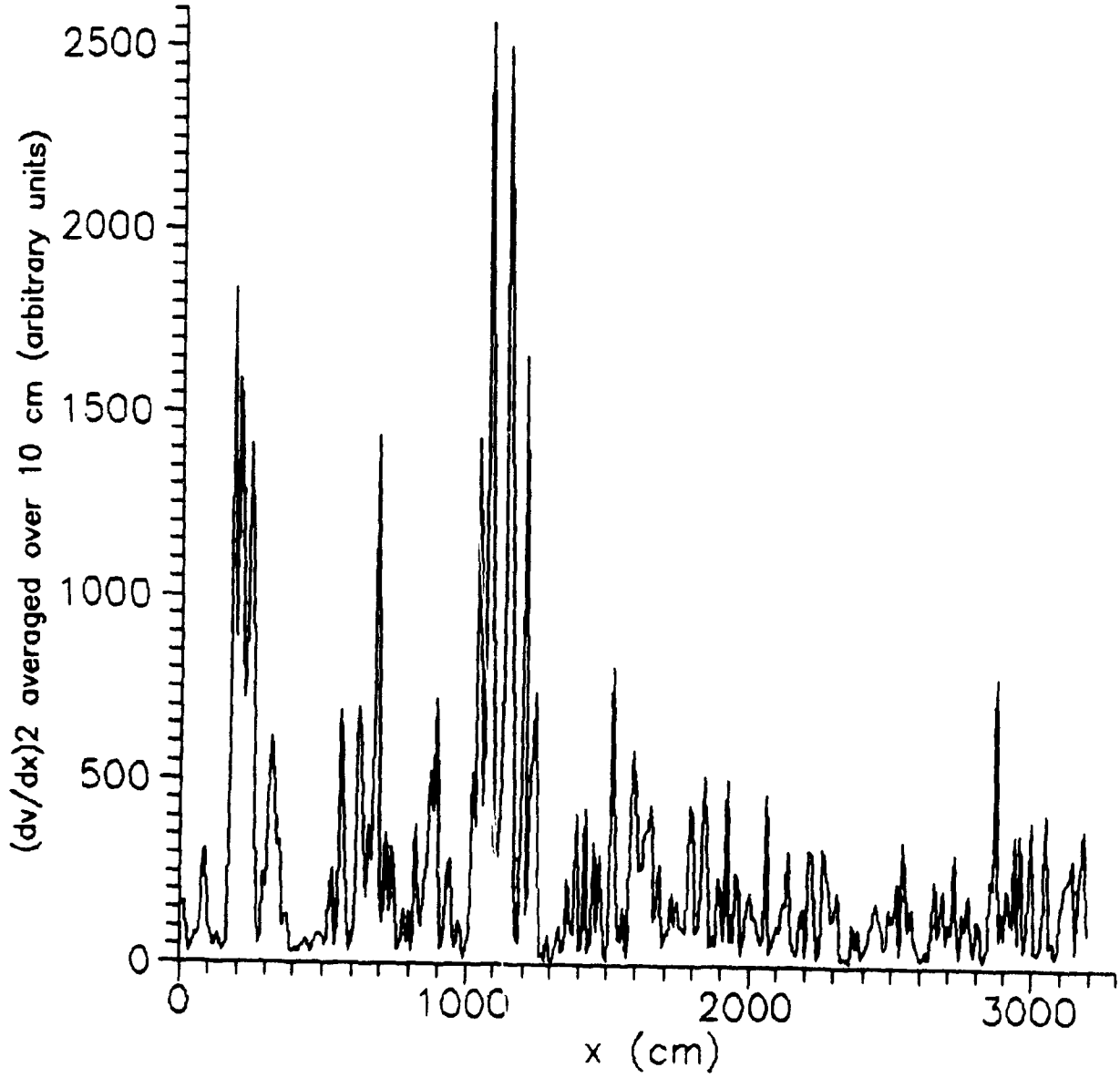

Figure 8.18: Values of the measures of 10 cm intervals for the field $(\partial u/\partial x)^2$.

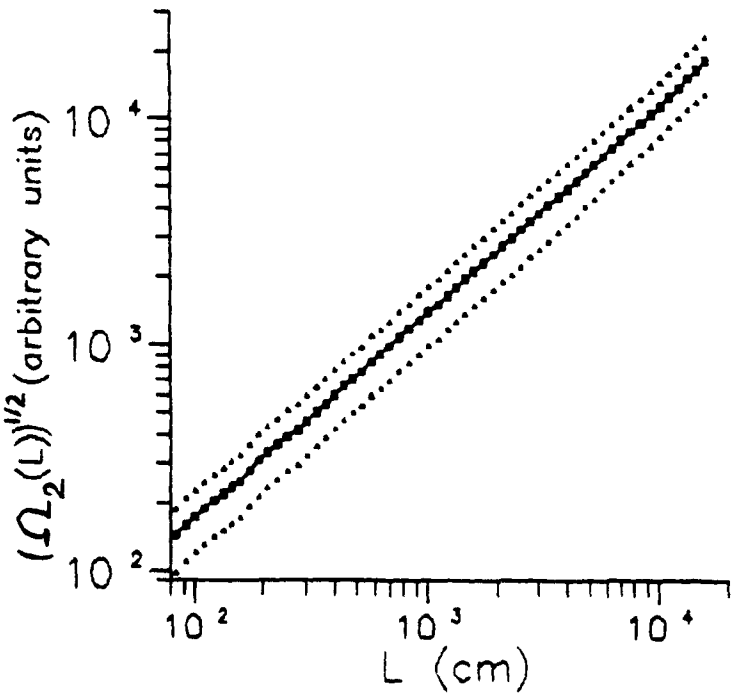

Figure 8.19: $<\Omega_2(L)>$ measured on the energy dissipation field. The solid curve corresponds to an averaging over the whole sample, while the dotted curves corresponds to averaging over the first and second halves of the sample. The differences between these curves clearly show that $\Omega_2(L)$ has not converged yet. However, the scaling exponents obtained with linear regressions are almost the same (less than 1% of difference).

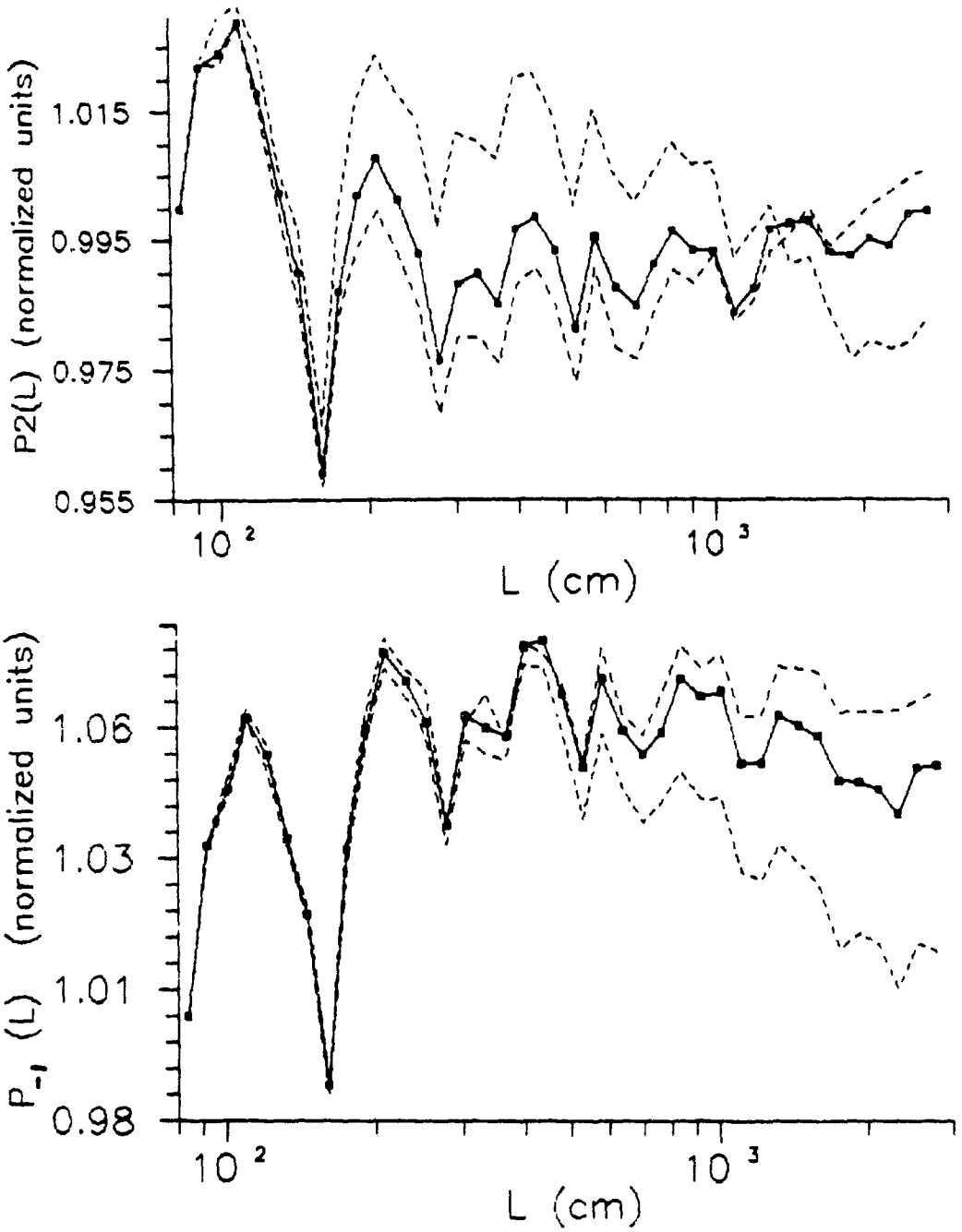

Figure 8.20: Prefactor functions of $\Omega_q(L)$ (see text for the definition) obtained with q = 2 (top) and q = -1 (bottom). The solid line corresponds to an averaging over the whole sample, while the dashed curves are related to the averaging on the first and second halves of the sample. Systematic oscillations are visible. Prefactors obtained with different samples (i.e. the first and second halves) have their up and downs at the same scales. These oscillations are therefore real, even if they are not very accurate. Their periodicity is not striking but they have their up and downs fairly regularly. A clear change in behavior occurs between the ranges $L \leq 3$ m and $L > 3$ m, which is not necessarily surprising since the altitude is about 4 meters. In the range $L \leq 3$ m, two large oscillations occur with a periodicity corresponding to $r \approx 1/2$. In the range $L > 3$ m, at least four oscillations (smaller in amplitude and period) occur with a periodicity corresponding to $r \approx 1/1.4$.

8.2.5 Conclusions about prefactor oscillations

We found that periodic prefactor oscillations of scaling quantities usually exist in random single-scale models, i.e. the periodic prefactors are rarely constant. For correlation functions these oscillations may be difficult to observe because of their small amplitude, and it is usually necessary to focus on high order correlation functions to enhance them. The analysis of $\Omega_q(L)$ on the energy dissipation field revealed systematic prefactor oscillations, with fairly regular up and downs, but the accuracy of the prefactors was not sufficient to establish periodicity. The oscillations were found to be consistent with $r \approx 1/2$ in the isotropic range (i.e. $L \leq 3$ m), and consistent with $r \approx 1/1.5$ in the non-isotropic range (i.e. $L > 3$ m). The prefactors do not appear to be periodic over the whole scaling range. We emphasize that the existence of a privileged scale ratio leads in general to prefactor oscillations but that the converse may not always be true. In other words, the prefactor oscillations of $\Omega_q(L)$ might have a different origin, especially in the non-isotropic range.

The numerical experiment with the Novikov pulse-in-pulse model showed that small power spectrum oscillations did exist in this model but that an accuracy of at least 5% on the spectrum was needed to observe them (in the specific cases examined). Our measurements of the power spectrum of $(\partial u/\partial x)^2$ in the atmosphere, involving a 50% statistical error, were not accurate enough for such a small oscillation to be detected.

CONCLUSION

Pour obtenir des résultats valables il faut d'abord choisir correctement son objectif, et savoir se contenter d'une description incomplète de la nature.

Hubert Reeves (from *Malicorne, réflexions d'un observateur de la nature*)

1) Cascade models and the energy dissipation field

We shall first reexamine the findings listed in the section *Contributions to original knowledge* from the viewpoint of one of the questions originally posed in the introduction: Can we distinguish the energy dissipation field (EDF), as measured with a hot wire anemometer in the atmospheric surface layer, from multiplicative cascade processes ? Let us review the five different analyses we made to check the validity of these various models:

i) Single-box scaling: One of the simplest property of multiplicative processes is the scaling behavior of the moments of the measure $\langle(\mu(\delta))^q\rangle \propto \delta^{\tau(q)+D}$. This property had already been found to be well supported for one-dimensional averages of $(\partial u/\partial x)^2$ by Meneveau and Sreenivasan. Our data also exhibits a convincing scaling behavior and we obtained approximately the same function $\tau(q)$ (section 6.4). The stability of the exponents for different flows is consistent with the Kolmogorov hypothesis of universality for small scale turbulence in the limit of infinite Reynolds number. We emphasize that for $q > 0$ the scaling of $\langle(\mu(\delta))^q\rangle$ is good but nevertheless the prefactor $\langle(\mu(\delta))^q\rangle\ \delta^{-\tau(q)-D}$ exhibits irregular oscillations. It is interesting to note that the scaling range extends over scales much larger than the range over which isotropy might hold.

ii) Two-box scaling: A calculation of correlations in single scale multiplicative processes showed that the quantities $\langle(\mu(\delta))^{p+q}\rangle$ and $\langle(\mu_l(\delta))^p(\mu_{l+1}(\delta))^q\rangle$, where $\mu_l(\delta)$ and $\mu_{l+1}(\delta)$ denote the average energy dissipation in boxes separated by a distance δ, should both scale with identical exponents $A(p, q)$ for wide domains of the (p, q) plane (i.e. the "CD-scaling"

region). The analysis of the EDF showed that for $p = q$ (in the CD-scaling region) this property was well satisfied, which supports multiplicative processes. In the non CD-scaling domain a scaling transition occurs for single scale multinomial models. A similar transition was observed in the EDF but in this region the scaling exponents $A(p, q)$ were found to be significantly different from the exponents predicted by the model. This result is interesting for at least two reasons: Firstly, the scaling transition predicted in the model actually occurs in the EDF; secondly, for some (p, q) the exponents $A(p, q)$ allow to distinguish the EDF from single scale cascades.

iii) Central limit theorem: In chapter three we showed that another way of testing finite variance multiplicative processes was to check that the moments of $\log(\varepsilon(\delta))$, where $\varepsilon(\delta)$ is the field $(\partial u/\partial x)^2$ line-averaged over a scale δ, could be obtained from the gaussian approximation. This was reasonably supported by the data (section 7.3), thus providing indirect support for the hypothesis of finite variance required for the central limit theorem to apply, although the infinite variance cases were not considered.

iv) Prefactor analysis: We tried in chapter 8 to determine whether the hypothesis of a privileged scale ratio in the EDF could find support in the data. Such privileged scale ratios are obtained for example in cascade processes where each eddy splits in a fixed number of eddies of the same size. For such models the existence of periodic prefactor oscillations in either power spectrum (section 2.4.3) or generating functions (section 5.4) can be used to reveal the underlying scale ratio. Prefactors were found to be sensitive to the box-counting grid in both sets and measures. Hence the usual methods involving grids used to obtain the box-dimension or the mass exponents cannot always be used to estimate prefactors. We consequently developed new "grid insensitive" methods to measure prefactors accurately in either sets or measures (section 8.1). These methods were tested numerically on artificial sets and measures (sections 8.2.1-2-3). The analysis of $\Omega_q(L)$ on the energy dissipation field revealed oscillating prefactors with fairly regular up and downs, but our estimation of the prefactors was not

accurate enough to establish periodicity. In the isotropic range (i.e. $L \leq 3$ m) the oscillations suggest a periodicity with $r \approx 1/2$; in the non-isotropic range (i.e. $L > 3$ m), they suggest a rough periodicity with $r \approx 1/1.4$. In any case, the prefactors are not periodic over the whole scaling range. We emphasize that the existence of a privileged scale ratio leads in general to prefactor oscillations, either for correlation functions or spectra, but that the converse may not always be true. In other words, the prefactor oscillations of $\Omega_q(L)$ might have another origin, especially in the non-isotropic range.

v) **Divergent versus non-divergent cascades:** Random multiplicative processes can be grouped in two classes called microcanonical and canonical (section 5.4). As pointed out by Mandelbrot (1974), canonical models make room for measures with divergent moments $<\mu^q(\delta)>$, and we showed in section 5.4.3 that divergence of moments leads to an effectively vanishing mass exponent $\tau(q)$ for large q. This behavior was not observed in the EDF for $-10 \leq q \leq 10$. Indeed $\tau(q)$ rather exhibits an asymptotically linear $\tau(q)$ for large |q|. This suggests that divergent cascade processes are not relevant to the modelling of the EDF, although we could not eliminate the possibility of the divergence of sufficiently high order moments.

The main disagreements between single-scale multinomial models and the real EDF were on one hand the scaling exponents A(p, q) of the correlations $<(\mu_i(\delta))^p(\mu_{i+1}(\delta))^q>$ in the non CD-scaling domain, and on the other hand the prefactor oscillations of $\Omega_q(L)$ that are not periodic over the whole scaling range. The other analyses give support to multiplicative processes, which is an interesting results in itself. The failure of the single scale multinomial model to account for the scaling of correlations for some (p, q) suggests that more general models, maybe multiscale cascade processes, may be more adequate for the energy cascade process. It should be noticed that this failure is consistent with the lack of periodicity of the prefactor of $\Omega_q(L)$ over the whole scaling range, that also rejects the hypothesis of a single scale ratio. The double-box scaling exponents A(p,q) may not always be related in a simple manner to $\tau(q)$, in which case they would provide a more complete description of a scaling field. iii)

and v) suggest that the 1-D multiplicative process that best fits the EDF, as measured on a line with a hot wire anemometer, should have multiplicative factors W with finite $<(\log W)^2>$, and be non-divergent (i.e. $\tau(q) > 0$ for $q > 1$) if canonical. Besides the actual form of the mass exponents $\tau(q)$, that were measured in chapter 6, these are the main informations obtained about the EDF.

2) Kolmogorov inertial range theories

We shall now come back on our main conclusions about some questions raised by the Kolmogorov theories. Landau's criticism of the original 1941 Kolmogorov theory, in essence, is that the $k^{-5/3}$ law is not invariant with respect to the composition of statistical subensembles. The K41 theory could escape this problem only if the volume-averaged EDF $\varepsilon(\delta)$ was constant for $\delta \geq \eta$, where η is the dissipation scale, which is found experimentally not to be the case. It follows that the K41 theory, although making remarkably accurate predictions for the energy spectrum, is in principle invalid. This problem lead Kolmogorov and Obukhov to develop a refined theory, rather questionable actually, on which we shall not further comment here. We made an interesting observation in connection with the general relevance of Landau's idea: Most statements made in statistical fluid mechanics, such as the law of the logarithmic boundary layer that describes the mean velocity profile over an infinite flat surface, are found not to be invariant with respect to the composition of statistical subensembles. It follows that Landau's objection equally applies to these statements, that should therefore be regarded as only approximate. This fact does not appear to have been noticed previously since many of these laws, e.g. the law of the logarithmic boundary layer (Monin and Yaglom, 1975), are presented as *exact* implications of the Reynolds equations. It follows that the universal constants involved in these statements, such as the von Karman constant, are not universal, which might explain the scatter of the estimations of this constant as made by various experimenters.

The Kolmogorov original theory predicts that the structure functions take the form $<(\Delta v(L))^h> = c(h)\ (\varepsilon_0 L)^{h/3}$, where c(h) is a universal function of h. According to Landau this result cannot be rigorously correct. However, Frisch argued that if the formal stretching symmetry of the Euler equation is obeyed by the velocity field in a statistical sense, the simple scaling $<(\Delta v(L))^h> \propto L^{h/3}$ should be obtained without necessarily having universal prefactors involving ε_0. This argument is interesting because the lack of universality of the prefactors does not allow the Landau's objection to apply. Hence the possibility of simple scaling remains and one must then explain why high order moments actually yield $<(\Delta v(L))^h> \propto L^{\zeta(h)}$, where $\zeta(h) \neq h/3$ for $h > 4$. This has been the object of a controversy. On one hand, Frisch simply interpreted the non-linearity of $\zeta(h)$ as an evidence for the breakdown of the stretching symmetry in turbulent fluids. On the other hand, Schertzer and Lovejoy argued that even if simple scaling was strictly obeyed for the probability distributions of $\Delta v(L)$, the linearity of the exponents $\zeta(h)$ measured on a sample could be broken if $\Delta v(L)$ had divergent moments for $h > 5$. From this point of view the non-linearity of $\zeta(h)$ is regarded as a statistical bias that does not disprove the validity of simple scaling.

In order to determine which of these two alternatives was correct, we examined the probability distributions of the velocity differences $\Delta v(L)$. Firstly, the probability distributions were not found to be convincingly hyperbolic. More importantly however, a statistical test made on suitably scaled histograms showed that simple scaling, apparently fairly well satisfied as judged by simple graphs, did not hold on a strict statistical basis. We also observed that simple scaling was increasingly broken for large values of $\Delta v(L)$, which explains the non-linearity of $\zeta(h)$ for h large. By contrast with previous tests of simple scaling (Anselmet, 1984), based on the linearity of $\zeta(h)$ for high order structure functions and possibly biased by divergence of moments, our method does not require an accurate estimation of the moments and remains valid even if $\Delta v(L)$ has divergent moments. We conclude that simple scaling is

definitely broken in the statistical sense but that it is obeyed sufficiently accurately for relatively small values of $\Delta v(L)$ to yield accurate scaling predictions for low order moments.

A slight improvement on previous formulations of the third Kolmogorov hypothesis was also made by suggesting that the moments of $\log\varepsilon(\delta)$ should be possible to obtain using the gaussian approximation. This conjecture was found to be reasonably supported by the data, which also supports indirectly the concept of multiplicative process, as mentioned above. We emphasize that this is a weaker version of the third Kolmogorov hypothesis, since it does not allow the calculation of the moments of $\varepsilon(\delta)$.

APPENDIX 3.1 : CENTRAL LIMIT THEOREM (BY KHINCHIN)

Consider the random variable

$$S_n = Y_1 + ... + Y_n$$

where the Y_i are identically distributed and independent random variables such that $\langle Y_i \rangle = 0$. Let u(y) denote by the probability density of Y and define $F(t) = \int e^{ity} u(y) dy$ the characteristic function. Khinchin results (section 3.2) about the probability density $\gamma_n(s)$ of S_n holds if Y satisfies the following conditions:

1 - u(y) possess continuous derivatives and there exists a positive constant A such that $\int |u'(y)| \, dy < A$,

2 - $\langle Y^p \rangle < \infty$, $p = 2, 3, ..., 5$,

3 - there exists positive constants a and b such that for $|t| < a$, $|F(t)| > b$,

4 - for each interval $[c_1, c_2]$ $(c_1 c_2 > 0)$ there exists a number $\rho(c_1,c_2) < 1$ such that for any $t \in [c_1, c_2]$ we have $|F(t)| < \rho(c_1,c_2)$.

APPENDIX 3.2 : THE MELLIN TRANSFORM THEOREM

Suppose that $f^*(z)$ is a function of the complex variable $z = \sigma + i\tau$ which is regular in the strip $S = \{ s : a < \sigma < b \}$ and that for any arbitrary small positive number ν, $f^*(z)$ tends to zero uniformly as $|\tau| \to \infty$ in the strip $a + \eta \leq \sigma \leq b - \eta$. Then the integral

$$\int_{-\infty}^{+\infty} f^*(\sigma + i\tau)\, d\tau$$

is absolutely convergent for each value of σ in the interval $]a, b[$, and if for positive real values of x and a fixed $c \in]a, b[$ we define

$$f(x) = \frac{1}{2\pi i} \int_{c-j\infty}^{c+j\infty} x^{-z} f^*(z)\, dz$$

then, in the strip S,

$$f^*(z) = \int_0^{\infty} x^{z-1} f(x)\, dx \ .$$

$f^*(z)$ is called the Mellin transform of f(x) (from Sneddon, 1972).

APPENDIX 4.1: SOLUTION OF THE MULTISCALE RENORMALIZATION EQUATION

Consider the linear equation

$$P(\delta) = \sum_{i=1}^{M} w_i P(\delta/r_i) \tag{1}$$

where $r_i < 1$ for all i and

$$\sum_{i=1}^{M} w_i = 1. \tag{2}$$

The general solution of (1) is a linear combination of elementary solutions of the form δ^{-d}, with d complex. The trial solution δ^{-d} replaced in (1) leads to the characteristic equation

$$\sum_{i=1}^{M} w_i r_i^{d} = 1. \tag{3}$$

$d = 0$ is a real root of (3). The complex roots of (3), denoted by $d = d_R + i\, d_I$, are solutions of the system

$$\sum_{j=1}^{M} w_j r_j^{d_R} \cos(d_I \log r_j) = 1 \tag{4a}$$

$$\sum_{j=1}^{M} w_j r_j^{d_R} \sin(d_I \log r_j) = 0 \tag{4b}$$

The complex roots with $d_R \neq 0$ are complex conjugate pairs which can be seen from (4a) to satisfy $d_R < 0$. There are other complex roots with $d_R = 0$ only if $d_I \log r_j = 2\pi n_j$ for all j, which implies that the ratios are of the form

$$r_j = r_0^{\,n_j}, \quad j = 1, 2, \ldots, M, \tag{5a}$$

where r_0 is a constant. In this case the imaginary parts are the solutions of $d_I \log r_j = 2\pi m_j$ that holds for all j, which implies with (5a) that $m_j = nn_j$, and therefore

$$d_I(n) = \frac{2\pi n}{\log r_0} \quad , n \in Z. \tag{5b}$$

Two cases must therefore be distinguished for the general solution:

(i) <u>generic case</u> : The r_j are not integer powers of some common ration r_0. Then the general solution is

$$P(\delta) = c_0 + R(\delta) \tag{6}$$

where

$$R(\delta) = \sum_n c(n)\, \delta^{-d_R(n)} \exp(-i\, d_I(n) \log\delta)$$

and $d_R(n) < 0$ for all values of n. It follows that $R(\delta) \to 0$ as $\delta \to 0$ and therefore $P(\delta)$ is constant in the limit $\delta \to 0$. If $d_R(n) = 0$ for some values of n the oscillations could survive over finite ranges of scale because of the slow damping rate.

(ii) <u>special case</u>: The values of r_j are of the form (5a) and the imaginary parts of the complex roots with $d_R = 0$ are given by (5b). The general solution becomes

$$P(\delta) = F(\log\delta) + R(\delta)\,, \tag{7}$$

where $F(x) = F(x + \log(1/r_0))$.

APPENDIX 5.1: ASYMPTOTIC LINEARITY OF $\tau(q)$ FOR FINITE $f(\alpha)$

For a scaling measure with finite $f(\alpha)$ spectrum ($\alpha \in D_f = [\alpha_-, \alpha_+]$)

$$\tau(q) \sim \alpha_{\mp}\, q - f(\alpha_{\mp}) \quad \text{as} \quad q \to \pm\infty.$$

This result can be derived as follows: On one hand $f(\alpha) \geq K = \min\{f(\alpha_-), f(\alpha_+)\}$ for all $\alpha \in D_f$; Young's inequality $\alpha q - \tau(q) \geq f(\alpha)$ (which follows from the definition of f) then implies that $\alpha q - \tau(q) \geq K$ for all $(\alpha, q) \in D_f \times \mathbb{R}$. On the other hand the concavity $\tau'' \leq 0$ implies that $\tau'(q) \geq \tau'(\infty) = \alpha_-$. Therefore

$$\alpha_- q - \tau(q) \geq K \quad \text{and} \quad \partial/\partial q\{\alpha_- q - \tau(q)\} \leq 0,$$

i.e. the function $\alpha_- q - \tau(q)$ is monotonely decreasing and bounded from below. Hence there must be a number $a_+ \geq K$ such that

$$\lim_{q\to\infty} \alpha_- q - \tau(q) = a_+, \quad \text{i.e.} \quad \tau(q) \sim \alpha_- q - a_+ \quad \text{as} \quad q \to \infty$$

Using $f(\alpha) = \tau'(q_0(\alpha))q_0(\alpha) - \tau(q_0(\alpha))$, where $\tau'(q_0(\alpha)) = \alpha$ which follows from (5.2.12) (see section 5.2.6.2 for more details), and replacing τ by its asymptotic form $\tau(q) \sim \alpha_- q - a_+$ yields $a_+ = f(\alpha_-)$ in the limit $q_0(\alpha) \to \infty$. Similarly it can be shown that there is an $a_- \geq 0$ such that $\tau(q) \sim \alpha_+ q - a_-$ as $q \to -\infty$, where $a_- = f(\alpha_+)$.

BIBLIOGRAPHY

Aitchison, J. and J. A. C. Brown. 1976. The lognormal distribution, with special references to its uses in economics. Cambridge University Press. Cambridge, New York, Melbourne.

Anselmet, F., Gagne, Y., Hopfinger E.J. 1984. *J. Fluid Mech.* **140**, pp. 63-89.

Antonia, R. A. 1981. Conditional sampling in turbulence measurement. *Ann. Rev. Fluid Mech.* **13**, 131-156.

Arnold, V. Mathematical Methods of Classical Mechanics (Russian edition, Moscow, 1974; French edition, Moscow, Editor *Mir*, 1976).

Badii, R. and A. Politi. 1985. Statistical Description of Chaotic Attractors: The Dimension Function. *Journal of Statistical Physics*, **40**, # 5/6.

Balatoni, J. and A. Renyi, *Publ. Math. Inst. of the Hungarian Acad. of Sci.* **1** (1956) p. 9 (Hungarian). English translation, Selected papers of A. Renyi, **1** (Acadeiai Budapest, Budapest, 1976), p. 558. See also A. Renyi, *Acta Mathematica* (Hungary) **10** (1959) p. 193.

Barnsley, M. 1988. Fractals everywhere. Academic Press, New York.

Bartello, P and T. Warn. 1988. A one-dimensional turbulence model; enstrophy cascades and small-scale intermittency in decaying turbulence. *Geophys. Astrophys. Fluid Dynamics*, **40**, pp. 239-259.

Batchelor, G.K. and Townsend. 1949. The role of big eddies in homogeneous turbulence, *Proc. Roy. Soc.* (London), **A195**, # 1043, pp. 513-532.

Bender, C.M. and S.A. Orszag. 1978. Advanced mathematical methods for scientists and engineers. McGraw-Hill. New York, Montreal, Paris.

Benzi, R., Paladin, G., Parisi, G., and A. Vulpiani. 1984. On the multifractal nature of fully developed turbulence and chaotic systems. *J. Phys. A: Math. Gen.* **17**. pp. 3521-3531.

Cates, M. E. and J. M. Deutsch. 1987. Spatial correlations in multifractals. *Physical Review A*. **35**, # 11. pp. 4907-4910.

Chhabra, A. B., R. V. Jensen, K.R. Sreenivasan. 1989. Extraction of underlying multiplicative processes from multifractals via the thermodynamic formalism. *Physical Review A*, **40**, #8.

Combes, J.M., Grossmann, A. and Tchamitchian, P (editors). 1988. Wavelets (Springer-Verlag, Berlin) and references therein.

Devaney, R.L. 1986. An Introduction to Chaotic Dynamical Systems. Benjamin/Cummings Publishing Company, Inc. Reading (Massachusetts), Don Mills (Ontario).

Eggleston, H.G. 1949. The fractional Dimension of a Set Defined by Decimal Properties, *Quart. J. Math. Oxford*, Ser. 20, pp 31-36.

Falconer, K.J. 1985. The geometry of fractal sets. Cambridge University Press. New York.

Falconer, K. 1990. Fractal geometry, mathematical Foundations and applications. John Wiley&Sons. Chichester, New York, Toronto.

Farmer J.D., E. Ott and J.A. Yorke. 1983. The dimension of chaotic attractors. *Physica 7D*, pp. 153-180.

Feder, J. 1988. Fractals. Plenum Press, New York, London.

Feigenbaum, J. F. 1987. Some characterizations of strange sets. *Journal of Statistical Physics*, **46**, # 5/6.

Feller, W. 1966. An introduction to probability theory and its applications. Vol. I and II. John Wiley & Sons. New York, Toronto.

Fourcade, B. and A.-M. S. Tremblay. 1987. Anomalies in the multifractal analysis of self-similar networks. *Physical Review A*. **36**, # 5, pp. 2352-2358.

Frisch, U. 1983. Fully developed turbulence. Proceedings of the international school of physics "Enrico Fermi", *Italian Physical Soc.*, Bologna, Italy.

Frisch, U. and S. A. Orszag. January 1990. Turbulence: Challenges for theory and experiment. *Physics Today*.

Frisch, U. and P. Sulem. 1978. A simple dynamical model of intermittent fully developed turbulence. *J. Fluid Mech.* **87**, part 4, pp. 719-736.

Grant, H. L., R. W. 1962. Stewart, A. Moilliet, *J. Fluid Mech.* **12**, p. 241.

Grassberger, P. and I. Procaccia. 1983. Measuring the strangeness of strange attractors. *Physica 9D*, pp. 189-208.

Grossmann, A. and Morlet, J. 1987. In Mathematics and Physics, Lectures on Recent results, edited by L. Streit (World Scientific, Singapore).

Halsey, T.C., M. H. Jensen, L. P. Kadanoff, I. Procaccia, B. I. Shraiman. 1986. Fractal measures and their singularities: The characterization of strange sets. *Physical Review A*. **33**. pp. 1141-1151.

Hentschel, H.G.E. and I. Procaccia. 1983. The infinite number of generalized dimensions of fractals and strange attractors. *Physica 8D*. pp. 435-444.

Hutchison, J. E. 1981. Fractals and self-similarity. *Indiana University Mathematics journal*, **30**, # 5. pp. 713-747.

Kadanoff, L. P. 1990. Scaling and universality in statistical physics. *Physica A*, **163**, pp. 1-14.

Kahane, J.P. and J. Peyrière. 1976. Sur certaines martingales de Benoit Mandelbrot. *Advances in mathematics*. **22**, # 2, pp. 131-145.

Khinchin, A. I.. 1949. Mathematical foundations of statistical mechanics. Dover Publications, New York.

Kolmogorov, A. N.. 1941a. Local structure of turbulence in an incompressible fluid at very high Reynolds numbers, *Dokl. Akad. Nauk SSSR*, **30**, # 4, pp. 299-303.

Kolmogorov, A. N.. 1941b. Logarithmically normal distribution of fragmentary particle sizes, *Dokl. Akad. Nauk. SSSR*, **31**, # 2, pp. 99-101.

Kolmogorov, A. N.. 1962. A refinement of previous hypothesis concerning the local structure of turbulence in an incompressible viscous fluid at high Reynolds numbers. *J. Fluid Mech.*, **13**, # 1, pp. 82-85.

Kolmogorov A.N.. 1958. A New Invariant for Transitive Dynamical Systems, *Dokl. Akad. Nauk SSSR*. **119**, pp. 861-864.

Kraichnan, R. H., 1974. On kolmogorov's inertial-range theories. *J. Fluid Mech.* **62**, part 2, pp. 305-330.

Kuo, A. Y-S., and S. Corrsin, 1971. Experiments on internal intermittency and fine-structure distribution function in fully turbulent fluid, *J. Fluid Mech.*, **50**, # 2, pp. 285-320.

Landau, L.D. and F.M. Lifshitz. 1989. Fluid Mechanics. Pergamon Press, New York.

Lavallée, D., Schertzer, D., Lovejoy, S., 1990. On the determination of the codimension function, in Scaling, Fractals and Non-Linear Variability in Geophysics, edited by D. Schertzer and S. Lovejoy, Kluwer, Holland, in press.

Lee, S. J. and T. C. Halsey. 1990. Some results on multifractal correlations. *Physica A.* **164**. pp. 575-592.

Lovejoy, S. 1985. Fractal properties of rain, and a fractal model. *Tellus*, **37A**, pp. 209-232.

Lovejoy, S. and D. Schertzer. 1986. Scale Invariance, Symmetries, Fractals, and Stochastic Simulations of Atmospheric Phenomena. *Bulletin of the American Meteorological Society*, **67**, # 1.

Mandelbrot B.B., 1988. An introduction to multifractal distribution functions. Proceedings volume Fluctuations and pattern formation (Cargèse 1988). Edited by H.E Stanley and N. Ostrowsky. Dordrecht, Boston.

Mandelbrot B.B., 1983, The Fractal Geometry of Nature, W. H. Freeman and Company, New York.

Mandelbrot, B. B. 1972. Possible refinement of the lognormal hypothesis concerning the distribution of energy dissipation in intermittent turbulence. Models and Turbulence, Proceedings of the Symposium at San Diego, July 15-21, 1971. (M. Rosenblatt and C. Van Atta, eds.) *Lecture Notes in Physics* **12**, Springer-Verlag, Berlin-Heidelberg-New York, pp. 333-351.

Mandelbrot, B.B. 1974. Intermittent turbulence in self-similar cascades: Divergence of high moments and dimension of the carrier. *J. of Fluid Mechanics* **62**, pp. 331-358.

Mandelbrot, B. B. 1975. On the geometry of homogeneous turbulence, with stress on the fractal dimension of the iso-surfaces of scalars. *J. Fluid Mech.*, **72**, part 2, pp. 401-416.

Meneveau, C. and K. R. Sreenivasan. 1987a. Simple multifractal cascade model for fully developed turbulence. *Phys. Rev. Lett.* **59**, p. 1424.

Meneveau, C. and K. R. Sreenivasan. 1987b. in The physics of chaos and systems far from equilibrium, edited by Minh-Duong Van (North-Holland, Amsterdam, p. 49.

Meneveau, C. and K. R. Sreenivasan. 1987c. *Nucl. Phys. B (Proc. Suppl.)* **2**, p. 49.

Meneveau, C., K. R. Sreenivasan, P. Kailasnath, M. S. Fan. 1990a. Joint multifractal measures: Theory and applications to turbulence. *Physical Review A*, **41**, # 2.

Meneveau, C. and A. B. Chhabra. 1990b. Two points statistics of multifractal measures. *Physica A*, **64**, pp. 564-574.

Monin, A.S. and A.M. Yaglom. 1975. Statistical fluid mechanics. Vol. 1-2. Edited by J.L. Lumley. Cambridge (Massachusetts), London (England).

Novikov, E. A., and R. W. Stewart. 1964. Intermittency of turbulence and spectrum of fluctuations in energy dissipation, *Izv. Akad. Nauk SSSR*, Ser. Geofiz., **3**, pp. 408-413.

Novikov, E. A., 1965. High-order correlations in a turbulent flow, *Izv. Akad. Nauk SSSR, Fiz. Atmosf. i Okeana*, **1**, # 8, pp. 788-796.

Novikov, E. A., 1966. Mathematical model for the intermittence of turbulent flow. *Dokl. Akad. Nauk SSSR* **168/6**, p. 1279. Sov. Phys. Dokl. **11**, pp. 497-499.

Novikov, E.A., 1970. Intermittency and scale similarity of the structure of turbulent flow, *Prikl. Mat. Mekh.*, **35**, # 2, pp. 266-277.

Novikov, E. A. 1990. The effects if intermittency on statistical characteristics of turbulence and scale similarity of breakdown coefficients. *Phys. Fluids A* **2**, p. 5.

Orszag, S. A.. 1970. Indeterminacy of the moment problem for intermittency turbulence. *Physics of Fluids*, **13**, pp. 2211-2212.

Orszag, S.A. 1977. Lectures on the statistical theory of turbulence. In Fluid Dynamics, Les Houches, 1973 (R. Balian and P.L. Peube ed.), pp. 235-374. Gordon and Breach, New York.

Peitgen, H.O and D. Saupe, 1988. The Science of Fractal Images. Springer-Verlag, New York.

Pond, S., and R. W. Stewart. 1965. Measurements of statistical characteristics of small scale turbulence, *Izv. Akad. Nauk SSSR, Fiz. Atmosf. i Okeana*, **1**, # 9, pp. 914-919.

Press, H. W., B. P. Flannery, S. A. Teukolsky, W. T. Vetterling. 1986. Numerical Recipes, the Art of Scientific Computing. Cambridge University Press, New York.

Raupach, M. R. 1981. Conditional statistics of Reynolds stress in rough-wall and smooth-wall turbulent boundary layers. *J. Fluid Mech.*, **108**, pp. 363-382.

Sandborn, V. A., 1959. Measurements of intermittency of turbulent motion in a boundary layer, *J. Fluid Mech.*, **6**, # 2, pp. 221-240.

Schertzer, D. and S. Lovejoy. 1984. On the dimension of atmospheric motions. In: Turbulence and chaotic phenomena in fluids. T. Tatsumi. North-Holland.

Schertzer, D. and S. Lovejoy. 1985. The dimension and intermittency of atmospheric dynamics. In: Turbulent shear flows 4. Editor: L.J.S. Bradbury. Springer-Verlag, Berlin, Heidelberg.

Schertzer, D., S. Lovejoy, 1985b. Generalized scale invariance in turbulent phenomena. *P.C.H. Journal*, **6**, pp. 623-635.

Schertzer, D. and S. Lovejoy. 1987. Physical modeling and analysis of rain and clouds by anisotropic scaling multiplicative processes. *J. Geophys. Res.* **92**, # D8, pp.9693-9714.

Schertzer, D. and S. Lovejoy. 1989. Nonlinear variability in geophysics: Multifractal simulations and analysis. In Fractals, edited by L. Pietronero (plenum Press)

Shaw, W. J. and J. A. Businger. 1985. Intermittency and the organization of turbulence in the near-neutral marine atmospheric boundary layer. *Journal of the atmospheric sciences*, **42**, # 23, pp. 2563-2584.

Siebesma, A. P. and L. Pietronero. 1988. Correlations in multifractals. *J. Phys. A: Math. Gen.* **21**. pp. 3259-3267.

Smith, L.A., J.D. Fournier, E.A. Spiegel. 1986. Lacunarity and intermittency in fluid turbulence. *Phys. Lett. A.* **8**, p. 9.

Sneddon, I. N. 1972. The use of integral transforms. McGraw-Hill Book company. New York, Montréal, London.

Sreenivasan, K. R. and C. Meneveau. 1988. Singularities of the equations of fluid motion. *Physical Review A.* **38 # 12**, pp. 6287-6295.

Stewart, R.W., J.R. Wilson, R.W. Burling. 1970. Some statistical properties of small scale turbulence in an atmospheric boundary layer. *J. Fluid Mech.*. **41**, part 1, pp. 141-152.

Townsend, A. A.. 1947. The measurement of double and triple correlation derivatives in isotropic turbulence, *Proc. Cambr. Phil. Soc.*, **43**, **# 4**, pp. 560-570.

Tricot, C. 1973. Sur la notion de densité, *Cahier du département d' économétrie de l' Université de Genève.*

Van Atta, C. W., and W. Y. Chen, 1970. Structure functions of turbulence in the atmospheric boundary layer over the ocean, *J. Fluid Mech.*, **44**, **# 1**, pp. 145-159.

Van Atta, C. W., and J. Park, 1971. Statistical self-similarity and inertial subrange turbulence. Statistical Models and Turbulence. Proceedings of the Symposium at San Diego, July 15-21, 1971, (M. Rosenblatt and C. Van Atta, eds.) *Lecture Notes in Physics* **12**, Springer-Verlag, Berlin-Heidelberg-New York, pp. 402-426.

Wong, R. 1989. Asymptotic approximation of integrals. Academic Press, inc.. New-York, Boston, Toronto, London.

Yaglom, A. M.. 1966. Effect of fluctuations in energy dissipation rate on the form of turbulence characteristics in the inertial subrange, *Dokl. Akad. Nauk SSSR*, **166**, **# 1**, pp. 49-52.